12-2010

ADVANCED AUTOMOTIVE THERMAL MANAGEMENT - OPERATION OF AN ELECTRIC RADIATOR FAN ARRAY FOR REDUCED ELECTRIC POWER CONSUMPTION

Amit Jagarwal
Clemson University, ajagarw@clemson.edu

ADVANCED AUTOMOTIVE THERMAL MANAGEMENT – OPERATION OF AN ELECTRIC RADIATOR FAN ARRAY FOR REDUCED ELECTRIC POWER CONSUMPTION

A Thesis
Presented to
The Graduate School of
Clemson University

In Partial Fulfillment
of the Requirements for the Degree
Master of Science
Mechanical Engineering

By
Amit Harendra Jagarwal
December 2010

Accepted by:
Dr. John Wagner, Committee Chair
Dr. Darren Dawson
Dr. Todd Schweisinger

ABSTRACT

The depletion of fossil fuel reserves and the limited renewable energy resources have raised public awareness about the need to improve fuel efficiency in ground transportation vehicles. The internal combustion engine remains one of the primary industrial machines using gasoline or diesel fuel to produce mechanical work. In these engines, the cooling system performs the vital role of removing waste heat to ensure normal combustion processes in the cylinders. To accomplish this task, the radiator, the radiator fan(s), the thermostat valve, and the water pump operated by circulating cooling fluid through the engine block and rejecting heat to the atmosphere. Studies have shown that the cooling system removes approximately 30% of the engine`s indicated power as waste heat. Since the cooling system consumes a portion of the engine power, it is important that its operation use minimum input energy. In this study, multiple radiator fans were controlled to minimize energy usage for subsequent efficiency gains. Simply put, this research found that improvements in the thermal management system can improve overall engine efficiency.

A reconfigurable smart cooling system test experimental bench was fabricated at Clemson University to test and analyze the cooling effect multiple electric radiator fans. This cooling system emulated a 6.8L International Truck and Engine Corporation V8 diesel engine application with an array of 3 rows by 2 columns (6 total) radiator fans. The speed of each fan was controlled from 0% to 100% maximum capacity. A dedicated controller area network (CAN) bus controller was interfaced to

the fan driver hardware and electric power source to control the system operation. The air speed, coolant flow rate, fluid (air, coolant) temperature, and power consumption sensors were connected to a dSPACE data acquisition board, on which data were recorded. The dSPACE and Plus+1 hardware were controlled in real-time using a MATLAB/Simulink algorithm operating at a 10 Hz frequency.

A series of laboratory tests were conducted with different fan combinations and rotational speeds, the objective being to cool a constant thermal loaded engine. A simplified mathematical model for the combustion process and the forced convection radiator system was developed to establish a basis to formulate a smart cooling control problem. The collected data was analyzed to determine the fan power consumption and radiator system cooling effectiveness. The experimental results demonstrated that the selection of specific fan combinations and fan motor speeds can achieve up to a 20% reduction in fan matrix power consumption for the specified cooling load. Further, air velocity surface plots offered a visual representation of the air flow profile across the radiator for different fan matrix configurations.

ACKNOWLEDGMENTS

I would like to thank Dr. John Wagner for his guidance and support throughout my research efforts. I would also like to express my appreciation to Dr. Darren Dawson and Dr. Todd Schweisinger for serving on my research advisory committee. I wish to thank my parents, Mr. Harendra Jagarwal and Mrs. Kanchan Jagarwal, for all the moral support and love they have provided throughout my life. Finally, I would also like to thank my colleagues and friends in the Mechanical Engineering Department at Clemson University for their help when it was needed.

TABLE OF CONTENTS

Page

Table of Contents (Continued)

Page

LIST OF TABLES

LIST OF FIGURES

NOMENCLATURE

Symbol	Units	Description
A	m^2	Surface area
a	-	Polynomial coefficients
A_c	m^2	Surface area on the coolant side of the combustion cylinder
A_e	m^2	Effective conduction heat transfer area
A_g	m^2	Inner surface area of the combustion cylinder
A_p	m^2	Surface area of the piston head
b	*m*	Bore size of the piston head
C_p	KJ/kg °K	Specific heat of water at constant pressure
d	kg/m^3	Air density
D	M	Fan diameter
d_P	Pa	Air pressure
G_{DS}	-	dSPACE Gain for motor speed
$G_{DS,T}$	-	dSPACE Gain for thermocouple
h_c	$W/m^{2\circ}K$	Convective heat transfer coefficient of the coolant
h_g	$W/m^{2\circ}K$	Convective heat transfer coefficient of the combustion gases
i	Amp	Fan motor matrix current
K	W/m°K	Thermal conductivity

K_C	W/m°K	Thermal conductivity of coolant
$K_{C,J}$	-	Conversion factor J-type thermocouple signal
$K_{C,K}$	-	Conversion factor K-type thermocouple signal
K_g	W/m°K	Thermal conductivity of combustion gases
K_M	-	Conversion factor for DC motor signal
K_w	W/m°K	Thermal conductivity of the engine block material
L	M	Significant length
$\dot{m}_{air}$	m^3/sec	Air discharge
$\dot{m}_C$	kg/sec	Coolant circulation rate
M_{DC}	VDC	Motor control signal
N	RPM	Fan motor speed
N_{DC}	RPM	Coolant motor speed
n_{fan}	-	Number of fans operating
N_u	-	Nusselt number
P	W	Fan motor matrix power consumption
P_{FAN}	KW	Impeller power of the fan
q	m^3/sec	Volume flow rate
$\dot{Q}$	KW	Heat transfer rate
$\dot{q}_{air}$	m^3/sec	Air volume flow rate
$\dot{q}_{air,1}$	m^3/sec	Individual fan air volume flow rate
$\dot{Q}_{HEAT}$	KW	Heat recirculated to the cooling system

$\dot{q}_{HEAT}$	W	Heat recirculated to the cooling system by radiator channel
$\dot{Q}_{IN}$	KW/sec	Heat input rate in the cooling system
$\dot{q}_{IN}$	W	Heat input rate in radiator channel
$\dot{Q}_{OUT}$	KW/sec	Heat rejection rate by the radiator
$\dot{q}_{OUT}$	W	Heat rejection rate by the radiator channel
$\dot{q}_{RC}$	W	Heat rejection rate from vertical radiator channel
$\dot{q}_{RF}$	W	Heat rejection rate from single radiator fin
R_e	-	Reynolds's number
$R_{e,g}$	-	Reynolds number for the combustion gases
r_h	m	Fan hub radius
r_m	m	Fan mean radius
r_t	m	Fan tip radius
S_X	-	Standard deviation
t	sec	Time period
T	$^\circ$C	Temperature level
T_{air}	$^\circ$C	Temperature of air
T_c	$^\circ$C	Temperature of circulating coolant
T_g	$^\circ$C	Temperature of gases
T_{HI}	$^\circ$C	Heat exchanger inlet temperature

T_{HO}	$^{\circ}C$	Heat exchanger outlet temperature
T_J	$^{\circ}C$	Temperature of coolant
$t_{v,95}$	-	t distribution variable
T_{RI}	$^{\circ}C$	Radiator inlet temperature
T_{RO}	$^{\circ}C$	Radiator inlet temperature
Ts	-	Transfer function
T_{SINK}	$^{\circ}C$	Air outlet temperature
t_w	m	Combustion chamber wall thickness
T_w	$^{\circ}C$	Temperature of water
T_{∞}	$^{\circ}C$	Ambient temperature
U	$W/m^2\,^{\circ}K$	Overall heat transfer coefficient
u_{C_p}	-	Uncertainty of the specific heat value
$u_{\dot{m}_c}$	-	Uncertainty for coolant mass flow rate
u_q	-	Uncertainty of heat flow rate
u_T	-	Uncertainty for temperature measurement
v	-	Hub ratio
v_{air}	m/sec	Air velocity
V_S	VDC	Fan motor matrix supply voltage
X	m	Width of radiator
x	m	Distance along the X-axis of radiator

X_J	VDC	Signal from K-type thermocouple
X_M	-	User input variable
Y	m	Height of radiator
y	m	Distance along the Y-axis of radiator
Y_J	-	Transfer function output
ΔT_m	$^\circ$C	Mean effective temperature difference
ΔT	$^\circ$C	Temperature difference
ρ	kg/m^3	Density
ρ_{air}	kg/m^3	Air density
μ	kg/m-sec	Dynamic viscosity
ν	m^2/sec	Kinematic viscosity
η_M	-	Electrical motor efficiency
Φ_m	-	Fan flow rate coefficient

CHAPTER ONE

INTRODUCTION

The fuel efficiency of a vehicle is an important concern given the depletion of fossil fuels and the growing environmental impact of greenhouse gases. Many automotive technological strategies have been adopted to reduce the use of fossil fuels including the introduction of hybrid electric vehicles and the development of bio fuel engines. However, the majority of ground transportation platforms still rely heavily on internal combustion (IC) engines which use either gasoline or diesel fuel. Consequently, one important design goal for researchers in this area is the efficient use of fuel and the minimization of harmful exhaust gases. The modern IC engine contains complex physical subsystem interactions which regulate the operation of the electro-mechanical component, the fuel pump, the forced air cooling system, the inlet air system including the idle air circuit, the exhaust gas circuit, the turbo charger with adjustable compressor blades, and the spark ignition system. These components control the parameters defining the engine`s operation which may be measured by such quantities as the air-fuel ratio, injection timing, engine temperature, and crankshaft speed. These physical subsystems are usually controlled by various actuators with their signals being generated by the on-board engine controller.

A key internal combustion engine subsystem which consumes accessory torque is the thermal management system. This cooling system consists of the radiator, water pump, thermostat valve, radiator fan(s), hoses, coolant reservoir,

temperature sensor, and engine water jacket. On average, in a gasoline engine 25% (38% for diesel engines) of the total energy generated from combustion is lost to the cooling system, 46% (27%) to exhaust gases and about 26% (35%) gets converted to useful brake power (Heinz, 1995, Heywood, 1988). Thus, the cooling system must accommodate a significant amount of heat while operating under reasonable power demands. The cooling systems also impacts the engine warmup time, general thermal transients, and peak operating temperature, all of which in turn affect the tailpipe emissions and fuel efficiency (Koch *et al.,* 2000). The cooling system must have a quick response time with an ability to maintain the prescribed temperature range to accommodate normal combustion.

The cooling system, which has evolved over a 100 year time period, is similar in both ground vehicles and stationary power generators. In fact, large power plant condensers also use the same type of components and designs; however, the heat transfer medium is different, involving various layouts, flow passages, actuators, control strategies, and accessories of heat conductive materials. The system of interest in this study is a multiple fan radiator cooling system monitored by sensors and controlled by a programmed microprocessor using electric actuators. This radiator system is a forced convection cooling system using electrical energy to provide power to its coolant pump, sensors, valve actuators, and fan matrix. These systems, which are not coupled to engines directly and can be independently controlled using a pre-programmed algorithm and control signal generators, offer several advantages. The multiple fan systems use electric actuators, which are easier to control than a fan

directly coupled to the engine. Better control of the electric motors and the large range of speeds and power output can help achieve efficient heat transfer and minimize power consumption. The electrical signal generation and processing is fast and accurate, thus enabling better response from the electric actuators, and electrically controlled systems are lighter and the equipment operates cleaner, thus proving to be a convenient, light-weight solution for a power efficient cooling system.

Depletion of fossil fuel reserves has triggered higher fuel prices, and its increasing environmental impact has lead to tighter emission norms, these restrictions requiring devices converting heat energy into mechanical work to be more efficient. An IC engine converts approximately 35% percent of its indicated power into mechanical work, making them inefficient devices for energy conversion since the rest of the energy is lost to the cooling system (30%) and to the exhaust (35%). The limitation of material heat transfer properties; the mechanical inertia of moving components; friction; and non-controllable variables such as ambient temperature, pressure conditions, and exhaust back pressure have created challenges in making IC engines efficient and environmentally clean. Current efforts focus primarily on controllable engine parameters; for instance, combustion temperature, fuel flow, and operation timing, to improve the fuel efficiency. Dynamic control of engine subsystems generating increasingly accurate parameter values have shown to improve engine fuel efficiency; these parameters include the coolant temperature, the air-fuel mixture, and the pressure from supercharger. A close control of these parameters

requires improved controllable engine sub-systems, addressing varying engine requirements over the operating cycle (Rocklege *et al*., 2006).

The cooling system of an engine is an important subsystem, maintaining dynamic engine temperatures within the required operating limits. There are many methods for achieving engine cooling within the required limits of these parameter values. The majority of these approaches use the circulation of a water and ethylene-glycol mixture in the coolant jackets surrounding the combustion chamber in an engine block. Coolant mixtures capable of withstanding higher temperature range have been developed to speed the heat transfer process under various climatic conditions. These mixtures are chemically engineered to maintain the required viscosity and thermal properties at low, as well as high, temperatures by reducing the freezing point of the coolant and raising its boiling point.

Along with natural convection, which is primarily a function of vehicle speed, a radiator may require additional forced convection to meet the thermal load, depending on its size and type of cooling system. Forced convection is obtained by rotating fan blades, operated using energy from the engine by either mounting them directly on the crank shaft or by driving the fan motors converting a portion of engine power into electric energy. On the other hand, vehicle speed can create ram air across the engine which offers forced convection. Increased control of the fan motors is possible with electric actuators as they have the potential of making the decoupled fan matrix cooling system energy efficient, leading to a reduction in fuel consumption in

the engine. In addition, a highly controllable cooling system running on feedback from dynamically acquired sensor data using embedded control algorithms has been shown to help reduce emissions (Choi *et al.*, 2007).

A forced convection cooling system with an array of electric fans and a radiator cooling circuit has been developed in the Mechanical Engineering Department at Clemson University. This system includes multiple fans and independent controllers to operate them, using the feedback collected across the system. The system is monitored and controlled using a dSPACE platform and MATLAB/Simulink control algorithms running in tandem. The data collected have been used to determine the system behavior at different fan configurations (various combinations of different numbers of fans operating at uniform speeds). A control problem has been formulated based on the observed input and output parameters, and the system is modeled with the goal to achieve optimization in power consumption.

The experimental setup represents a cooling circuit for vehicles and with minor changes in equations can also be used to simulate relatively stationary applications (for example mining equipment, power plants, portable generator sets). Further, with minor changes in assumptions, this setup can be considered to be equivalent to any forced convection radiator cooling system that needs an external power supply for heat rejection. The data obtained and the control algorithm developed are useful in a wide variety of applications with subsystems consisting of a

heat source, a heat pump, and a heat sink with a multiple fan matrix for accelerated heat rejection.

1.1 Automotive Thermal Management System

Automotive thermal management systems consist of a mechanism which is, in principle, a heat pump operating in reverse, i.e., removing heat from higher temperature source, the engine block, to the lower temperature sink, the atmosphere. It has the primary function of limiting the temperature level in the engine block to a specified range. These systems can be broadly classified as either open or closed thermodynamic circuits. Since the heat transfer is from the higher temperature source to the lower temperature sink, the external power source in this case is used to increase the rate of energy transfer. The system may use either a single medium or a number of consecutive mediums for this heat transfer to occur effectively. The primary objective of thermal management is to use a minimum of the energy input to obtain a maximum and fast rate of heat flow from the source to the sink.

The role of automotive thermal management systems has widened from maintaining safe engine temperatures to preventing harmful emissions and improving the fuel efficiency. Carbon dioxide, CO_2; carbon monoxide, CO; nitrogen oxides, NO_X; and hydrocarbons such as heptanes and octane are the major pollutants attributed to the internal combustion engine (Choi *et al*., 2007). Carbon dioxide is the product of the exothermic chemical reaction (i.e., combustion) between the air and the hydrocarbon fuel, while carbon monoxide is formed due to an insufficient supply

of oxygen, O_2, for combustion. Nitrogen oxides, which form when nitrogen and oxygen are subjected to very high temperatures in the combustion chamber, can be reduced by controlling the engine intake/exhaust valve timing and the engine operating temperature. In many instances, corrective actions can be taken such as processing the exhaust to remove or chemically transform the pollutants into less harmful compounds. However, engine temperature must also be controlled over the wide range of temperatures that the vehicle may experience.

The response of the cooling system depends on the horsepower of the engine, the radiator, the pump, and the fan(s) sizes as well as the control algorithm. For example, when cold starting, the IC engine needs to warm up fast, so the radiator fluid flow should be minimal. Slower heating up of the engine to the optimum temperature increases the level of hydrocarbon pollutants emitted. Thus, the cooling system is required to adapt to the temperature needs of the engine as fast as possible. Since the coolant circuit uses a control system that runs on the energy generated by the engine itself, a better control algorithm may demand higher power for accurate and fast operation; this requirement in turn increases the load on the engine as the power requirement of the coolant system increases. The cooling system, thus, needs to have all of these controlling abilities but must minimize the energy consumption, meaning while maintaining the energy efficiency of the radiator, it must also be capable of proper engine temperature control and, consequently, the engine emissions.

An automotive cooling system can be classified into two major types (refer to Figure 1.1): crank coupled systems, which consume power through a coupling to the engine crank shaft, and decoupled systems that rely on electrical power to drive electric actuators from the alternator via the batteries. A coupled system includes various parameters derived from the engine itself including the fan speed and coolant pump input power; the inability to control these parameters independently hampers the efficiency of such a cooling system. A decoupled system facilitates independent control of fan speed and pump power as well as providing flexibility in system layout and component mounting.

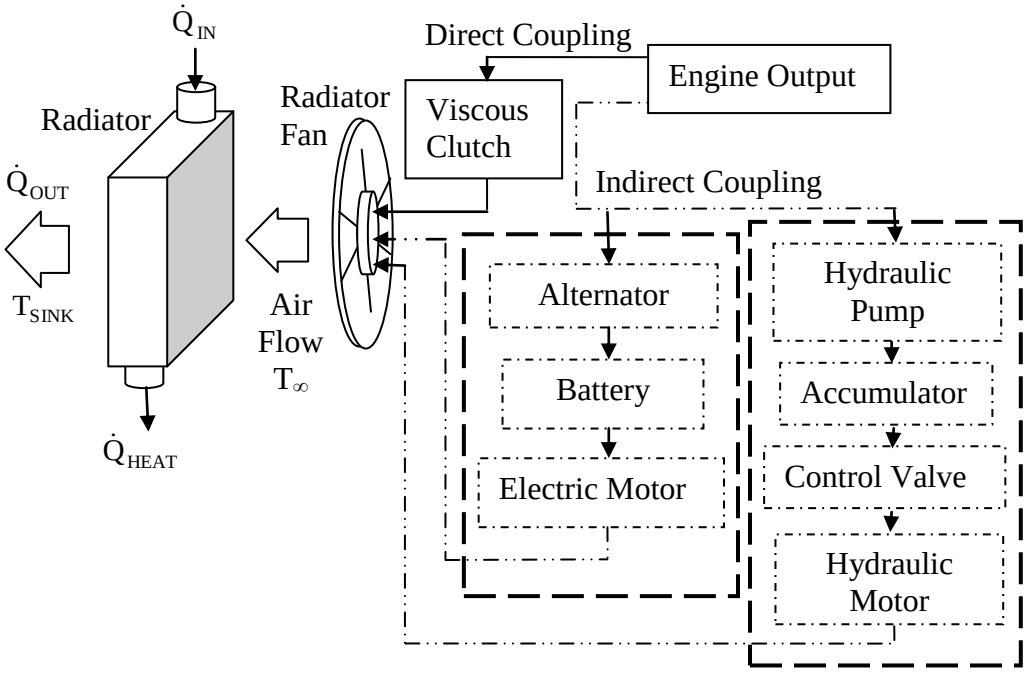

Figure 1.1: Direct and indirect engine coupling for an automotive (electric and hydraulic drive) forced convection cooling system.

In forced convection cooling systems, the classification is also based on the number of fan actuators and their location; broadly they can be classified as single or multiple fan systems. Single fan systems generally serve small heat load applications and require a single controller to achieve varied air flow over the radiator fins; however, the air flow pattern over the radiator is limited. On the other hand, a multiple fan system has complex control capabilities, and with the possible variations in fan speeds and matrix arrangements, it can achieve a varied flow pattern over the radiator surface area. Since the air flow pattern governs the rate of heat transfer, a multiple fan system can adapt better to the continuously varying heat load scenario often encountered in an automotive cooling system.

1.2 Operation of Heat Exchangers

A heat exchanger transfers heat between two mediums at different temperature levels, from the one at the higher temperature to the one at the lower temperature. The radiator is essentially an enclosure made of a thermally conductive material designed to provide fluid passages with a maximum heat transfer surface area, to facilitate a fast heat exchange. Material and object properties such as thermal conductivity, surface area, and viscosity are important parameters to be considered when designing a radiator. Materials in a liquid state facilitate the transport of heat energy because of their ease of transportation and collective heat transfer properties. Similarly, solid metals having high conductivity offer effective and efficient heat transfer. These two properties, when combined, result in a radiator cooling system

that can achieve higher heat transfer rates between two distinct fluid mediums which do not mix.

To increase the heat transfer rate in a radiator, a fan system generates forced air convection over the radiator passages (fins) (refer to Figure 1.2). This air cools the fluid through surface air convection, conduction through the metal and fluid convection inside the radiator, cooling the circulating fluid inside. The factors contributing to the amount of heat transfer in such a system are the geometry of the fins, the fluid thermal properties, the radiator material, the properties of the fluid flow, and the ram air flow over the fins; of particular interest to the study reported here is the external airflow due to the fan(s). The rate of heat loss through a radiator is proportional to the amount of power input to these fan(s).

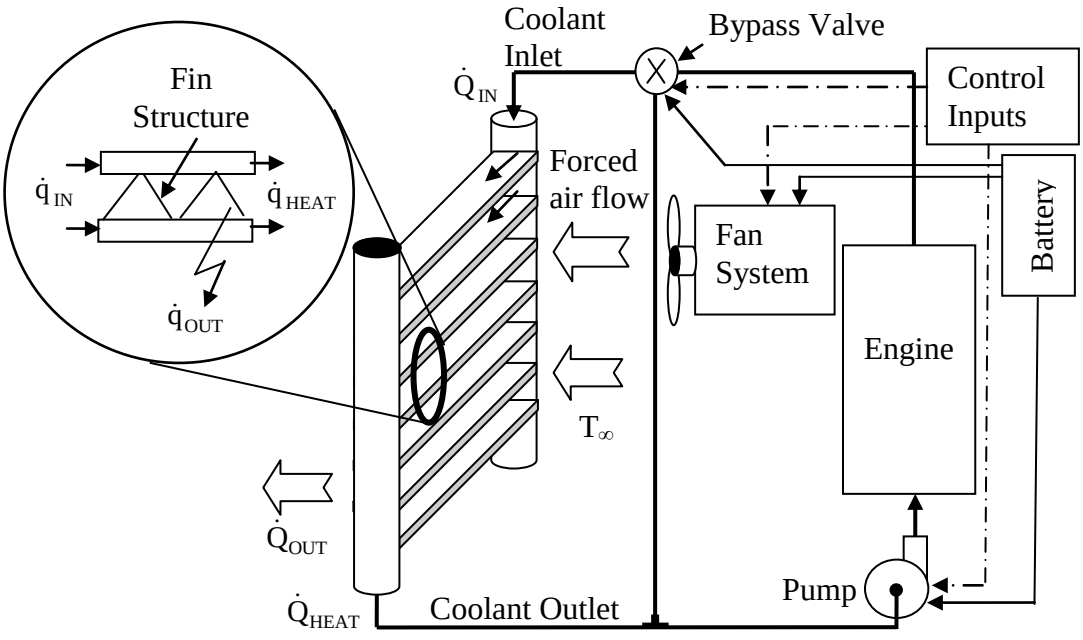

Figure 1.2: Cross flow radiator indicating the flow directions, heat transfer surface of the radiator and electromechanical actuators in the system.

In a decoupled fan radiator cooling system, the electric energy is converted into the mechanical rotation via motors and eventually into the kinetic energy of air motion.

A standard automotive cooling system in Figure 1.2 is comprised of a coolant which receives heat from the engine and then rejects it through the radiator. The operating fluid undergoes heating and cooling to control the tempertaure in the engine block. The operating fluid, i.e., the coolant, gains the heat in the engine jackets and after loosing this energy, $\dot{Q}_{OUT}$, in the radiator it circulates back to the engine to form a basic closed loop heat transfer circuit. The heat rejection, $\dot{Q}_{OUT}$, is the sum of the heat loss, $\dot{q}_{OUT}$, from the individual fins and in the radiator fluid passages. The pump flow rate, the fan speed, the coolant properties, and the radiator mesh size determine the overall capacity of a radiator cooling system.

The power required to achieve a given amount of heat transfer depends on the performance of such auxiliary equipment as the fan and pump motor system used in forced convection radiator cooling system. The relationship between the fan blade motion, air circulation, and the subsequent increase in heat transfer is non-linear. The solution for the relationship between convective air flow and the heat rejected by the radiator is found mathematically by using models built to scale and taking measurements under standard operating conditions or through analytical models. These measurements are plotted, and values for actual systems are predicted using these graphs as a reference. Thus, power consumption by a fan motor cooling system

for a given heat load is estimated from the performance curves of the standard model tests. The accuracy of these predictions depend on the sensitivity of the measuring instruments and the selection of the appropriate standard values.

Thermal management systems use several strategies (refer to Figure 1.3) to achieve effective heat transfer with minimum power requirements. An automotive cooling system requires a solid mechanical design, a good system component arrangement, approximately sized actuators, sensors, and robust control algorithms. The complexity of the cooling system determines the control level achieved in the system; however, not every application of an IC engine needs accurate control. The simplest cooling system is ram air cooled engine which uses fins on a cylinder block and cylinder head to reject heat (refer to Figure 1.3a). In this system the mechanical design and the air flow over the fins cools the engine.

A more complicated cooling system is a forced convection cooled engine; this arrangement has a fan actuator to increase air flow over the engine fins, achieving a more efficient cooling than the natural ram air effect in moving vehicles (refer to Figure 1.3b). However, temperature feedback is not typically used to control such systems which are designed to operate continuously for maximum possible heat load from the engine. The complex thermal management systems illustrated in Figure 1.3c and Figure 1.3d, demand improved mechanical design, and a strategic location for components as well as sensors and actuators to monitor the system. An automotive thermal management system is one such system that has a varying heat load and uses

feedback control to achieve improved fuel efficiency. The final cooling system heat transfer strategy is found in marine engines which pump fresher sea water to a heat exchanger instead of using forced air convection to remove heat from the coolant. Sea water pumps and coolant circulation are controlled for effective and efficient heat transfer.

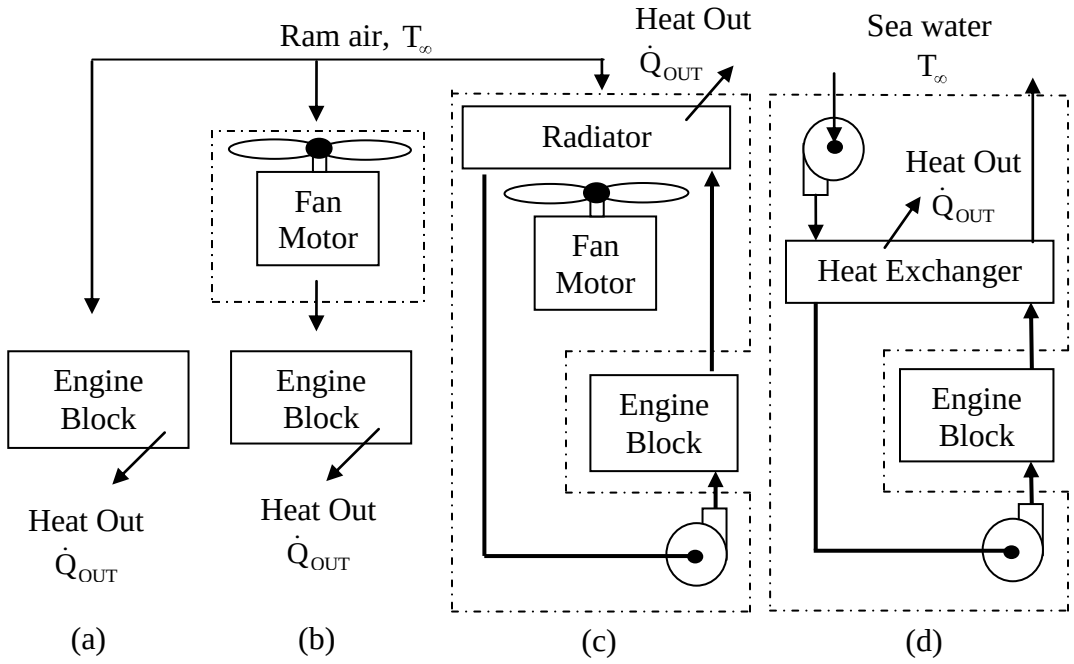

Figure 1.3: Strategies in achieving thermal management, (a) air cooled engine with fins, (b) forced convection cooled engine, (c) controlled forced convection cooled automotive engine, and (d) sea water cooled marine engine.

1.3 Outline of Thesis

In this research project, a multiple fan automotive cooling system and associated components will be investigated with the goal to minimize energy consumption in the auxiliary vehicular subsystem. The thermal management system was designed and packaged to facilitate experimental testing under representative

operating conditions followed by the analysis of results. Chapter 2 contains the literature review of the research on automotive thermal management systems which helped to establish an understanding of the cooling systems and the design basis for the experimental test bench. Chapter 3 describes the data acquisition setup used to collect and transmit data signals to the computer software, allowing data storage and feedback control. The control algorithm used to plot system performance from the data is also described. The experimental test runs conducted using the test bench with various fan configurations are presented in Chapter 4. It describes the data recorded during the runs and the resulting plots which indicate the performance of the multiple fan matrix radiator cooling system. It presents the analytical mathematical model for the multiple fan and radiator cooling system to determine its theoretical performance based on various parameters. Chapter 5 summarizes the results obtained, observations pertaining to system performance and their potential future applications in determining energy efficient multiple fan cooling system configurations. The appendices provide the step-by-step operating sequence for the test bench and the plots of the test results.

CHAPTER TWO

LITERATURE REVIEW

A number of research studies have been conducted exploring the modeling and analysis of advanced vehicle thermal management systems. These investigations have examined the effect of parameter selection on cooling system performance, derived mathematical models to describe system operation, and designed control algorithm and/or experiments for laboratory and in-vehicle tests.

2.1 Thermal Management Systems Methods and Analysis

One of the strategies for improving cooling system performance to maintain accurate engine temperatures and energy efficiency is the development of new components designs capable of accurate thermal control. Hyun and Heon, (1998) described an adjustable viscous flow radiator fan clutch to reduce energy consumption in a direct coupled radiator cooling system. This clutch controlled the power drawn from the engine crankshaft based on temperature feedback signals. This design adjusted fan speed by varying the fluid flow between drive disks within the viscous clutch. The prototype tests demonstrated increased fuel efficiency, a reduction in fan noise, and improvements in cooling system NVH properties. The researchers suggested improvement in cooling system operation by incorporating a controllable fluid control valve.

Research and development of advanced materials with enhanced thermodynamic properties have also helped improve automotive cooling system performance. Wambsganss, (1999) studied a hybrid forced convection/nucleate boiling system which used the high heat absorbing capacity of a coolant at its nucleate boiling stage. Their study recommends the use of water/ethylene-glycol solutions as coolants in the circuit, a suggestion that can increase thermal conductivity by 40%. In addition, they proposed the use of smart materials in radiator fins or air directing louvers that react to changing temperature to ensure maximum heat flow. The thermal expansion properties of metals are used for sensing, for example, in the bimetallic thermostat valves. However, studies have shown that the material properties alone cannot result in effective control; there is a need for electric actuators. Mitchell *et al.* (2009) studied the role of thermostatic valves in vehicle cooling systems, comparing the performance of various cooling system configurations. These authors designed thermal models of cooling systems having two-way, three-way, and no valve designs. Control laws were formulated based on these models and experiments conducted to investigate their validity. This investigation showed that a two-way wax thermostat controlled only 42% of maximum radiator flow for temperature control. The study concluded that the three-way and valve absent configuration were the most effective for efficient thermal management.

Further experiments focused on the control of individual cooling system components to achieve energy efficient radiator heat transfer. For example, Chanfreau

et al. (2003) demonstrated improved cooling system efficiency with controlled fan valves and pump actuators. The cooling system efficiency was analyzed during engine warm-up, cabin cooling/heating, and shutdown. They also suggested a requirement for high resolution, progressive and quick response coolant flow control valves. Their tests conducted using a Fantronic variable speed fan, a 200 watt water pump, and a three-way electric water valve indicated a high cooling loop response time of 8.0 seconds to reach 100 °C and 25.0 seconds for 90 °C. The authors concluded that further improvement in the response time was not possible until the radiator increased its cooling capacity. Similarly, Chalgren, (2004) conducted a series of experiments with an electric coolant pump and an electric two-way flow control valve for faster engine and passenger cabin warm-up. Their research attempted to control both the coolant flow rate and the engine coolant temperature. An EMP C20 mixed flow electric water pump, an EMP two-way flow control valve, and two BLDC motor driven electric fans were controlled by an EMP V4 controller. Their results showed a reduced warm-up time of 35% - 40% after the coolant temperature reached 40°C; the tests also demonstrated improvement in the warm-up rate of the passenger cabin.

However, the use of these advanced electric actuators requires an improved control algorithm for an energy efficient fan radiator cooling system. Alfano and Judkins, (1998) studied control methodologies for a brushless DC fan motor to improve performance and increase operating life. Their studies showed that better temperature control was obtained using a temperature-based proportional speed

controller than an on/off fan control strategy for the radiator fans. Specifically, a Pulse Width Modulation (PWM) power fan motor control method was more energy efficient. In similar research, Page *et al*. (2005) investigated a PID control system featuring multiple electric radiator fans with heat control valves (thermostats). They reported a 10% reduction in peak fuel consumption. This decreased fuel usage may be attributed to reduced parasitic losses achieved by decoupling the cooling system components from the engine shaft and adjusting the coolant pump speed (i.e., coolant flow rate). The coolant set point temperature was increased from 93°C to 105°C to reduce both fluid viscosity and viscous friction effects. This study suggests using PID controllers with fast data processing capabilities with electro-mechanical equipment exhibiting fast response times.

Setlur *et al.* (2005) studied nonlinear control strategies for servomotor driven radiator fans, water pumps, and thermostatic valves. The authors developed a mathematical model to describe system behavior based on physical system variables such as temperature and flow. An experimental cooling system was fabricated to test and validate the control model, the results indicating a 42% reduction in the warm-up time. Badekar *et al.* (2006) described a microprocessor-based controller for automotive radiator fans to reduce power consumption and to optimize component size. Their algorithm operated the fans based on the coolant temperature rate of change. Highway and city tests were conducted, the results being compared to a bimetallic thermostat to validate the cooling system performance. The findings showed a 70% improvement in temperature control, a reduced reaction time of 50%

and a reduced fan operation duty cycle of 66%. Jiangjiang *et al*. (2007) studied control strategies to regulate the hot water temperature in heating systems and the air temperature in cooling systems. A basic cooling system control with proportional and feed forward controllers was investigated and described.

Since improved control was possible using electric signals, experiments were conducted to design and validate actuator control algorithms. Chanfreau and Joseph, (2001) built a 42V vehicle model with electrically controlled cooling circuit components. With this model they achieved improved control over the coolant temperature, quick engine warm up, and reduced carbon emissions. The model simulated the Valeo engine cooling system; the control algorithm achieved better coolant temperature control than the temperature predicting model used in other systems. Rocklage *et al*. (2001) explored digital cooling components for onboard control systems. The real-time algorithm adjusted the amount of heat rejection to satisfy operational demands and, thus, minimize power consumption for a given cooling load. Their research demonstrated that the increased coolant operating temperatures improved overall energy efficiency.

The cooling system models based on thermodynamic principles and control theories have significantly improved the accuracy of cooling system analysis. Koch and Haubner, (2000) developed a detailed thermodynamic model to simulate the material thermal interactions and heat flux within an engine. Their model depicted thermal interactions between the engine block and the coolant passages. Using this

model, they analyzed the effects of these interactions on engine cooling thermodynamics. A control algorithm was developed using this cooling system thermal model. The researchers achieved faster engine warm-up and a 5% fuel efficiency improvement. Wagner *et al.* (2002) studied the integration of an electrical water pump and an intelligent thermostat valve to achieve faster engine warm-up, reduced temperature fluctuation, and efficient cooling. These researchers developed a lumped mathematical thermal model of an engine cylinder head assembly to represent real-time heat flow during operation as well as to describe the cooling system components. Three scenarios were simulated using these mathematical models; the results suggested the use of coolant temperature feedback to achieve reduced cooling system fluctuations.

Since numerical simulations have successfully reduced design development time and prototype testing costs, many researchers have created computer simulations to study cooling system performance. Choukroun and Chanfreau, (2001) formulated a thermal management system control algorithm with the input parameters being selected through simulated tests. The controller development time was reduced by avoiding wind tunnel tests. The strategy for achieving minimum fuel consumption and emissions, while at the same time offering maximum passenger comfort, was to allow the engine to heat quickly to the operating temperature range. The tests indicated that heat loss was minimized by reducing coolant circulation during the initial warm-up period. A second strategy suggested was to increase the coolant temperature level inside the engine block, which, in turn, increased the oil

temperature and ensured better lubrication. System errors (for example hydraulic errors in valves, pump flow errors after actuator initialization) were reduced using a PID controller to regulate the electric water pump, water valve, and fan components.

Mahmaud *et al.* (2003) developed simulation techniques to design and performed computer based study of conceptual thermal management systems instead of building and testing prototypes. This approach achieved a reduction in development costs. Using FEA and CFD codes to build one-dimensional and three-dimensional scalable models, they analyzed variables such as heat transfer in the power train, the exhaust system, under the hood, and in the passenger cabin. Various software platforms were used to obtain reliable values for the input variables. The numerical results demonstrated a cost-effective way to analyze conceptual thermal management using mathematical models. Taken together, these models helped to generate a complete picture of thermal system behavior, from the powertrain heat load to human comfort in the vehicle cabin. Rehman and Son, (2003) used Monte Carlo simulation techniques to study the probabilistic properties of uncertain responses in a cooling system. The statistical analysis tools were applied to data obtained from cooling systems with uncertain input parameters. This analysis helped construct a probability distribution curve which was then used to tune the components of the cooling system to achieve the desired mean value and best distribution.

Cho *et al.* (2007) investigated controllable electrical coolant pumps, comparing them to traditional mechanical pumps. The authors used GT-Cool

software to model the engine cooling system and simulate the pump option implemented on a class 3 pickup truck. Their analysis showed improvement in energy efficiency (a reduction in power consumption of 87%) and a possibility of downsizing the radiator by more than 27% using electric coolant pumps. Staunton *et al.* (2008) constructed a one-dimensional model to simulate an automotive cooling system undergoing a constant duty cycle. Their study suggested considerable energy savings (14.5 KW for a standard diesel engine) when using an array of small electrical fans rather than a single mechanically driven fan. According to the authors, a minimum voltage level was required for the electro-mechanical actuators to operate properly.

Several studies have analyzed the environmental impact due to the introduction of advanced cooling system components and their operating strategies. Choi *et al.* (2007) explored the advantages of electrical actuators (such as brushless DC motors and solenoid controlled valve spools) over the traditional wax-based thermostat used in diesel engine cooling systems. They conducted standard test cycles on a 2.7 high speed diesel injection (HSDI) engine using an experimental test bench to collect emission data. Their test results demonstrated a 15% reduction in greenhouse gases, hydrocarbons, and carbon monoxide, attributed to improved temperature control. However, these authors reported an increase in the NO_x emissions due to reduced coolant circulation. Fulton and Repple, (2008) studied a mechanical coolant pump application with integrated bypass valve functionality for cooling system circuits. Their prototype hardware used a non-positive displacement vane pump with adjustable guide vanes at the pump inlet to provide variable coolant

discharge rates. Their proposed design required temperature feedback to adjust the vane position. In-vehicle tests conducted using a prototype showed a 1.2% increase in fuel economy. Their analysis indicated an 8% reduction in hydrocarbons and 23% reduction carbon monoxide; however, increased engine operating temperature increased the NO_x content in the exhaust.

Choi *et al.* (2009) investigated an HSDI engine cooling system using a New European Drive Cycle. They conducted experiments using an electric pump and electronic valves, the results indicating an improvement in brake specific fuel consumption (BSFC) of 3%, a reduction in CO emissions of 20%, and a faster engine warm up of 30% when compared to traditional systems. However, they also reported a 10% increase in NO_x emission due to higher operating temperatures.

The literature review of various works mentioned in this Chapter helped in the understanding of the engine cooling systems, system design strategies, and analysis methods. The following Chapters will describe the experimental test setup, test data with observations, and subsequent conclusions.

CHAPTER THREE

EXPERIMENTAL SYSTEM DESIGN AND CONSTRUCTION

The experimental setup used a laboratory test bench to simulate an automotive engine cooling system with a matrix of multiple radiator fans. The physical layout of this experimental setup closely resembled the actual application in terms of the packaging. Similarly, the connections between the subcomponents and the components are of the same specifications as those on the vehicle mounted cooling system. In addition, care was taken in the test bench design and setup to minimize parameter value deviations from an actual vehicle cooling system. For example, the wind tunnel, which forms the outer boundary of the test bench, has an inlet air flow area similar to the flow area in a compact engine compartment on a vehicle. However, since sensor data acquisition was one of the primary objectives of the test bench, the position of several subcomponents had to be changed from the original configuration. To prevent any variations in their parameter values, these changes were accommodated by design modifications. For example, the connecting pipes in the cooling system are longer than those in the actual system providing more surface area for parasitic heat losses. The design modification addressing this issue is the addition of foam insulation on the pipes to prevent excessive heat loss through this larger heat transfer surface.

3.1 Overall Design

The experimental setup consisted of three important components required for a basic automotive cooling circuit; a heat source, a heat pump, and a heat sink (refer to Figure 3.1). The heat source was a low pressure steam supply line which provided energy equivalent to the average engine heat output to the cooling system. In this setup, the heat sink was the atmospheric volume surrounding the actual engine. The forced convection air flow over the radiator fins increased the heat transfer to the heat sink. Two heat exchangers, one at the heat source, and one at the heat sink, allowed heat to be exchanged between the source and the sink through a liquid coolant, in continuous circulation between the heat exchangers. The circulation of the coolant was achieved using an electric motor driven centrifugal water pump, and a bypass valve could alter the coolant flow direction during operation. The heat transfer from the radiator on the sink side was increased by the forced air convection created by electric motor driven external radiator fans.

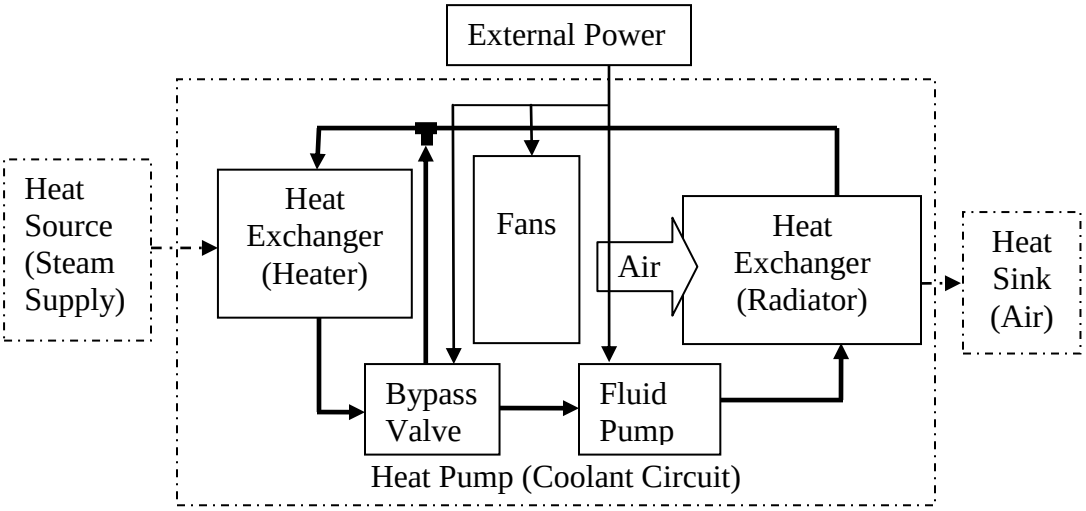

Figure 3.1: System block diagram showing main components of the test bench

In addition to the steam supply, an external energy input was also needed for the electric motor driven forced convection fan system, the bypass valve, and the centrifugal coolant pump. The energy output from the system results primarily through the heat loss from the radiator and the parasitic heat loses from the engine block and coolant carrying pipes.

3.2 Steam Supply

A low pressure (LP) steam source was used to simulate the heat addition of an IC engine in operation; a multi-pass heat exchanger was used to facilitate heat transfer from the low pressure steam to the circulating coolant in the system (refer to Figure 3.2). The steam was pumped through insulated piping that was monitored by safety equipment such as a pressure regulator, a pressure gauge, and a safety valve. A shut-off valve on the return steam line offered additional flow control while a drain valve removed condensate during maintenance and dismantling of the heat exchanger.

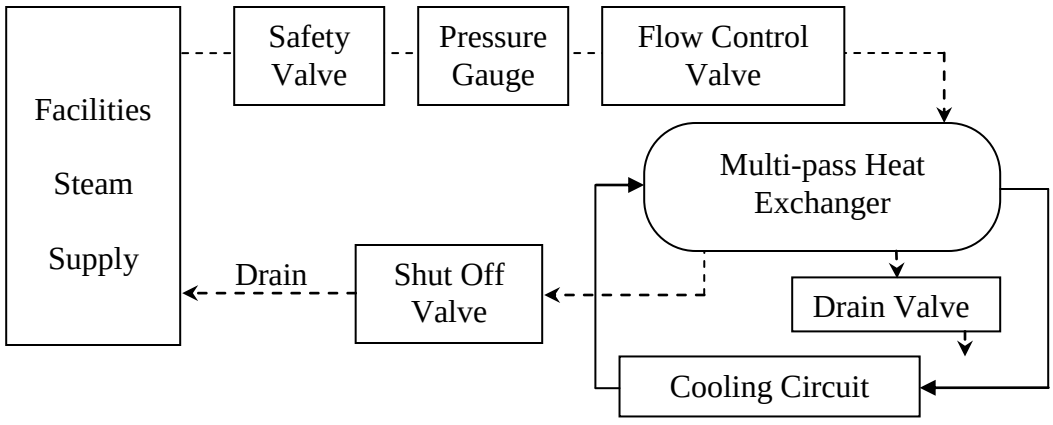

Figure 3.2: Schematic layout of the steam circuit used to add heat to the cooling circuit

When heat was needed in the system, a continuously metered quantity of steam was allowed into the circuit, regulated by a manual flow control valve; the heat input capacity could be further increased if needed by increasing the steam supply pressure. The intial opening of the steam flow control valve may have introduced high velocity steam into the heat exchanger causing water hammer to occur. This phenomenon results in steam condensation and water accumulation inside the heat exchanger during inoperation. This water hammer effect which must be minimized to prevent excessive pressure and internal erosion leading to catastropic failure, may be avoided by controlling the opening of the manual flow control valve as the steam is first introduced into the exchanger. In addition, a shut-off valve at the steam outlet of the heat exchanger must be opened before steam is introduced into the heat exchanger. This procedure drains the accumulated condensate and prevents excessive water hammer. Continuous water hammer in the heat exchanger compromises the reliability of the heat input supplied to the system. Heat exchangers are equipped with a drain plug that can be used to remove sediment deposition on the coolant side to help achieve unobstructed coolant circulation.

The heat obtained from the low pressure steam leads to an immediate increase in the coolant oulet temperature from the heat exchanger. However, the temperature of the radiator inlet does not change as fast as the coolant outlet of the heat exchanger because the thermal capacitance of the engine used in the circuit, acts like a heat accumulator (refer to Figure 3.3). Thus, to achieve a steady temperature reading

across the coolant circuit requires a certain amount of time which is dependent on the coolant flow rate and airflow over the radiator, and size of the engine.

3.3 Coolant Circuit

The coolant circuit acts as the heat carrier within the automotive thermal management system. It is comprised of the heat exchanger, the engine cooling jacket, the bypass valve, a coolant pump, and the radiator with fans. The coolant undergoes a heating and cooling cycle which may be explained using Figure 3.3. The coolant gains heat from the steam in a multi-pass heat exchanger; from the heat exchanger it is pumped into the cooling jacket of the engine block which also acts as a heat reserve to minimize heat fluctuations in the circuit. From the outlet of the engine cooling jacket, the coolant flows into a direction control valve which, according to the set point temperature, diverts the coolant back into the heat exchanger or into the radiator. For this study, the thermostat valve directs all fluid through the radiator. The coolant enters the radiator from the top inlet port and flows through a mesh of pipes with attached fins, losing its heat energy. The fluid exits through an outlet in the bottom portion of the radiator into the inlet of the centrifugal pump. The pump circulates it back to the steam heat exchanger, thus completing the cycle. Insulated galvanized pipes and pipe connections are used to circulate the coolant between the cooling system components in the system.

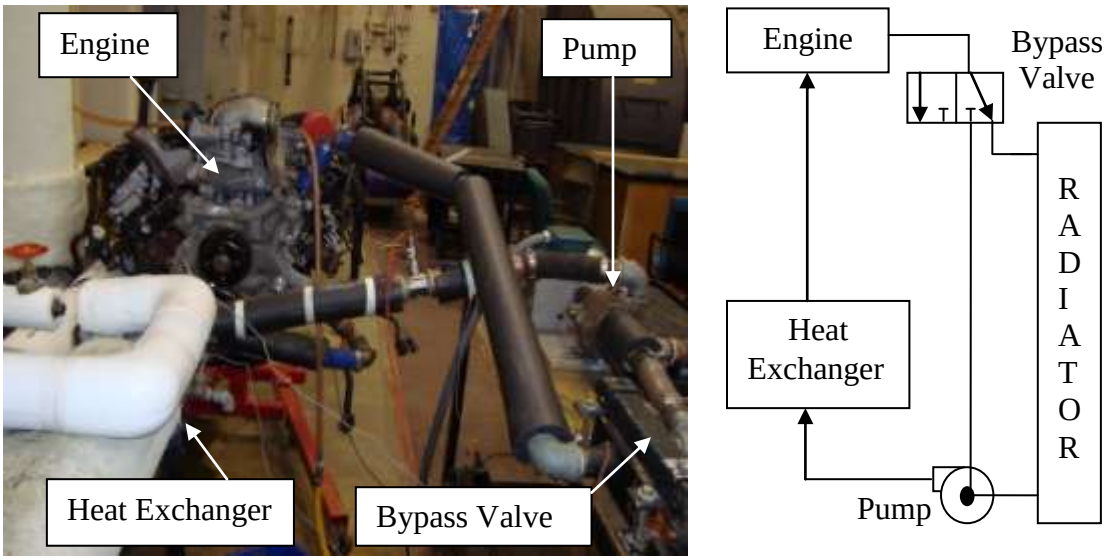

Figure 3.3: The pipe connections for the coolant flow and hydraulic schematic of bypass valve

The experimental coolant circuit subsystem components can also simulate the bypass valve function required in automotive cooling systems. A 3/2 (ports/positions) direction control valve (DCV) is actuated using a DC motor and used as the bypass switch in the coolant circuit as illustrated in Figure 3.3 and Figure 3.4. The path of coolant flow can be altered progressively using an electro-mechanical spool operated bypass valve with its spool operated using a spring coupled solenoid. This bypass valve performs the important function of directing the heat flow into one of two paths: the recirculation path in which heat continues to be added to the coolant circuit and the path that allows heat transfer from the heat source to the atmospheric sink. As stated previously, the valve was not actively controlled but rather diverted all fluid to the radiator during the experimental runs.

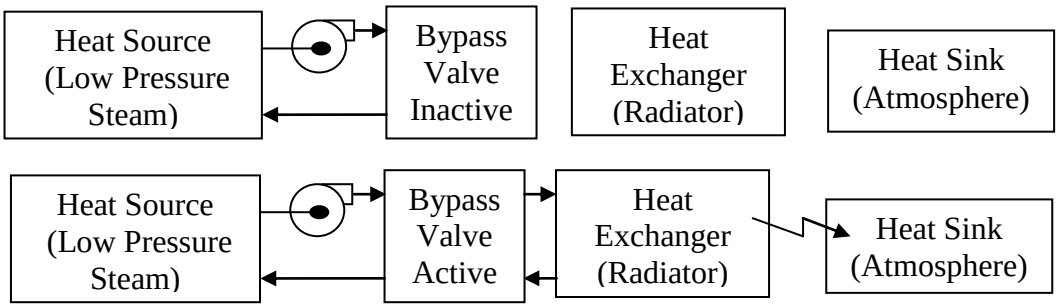

Figure 3.4: Schematic block diagram of bypass valve positions and coolant flow options.

3.4 Wind Tunnel

In the experimental test bench, the heat rejection from the radiator to the atmospheric sink occurred in a wind tunnel illustrated in Figure 3.5. This tunnel was rectangular, 1.5m × 1.4 m and 2.2 m long, built to accommodate radiators up to dimensions of 44″ × 40″ (1.11m × 1.01m) while resembling the general layout of the fan radiator cooling system found in an automobile. The shape of wind tunnel air-flow passage was determined by considering the geometry of the radiator face.

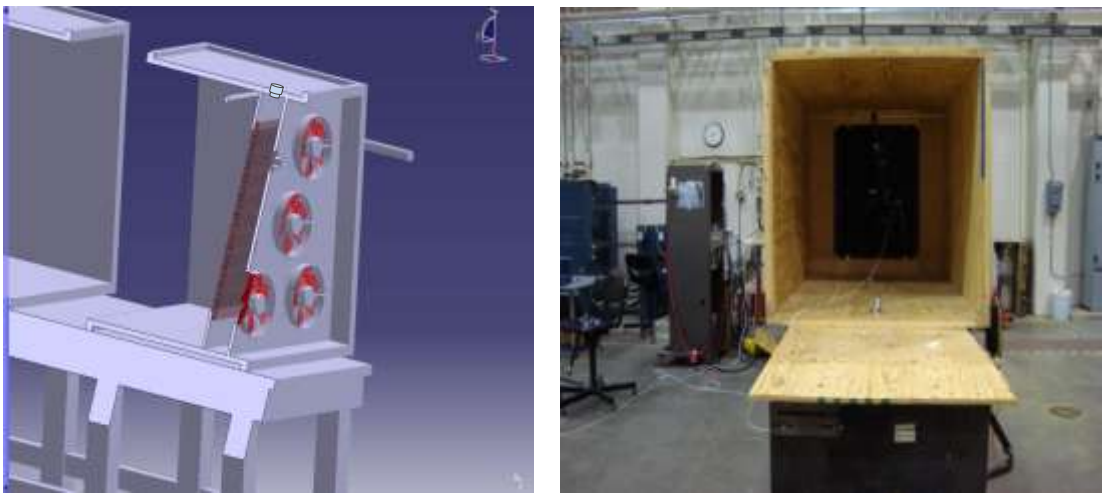

Figure 3.5: CATIA model showing section of the wind tunnel and test bench wind tunnel

The length of the wind tunnel was divided into two openings; the entry side and the exit side. The entry side supported a matrix of six fans while the air discharge generated by these fans was channeled via the wind tunnel exit (refer to Figure 3.6). The fans were mounted in close proximity to the entry of the wind tunnel; thus, the entry of air into the fan matrix was not affected by the boundary wall of the wind tunnel. The wind tunnel included small bore holes to measure the back air pressure between the fan matrix and the radiator. The wind tunnel also had openings to support the radiator coolant input and output pipe connections. The wind tunnel was constructed of plywood to mount sensors and their accessories.

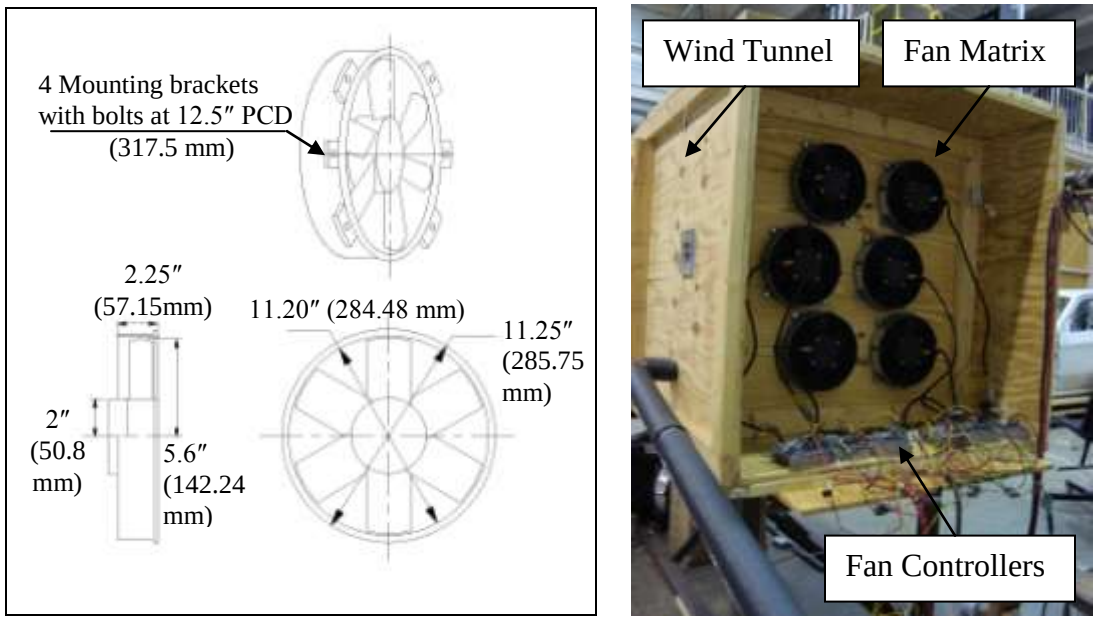

Figure 3.6: EMP fan dimensions and installation on the wind tunnel

The wind tunnel has a rectangular matrix arrangement with six fans arranged in 3 rows and 2 columns, each connected to a power supply for speed control. All the fans have the same specifications and dimensions, a 14″ (355.6 mm) diameter frontal

area casing. The fans were mounted on the wind tunnel using four bolts attached to the plywood; for safety, the fan blades were covered by a plastic shroud on the exposed side. This fan arrangement ensured that the forced convection through the radiator was due to the fan matrix alone, preventing any other air flow that might contribute to the heat transfer mass (i.e., no ran air effect occurred).

The fan motors were 30V brushless DC motors; a Techron power source (Model# 5530) with variable DC voltage and current supplied the power required for the fans and the control system. The power to the fan motor comes from an EMP BLDC power controller (refer to Figure 3.7), which by varying the power input achieves a given motor speed. The change in power input was based on the control signal the power controller receives; a Sauer Danfoss Plus+1 microprocessor fed a control signal to the input of the power controller. This control signal generated by the microprocessor is based on controller area network (CAN) signals originating from the computer interface.

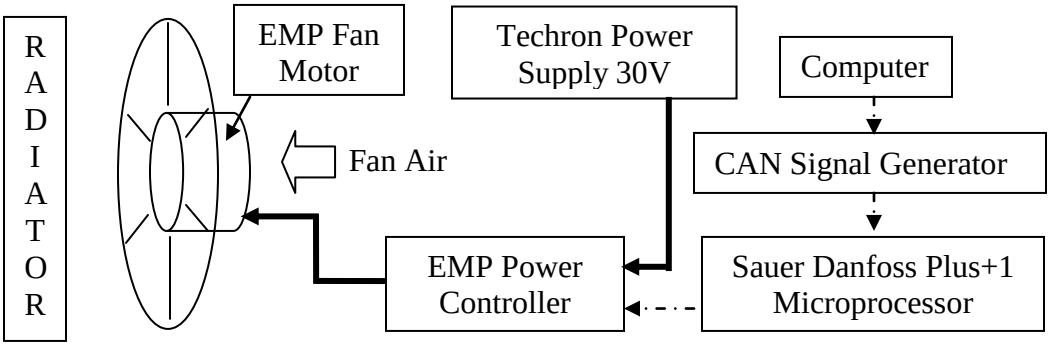

Figure 3.7: Schematic of the fan control and power signals

The number of fans operating at a given time could be changed by connecting or disconnecting their individual power sources.

3.5 Data Acquisition Circuit

The experimental test setup contained electrical, electronic, and computer subsystems to acquire, process, record, and display data generated during a given test run. Based on their functionality, the components may be classified as either sensor, data acquisition hardware/software, computer interface, or actuator. The analog signals generated by temperature, flow, and speed sensors (refer to Figure 3.8) were converted into proportional voltage values using dedicated signal conditioners; the continuous analog data were then fed into the dSPACE data acquisition board (Model# DS 1103 PPC). This board converted the collected analog data into digital form at a frequency of 100 Hz that can be read by the computer interface and can further be used as input for the control algorithm. The computer interface generated an output control signal for the actuators and recorded parameter data for later analysis.

3.6 Sensors Systems

The sensors used in the setup generated a signal proportional to the measured parameter value it is designed to detect. The sensors used in this experiment included a velocity sensor, a turbine type flow meter, a linear variable differential transducer, five thermocouples, and an ammeter. These sensors generated DC voltage, pulse or

electrical resistance signals; the signals were converted to proportional voltage and fed as a continuous analog signal to the signal conditioners. The sensors, their properties, specifications, and function in the experimental test bench are further explained below.

The air velocity at the radiator outlet inside the wind tunnel was measured using a flexible stand mounted velocity sensor. The sensor used here was FMA-900 Series Air Velocity Transducer, with an accuracy of ±1.5% for Full Scale (0-100 feet/second or 0-30.5 m/sec) at room temperature. The sensing element was a temperature compensated polymer capacitor for detection of humidity, coupled with a solid state velocity sensor. The signal generated by it was converted to a proportional voltage value in the range of 0-5 V DC in its individual converters. During test runs, the velocity sensor was located at distance of 3.0 inches (76.2 mm) from the radiator front face. Flexible mounting helped to locate and lock the sensor in place at various points along the radiator front face.

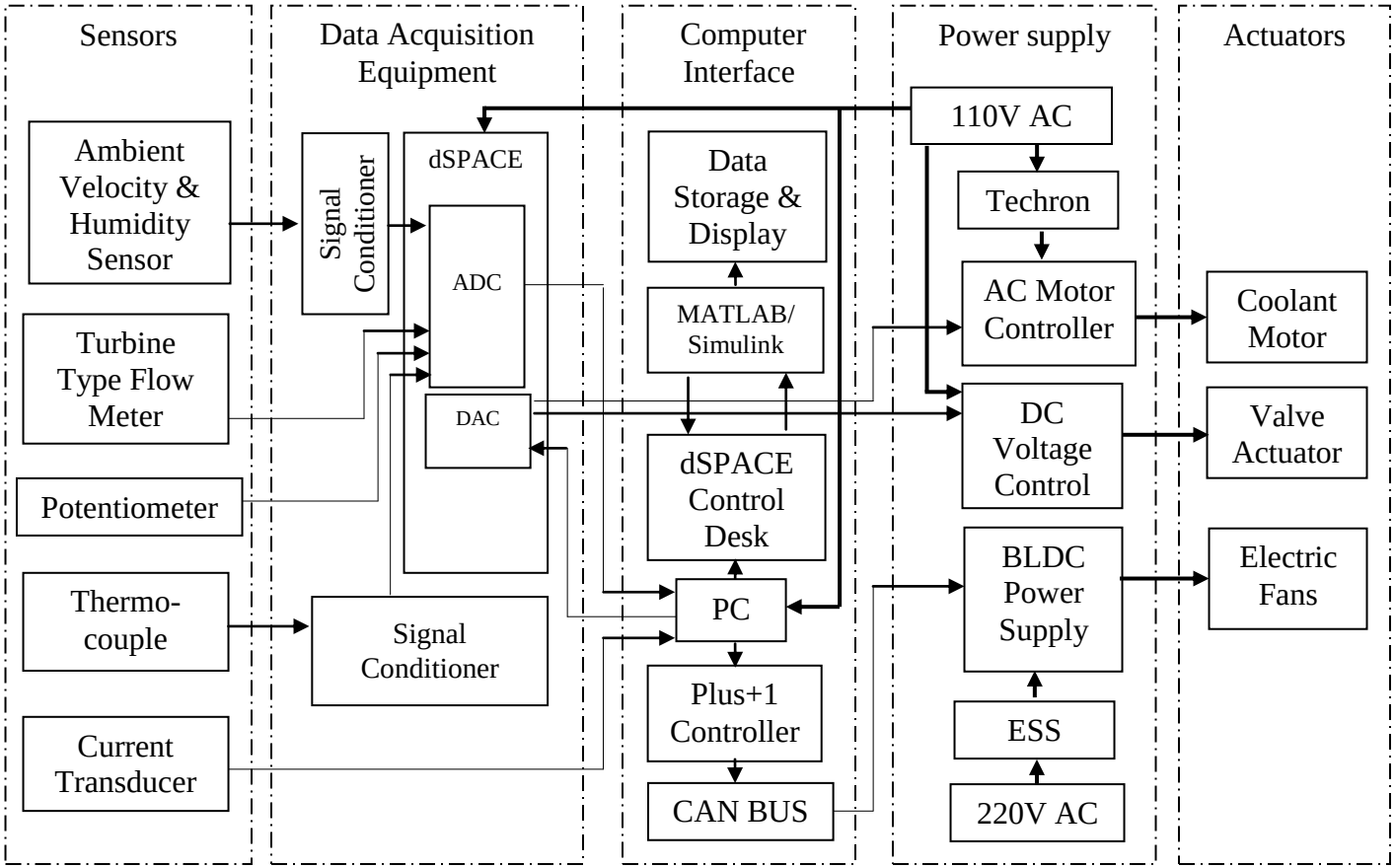

Figure 3.8: Block diagram for data flow among the sensors, data acquisition equipment, computer interface, and actuators.

A turbine type flow meter, TR – 1100 Series manufactured by the AW Company, was used in the setup used in this research to determine the rate of coolant circulation during the experimental runs (refer to Figure 3.9). This flow meter, which was near the pump outlet in the coolant circuit, can handle up to 5000 GPM (22,730 liter/minute), the smallest flow it measured was 0.6 GPM (2.72 liter/minute). Its accuracy is in the range of $\pm$1% of actual flow. It had a maximum pressure rating of 5000 psi (34,473 KPa) and better accuracy for low viscosity fluid such as water. It operates safely in the temperature range of -150 °F (-101°C) to 450 °F (232 °C), and in the current setup it was subjected to a range of 68°F (20 °C) to 200°F (93.33 °C). The turbine type flow meter had a metal turbine wheel mounted on a precision bearing and a magnetic pick up over it that detected the passage of the turbine blades underneath as seen in Figure 3.9b. For a signal output of sufficient strength and accuracy, the magnetic pick up of the flow sensor has an MG-300 and the JV 400 signal amplifier to proportionally increase the signal output.

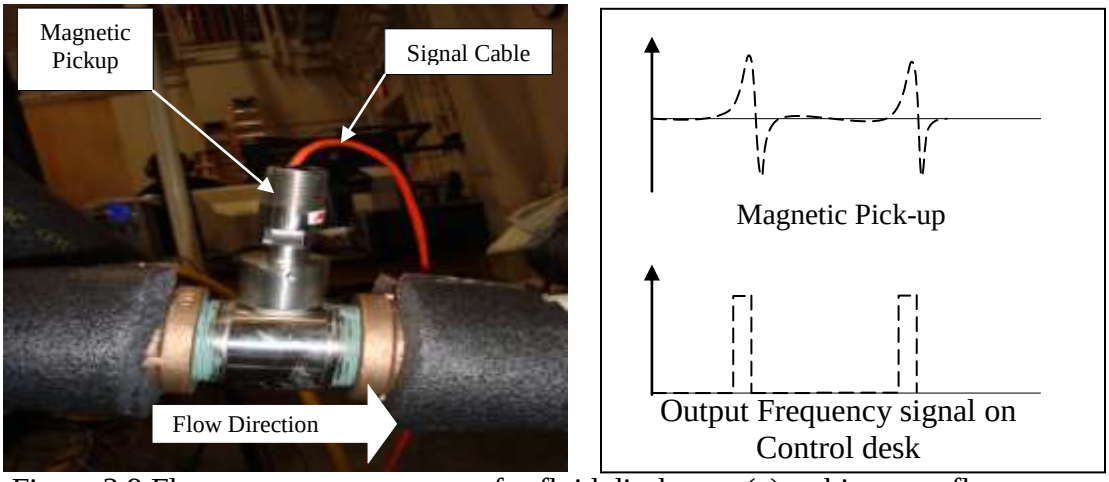

Figure 3.9 Flow measurement sensor for fluid discharge, (a) turbine type flow meter, and (b) the magnetic pick-up signal

The J-type and the K-type Omega thermocouples monitored the coolant temperature throughout the system. The J-type thermocouple can measure temperatures in the range of -210°C to 1200°C, while a K-type thermocouple senses temperature in a range of -271°C to 1372°C. Both sensors have a hot junction enclosed in the probe that can be placed into the coolant`s flow to measure the temperature. This probe is covered by a 304 stainless steel sheath for enhanced durability. It was integrated into the system by its 0.25" external pipe threads and a pipe sealant to create a water tight joint with the coolant pipe. The probe included insulation and mesh protect the 72" (1.82 m) wire leads that were directly connected to the data acquisition hardware. The shielded wiring protects the sensor signal from external disturbances such as electromagnetic fields and high temperatures.

A current transducer was used in the electrical circuit to monitor the current supplied to the fan motor matrix and help determine the total fan power consumption. Specifically, a Ultrastab 867 current transducer was used here, its design is based on the zero flux principle for measuring galvanically isolated currents. It can take a maximum non-destructive load of 500 Amps within a current range of 0 to 700A. This sensor requires a 15 Volts DC supply to generate the linear proportional voltage measurement signal that is transmitted to the ADC port of the dSPACE hardware in form of a continuous analog signal.

A Viatran pressure sensor (Model# 245FYGDWTU) with a pressure sensing range of 0-15,000 PSI. This pressure sensor has one port that can be connected via tubes to the chamber in which the pressure needs to be measured. Pressure reading is

available at the sensor output as an analog voltage signal of maximum range 0-5 VDC. Tubes were connected on three sides of the wind tunnel to measure the overall pressure developed between the radiator and the fan matrix. These three tubes were merged into a single outlet using cross pipe joint and this outlet was connected to the input port of the sensor.

High operating temperatures and steam pressure require the sensors to be accurate for operation safety. The fluid temperature, fluid velocity, and electrical power values were verified using hand-held sensors and instrument displays. To verify the velocity profile created by the fan matrix at the radiator frontal area, a hand-held air flow meter (Model# Kestrel 1000, 0 - 25 meter/second range) was used. The rotary speed of the fan motor was verified with that in the Plus+1 control software using a strobe light. The temperature at different points in the cooling circuit was validated using mercury thermometers of different temperature ranges. Thermometers were also used in the initial test runs conducted on the setup to ensure the desired heat flow and to determine the temperature levels resulting in the system through the low pressure (lp) steam heat input. The pump discharge specifications estimated the discharge through the pump outlet at a given pump speed. The power consumption of the fans could also be derived from the voltage and current displays of the ESS power supply units.

3.7 Data Acquisition Equipment

Data collected from the sensors needs to be converted from an analog to a digital format before they can be transmitted and processed by the computer hardware. Data acquisition equipment (DAQ) uses solid state microprocessors and electronic circuits to process signals from sensors into a usable data format. The data acquisition equipment used in this setup included signal conditioners (OM-5) and dSPACE hardware (DS 1103 PPC Controller). Data received from continuous analog sensors were required to be broken into finite data sets per second, called the data acquisition frequency; all DAQ equipment is capable of communicating at a certain frequency range to facilitate interconnectivity. The Table 3.1 illustrates the data acquisition system used, the input/output signal type and the corresponding parameters collected.

DAC system	Input signal	Output signal	Parameter
dSPACE	Frequency	Digital	Flow (GPM)
Plus+1	Digital	Digital	Fan Speed (FPM)
dSPACE	Analog	Digital	Air Velocity (m/sec)
OM5 Signal Conditioner	Analog	Analog	Temperature (ºC)
dSPACE	Analog	Digital	Temperature (ºC)

Table 3.1: DAC equipment, I/O signal type and parameters list

The signal conditioners were used to amplify the thermocouple signals to achieve a higher proportional voltage within the range of 0-5 VDC. The signal conditioners used had a 4Hz bandwidth with ±0.38°C accuracy for the K type [model:

OM5-LTC-K2-C] thermocouple and ±0.36°C for the J type [model: OM5-LTC-J3-C]. Both can generate proportional signals to measure temperatures from 0°C to 500°C. Though the thermocouple can detect temperatures in the range of -100°C to 600°C, the required range was 0°C to 150°C for the experiments conducted here. The maximum coolant temperature was not expected to reach boiling point (212°F or 100°C). Since the coolant circuit was closed, potentially building significant pressure inside the circuit, the boiling point may rise, and, thus the maximum temperature was set above 100°C.

The signal conditioners had a pinout (refer to Figure 3.10) that connected to the sensor on one side and the dSPACE DAC board on the other. The thermal signal conditioners used the Omega OM5-BP-16-C backplane to connect with the DAQ setup. The backplane was a robust printed circuit board designed to accommodate 8 to 16 signal conditioners and their corresponding sensors. The power supply required for the mounted signal conditioners was provided by the backplane through its common power port (refer to Figure 3.11). The backplane circuit included an 18 pin output port, which provided a single location to obtain output signals from all the mounted signal conditioners. The backplane pinout was divided in separate wire conductors, and the voltage signal was transmitted to the dSPACE ADC ports.

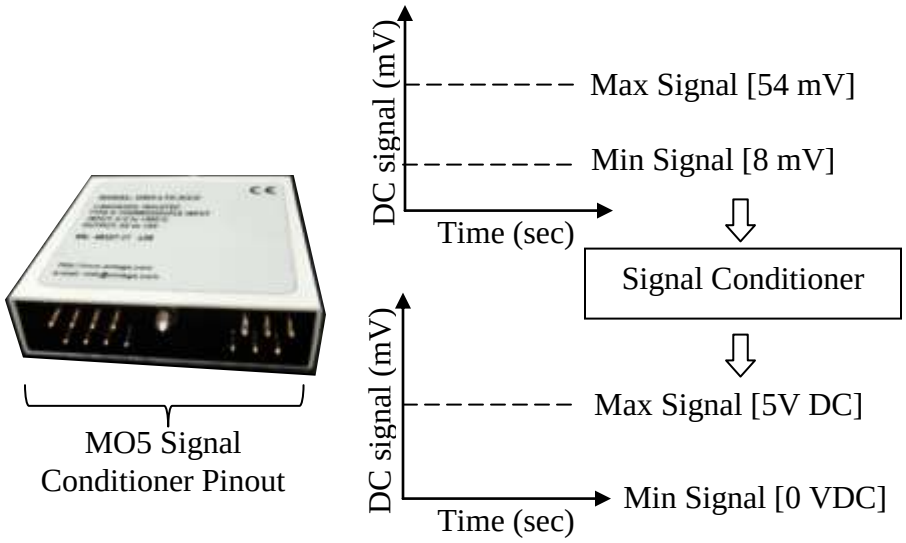

Figure 3.10 Signal conditioner OM5-LTC-J3-C pinout for J type thermocouple

The signal conditioner type should match the corresponding thermocouple type (J or K) for the output voltage signal to be within the specified (0-5 VDC) range.

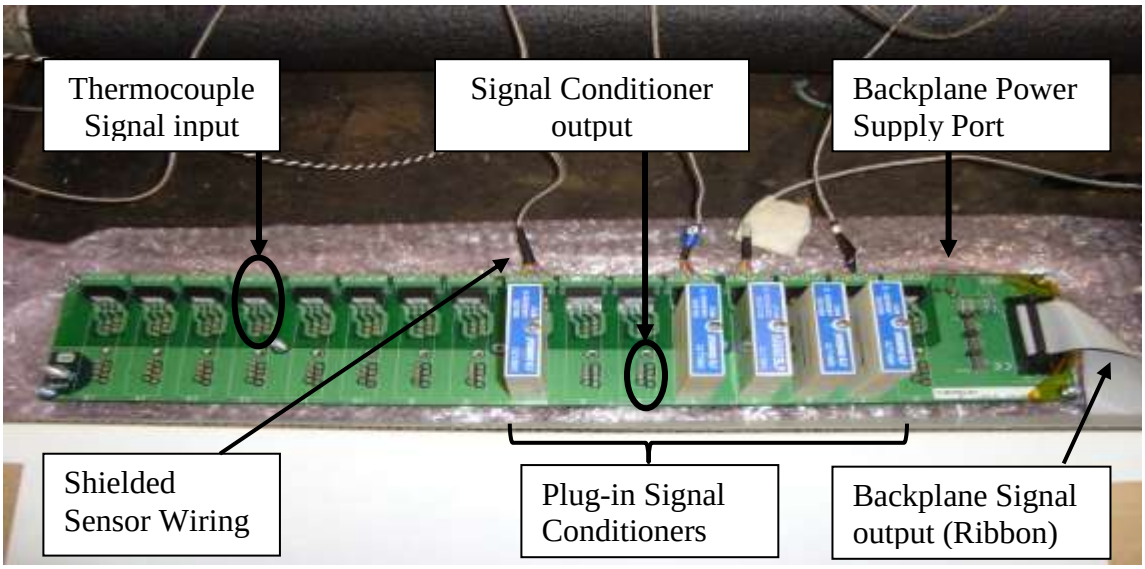

Figure 3.11: Omega backplane with plug-in signal conditioners and computer interface ribbon (bus).

The dSPACE hardware interface (DS1103 PPC Controller) had 8 DAC (digital-to-analog converter) outputs and 36 ADC (analog-to-digital converter) inputs, each connected via a ribbon cable to the PC. It operates using a power supply of 12 VDC at 0.75 Amps or 5 VDC at 4 Amps. In the experimental setup used here, the dSPACE hardware collected and processed signals from the five temperature sensors, one pressure sensor, one flow meter, in addition to the wind speed, and humidity, and from the potentiometer. The sensor outputs were connected through the dSPACE board ADC port which offers 16 bit resolution and an input voltage range of ±10VDC. The output control signals generated by the computer were communicated to the actuators through the dSPACE DAC output ports. The DAC port also has 16 bit resolution and maximum output voltage range of ±10V. The processed digital sensor data is communicated to the computer (PC) in real-time and becomes available to be stored on the hard drives.

The air speed sensor in the wind tunnel used a resistance temperature detector (RTD) to generate a sensor signal proportional to the wind speed. A signal conditioner was required to covert the resistance change into a proportional voltage signal for the DAQ. This signal conditioner requires a power input of 15 to 18 VDC at 300 mA. The output is an analog DC voltage signal linearly proportional to the air velocity; the signal obtained is in the range of 0-5 VDC, corresponding to the air velocity of 0 to 100 feet per second (30.5 meter per second). The signal conditioner and connected wiring are shielded to prevent errors due to external electromagnetic interferences.

A turbine type (TRG-1100) fluid flow sensor was used in the system, to provide an output frequency different from the proportional voltage of other sensors. The sensor output was in the form of square wave pulses, the frequency of waveform which was used to determine the flow rate. The signal generated was directly connected to the ADC of the dSPACE board using a shielded cable. The DS1103 PPC Control board can acquire an input signal frequency count in the range of 6.6 MHz. This frequency count along with a specified K-factor of $\left(\frac{1}{208}\right)$ can thus be used to compute the real-time flow rate.

3.8 Computer Interface

The computer interface included the software programs MATLAB/Simulink, the Plus+1 service pack, dSPACE, and the Control Desk. These software utilities were used to acquire sensor data, perform math control operations, develop control signals, and store data. The signal inputs were recieved through the dSPACE hardware board, while the output control signals were transmitted via the Plus+1 microprocessor and dSPACE DAC.

The MATLAB/Simulink environment was used for unit conversions, calculations, and data storage. The software functionalities were utilized for temperature sensing, potentiometer feedback, the coolant pump motor speed, and the bypass valve actuator position. The voltage readings received from the sensors were converted to the SI unit system to maintain a measurement standard and for ease of

calculation. According to the thermocouple type (J-type or K-type), the equations were formulated for the interpretation of the measured voltage signal into a corresponding temperature reading. The J type thermocouple has a temperature range of -210°C to 1200°C while K type has a temperature range of -270°C to 1372°C. The signals were amplified and processed by (Omega OM5-LTC-J2-C and OM5-LTC-K2-C) signal conditioners in the range of 0-5 VDC, while the limit for the temperature measurement dictated by the capacity of the signal conditioners was 0°C - 500°C and -100°C to 300°C respectively. A transfer function $\left(\frac{1}{Ts+1}\right)$ was used to filter the input signals and for removal of excessive fluctuations, where T=1. The output from this transfer function is represented as

$$\frac{Y_J}{X_J} = \frac{1}{Ts+1} \tag{3.1}$$

where X_J is the signal from the K-type signal conditioner and Y_J the corresponding output from the transfer function. This Y_J value can be further converted to indicate temperature level by the equation,

$$T_J = K_{C,J} Y_J - 100\,; \quad K_{C,J} = 400/5\, G_{DS,T} \tag{3.2}$$

where $G_{DS,T}$ is the gain of value 10, added in the signal as per specifications by dSPACE. Further, the signal requires a conversion factor $K_{C,J}$, a gain of 400/5, that is needed to bring the voltage reading equal to the temperature reading, T_J in °C. The temperature range for the J type thermocouple is from -100°C to 300°C. Thus, the

total range is 400°C, and to fit the complete range in a 0-5 volts range, a gain of 400/5 is required. For 0 volt the corresponding temperature read is -100°C thus, to account for the Y axis intercept addition of constant offset value of -100 was required in the equation (3.2).

As Figure 3.12 shows a MATLAB/Simulink algorithm was used to process the signal from 4 dSPACE ADC ports. The first port acted as a feedback port for the valve, conveying the actual position of the valve and adding input to the PID to achieve corrective action in next control signal. The valve position was governed by the control desk slide bar function, added to the signal for the DAC that connected the valve operating motor. A reported earlier, the valve was maintained such that all flow travelled through the radiator. The second port was connected to determine temperature from a thermocouple, it had appropriate gains as described by equations (3.2). Note that the remaining four temperature signals were processed using same MATLAB/Simulink algorithm as discussed in Figure 3.12. The third port was connected to the pressure sensor and its gain increased the signal to the value equal to the gauge level PSI. The last port, the air velocity sensor, included a transfer function to smooth out the signal, further the appropriate gain is multiplied to the signal to obtain reading in FPM or in MPS. A saturation block was used in most of the feedback signals to prevent accidental high signals for the actuators running using this feedback signal.

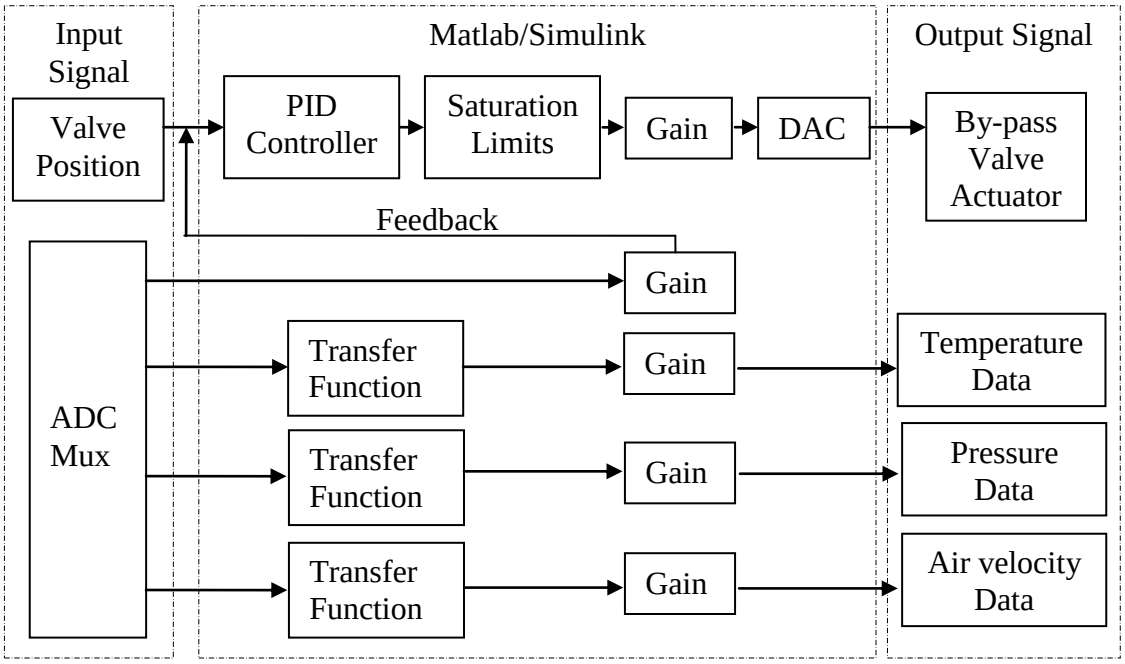

Figure 3.12: MATLAB/Simulink algorithm for measurement of parameters including air speed, valve position, and pressure readings; also shown are the low pass filters and the required gains

The motor control, provided from the Control Desk slide bar which can feed incremental numeric values to the Simulink constant block, it is further multiplied by the gain, and there final value is converted to the voltage signal of the final value and fed to, DAC. This signal for the motor control can be stated as

$$M_{DC} = X_M \times G_{DS} \tag{3.3}$$

where M_{DC} is the DC voltage control signal, X_M the user input variable in range of 1 to 10, and the G_{DS} is the dSPACE gain of 0.1. The motor speed can be expressed as

$$N_{DC} = X_M \times G_{DS} \times K_M \tag{3.4}$$

where N_{DC} is the motor speed (RPM), X_M the user input variable (range 1-10), K_M the conversion factor for voltage value to RPM the conversion factor was gain of 368, and G_{DS} the dSPACE gain of 0.1.

Parameter	Nomenclature	Value
K type thermocouple conversion factor	$K_{C,K}$	100
J type thermocouple conversion factor	$K_{C,J}$	80
dSPACE gain for thermocouples	$G_{DS,T}$	10
User input variable for motor speed	X_M	1-10 range
dSPACE gain for motor speed	G_{DS}	0.1
Voltage value to RPM conversion factor	K_M	368

Table 3.2: Gains and conversion factor list in MATLAB/Simulink model

The DAC port connected to the motor controller provides signals to change the coolant pump motor speed depending on the Simulink output. A saturation block blocks signals above the specified low and high signal points. A volt-to-RPM block indicates the ideal RPM the coolant pump motor should possess at that particular feedback signal; however, it may vary by some amount depending on the motor condition and response speed of the mechanical system. The value input through the Simulink Constant block generates a proportional signal ranging from 0 to 10, with 10 indicating the maximum speed of the motor.

The output recorded via the Control Desk has dynamic signal characteristic, classified as a non-deterministic variable. Data output from dSPACE is discrete time; the time step which can be adjusted in the Control Desk. Generally, a small time step ($\Delta t < 0.01$ seconds) offers more details about the system behavior by increasing the

data resolution. The MATLAB algorithm prepared signals for export from the dSPACE digital to the analog converter (DAC) in the board. The dSPACE and Control Desk utilities require C code to communicate data from each other.

3.9 Power Supply Control for Actuators

The experimental power supplies channels metered amounts of power to the actuators: fan motor (EMP BLDC Controller), the coolant pump motor (Genesis AC motor controller, Model# KBE2-2202-P), and the bypass valve. The power flow can be continuously varied based on control signals from the computer. The power flow systems in the experimental setup reported here and the corresponding actuators controlled are described below. All the power systems received their power supply from either the 115 VAC or the 240 VAC main supply.

The power supply system for the fan motor matrix is shown in Figure 3.13. A high capacity constant DC power source was required by the EMP power controller, a Lambda ESS power supply with a power input of 240 VAC was used. The maximum current obtainable was 0 – 400 Amps and the voltage range 0 - 50 VDC. The output from the ESS was split to supply 30VDC to all six fan motors in the circuit. The controlled power supply used in the experimental setup was the EMP BLDC Controller (Model C20), capable of accepting the CAN commands that define speed and direction of the motor. It can be used in 12-24VDC circuits having a rated current of 20 Amps continuous and rated voltage in the range of 9-32 VDC. The control commands originating in the Plus+1 Controller software were transmitted from the

PC to a Plus+1 microprocessor, which then transmited the CAN format signal to the EMP BLDC controller.The brushless DC motor (BLDC) runs with a desired speed using the controlled power from EMP BLDC motor controller. A 24 VDC motor is used for operating the fans.

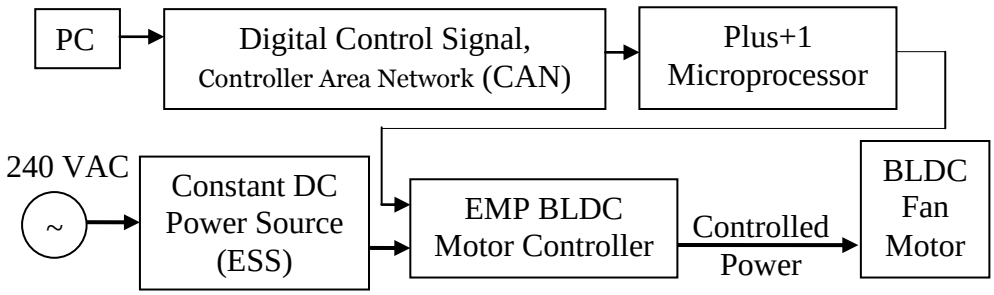

Figure 3.13:Block diagram of the digital signal and power flows for a single fan motor.

The motor speed for the coolant pump and the bypass valve actuator was controlled using the Genesis 3-phase AC drive digital power controller (refer to Figure 3.14). Model KBE2-2202-P, needs a power supply of 230VAC at its input; at the output it can control up to a 2HP motor with a voltage and current output of 220 VAC and 7.5 Amperes. It could withstand a maximum load of 100 Ampere for two minutes; the switching frequency was 8 kHz and the acceleration / deceleration time 0.1-180 /0.3-180 seconds. This power supply controlled the Reliance 2HP motor speed in a range of 0-3450 RPM for varying the coolant pump speed. Similarly, the control power supply was also provided to the bypass valve operating DC motor.

A constant DC power supply source was required for such sensor signal conditioners as the thermocouple OM5 conditioners and the air velocity sensor signal

conditioners. Solid-state AC to DC converters were used for this purpose where the current requirement was low.

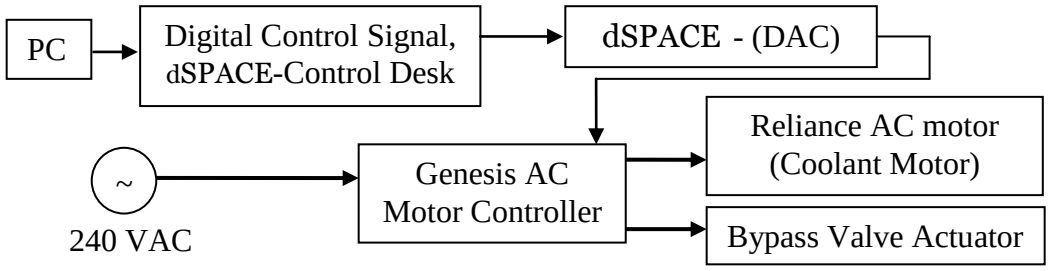

Figure 3.14:Block diagram of the dSPACE signal and power flows for the coolant pump motor and by-pass valve actuator.

The power supply units were housed in a cabinet for safety and ease of mounting and connections (refer to Figure 3.15)

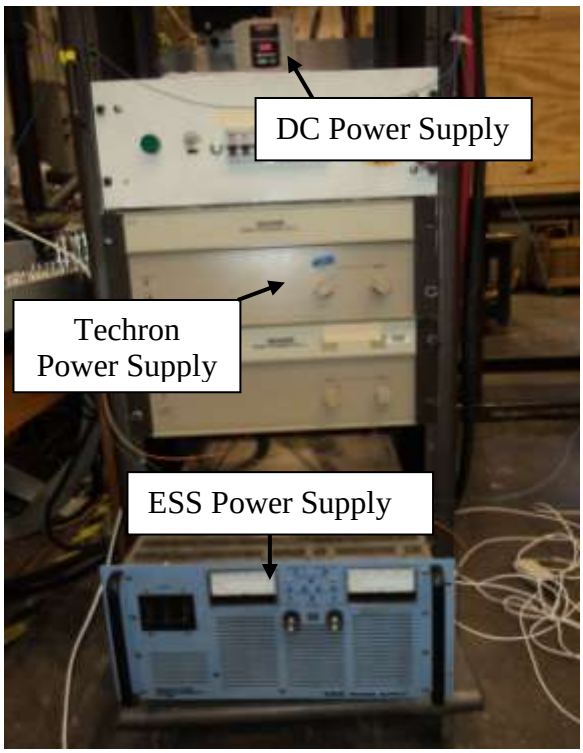

Figure 3.15:Cabinet for power supply units - the Techron, ESS, AC motor controller and the 5 VDC converter.

3.10 Test Methods and Procedure

The experimental setup was used for heat rejection and air velocity experiments. This system was run using different configurations of the installed sensors and actuators. They involved sequential steps needed to run and acquire data correctly. Safety during test runs was ensured by following the sequence described in Section below, these procedures providing guidelines for operating the test bench.

3.10.1 Heat Rejection Experiments

The heat rejection experiments involved the coordinated operation of all the test bench components such as power supply, the actuators, sensors, and data acquisition hardware/software. The experimental test runs were conducted using ten fan configurations working at specified speeds in the range of 1,000 to 5,000 RPM in increments of 1,000 RPM. The experiment for each fan configuration was conducted in three steps: (1) the system preparation and start-up, (2) the heat input and data acquisition, and (3) the system cooling and shut down.

System Preparation and Startup

The system preparation and start-up procedure involved checking and replenishing, if needed, the coolant level in the coolant circuit. This circuit required 30.4 liters of plain coolant water as it encountered temperatures up to 90°C. The coolant was lost during the runs because of evaporation and the vapor pressure build up; some coolant fluid was lost over the pressure relief valve in the coolant circuit.

The system was observed to produce contamination due to wear and rusting into the flow path. Thus, the system needed to be flushed completely after every 5 runs to prevent clogging of the narrow radiator passages. Once the coolant level was checked and maintained the coolant circuit was sealed using a threaded plug. Plain water was used as coolant as the peak coolant temperatures did not exceed 90°C and the fact that the system required frequent flushing.

The next step was to start sequentially the power supplies for all the sub-components (sensors, DAQ systems, and actuators) on the test bench. First, the power supply for the sensors, computer systems, and control signal generators was required to be connected, followed by power to the actuators. This order was required because the actuators in the system could recieve unintended signals through the data acquisition dSPACE board as well as the Plus+1 controller. After the sensors were supplied with their corresponding power supply, the computers (PC, dSPACE, and Plus+1 controller), and then the corresponding control softwares (MATLAB/Simulink, dSPACE-Control Desk, and Plus+1 service pack) had to be opened and run. The MATLAB/Simulink code and the Control Desk were interlinked, requiring the Control Desk program to start first and the MATLAB/Simulink code to compile later. The Plus+1 service pack needed to be operational based on the corresponding control code for the fan motor matrix. Before power could be supplied to the fan matrix, the Plus+1 software had to be continuously communicating the speed and directional signals to the Plus+1 microprocessor. Failure to do so could lead to excessive motor speeds.

The Control Desk, MATLAB/Simulink algorithm, and the dSPACE hardware were required to be operating before the coolant motor controller was started. The Control Desk provided control values for the motor controller; thus, it was necessary for the proper variable values to be communicated before starting the motor power supply. Starting the sensors, the PC, and the software applications also gave an indication of the temperature levels in the system before heat was added, this was a precautionary measure to prevent excessive heat addition and the ensure proper sensor operation. Once the control systems were connected to supply and operational, the actuator power supply systems were be connected to their respective power supply. The 240 VAC supply for the fan motor matrix was started using the connector bus bars in the Lambda ESS power supply. The coolant motor power supply was connected using the Run Command on the digital display of the Genesis 3-phase controller.

The Heat Input and Data Acquisition

The second phase of the experiments involved adding heat to the coolant using low pressure steam, operating the fan matrix using different combinations, and collecting sensor data. Once the power supply using provided to the experimental test system, the fan motor matrix operated at a uniform minimum base speed of 1,000 RPM. Then the coolant pump motor was set to a fixed discharge of 93.8 liter/min. The coolant circulation and forced convection from the fans prevented the system from overheating and evaporation subsequently resulting to build-up of steam

pockets. Higher coolant temperatures were observed near the heat exchanger than the other parts of the circuit, even when the steam supply was shut off due to parasitic heat conducted via the metal of the steam pipe to the heat exchanger. An initial settling time of approximately 15 minutes was provided after starting the fan matrix and the coolant circulation to ensure uniform coolant temperatures across the cooling circuit.

Once the temperature sensors indicated a uniform coolant temperature across the cooling circuit, the addition of heat into the system began. The low pressure steam supply was gradually increased in the heat exchanger to achieve a coolant outlet temperature in range of 78-82°C. The coolant temperature at this level was allowed to stabilize in the cooling circuit for approximately 10 minutes. The real-time temperature level display on the Control Desk panel was used to determine when the system reached stability. The data recording was begun after temperatures across all the measurement points in the cooling circuit were stable; data were collected for t = 400 to 600 seconds during each test run. After data collection the fan speeds were increased by 1,000 RPM and data recording procedures repeated. The data collection cycles were repeated until the fan motor speeds reached 5,000 RPM, after which the system was allowed to cool and the shut down procedures were implemented.

The System Shut Down

After a fan configuration went through five run cycles at incremental fan speeds, the system was shut down using a predetermined sequence. Before the cooling system actuators (the coolant pump and the fans motors) were stopped, it was necessary to reduce the coolant circuit temperatures to $T_{HO} < 40°C$. to prevent the formation of steam pockets from the residual heat in the heat exchanger and possible pressure build-up in the coolant pipes. The heat input from the low pressure steam was gradually stopped using a manual shut off valve. The coolant pump motor and the fan motors were allowed to run at 2,000 RPM until the temperature sensors began showing values below 40°C. Once the coolant temperatures were lowered, the fan motors were stopped through the zero speed control signal in the Plus+1 BLDC controller using the Plus+1 software interface. Subsequently, the power supply to the fans was disconnected using the Lambda ESS bus bar switch. The Plus+1 service pack software was terminated only after the DC power supply for the fan motors was disconnected to prevent any erroneous control signals to the fan actuators.

Similarly, the coolant pump motor was stopped using the dSPACE-Control Desk slide bar control. As the coolant motor stopped, the power supply to the motor controller was disconnected. After all cooling system actuators were stopped, a final check of the temperature indications was required, and the coolant pump and fan motors were restarted if the coolant temperature at any point in the system was found to exceed 40°C. The dSPACE-Control Desk and MATLAB/Simulink applications

were terminated and the power supply to the computer systems could be disconnected.

3.10.2 Air Speed Experiments

A start-up procedure similar to that discussed in the previous sections was used to measure and record the air velocity over the frontal area of the radiator. However in this system, the fans, and the air velocity sensors were used only to collect the required data. The procedure for collecting the data for the velocity profile involved using an Omega – FMA 900 velocity sensor was suspended in place by a 6 degree-of-freedom clamp that could be adjusted and clamped to any position across the radiator face. The velocity readings were obtained from the dSPACE-Control Desk applications where the signals were processed by the MATLAB/Simulink model. Initially, the probe was located against the point at which the velocity was to be measured using a series of clamps. A distance of 3 inches (76.2 mm) was maintained between the radiator face and the opening for the sensing element (RTD). Then, the fans were run at 1000 RPM and the flow stabilized for 10 minutes; the velocity indicated by the sensor was recorded. While keeping the sensor at the same location, the fan motor speed was increased by 1,000 RPM and the readings recorded after a 10 minute time period. This measurement cycle was repeated for all points on the surface of the radiator and tables for each fan speed at a fan configuration were obtained. A surface profile indicating the velocity over the frontal area of the radiator was created using the CATIA software`s surfacing tool.

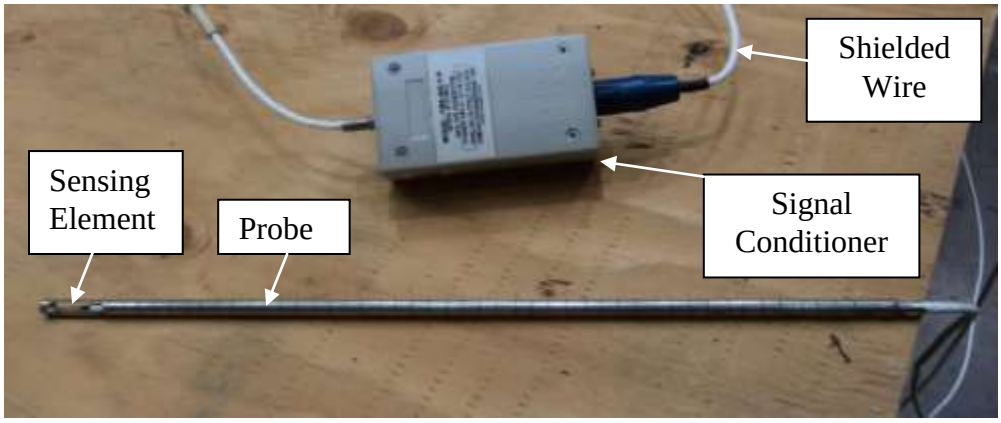

Figure 3.16:Air velocity probe for Omega – Model# FMA 900 with signal conditioner and shielded wire.

CHAPTER FOUR

EXPERIMENTAL TEST RESULTS

The thermal management system experimental test configuration, described in Chapter 3 to investigate the engine heat generation and multiple fan radiator heat rejection, will be applied to a variety of test cases. As shown in Table 4.1, a series of tests were conducted using various fan locations and fan speed configurations. The cooling circuit actuators, embedded sensors, the data acquisition system, and the software programs, various parameters (temperature, coolant flow, air velocity) were recorded in real-time. The recorded data was plotted against time; temperature changes and the forced convection air flow generated by the fan matrix configurations were analyzed to evaluate system performance.

Test Set No.	Heat Exchanger Outlet Temp. Range	Ambient Temp.	Coolant Flow Rate	Fan Speed Range In Steps Of 1,000 RPM	Operating Radiator Fans					
	°C	°C	LPM	RPM	1	2	3	4	5	6
1	78-81	22	93.8	1,000 – 5,000		•				
2	79-82	24				•		•		
3	79-81	22				•		•		•
4	78-81	23			•	•		•		•
5	79-82	23			•	•	•	•		•
6	78-81	23			•	•	•	•	•	•
7	79-82	22			•	•				
8	78-81	22			•	•		•		
9	78-81	23			•	•	•	•		
10	79-82	23				•	•	•		•

Table 4.1: Fan matrix and speed combinations for the experimental runs

The air speed values at different points on the radiator face were measured and used to construct air velocity profiles. The temperature data plots provided the average temperature values which were used to determine the heat rejection behavior of a multiple fan system for the ten different configurations. Finally, the measured current and voltage for the fan allowed the power consumption to be monitored and analyzed for ultimate fuel savings.

4.1 Heat Rejection Experiment Results

A comprehensive set of ten tests were completed to explore the thermal behavior of the radiator fan system. For simplicity, the sixth test will be discussed in detail which corresponds to all radiator fans operating. The temperature responses of the heat exchanger and radiator (inlet and outlet) for Test #6 at 1,000 RPM are shown in Figure 4.1. The heat gain and heat lost can be calculated from these temperature values; the heat supplied to the coolant by the low pressure steam exchanger, $\dot{Q}_{IN}$, can be expressed as

$$\dot{Q}_{IN} = \dot{m}_c C_P \left(T_{HO} - T_{HI} \right) \tag{4.1}$$

where $\dot{m}_c$ is the mass flow rate of the coolant circulation generated by the pump, C_P is the specific heat of the coolant (water) at constant pressure, and T_{HO} and T_{HI} are the temperatures recorded at the heat exchanger inlet and outlet, respectively (refer to Figure 4.2). Similarly, the heat lost in the radiator to the atmosphere, $\dot{Q}_{OUT}$, becomes

$$\dot{Q}_{OUT} = \dot{m}_c C_P \left(T_{RI} - T_{RO} \right) \tag{4.2}$$

where T_{RI} and T_{RO} are the temperatures recorded at the radiator inlet and outlet.

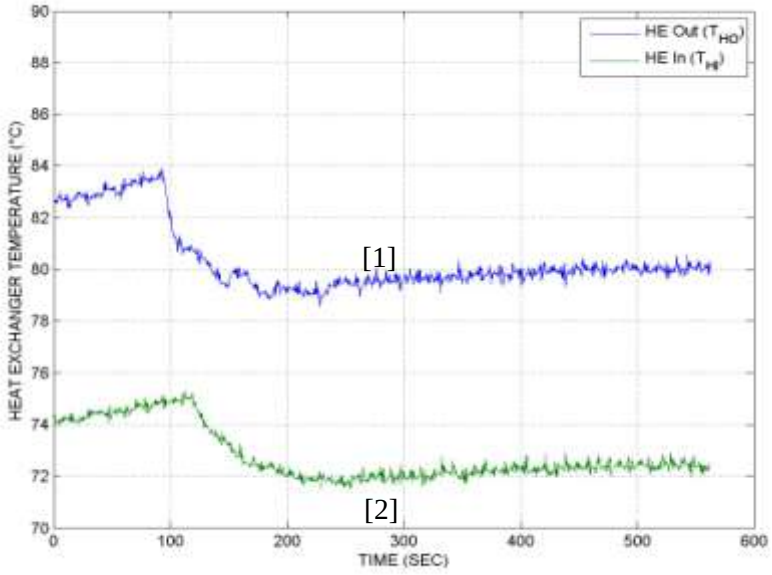

(a)

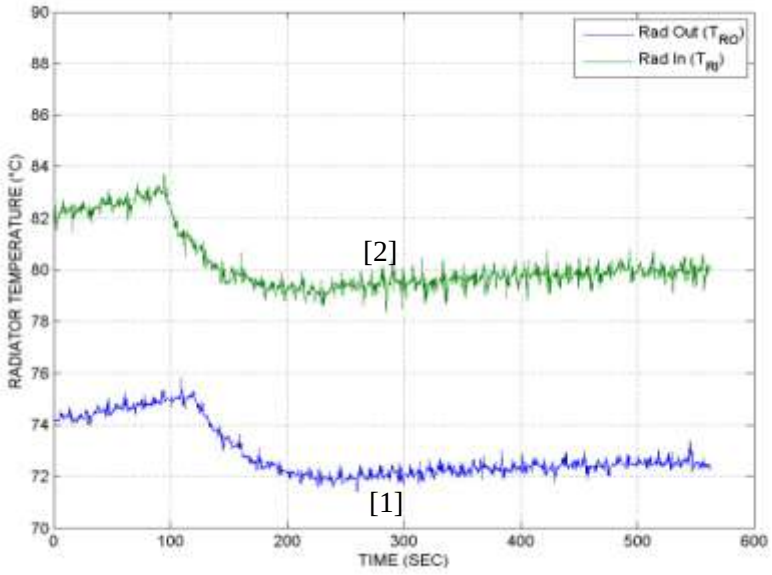

(b)

Figure 4.1: Temperature data plot for Test #6 at 1,000 RPM - (a) heat exchanger outlet [1] and inlet [2] temperatures, and (b) radiator outlet [1] and inlet [2] temperatures.

As Figure 4.1 shows, there is a 5°C decrease in the temperatures at t=100 seconds that may be attributed to the manual reduction in the steam supplied to the system by closing the manual steam valve. The ideal heat exchanger outlet temperature was T_{HO} = 80°C which corresponds to the target engine coolant temperature for the study. Note that T_{HO} and T_{RI} plus T_{HI} and T_{RO} are essentially the same profiles as expected when the bypass valve was closed. It is important to note that the bypass valve was closed for all the tests conducted on the experimental test bench. Thus, little heat was lost from the coolant due to the insulation layer on the coolant pipelines between these two components.

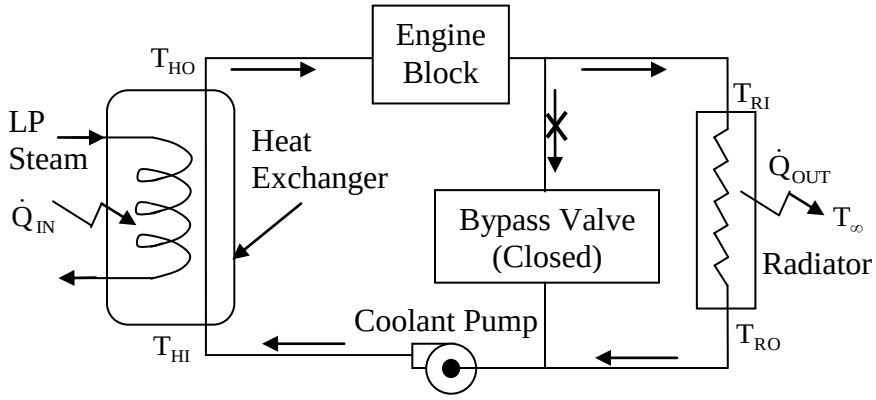

Figure 4.2: Schematic of the coolant circuit and temperature measurement locations

The temperature drop across the radiator was 7.7°C, while the temperature gain from the heat exchanger was 7.9°C. The coolant circulation rate, $\dot{m}_c$, was maintained at a constant value of 1.15 kg/sec thus the heat gain, $\dot{Q}_{IN}$, and heat rejected, $\dot{Q}_{OUT}$, were 38 KW and 37 KW, respectively. A parasitic heat loss of 1 KW existed considered due to engine and coolant pipe radiation as evident by the 0.2°C

temperature difference. The system operated in a steady-state equilibrium state (i.e., heat input equals heat lost, $\dot{Q}_{IN} = \dot{Q}_{OUT}$) during the test runs. This effect can be observed in the heat input and heat rejection plots of Figure 4.3.

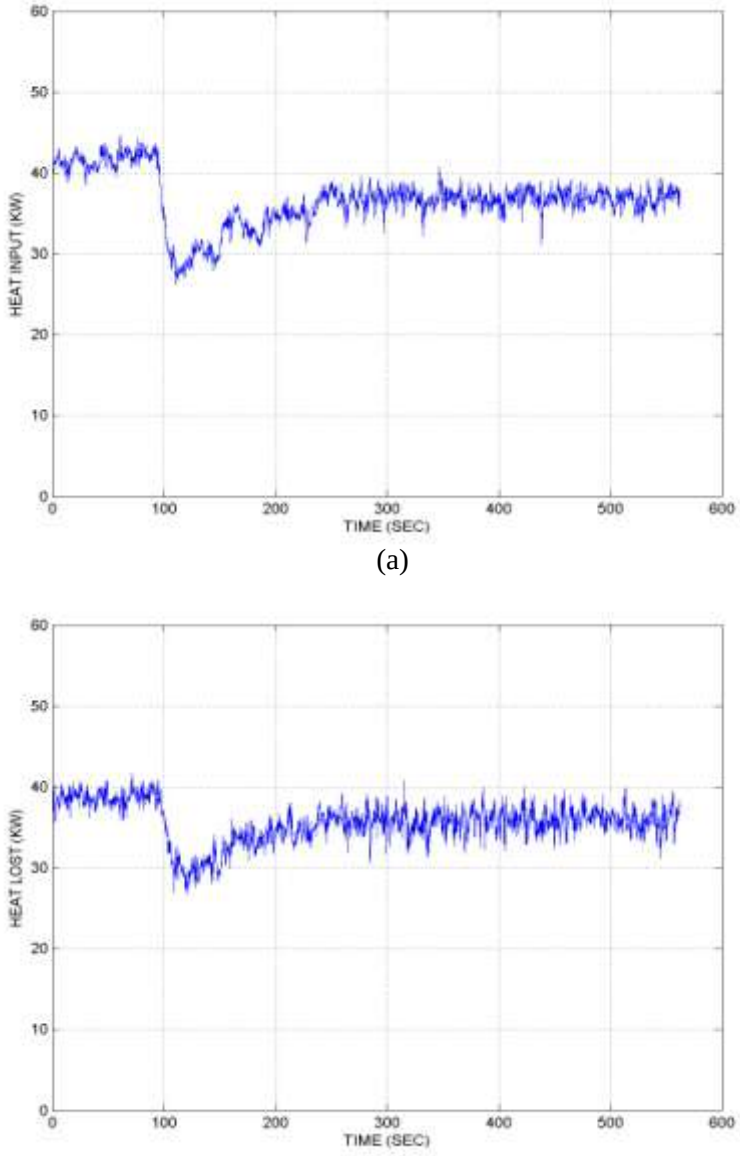

Figure 4.3: Heat data plot for Test #6 at 1,000 RPM - (a) heat exchanger heat input, and (b) radiator heat rejected

The coolant temperature at the heat exchanger outlet, T_{HO}, was maintained in the range of 78°C < T_{HO} < 82°C but ideally 80°C for all test configurations listed in Table 4.1, for a t ≈ 400 second time period over a 0 < t < 600 second test. For all tests, the fan motor speed was increased in 1,000 RPM increments and subsequent adjustments in the steam supply were made to maintain the coolant temperature in the desired range. This procedure was repeated until the fan motor speeds reached 5,000 RPM. Figure 4.4 summarizes the ten test cases and these scenarios will be discussed below.

Uncertainty Analysis for Data Measured

The temperature measurement was performed using thermocouples, their signal condtioners, and the dSPACE data acquisition board. Each of these components may introduce certain errors in the recorded temperature values due to the sensor calibration and accompanying instrument errors. As the true value of the measured parameter is not exactly known, a probable estimate may be calculated to determine the measurement error. This process is typically called uncertainty analysis during which the errors are identified and quantified (Figliola and Beasley, 1995).

The heat input, $\dot{Q}_{IN}$, and heat output, $\dot{Q}_{OUT}$, were the calculated parameters which were analyzed for errors based on system measurements. The Equations (4.1) and (4.2) indicate that the heat input and output values depend on the coolant mass flow rate, $\dot{m}_c$, the specific heat, C_p, and the temperature,T. The combined

uncertainty of the measurement of these three parameters represents the uncertainty in the heat input and heat output calculations. A basic heat flow rate equation can be stated as

$$\dot{Q}=\dot{m}_c C_P \Delta T \tag{4.3}$$

The combined uncertainty for heat flow using the Equation (4.3) may be stated as

$$u_q=\sqrt{\left(\frac{\partial \dot{Q}}{\partial \dot{m}_c}u_{\dot{m}_c}\right)^2+\left(\frac{\partial \dot{Q}}{\partial C_p}u_{C_p}\right)^2+\left(\frac{\partial \dot{Q}}{\partial \Delta T}u_T\right)^2} \tag{4.4}$$

where u_q is the probable uncertainty of heat flow rate measurement. In addition, the term $u_{\dot{m}_c}$, is the uncertainty for coolant mass flow rate measurement, u_{C_p}, denotes the uncertainty of the specific heat value, and, u_T represents the temperature measurement uncertainty. When the partial derivation in Equation (4.4) is completed, the expression becomes

$$u_q=\sqrt{C_p \Delta T u_{\dot{m}_c}{}^2+\dot{m}_c \Delta T u_{C_p}{}^2+\dot{m}_c C_p u_T{}^2} \tag{4.5}$$

In reverse order, the uncertainty for the temperature measurement, u_T, is given by

$$u_T=\pm t_{\nu,95} S_X \tag{4.6}$$

where S_X is the standard deviation of a set of data points measured during steady state operation of the cooling system, and $t_{v,95}$ is the variable obtained from the t distribution table for a probability of 95%. A sample set of 250 data points for the temperature measurement were statistically analyzed; the calculated standard deviation was, $S_X = 0.05$. The variable value, $t_{v,95}$ was obtained from a standard t distribution chart as $t_{v,95} = 1.96$. Using Equation (4.6), the uncertainty for temperature measurement was calculated as $u_T = 0.09$.

The value for unceratainty of specific heat of water at constant pressure is, $u_{C_p} = 0$ since the value is selected from standard table for fluid properties.

The uncertainity for the coolant mass flow rate, $u_{\dot{m}_c}$, could not be determined due to single data point measured during the experiment (i.e., coolant pump operated in a steady-state manner at fixed flow rate of 93.8 liters/min). However, to determine the uncertainty that contributes significantly to increase the heat flow rate uncertainty, u_q, it was assumed that the temperature measurement uncertainty is equal to the coolant mass flow rate unceratinty, (i.e., $u_{\dot{m}_c} = u_T = 0.09$). Substituting the values for the coolant flow rate, specific heat, and the temperature difference from Figure (4.1a) yeilds $C_p = 4.18$KJ/kg°C, $\dot{m}_c = 1.15$ kg/sec, and $\Delta T = 7.9$°C so that

Term #1 in Equation (4.5) is $C_p \Delta T u_{\dot{m}_c} = 2.9$

Term #2 in Equation (4.5) is $\dot{m}_c \Delta T u_{C_p} = 0$

Term #3 in Equation (4.5) is $\dot{m}_c C_p u_T = 0.43$

In the above scenario, the uncertainty in the coolant mass flow rate (Term #1) contributes the most to the heat flow rate uncertainty; however, it was also observed that when the coolant flow rate uncertainty, $u_{\dot{m}_c} < 0.01$, then the temperature measurement uncertainty, u_T, (Term #3) contributed more to the heat flow rate uncertainty. Substituting Term #1, Term #2, and Term #3 values in the Equation (4.5) generates the value for combined uncertainty of $u_q = 2.93$. Thus, the accuracy of heat flow, $\dot{Q}_{IN}$, is in range of $\pm 1.5\,KW$ from the mean value. In the similar manner, the combined uncertainty for the heat flow, $\dot{Q}_{OUT}$, becomes $u_q = 2.91$. Simply put the measured heat flow can vary in range of $\pm 4\,\%$.

The test configurations were split into two sets (I and II), each evaluating the heat rejection performance of the fan matrix at different fan motor and speed combinations. The fan selection is based on the fundamental thermodynamic principle that the amount of convective heat transfer is directly proportional to the fluid temperature difference which occurs across the heat exchanger, $\dot{Q} \propto \Delta T$ (Jorgensen, 1983). Specifically, the fan combinations ensured variable air flow over the radiator`s higher temperature regions to achieve maximum

forced convective cooling. The Set I configuration evaluates heat rejection achieved using an increasing number of fans starting with one fan through all 6 fans. The fans selected for this set include those directly behind the hottest temperature region on the radiator face (i.e., inlet fluid from engine). The fan motor combinations in Set II were alternative fan motor choices; their heat rejection performance was analyzed and compared with those from Set I. Again, the hottest region of the radiator received the most attention. The average temperature values and heat gain or lost calculations for the different tests have been summarized in Table 4.2. This table presents mean values of the heat exchanger inlet/outlet and radiator inlet/outlet temperatures recorded during the test runs, as well as the heat gain and heat lost values calculated from these mean temperatures using Equations (4.1) and (4.2). The air temperature rise across the radiator was not considered since the effect was indirectly measured through the coolant temperatures.

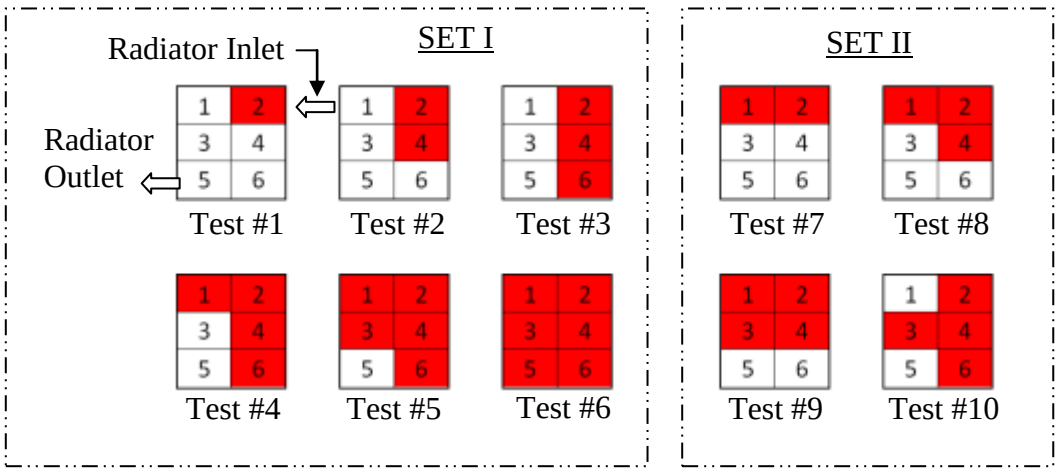

Figure 4.4: Fan selection for different test configurations (a total of 10 tests); arrows indicate the direction of coolant flow.

The power consumption of the fan motors was calculated using the voltage, V_S, and the current, i, values measured for the given configuration and operating speed (refer to Table 4.3). This fan power consumption data was essential in determining the energy usage by the cooling system for a given engine heat load. The steady state DC power consumption, $P = iV_S$, was observed to vary depending on the fan motor speed and the number of the fans operating at a given time.

TEST NO.	FAN CONFIG.	FAN MOTOR SPEED, N	RADIATOR IN T_{RI}	RADIATOR OUT T_{RO}	HEAT EXCH. IN T_{HI}	HEAT EXCH. OUT T_{HO}	HEAT GAIN $\dot{Q}_{IN}$	HEAT LOST $\dot{Q}_{OUT}$
		RPM	°C	°C	°C	°C	KW	KW
SET I								
1	2	1,000	80.1	78.2	78.1	80.2	10	9
		2,000	80.0	76.6	76.5	80.1	17	16
		3,000	79.7	75.7	75.4	79.8	21	19
		4,000	79.5	74.3	75.1	79.9	23	25
		5,000	80.2	74.2	74.1	80.5	31	29
2	2-4	1,000	80.4	77.0	76.9	80.5	17	16
		2,000	79.8	74.0	73.9	79.9	29	28
		3,000	79.9	72.0	72.1	80.2	39	38
		4,000	81.1	71.1	71.0	81.2	49	48
		5,000	80.7	69.5	69.4	80.8	55	54
3	2-4-6	1,000	80.7	76.5	76.4	81.0	22	20
		2,000	80.4	72.5	72.4	80.5	39	38
		3,000	80.4	70.0	69.9	80.5	51	50
		4,000	79.6	67.0	66.9	79.7	62	61
		5,000	80.0	65.1	65.1	80.0	72	72
4	1-2-4-6	1,000	79.5	73.9	74.0	80.4	31	27
		2,000	80.3	71.2	71.0	80.5	46	44
		3,000	79.7	67.3	67.2	79.8	61	60
		4,000	79.8	64.1	64.0	79.9	77	76
		5,000	80.9	63.7	63.6	81.0	84	83
5	1-2-3-4-6	1,000	80.9	74.0	73.9	81.0	34	33
		2,000	79.8	68.2	68.1	79.9	57	56
		3,000	79.9	64.4	64.3	80.0	76	75
		4,000	79.2	61.6	61.5	79.3	86	85
		5,000	79.9	59.8	59.7	80.0	98	97
6	1-2-3-4-5-6	1,000	80.1	72.4	72.3	80.2	38	37
		2,000	79.5	66.7	66.4	79.7	64	62
		3,000	80.3	63.5	63.3	80.5	83	81
		4,000	79.9	60.4	60.3	80.0	95	94
		5,000	80.0	57.7	57.6	80.1	109	108
SET II								
7	1-2	1,000	80.1	76.5	76.4	80.2	18	17
		2,000	79.9	74.7	74.7	79.9	25	25
		3,000	80.4	72.7	72.6	80.5	38	37
		4,000	81.0	72.3	72.2	81.3	44	42
		5,000	80.2	68.8	68.6	80.4	57	55
8	1-2-4	1,000	80.5	76.3	76.3	80.5	20	20
		2,000	79.8	71.9	71.9	79.8	38	38
		3,000	80.1	69.7	69.6	80.2	51	50
		4,000	80.9	68.1	68.0	81.1	63	62
		5,000	80.0	64.7	64.7	80.0	74	74
9	1-2-3-4	1,000	80.0	74.6	74.2	80.4	30	26
		2,000	79.9	70.8	70.7	80.0	45	44
		3,000	80.1	67.7	67.7	80.1	60	60
		4,000	80.7	66.0	65.9	80.8	72	71
		5,000	82.0	65.4	65.3	82.1	81	80
10	2-3-4-6	1,000	80.8	75.0	74.9	81.1	30	28
		2,000	79.7	70.4	69.8	80.2	50	45
		3,000	80.4	68.0	67.4	80.9	65	60
		4,000	79.8	65.3	64.7	80.2	75	70
		5,000	80.1	63.5	63.4	80.2	81	80

Table 4.2: Fluid temperature and heat transfer calculation results for different fan matrix configurations and motor speed combinations (Sets I and II).

SET I				
TEST NO.	FAN CONFIG.	FAN MOTOR SPEED, N	CURRENT, i	POWER CONSUMPTION, P
		RPM	Amperes	KW
1	2	1,000	2	0.060
		2,000	3.5	0.105
		3,000	9	0.270
		4,000	11	0.330
		5,000	20	0.600
2	2-4	1,000	3.5	0.105
		2,000	7	0.210
		3,000	11	0.330
		4,000	20	0.600
		5,000	35	1.050
3	2-4-6	1,000	5	0.150
		2,000	9	0.270
		3,000	15	0.450
		4,000	30	0.900
		5,000	51	1.530
4	1-2-4-6	1,000	7	0.210
		2,000	10	0.300
		3,000	20	0.600
		4,000	39	1.170
		5,000	71	2.130
5	1-2-3-4-6	1,000	8.5	0.255
		2,000	13	0.390
		3,000	30	0.900
		4,000	52	1.560
		5,000	98	2.940
6	1-2-3-4-5-6	1,000	9	0. 270
		2,000	15	0.450
		3,000	31	0.930
		4,000	67	2.010
		5,000	125	3.750
SET II				
7	1-2	1,000	3.5	0.105
		2,000	7	0.210
		3,000	11	0.330
		4,000	20	0.600
		5,000	35	1.050
8	1-2-4	1,000	5	0.150
		2,000	9	0.270
		3,000	15	0.450
		4,000	30	0.900
		5,000	51	1.530
9	1-2-3-4	1,000	7	0.210
		2,000	10	0.300
		3,000	20	0.600
		4,000	39	1.170
		5,000	71	2.130
10	2-3-4-6	1,000	7	0.210
		2,000	10	0.300
		3,000	20	0.600
		4,000	39	1.170
		5,000	71	2.130

Table 4.3: Current and power readings a constant voltage of, V_S = 30VDC for different fan matrix and speed combinations (Sets I and II)

Figure 4.5 shows the plot of the fan motor power consumption, P, for the various combinations in Set I versus the fan motor speeds, N. This graph displays the general trend that the increased power consumption is dependent on the number of fans and operating speeds. However, there were exceptions observed at 3,000 RPM for the single fan (Test #1) and for the five fan (Test #5) combinations. In these two cases, the power consumption increased. The power consumption was observed to be almost equal for speeds up to 3,000 RPM when either five (Test #5) or six (Test #6) fan motors operated. However, all the fan motor combinations have a comparatively smaller variation in power consumption for motor speeds up to 2,000 RPM .

The standard fan law give the mathematical relationship between the fan power consumption, P_{FAN}, the fan speed, N, the air pressure, dp, and volume flow, q, as

$$\frac{P_{FAN1}}{P_{FAN2}} = \left(\frac{N_2}{N_1}\right)^3 \left(\frac{D_2}{D_1}\right)^5 \left(\frac{d_2}{d_1}\right) \tag{4.7a}$$

$$\frac{q_1}{q_2} = \left(\frac{N_2}{N_1}\right) \left(\frac{d_2}{d_1}\right)^3 \tag{4.7b}$$

$$\frac{dp_1}{dp_2} = \left(\frac{N_2}{N_1}\right)^2 \left(\frac{d_2}{d_1}\right)^2 \tag{4.7c}$$

In this expression, P_{FAN}, is the impeller power of the fan in KW, N is the speed in RPM, D is the fan diameter in meters, d is the air density in kg/m^3, q is the

volume flow rate in m^3/sec, dp is pressure in Pascal, and subscripts 1 and 2 indicate initial and final states. The non-linear relationship show that a 10% fan speed increase results in a 10% air volume flow increase, a power increase of 33% and a pressure increase of 21%.

The impeller power, P_{FAN}, can be compared with the electrical motor power consumption, P, of a fan operating efficiency. The electrical motor efficiency, η_m, is about 98%, thus $P = \frac{1}{\eta_M} P_{FAN}$. For example, in Test #6 at speed N = 3000 RPM (refer to Table 4.3) the electrical power consumption is P = 0.93 KW which indicates that the impeller needs 0.93/1.02 = 0.91 KW to overcome the blade air drag. It should be noted that the fan law indicates the relationship between two performance variables of fans with similar flow conditions for turbo machinery (Jorgensen, 1983).

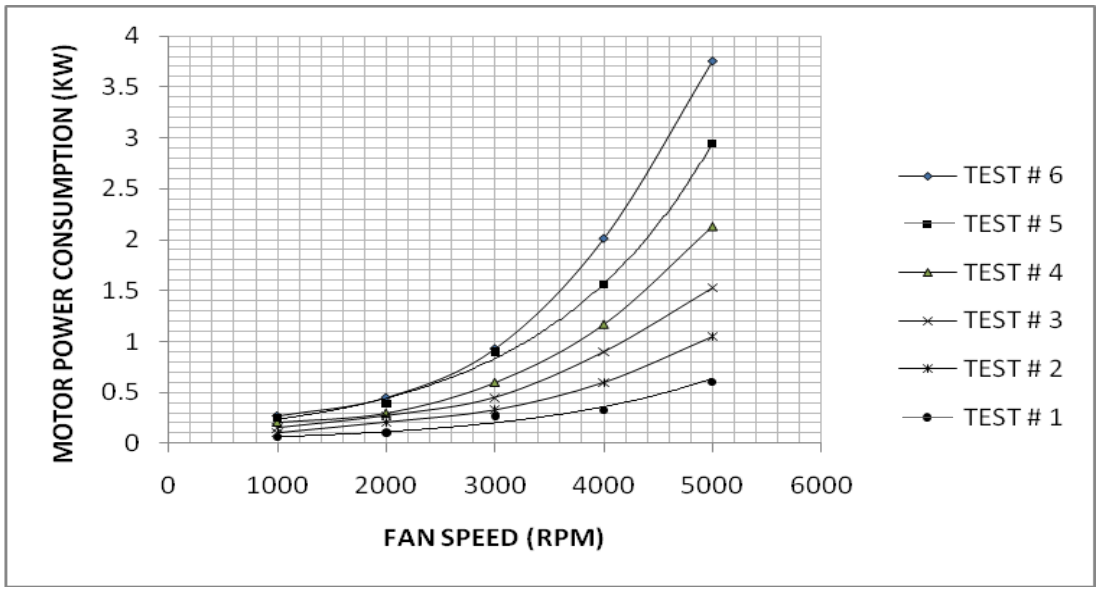

Figure 4.5: Total power consumption for various fan configurations in Set I; symbols on lines correspond to 1,000 RPM (left end) and 5,000 RPM (right end) with 1,000 RPM increaments in between them.

The fan power consumption, P, was checked to determine the validity of the data and the individual average fan motor power consumption for the multiple fan configurations of Tests #1 – #6 of Set I. Table 4.4 lists the calculated individual fan power consumption, P, at different fan configurations. These results indicate that the variations in the average fan power consumption range from 12% to 42% for Test #1 – #6. In other words, the measured fan power was divided by the number of operating fans to obtain the power per fan magnitude. The experimental results indicate that the fan power consumption is non-linear and dependent on the number of operating fans and their speed.

Speed, N	Average Power Consumption For a Single Fan in a Test Configuration, W						Maximum % Difference
RPM	#1	#2	#3	#4	#5	#6	%
1,000	60	52.5	50	52.5	50	45	25
2,000	105	105	90	75	78	75	28
3,000	270	165	150	150	180	155	42
4,000	330	300	300	292.5	312	335	12
5,000	600	525	510	532.5	588	625	18

Table 4.4: Average power consumption for a single fan motor in the speed range of 1,000-5,000 RPM for Test configurations #1 - #6.

The fan power, P, versus fan speed, N, plot shows the polynomial curve fitting that represents the trend of the data collected (refer to Figure 4.6). The power to speed plot indicates the confirmation of the Fan Laws in Equation (4.7) which offer a cubed relationship. The curve fit obtained gives a second order polynomial curve as well as a third order, using the least square method; which can be used to determine the current required, i, by the system for different fan combinations and motor speeds, N, provided the supply voltage V_S. The current required, i, may be represented as

$$i = \left(\frac{1}{V_S}\right)\left(a_2 N^2 - a_1 N + a_0\right) \tag{4.8a}$$

where $a_2 = 3\times10^{-5}$, $a_1 = 0.0784$, and $a_0 = 101.43$.

$$i = \left(\frac{1}{V_S}\right)\left(a_3 N^3 - a_2 N^2 + a_1 N + a_0\right) \tag{4.8b}$$

where $a_3 = 5\times10^{-9}$, $a_2 = 1\times10^{-5}$, $a_1 = 0.0486$, and $a_0 = 11.017$.

The power consumed by a single fan motor becomes, $P = iV_S$, based on the fan motor speed, N. The supply voltage, V_S, is constant at $V_S \approx 30$VDC. The coefficients are obtained from the statistical processes on the X and Y axis intercepts of the data points (30 points) presented in the Table 4.4.

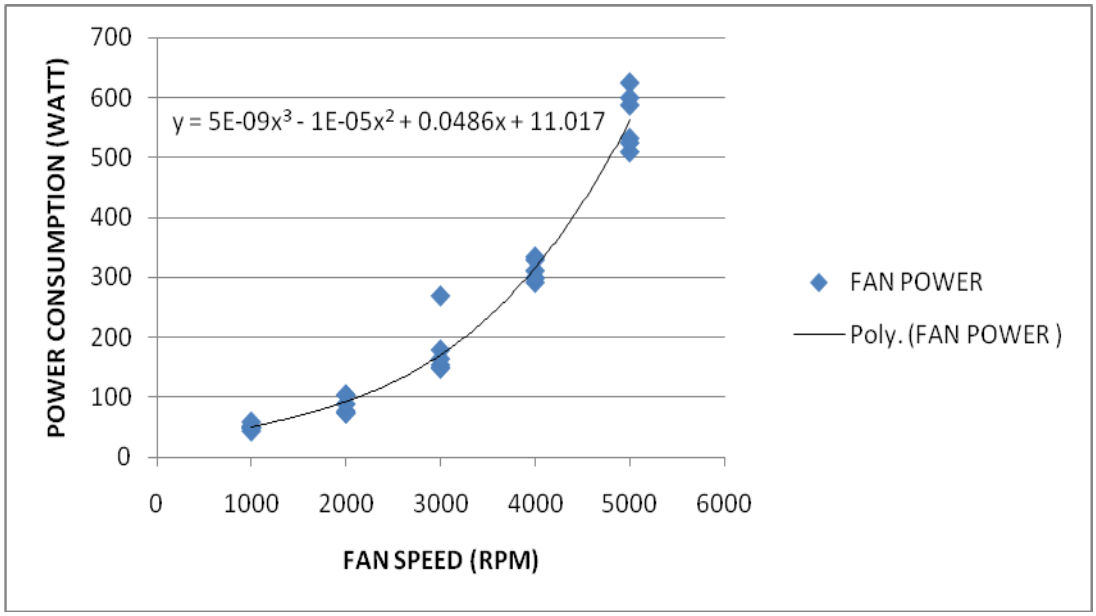

Figure 4.6: Power consumption versus fan speed for a single fan motor for all test configurations of Set I.

The power consumption of a single fan was experimentally observed without the radiator pressure drop to determine the power consumption and air velocities obtained at the speed range of 1,000 – 5,000 RPM in steps of 1,000 RPM. Table 4.5 presents the observed peak air velocities and the power consumption for a single fan. The power consumption of this single fan was observed to match with the power consumption of a single fan with radiator pressure drop at speeds 1,000 RPM and 4,000 RPM. However at 2,000 RPM, 3,000 RPM and 5,000 RPM the power consumption was reduced for the single fan without a radiator. The increased power consumption for the three cases was due to the presence of a radiator. A pressure increase in range of 0-137 Pascal (0.02 PSI) during Test #1 – Test #10 was experimentally increased between the radiator and the fan matrix.

Speed, N	Air Velocity, V	Voltage, V	Current, i	Power, P
RPM	m/sec	VDC	Amp	W
1,000	4	30	2	60
2,000	7	30	5	150
3,000	11	30	8	240
4,000	13	30	11	330
5,000	18	30	18	540

Table 4.5: Power consumption for a single fan motor in the speed range of 1,000-5,000 RPM without radiator interference.

Discussion of Graphical Results

In Figure 4.7, the graph of the heat rejected, $\dot{Q}_{OUT}$, versus fan power, P, for different fan configurations gives the information of fan speed (symbols on the given trace), fan configuration (Test #1 - #6), and corresponding power consumption

(horizontal axis) for the required heat rejection (vertical axis). The plot represents four parameters - heat rejected, $\dot{Q}_{OUT}$, fan speed, N, fan configuration, Test #, and the fan power consumption, P. For example, if the heat rejection rate is considered the "input" design parameter, then both the fan configuration and the fan speed must be selected to achieve the heat rejection. This graph may help select the automotive engineer to best energy efficient fan speed and fan matrix configuration for a given heat load.

Specifically, the data obtained from the Set I experiments indicate that reduced energy consumption by the all six fans operating configuration (i.e., Test #6) can be achieved for heat rejection rates above $\dot{Q}_{OUT} > 56$ KW. However, below 56 KW other fan configurations were observed to be more energy efficient. For example, a heat rejection rate of 48 KW shows, Test #5 with a fan matrix power consumption of P = 0.30 KW while Test #6 was 0.33 KW. This scenario represents a 10% decrease in power consumption while offering the same benefit.

If the curves are analyzed with respect to the fan power consumption, for smaller values, then all the fan configurations were observed to reject heat essentially proportional to their electrical power input. This can be explained using Figure 4.8 over a 0.5 KW range of fan power.

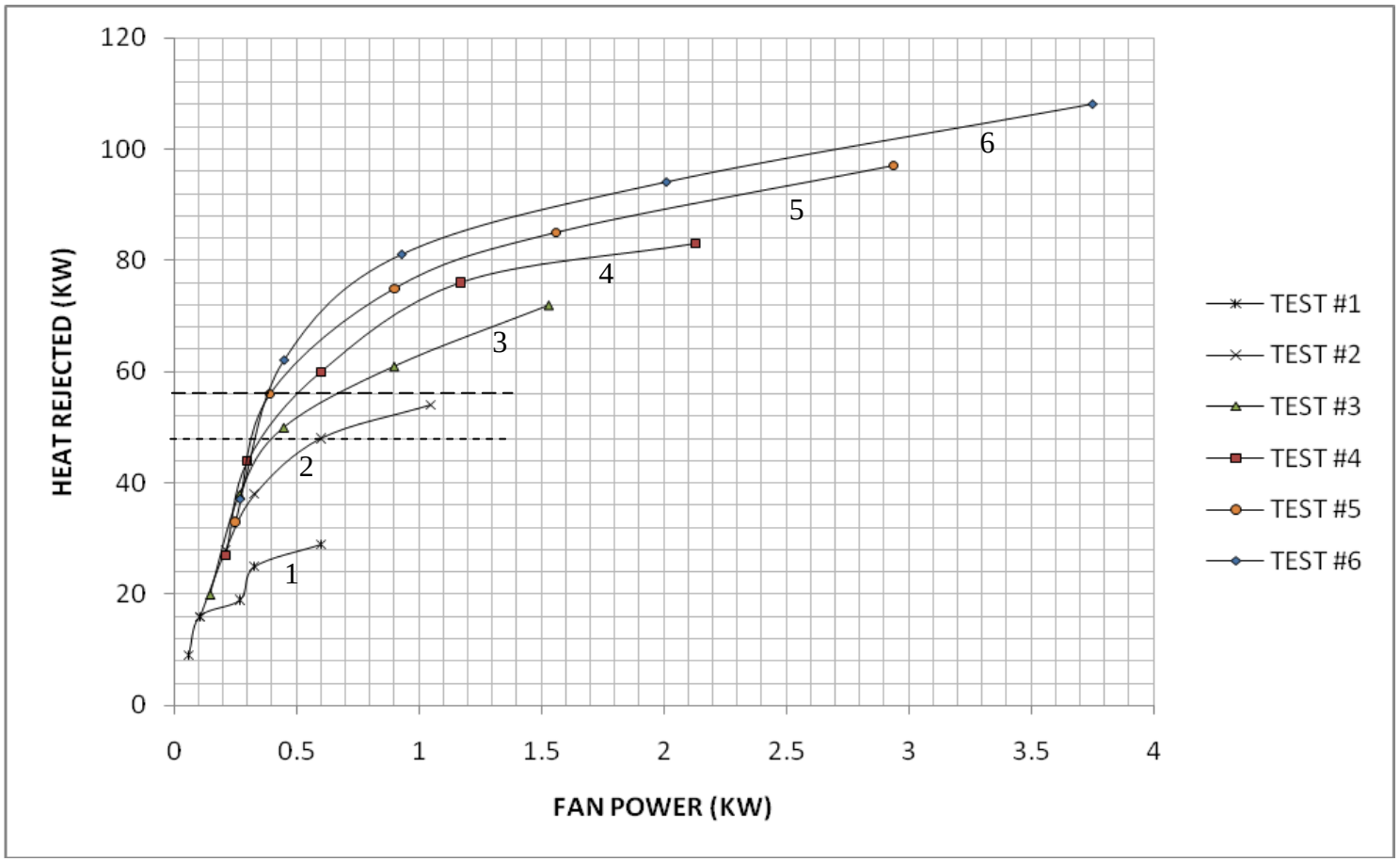

Figure 4.7: Fan power versus heat rejection at different fan and fan speed 1,000 to 5,000 RPM configuration (Test #1- #6) for Set I.

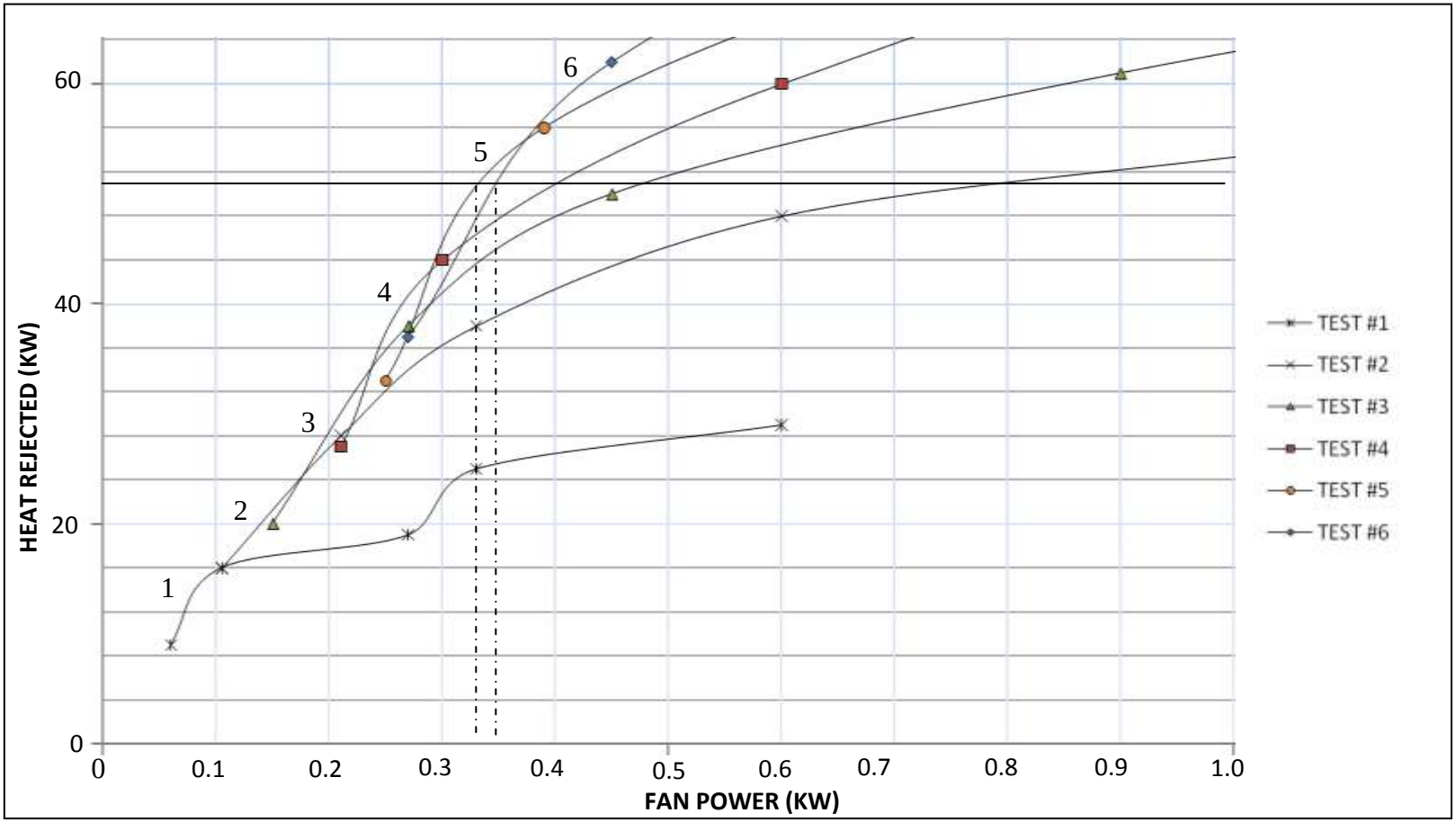

Figure 4.8: Fan power versus heat rejection at different fan and fan speed configurations for Set I for fan power, P, below 1KW.

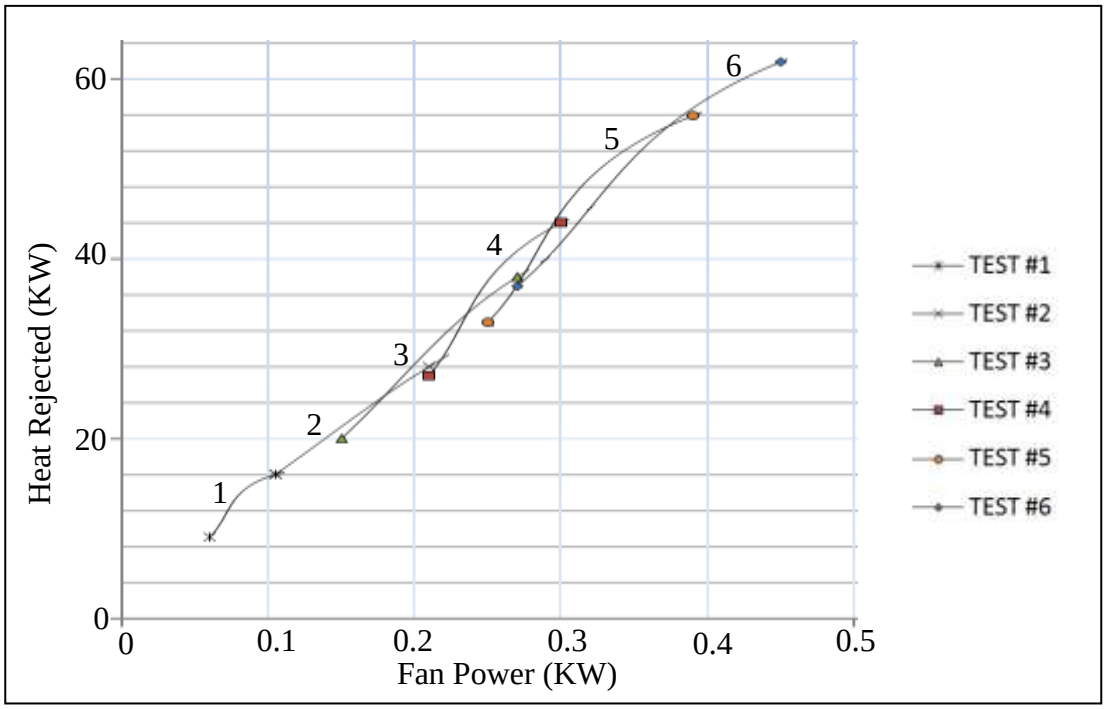

Figure 4.9: Test #1 - #6 with fan operating at 1,000 to 2,000 RPM and display of fan power versus heat rejection.

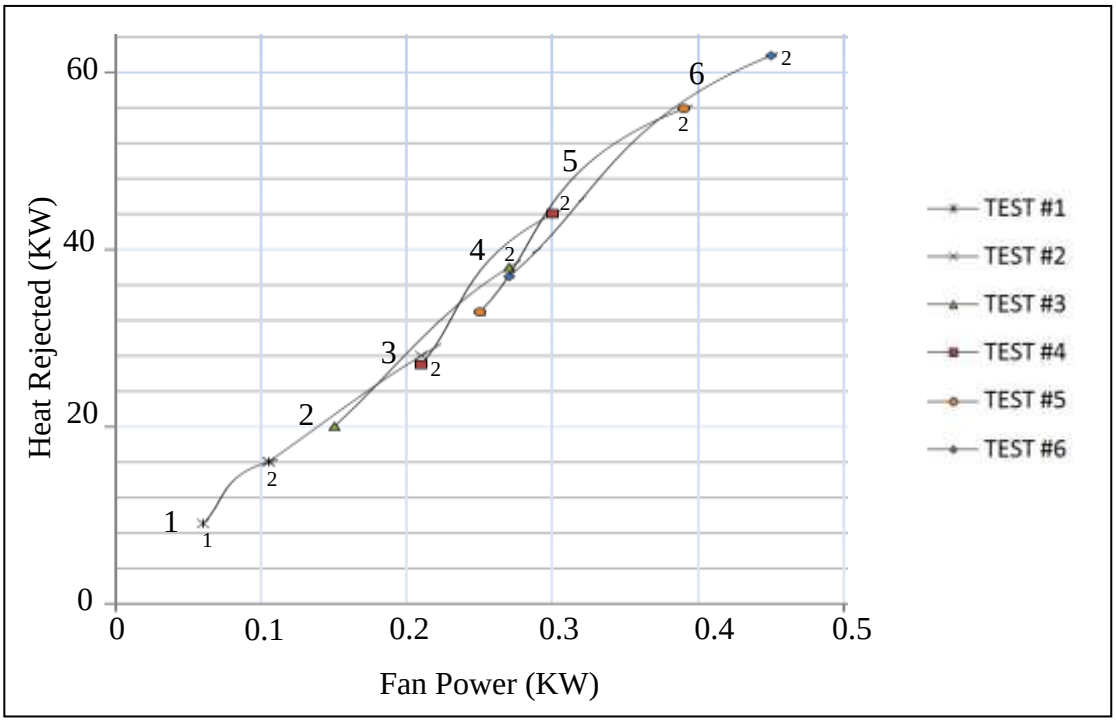

Figure 4.10: General rule applied to the 0-60KW heat rejection range for Test #1 - #6.

$\dot{Q}_{OUT}$ (KW)	Configuration (Fans)	Fan Power, P (KW)	Fan Speed, N (RPM)
0-16	Test #1	0-0.10	1,000-2,000
16-24	Test #2	0.10 - 0.18	1,000
24-35	Test #3	0.18 – 0.23	1,000
35-43	Test #4	0.23 – 0.30	1,000-2,000
43-56	Test #5	0.30 – 0.39	2,000
56+	Test #6	0.39 +	2,000

Table 4.6: Best observed combination for Set 1 heat rejection and fan power configuration.

For heat rejection of $0 < \dot{Q}_{OUT} < 16$ KW, then Test #1 was in the range of $1{,}000 \leq N \leq 2{,}000$ RPM. Next, $16 < \dot{Q}_{OUT} < 24$ KW and $24 < \dot{Q}_{OUT} < 35$ KW corresponds to Test #2 and #3 at N=1,000 RPM, respectively. If $35 < \dot{Q}_{OUT} < 43$ KW, then the Test #4 should operate at $1{,}000 \leq N \leq 2{,}000$ RPM. Finally, $43 < \dot{Q}_{OUT} < 56$ KW and $\dot{Q}_{OUT} > 56$ KW results in Test #5 and Test #6 at N=2,000 RPM, respectively.

General Rule for Radiator Fan Matrix Operation:

A rule of thumb can be formulated based on these experimental observations for heat rejection, between 0 – 56 KW. First start with a single fan (Test #1) and operate at N=1,000 to 2,000 RPM. If more heat rejection is needed, then bring another fan online (Test #2 – Test #5) till the all six fans (Test #6) operate at N=1,000 RPM (perhaps 2,000 RPM if needed). Above a heat rejection threshold of 56 KW, use all six fans and increase the fan speed as needed to 5,000 RPM.

A case study was done using Test #6 experimental data for fan speeds of 2,000 RPM. For the heat rejection rate of $\dot{Q}_{OUT}$ = 52 KW, the fan power consumption because P = 0.44 KW (6 fans operating at 2,000 RPM). If Test #5 configuration was used for same heat rejection the fan power consumption was observed to be 0.38 KW. Thus, the net benefit is 20% reduction in energy consumption. For the general rule the power consumption becomes 0.385 KW (5 fans at 2,000 RPM)

The heat rejection Data Set II in Figure 4.4 evaluates different fan matrix combinations to further explore fan placement behind the radiator. In Figure 4.11, the heat rejection, $\dot{Q}_{OUT}$, versus fan power consumption, P, has been displayed for these additional combinations to help determine the most efficient combination. The following three cases were identified and compared: Test #2 versus Test #7; Test #3 versus Test #8; and Test #4 versus Test #9 versus Test #10. The comparison between fan combinations in Test #2 and Test #7, in Figure 4.12 indicates slightly better energy efficiency per KW of heat rejection by Test #2 over the operating speed range of 0-5,000 RPM. However, it can be observed that Test #7 has slightly lower energy consumption for the fan power consumption of P > 1 KW (5000 RPM), where the curve for Test #7 intersects the curve for Test #2 and continues with a higher slope value. On comparing the fan configuration for Test #2 and Test #7 in

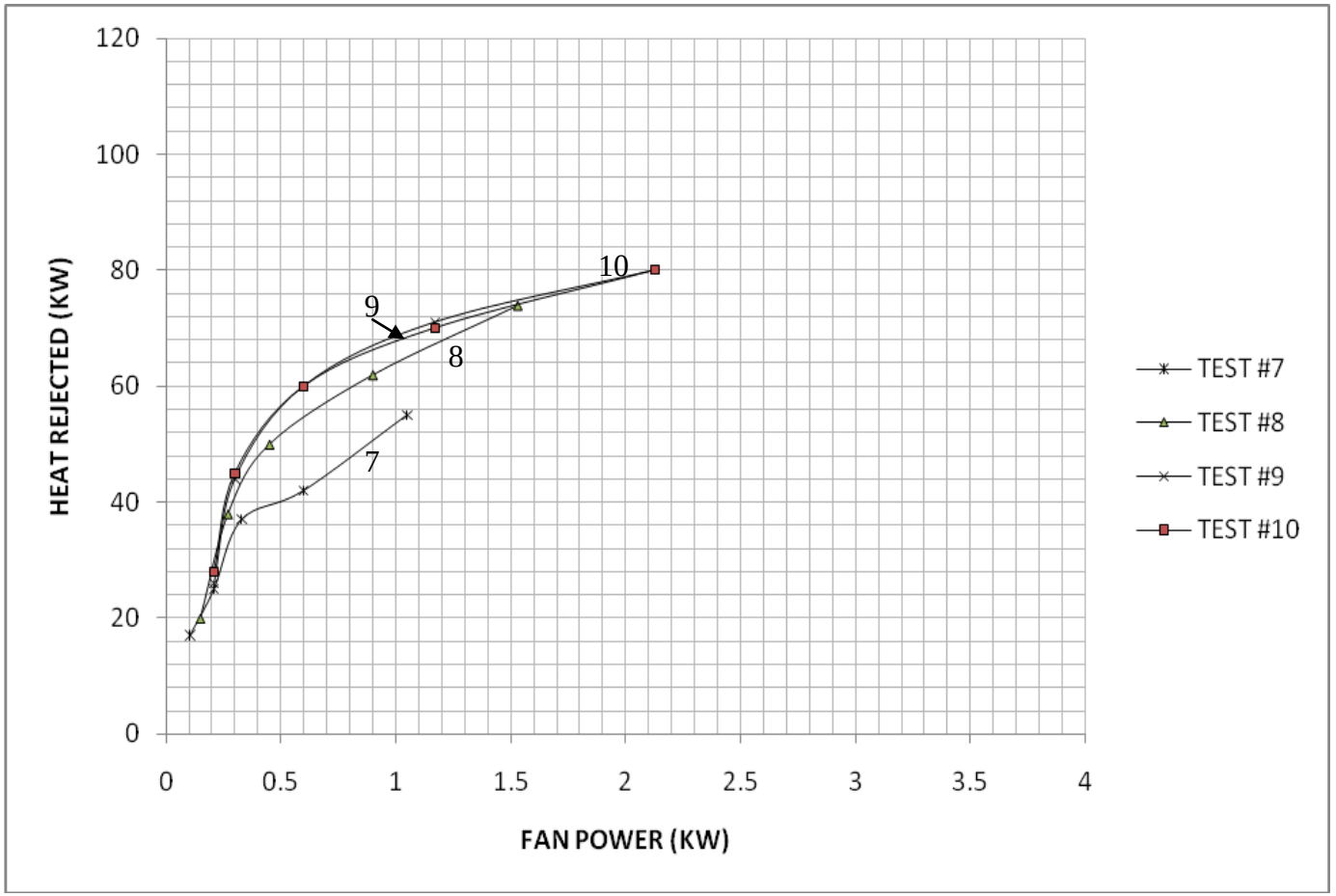

Figure 4.11: Fan power versus heat rejection at different fan and fan speed 1,000 to 5,000 RPM configuration (Test #7- #10) for data Set II.

Figure 4.4, this plot suggests that the location of the fans can significantly improve the heat transfer rate per KW of power consumed by the motors. The combination with fans located closer to the highest temperature region on the radiator (upper right hand corner) has higher energy efficiency.

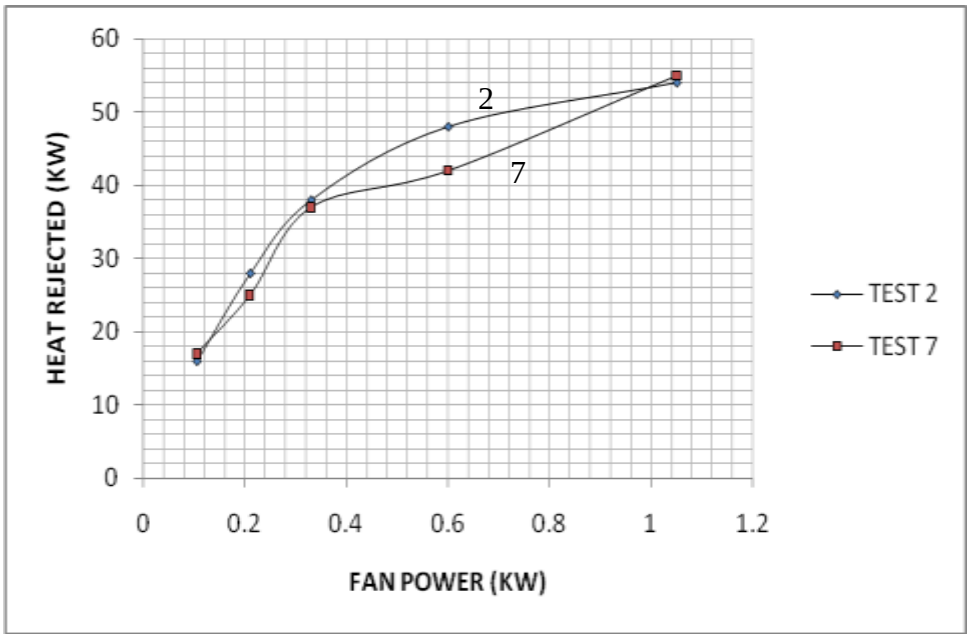

Figure 4.12: Total electric fan power versus heat rejection for Test #2 and Test #7 at fan speeds of 0-5,000 RPM.

The fan configurations for Test #3 and Test #8 show marginal differences in overall energy efficiency for the operating speed range of 0-5,000 RPM (refer to Figure 4.13). Test #8 shows a little higher efficiency on the fan power consumption versus heat rejection plots indicted by its higher slope when compared to the curve representing Test #8. Thus one can suggest that location of fan nearer to the radiator coolant inlet is more effective in increasing heat rejection.

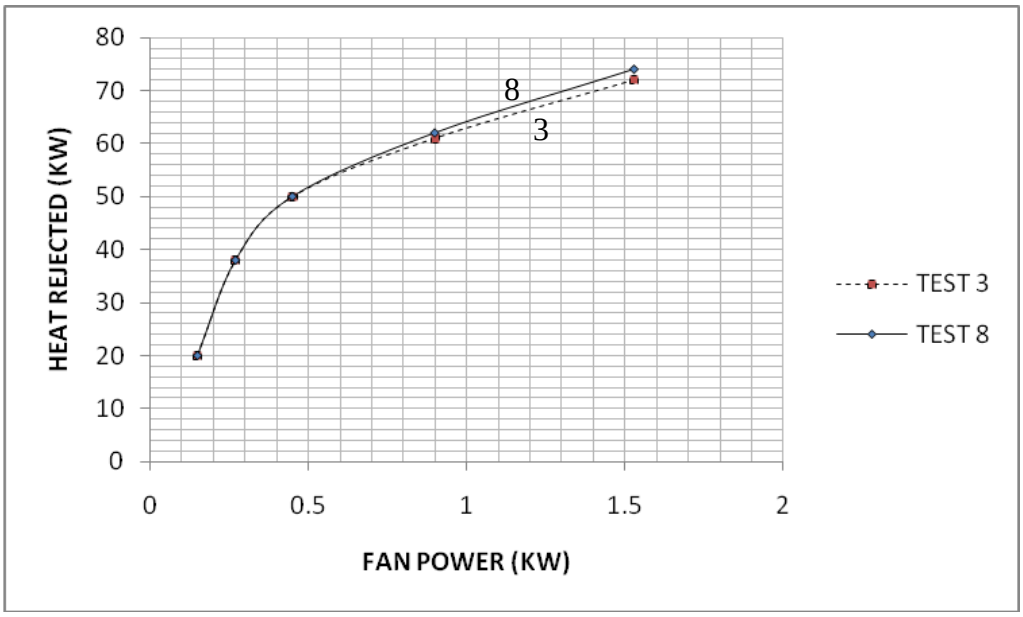

Figure 4.13: Fan power versus heat rejection for Test #3 and Test #8 at fan speeds of 0-5,000 RPM.

Comparing the energy consumption by the fan motors with the heat rejection rate among the fan combinations in Test #4, Test #9, and Test #10, shows that the fan matrix in Test #4 has a higher overall energy efficiency (refer to Figure 4.14). However the energy efficiency of this combination (i.e., Test #4) coincides with other two combinations, at speeds below N < 3,000. At fan power consumption value of p>0.6KW, significant efficiency increase in Test #4 fan configuration indicated by consistent higher heat rejection compared to other two test configurations is observed. If compared with fan locations for the test configurations in Figure 4.4, these plots display a trend indicating higher heat transfer rate for fans located near the highest temperature region on the radiator face. In other words, fluid travels downward for cooling and right-to-left. So Test #4 offer best since cools top-to-bottom and right-to-left on hottest row.

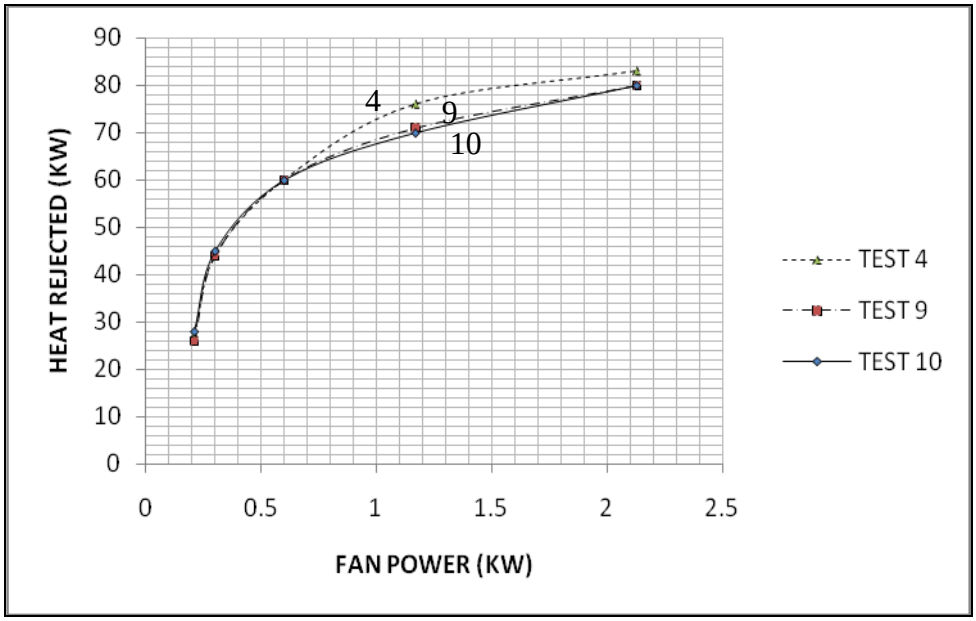

Figure 4.14: Electrical fan power versus heat rejection for Test #4, Test #9, and Test #10 at fan speeds of 0-5,000 RPM.

Estimation of Heat Rejection Requirements

To complement the experimental heat transfer results of the previous section, an analytical model for the combustion process generated heat and the air flow rate for forced air convection in the radiator fans. The heat rejection from an engine combustion chamber to the coolant, $\dot{Q}_C$, (Taylor, 1957) may be stated as

$$\dot{Q}_C = UA_p \left(T_g - T_c \right) \text{ or } U = \dot{Q}_C \left(\frac{1}{A_p \left(T_g - T_c \right)} \right) \tag{4.9}$$

where $\dot{Q}_C$ is the rate of heat flow from combustion chamber gases to the coolant in the coolant flowing through the coolant jackets, A_p is the surface area of the piston head, T_g is the mean effective gas temperature, and T_c is the coolant temperature.

The mean effective gas temperature, T_g, for a specific air-fuel ratio (AFR) can be obtained for a liquid and air cooled engine from Figure 4.15 (Taylor and Toong, 1958). The coolant temperatures,T_c , can be determined using temperature sensors in the coolant jacket surrounding the combustion chamber(s).

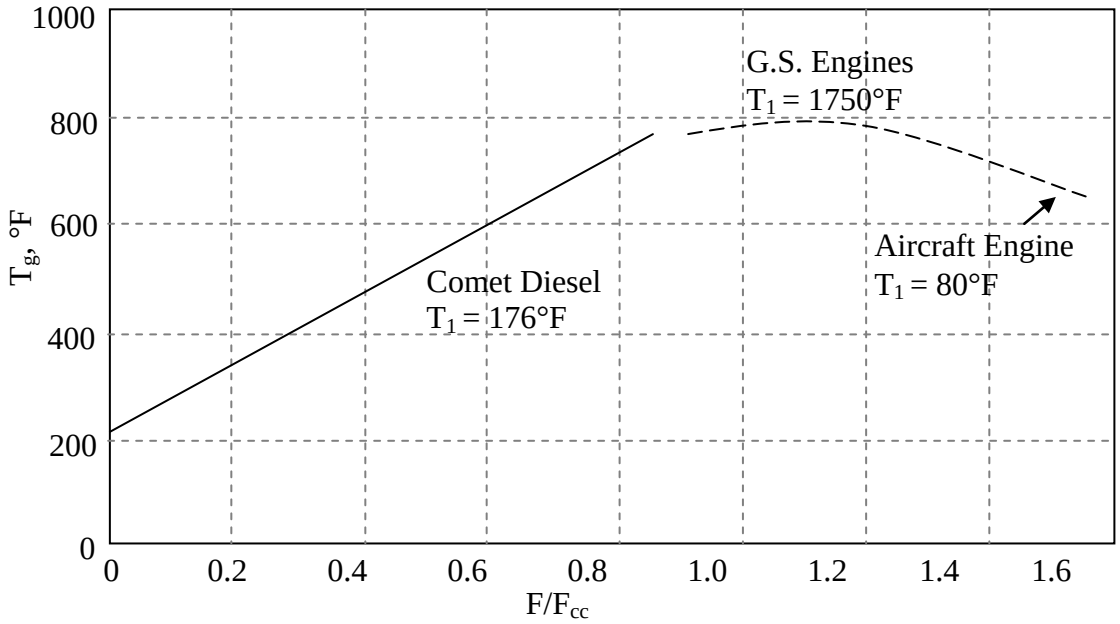

Figure 4.15: Mean effective gas temperature versus fuel-air ratio for a comet diesel engine, a G.S. engine and aircraft engine at compression ratio of 5.74, 5.74 and 13 respectively (reproduced from "Heat Transfer in Internal Combustion Engine" by C.F. Taylor and Tau-Yi Toong, 1958, pp. 15).

For convenience, the piston area has been selected rather than the actual heat transfer area. For an internal combustion engine, the equation for the overall heat transfer coefficient, U, between the combustion gases and the liquid coolant becomes

$$\frac{1}{UA_p} = \frac{1}{h_g A_g} + \frac{t_w}{K_w A_e} + \frac{1}{h_c A_c} \tag{4.10}$$

where h_g is the convective heat transfer coefficient of the combustion gases, A_g is the inner surface area of the combustion cylinder, h_c is the convective heat transfer coefficient of the coolant, and A_c is the surface area on the coolant side of the combustion cylinder, The parameters A_e, K_w, and t_w denote the effective conduction heat transfer area, the thermal conductivity of the engine block material, and the combustion chamber wall thickness, respectively. Equation (4.10) can also be written as

$$\frac{1}{U} = A_p\left(\frac{1}{h_g A_g} + \frac{t_w}{K_w A_e} + \frac{1}{h_c A_c}\right) \tag{4.11}$$

The multiplication of, A_p, with the right hand side of Equation (4.11) yields

$$\frac{1}{U} = \frac{1}{h_g}\left(\frac{A_p}{A_g}\right) + t_w\left(\frac{1}{K_w}\right)\left(\frac{A_p}{A_e}\right) + \frac{1}{h_c}\left(\frac{A_p}{A_c}\right) \tag{4.12}$$

Multiplying the Equation (4.12) by thermal conductivity of combustion gases, K_g the equation becomes

$$K_g\left(\frac{1}{U}\right) = K_g\left(\frac{1}{h_g}\left(\frac{A_p}{A_g}\right) + t_w\left(\frac{1}{K_w}\right)\left(\frac{A_p}{A_e}\right) + \frac{1}{h_c}\left(\frac{A_p}{A_c}\right)\right) \tag{4.13}$$

Dividing the Equation (4.13) by the engine combustion chamber bore size, b,

$$K_g\left(\frac{1}{b}\right)\left(\frac{1}{U}\right) = \frac{K_g}{b}\left(\frac{1}{h_g}\left(\frac{A_p}{A_g}\right) + t_w\left(\frac{1}{K_w}\right)\left(\frac{A_p}{A_e}\right) + \frac{1}{h_c}\left(\frac{A_p}{A_c}\right)\right) \tag{4.14}$$

Multiplying last term of Equation (4.14) by $\left(\frac{K_c}{K_c}\right)$

$$\left(\frac{K_g}{b}\right)\left(\frac{1}{U}\right)=\left(\frac{K_g}{b}\right)\left(\frac{1}{h_g}\right)\left(\frac{A_p}{A_g}\right)+\left(\frac{t_w}{b}\right)\left(\frac{K_g}{K_w}\right)\left(\frac{A_p}{A_e}\right)+\left(\frac{K_g}{K_c}\right)\left(\frac{K_c}{h_c}\right)\left(\frac{1}{b}\right) \quad (4.15)$$

Assuming $A_p = A_g = A_c$ the Equation (4.15) can be written as

$$\left(\frac{K_g}{b}\right)\left(\frac{1}{U}\right)=\left(\frac{K_g}{b}\right)\left(\frac{1}{h_g}\right)+\left(\frac{t_w}{b}\right)\left(\frac{K_g}{K_w}\right)\left(\frac{A_p}{A_e}\right)+\left(\frac{K_g}{K_c}\right)\left(\frac{K_c}{h_c b}\right) \quad (4.16)$$

The Nusselt number is given by

$$N_u = \frac{hb}{K} \quad (4.17)$$

In Equation (4.16), the terms on the right hand side can be written in terms of Nusselt numbers as:

- For gas side convective heat transfer (Term #2) $\left(\frac{K_g}{b}\right)\left(\frac{1}{h_g}\right)=\frac{1}{N_g}$ (4.18)
- For coolant side convective heat transfer (Term #4) $\left(\frac{K_c}{b}\right)\left(\frac{1}{h_c}\right)=\frac{1}{N_c}$ (4.19)
- For overall Nusselt number (Term #1) $\left(\frac{K_g}{b}\right)\left(\frac{1}{U}\right)=\frac{1}{N_U}$ (4.20)

For an overall Nusselt number, N_u, the heat transfer expression becomes

$$\left(\frac{1}{N_U}\right)=\left(\frac{1}{N_g}\right)+\left(\frac{t_w}{b}\right)\left(\frac{K_g}{K_w}\right)\left(\frac{A_p}{A_e}\right)+\left(\frac{K_g}{K_c}\right)\left(\frac{1}{N_c}\right) \quad (4.21)$$

where N_g and N_c are the gas side and coolant side Nusselt numbers, respectively. The ratio of the piston and conduction heat transfer areas, $\left(\frac{A_p}{A_e}\right)$, can be obtained from standard plots, while the thermal conductivities for the gas and coolant, K_g and K_c, can be obtained from reference books.

The combustion gas temperature, T_g, can help determine Reynolds number for the combustion gases, $R_{e,g}$, using standard graphs of similar engine combustion process. This Reynolds number can be used to obtain the Nusselt number using the standard Nusselt number versus Reynolds number plots. Using Equation (4.21), the Nusselt number for the coolant side can be calculated. Equation (4.17) for the Nusselt number can be used to calculate the convective heat transfer coefficients, h_g and h_c, for the engine used in the experimental setup.

Attention will now be focused on the performance of the fan within the cooling system to better understand the air flow and corresponding electric motor speed. A sample fan speed, N, of 3,000 RPM was selected for Test #6 configurations in Table 4.1. The total heat rejected by all six fan, $\dot{Q}_{OUT}$, using an experimental analysis was 81 KW (refer to Table 4.2). These fans displayed an average air speed of $v_{air,exp}$ = 4.0 m/sec (refer to Appendix B - Figure B3).

The corresponding analytical relationship may be stated as

$$\dot{Q}_{OUT} = \dot{m}_{air} C_P \left(T_{SINK} - T_{air} \right) \tag{4.22}$$

where $\dot{m}_{air}$ is the mass flow rate of the air in kg/sec, T_{SINK} is the exit air temperature for the wind tunnel it (observed to be T_{SINK} = 40°C), T_{air} is the air temperature at the radiator inlet (observed to be T_{air} = 22°C), and C_P is the specific heat of the air at as average air temperature of $T_{AVE} = \frac{T_{SINK} + T_{air}}{2}$ = 31°C.

Fluid Property	Symbol	Parameter Value
Density	ρ_{air}	1.1 kg/m^3
Specific heat	C_P	1 KJ/kg°C
Thermal Conductivity	K	0.025W/m°C
Kinematic viscosity	V	1.6×10^{-6}m^2/sec
Prandtl`s number	P_r	0.713

Table 4.7: Fluid properties for ambient air at T_{AVE} = 31°C

The observed values and the specific heat of the air from Table 4.7 may be substituted in to Equation (4.22) for the given heat transfer conditions. The resulting mass flow rate, $\dot{m}_{air}$ is calculated as $\dot{m}_{air}$ = 4.5 kg/sec. The mass flow rate can be converted to discharge, (i.e., the volume flow rate) using the relationship

$$\dot{q}_{air} = \frac{1}{\rho_{air}}\dot{m}_{air} \tag{4.23}$$

where $\dot{q}_{air}$ is the volume flow rate in m^3/sec. For an air density of ρ_{air} = 1.1 kg/m^3 at T_{AVE} = 31°C, the volume flow rate were calculated as, $\dot{q}_{air}$ = 4.09 m^3/sec.

The air flows through the radiator which has a height of 1.1 m and a width of 1 m. The air flow surface area, A_r through this radiator is approximately A_r = 1.1 m^2. The volume flow rate, $\dot{q}_{air}$, in Equation (4.23) can also be expressed as

$$v_{air} = \frac{\dot{q}_{air}}{A_r} \tag{4.24}$$

where v_{air} is the air speed through the radiator (m/sec). Substituting the values for the area, A_r, and the discharge, $\dot{q}_{air}$, into Equation(4.24), the analytical air speed becomes, $v_{air,ana}$ = 3.68m/sec. The experimental sir flow rate was 4.0 m/sec so a 0.32 m/sec

difference exists or a change of 8%. Remember that the heat rejection rate was 81KW (6 fans) with this fans air speed.

The experimental and analytical results for the fan motor speeds 1,000-5,000 RPM of Test #6 configuration have been presented in Table 4.8.

Test #6 Fan speeds (RPM)	Actual Heat Rejection (KW)	Analytical Air Speed, v_{air} (m/sec)	Actual Air Speed Range (m/sec); Average	Fan Motor Speed, N (RPM)
1,000	37	1.68	0.25 – 1.74; 0.99	1,589
2,000	62	2.82	0.43 – 3.31; 1.87	2,615
3,000	81	3.68	0.61 – 4.92; 2.7	3,435
4,000	94	4.27	0.75 – 7.43; 4.09	4,000
5,000	108	5.0	2.85 – 9.48; 6.16	4,666

Table 4.8: Summary of results for Test #6 configuration with fans running at 1,000 – 5,000 RPM for analytical and measured air speeds

The total volume flow rate, $\dot{q}_{air}$, through the radiator from the fan matrix can also help determine the fan motor required speeds. The volume flow rate, $\dot{q}_{air}$, in (m^3/sec), obtained from Equation (4.23) is generated by multiple fans. Thus, the flow rate of a single fan, $\dot{q}_{air,i}$, is calculated based on number of fans, n_{fan}, operating in the given test configuration

$$\dot{q}_{air,i} = \left(\frac{\dot{q}_{air}}{n_{fan}} \right) \tag{4.25}$$

For Test #6 configuration at an observed fan speed of 3,000 RPM, the air discharge was, $\dot{q}_{air}$ = 4.09 m^3/sec, so the individual fan discharge , $\dot{q}_{air,1}$ = 0.67 m^3/sec.

The speed, N, required for a single axial fan to generate volume flow rate, $\dot{q}_{air,i}$, is given by (Jorgensen , 1982)

$$N=\frac{\dot{q}_{air,i}}{4\pi^2 r_m{}^3 \Phi_m}\left(\frac{1+v^2}{1-v^2}\right) \tag{4.26}$$

where, r_m is the mean radius, v is the hub ratio and Φ_m is the flow rate coefficient. This first term in Equation (4.26) may be calculated using the tip and hub radius, r_t and r_h, respectively so that

$$r_m = \sqrt{\left(\frac{r_t^2 + r_h^2}{2}\right)} \tag{4.27}$$

The mean radius for a single fan in the experimental systems was calculated as, r_m = 0.1m based on tip and hub radius of, r_t = 0.14m and r_h = 0.04m. The hub ratio, v, can be expressed as, $v = \left(\frac{r_h}{r_t}\right)$, so v = 0.285. The flow rate coefficient, Φ_m, is obtained from standard plots for optimum values. In the study, Φ_m = 0.006, was selected from standard fan characteristic plots for low pressure developing axial flow fans (Jorgensen, 1982). Substituting the values obtained for the mean radius, r_m, the hub ratio, v, and the flow rate coefficient in Equation (4.26), the required fan speed was, N = 3,435 RPM. When compared to Table 4.8 entry for actual fan speed of N = 3,000 RPM, the difference is 435 RPM or 14.5% which may be attributed to the selection of Φ_m.

The heat transfer relations between different components in an engine cooling system starting from engine combustion to the radiator heat rejection to the atmosphere has been presented. The heat load to the coolant in the cooling system by an engine combustion process using a given air fuel ratio is in given by Equations (4.9) to (4.21). Equations (4.22) to (4.24), give the air volume flow rate required to achieve heat rejection equal to the heat addition by the engine combustion process. The Equations (4.25) to (4.27) help determine the fan speeds required to achieve the required volume flow rate of ambient air.

The total area of the radiator used for heat rejection is represented by, $A_r = Y \times X$ (refer to Figure 4.16). The variables, Q_{IN}, is the heat addition to the radiator, Q_{OUT} is the heat rejected by radiator fins and Q_{HEAT} is the residual heat circulated back to the circuit. An ideal radiator operation would reject all heat input, $Q_{IN} = Q_{OUT}$; however, some heated fluid circulates back to the engine, Q_{HEAT}, increasing the temperature level of engine in operation. This residual heat is important factor which determines engine performance and emissions. For example, higher Q_{HEAT} will help a faster engine warm up under cold weather conditions while a lower Q_{HEAT} in desert regions prevents engine from overheating.

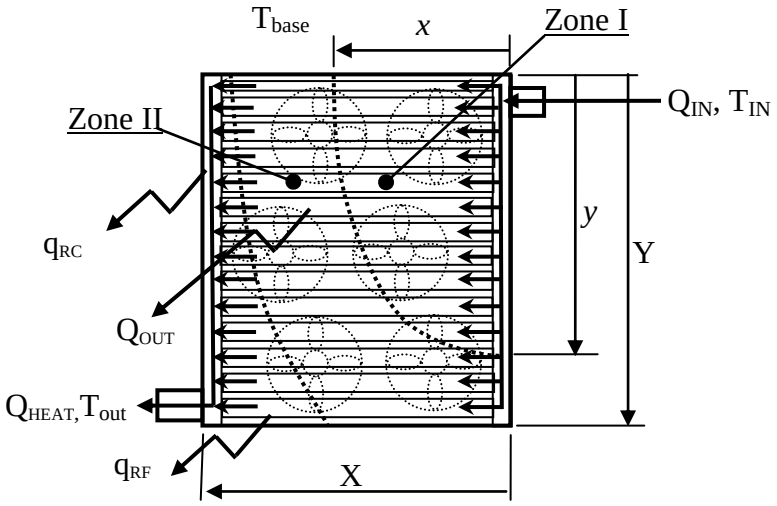

Figure 4.16: Radiator temperature zones, flow path, and general dimensions. Rear side view if radiator with fan matrix behind the radiator

Although the radiator is designed to maximize the heat rejection, the side channels have no fins and, thus, a very small low rejection rate, q_{RC}. Let the radiator fin heat rejection rate be, q_{RF}. Since $Q \propto \Delta T$, where ΔT is the temperature difference responsible for heat transfer, the temperature level falls as the heated coolant travels down the side channel. Thus, the side channel experiences descending temperature levels from the top input to the bottom of the radiator. It can be inferred that the temperature level, T, is inversely proportional to the distance Y and X indicated in Figure 4.17 from the radiator inlet, Q_{IN}. Similarly the radiator surface can be divided into different temperature zones. For example, zone indicated by x and y in Figure 4.17. Based on these distances and a decision for a given fan matrix, the fan motor speeds can be determined.

To verify the heat rejection rate obtained from the radiator in the test runs, a mathematical model for calculating the theoretical heat rejection based on heat transfer between coolant and air flow obtained from a geometrically similar radiator was calculated.

4.2 Wind Tunnel Speed Measurements

The air speed through the fins of the radiator determines the rate of the heat transfer between the ambient air, T_∞, and the circulating coolant, T_c. This speed profile across the length and width of the radiator for forced convection involving multiple fans differs from that of single fan forced convection scenario. The data representations of this air speed are presented in this Section. The fan matrix combinations used for the experiments are summarized in the Table 4.9.

Test No.	Fan Configuration.	Fan Motor Speed	Points On X-Axis	Points On Y-Axis	Total Measurement Points
		RPM	-	-	-
11	1-2-3-4-5-6	1,000	11	13	143
		2,000			
		3,000			
		4,000			
		5,000			
12	1-2	1,000			
		5,000			
13	3-4	1,000			
		5,000			
14	5-6	1,000			
		5,000			
15	1-3-5	1,000			
		5,000			
16	2-4-6	1,000			
		5,000			

Table 4.9: Air velocity measurements test matrix for different fan and speed combinations

For a single fan, the measurement is usually taken from a number of radially distributed points at varying distances from the fan hub to achieve an accurate air speed plot using a minimum number of measurement points. For the research

reported here, a dense measurement matrix for capturing the majority of the speed variations was assumed to be parallel to the radiator frontal plane (refer to Figure 4.17). The matrix of data collection points included 13(78.74 mm apart) × 11(80.00 mm apart) points for total of a 143 data point.

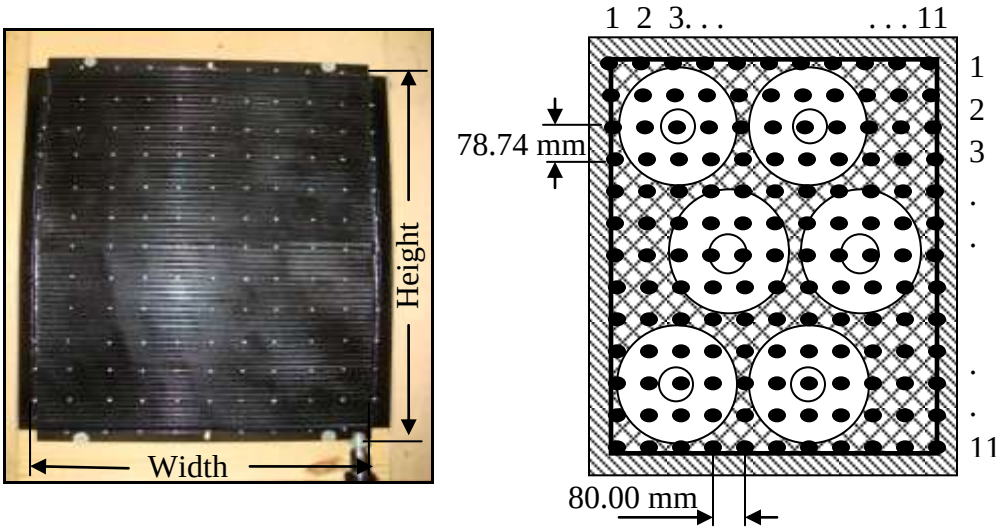

Figure 4.17: Matrix of points assumed on the radiator frontal area used as location points to measure air velocity. Note the radiator view shown is from rear side with fan matrix located behind the radiator

As the speed profile may be influenced by the Reynolds number, R_e, disturbances in the flow path and the boundary of the flow channel; in the current setup, there was no obstruction in the wind tunnel to the air flow. A clearance of 7.5 inches (190.5 mm) from the radiator as well as the walls of the wind tunnel was provided. The speed was measured at an offset distance which is before the flow reached the walls of the wind tunnel. The data collection format is has been listed in Table 4.10.

Fan Air Speed (m/sec) for Test #11 Speed 5,000 RPM											
Point	1	2	3	4	5	6	7	8	9	10	11
1	0	0	0	0	0	0	0	0	0	0	0
2	0	9.18	8.884	9.485	6.732	6.624	6.627	6.499	6.134	6.887	0
3	0	6.896	2.856	8.889	8.352	8.537	5.868	0.713	5.445	7.325	0
4	0	7.465	7.013	7.056	5.981	6.665	7.671	6.801	7.348	8.035	0
5	0	8.029	7.605	7.413	6.967	5.709	7.053	7.23	7.743	8.376	0
6	0	7.501	8.545	7.041	7.118	7.771	7.328	8.652	7.368	8.787	0
7	0	9.083	8.824	3.227	3.156	8.823	8.694	8.633	6.103	6.293	0
8	0	8.041	8.182	6.961	7.494	8.448	6.924	8.082	6.418	8.205	0
9	0	7.447	7.924	8.29	7.051	7.485	6.148	7.678	8.007	8.196	0
10	0	8.076	7.738	8.052	5.864	7.44	6.338	6.773	8.092	7.503	0
11	0	7.875	5.238	7.976	6.256	7.488	7.542	4.433	5.782	8.058	0
12	0	8.262	3.406	7.153	8.616	7.575	8.173	7.536	6.04	8.608	0
13	0	0	0	0	0	0	0	0	0	0	0

Table 4.10: Experiemntal air speed data in m/sec for the point matrix on the radiator frontal area for Test #11 at a speed of 5,000 RPM.

In Figure 4.18, the lines along the Z–axis of the plot indicate the speed value at the matrix point on the radiator. The speed lines covering the complete radiator surface generated a point cloud, with the point located at the extreme end of this speed line indicating the magnitude recorded by the air velocity sensor. This point cloud was used to construct a surface indicating the three dimensional air speed profile developed over the frontal area of the radiator by a given fan matrix. This speed profile can then be integrated over the entire surface of the radiator and used to determine the total flow rate for the different fan configurations at different operating speeds in the wind tunnel.

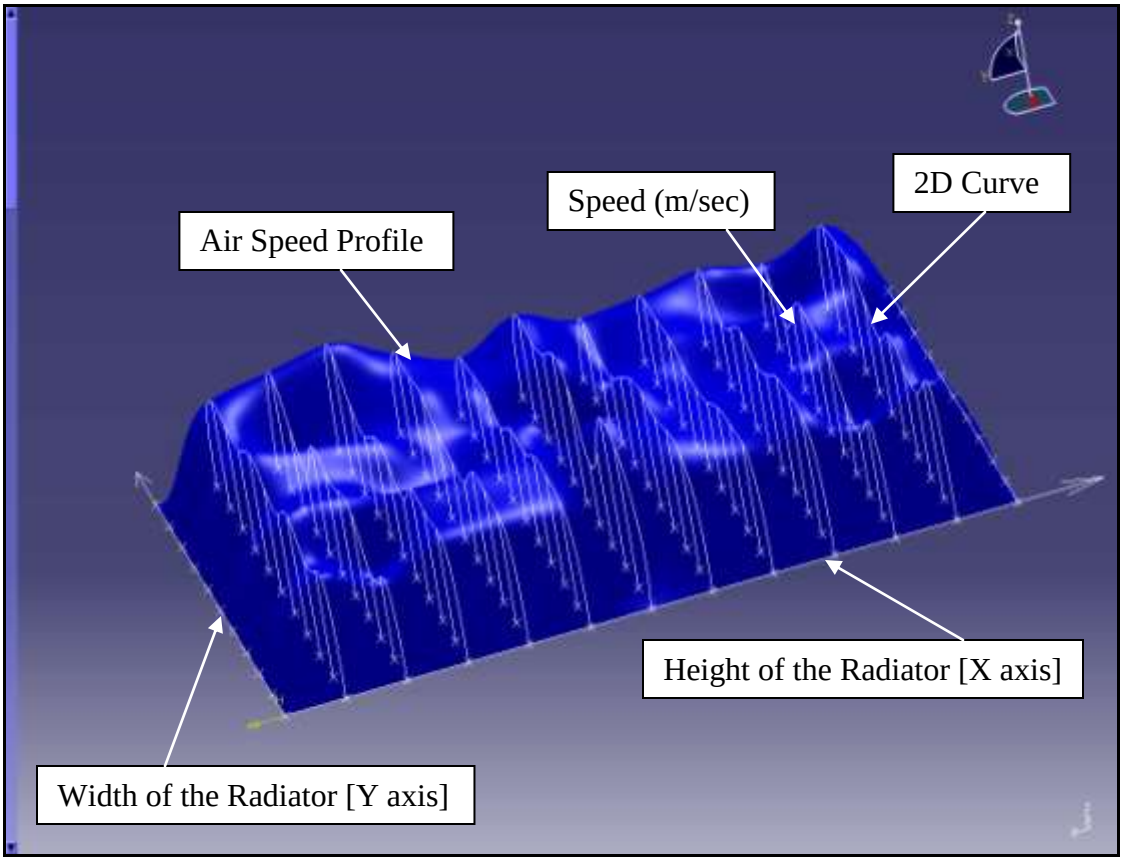

Figure 4.18: Speed profile construction using CATIA for Test #11 at 3,000 RPM

The surface was constructed in CATIA software application using the following procedure; curve fitting was done using the points in each of the rows of the measurement matrix. The 11 curves formed in addition to 2 straight lines representing nil air speed at the extreme edges of the radiator, were used to generate the speed profile surface. The 15 air speed profiles generated by the fan matrix configurations seen in Table 4.9 can be found in the Appendix B. These speed profiles, which provided a complete picture of the air flow development over the radiator, were subsequently used to calculate the average air speeds using various fan configurations.

CHAPTER FIVE

CONCLUSION AND FUTURE RESEARCH

The reconfigurable cooling system setup in the Department of Mechanical Engineering at Clemson University was build to study and analyze of a multiple fan radiator cooling system. The setup was used to conduct extensive experiments to analyze thermal behavior and air speed characteristics from a multiple radiator fan matrix. The observations based on the data obtained from tests conducted helped to analyze relations between the various system variables, (for example, the power consumption, heat rejection, fan speeds, and fan configurations). These experimental procedures can be used to model and predict the performance of similar radiator cooling systems. The unique test bench created and used here can help guide the design of similar experiments in the future.

5.1 Summary

The heat rejection versus fan power consumption plots provide a visual representation of the energy efficiency of the fan motor matrix and helps to assess the system behavior. The overall trend indicates that the more fans which operate in the matrix, then the larger the heat rejection capacity of the radiator. The heat rejection capacity of the system also increases with an increase in fan speed; however, the heat rejection rate drops with an increase in fan motor RPM, this is evident from the decreasing slope of the curves representing all the test configurations (refer to Figure 4.7). This inversely proportional relation with the heat rejection capacity remains the

same for all fan configurations. In addition, the multiple fan matrix in the test setup reported here exhibits more efficiency with fewer fans operating below a heat rejection rate of 55 KW. Thus, there is a heat rejection limit for a given fan motor matrix above which more operating fans are needed to increase the heat rejection capacity. Above 55 KW, the results indicate higher efficiency obtained only by using more fans, the increase in efficiency being substantial, a maximum of 50% being observed. Fan laws indicate that higher speeds demand proportionally higher power for operation ($P \propto N^3$), and power is proportional to the fan motors in operation ($P \propto$ Number of fan motors); thus, for more number of fans operating at lower speeds, the power consumption is lower than with fewer fans at higher speeds. However, this gap closes below 3000 RPM, and this conclusion is not valid below speeds of 1500 RPM using the current setup.

Similar to previous research, the independent control of the electric actuators used here was found to improve the overall efficiency. The variable speeds achieved using the Plus+1 controller and the BLDC power controller adjusted air flow over the radiator not directly coupled to the engine speed, preventing the loss of energy that usually occurs in an engine coupled fan radiator system due to the uncontrolled air flow over all the radiator regions. The comparison of different fans motor combinations with a fixed number of fan motors in operation indicates that operating fans in the high temperature regions of the radiator improves heat rejection. The reduction in energy consumption achieved was found to be upto 38% of the heat rejection capacity. As discussed in Chapter 4, the power consumption by the for heat

rejection rate of 48 KW, Test #7 consumes 0.68 KW while Test #2 needs 0.42 KW (refer to Figure 4.10), this illustrates a power saving of 38% using Test #2 fan configuration. In addition, this comparison study of power consumption versus heat rejection by various fan combinations indicates that operating the fans near the heat input source, i.e the radiator inlet, reduces the energy consumption of the fan matrix for a given heat load.

The air speed profile constructed in this study indicates a better flow distribution using multiple fans rather than a single larger fan. Since fans generate a lower air speeds near their hubs, a single large fan creates a significant decrease in air speed at the central portion of the radiator. With a fan matrix arrangement and an increased number of fans, the flow was observed to be more uniform across the radiator face. This larger number of fans forming a matrix was observed to minimize the lower air speed zone at the fan hub. Thus, a fan matrix arrangement was found to be more effective than a single large fan in generating the required air flow over a targeted high temperature region on a given radiator face area. The fan motor matrix run at higher speeds was also observed to build-up a positive pressure behind the radiator in range of 0-49 Pa; this positive pressure difference between the two sides of the radiator can help generate a uniform air flow over the radiator.

Air speed measurement tests conducted operating a single row or column of the fans was observed to generate considerable flow in the radiator regions where the fans were inoperative. At higher fan speeds the air speed profile indicates flow generated in range of 0.2 to 3.35 m/sec, leading to the conclusion that while targeting

high temperature regions on the radiator, the fan matrix provides sufficient residual air to the lower temperature zones. As Figure 4.5, showing the individual fan motor power consumption indicates, eliminating the activation of a single fan motor results in a minimum power saving of 50 Watts.

The data plots helped verify the validity of the system performance and to identify the errors, if any, in data collection by the sensors and the data acquisition equipment. It was observed during the test runs that the power consumption by each fan motor remains within a small range at any given fan speed, a situation found to be same for any fan combination with equal numbers of actuators. Thus, using this observation, the power requirement can be predicted for each actuator added to the fan motor using this observation.

The test runs conducted using this experimental setup helped understand the thermal aspects of a six fan matrix radiator cooling system. The results indicate improvement in energy efficiency using multiple fan radiator systems, suggesting the potential for this matrix to be an effective method of controlling coolant temperatures under most engine operating conditions.

5.2 Future Research

Future research could be conducted to develop a multiple fan cooling system for practical vehicle application. Such investigations would require tests involving standard engine operating cycles, coolant varieties, variation in fan matrices and the

corresponding flow profiles, ram air effects due to vehicle speed, and ease of integrating the controllers in a vehicle communication systems.

While experiments reported here involve a constant heat input into the radiator cooling system, in actual engine operation this is not the case; thus, the heat input could be varied in future experiments using standard engine operating cycles. A selection algorithm based on the current study could be used to select the fans in the matrix and to determine their speeds. This selection algorithm could also be investigated for varying heat loads, modified and tuned to particular engine requirements. In addition, various coolant combinations having different heat capacities could be investigated. This type of study would further modify the algorithm by taking into account the coolant properties. Coolants with different heat capacities and maximum temperature levels could be tested to determine the heat loss and heat gain at different fan speeds. Such trials would help determine proper coolant combinations and would improve the control algorithm by taking into account its physical properties.

In the air speed experiments, it was observed that more fans in a matrix helped generate a uniform air speed profile, allowing higher heat rejection from a given radiator heat transfer surface. The presence of a number of fans in the fan matrix was also observed to help direct localized air flow over the highest temperature region of the radiator, a primary factor contributing to the improved energy efficiency. Thus, further research needs to be conducted on test configurations including an increasing

number of fans, analyzing the air speeds they generate. The increased number of fans may provide more combinations in a fan matrix for achieving a desired air flow. However, an increased number of small fan motors may not be feasible since they consume more power for the same flow velocities generated using fewer actuators. Since blade sizes will be smaller in such a matrix to accommodate more fans, the implication on peak axial air velocities generated should also be investigated.

The most effective strategy found here for achieving improved cooling with reduced fuel consumption was to expose the highest temperature region on the radiator to the maximum air flow. Mounting thermal sensors in a matrix on the radiator face may provide additional information on the temperature level at a given location of the radiator at a given time. This feedback could be useful as a real-time update helping to select the fans closest to the high temperature region, in addition, the fan speeds could be selected using a look-up table. The higher the density of the sensor array on the radiator face, the better the accuracy in determining the temperature zones on the radiator however, the data processing capabilities of the controller would determine the optimum size of such an array.

Multiple fan matrices could be investigated using an external ram air source supplied by a wind tunnel of velocity equal to that encountered by a vehicle at a given speed. As the engine speed is related to the vehicle speed, the radiator could be provided with heat rejection load corresponding to particular engine load. Such a test platform would provide an opportunity to simulate and record actual cooling system

performance. Alternately, a multiple fan matrix cooling system could be mounted on a moving vehicle to generate the ram air effect and the engine heat rejection load as per the driving conditions.

A multiple fan radiator cooling system can potentially be used in mobile as well as stationary engine generator applications. This multiple fan cooling system, which requires a control algorithm to make decisions, could be achieved using an on-board microprocessor. Currently, the MATLAB/Simulink algorithm developed here could be fed into C codes, or an electronic circuit could be designed equivalent to the current decision models. The system in the experimental setup could communicate using CAN format, which is a standard method of control signal transfer in modern vehicles. In the current setup discussed in literature, the BLDC motors used these signals to operate the fan motor matrix; however the BLCD motors and individual power supply units (BLDC controller) may add weight that could reduce the fuel efficiency of the vehicle; however this weight would not be a criterion for stationary engine generator applications.

APPENDICES

Appendix A

Thermal Management System Test Results

The temperature plots constructed using the data collected during the experimental test runs (refer to Table 4.1) will be presented in this Section.

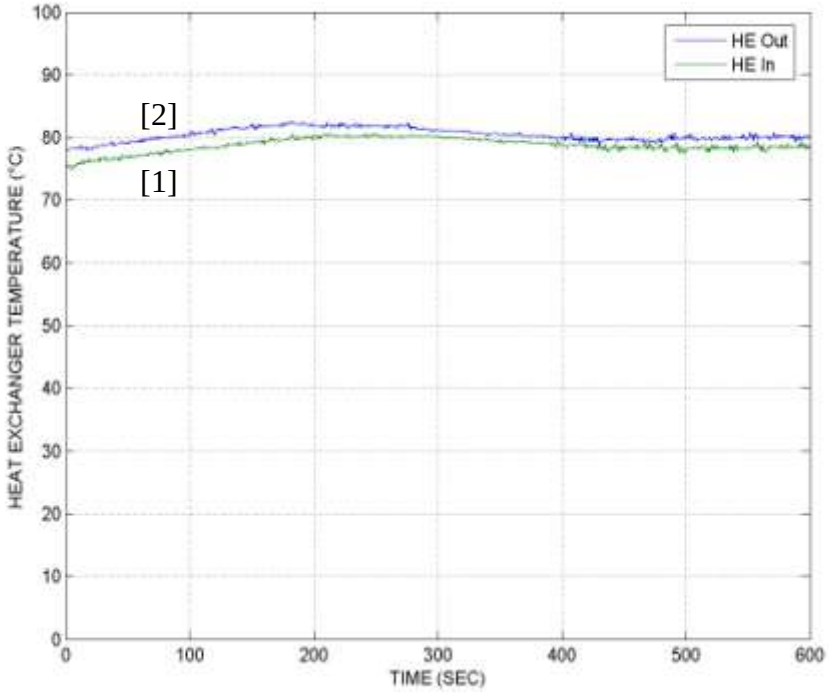
HE Out
HE In
[2]
[1]
HEAT EXCHANGER TEMPERATURE (°C)
TIME (SEC)
0
10
20
30
40
50
60
70
80
90
100
0
100
200
300
400
500
600

(a)

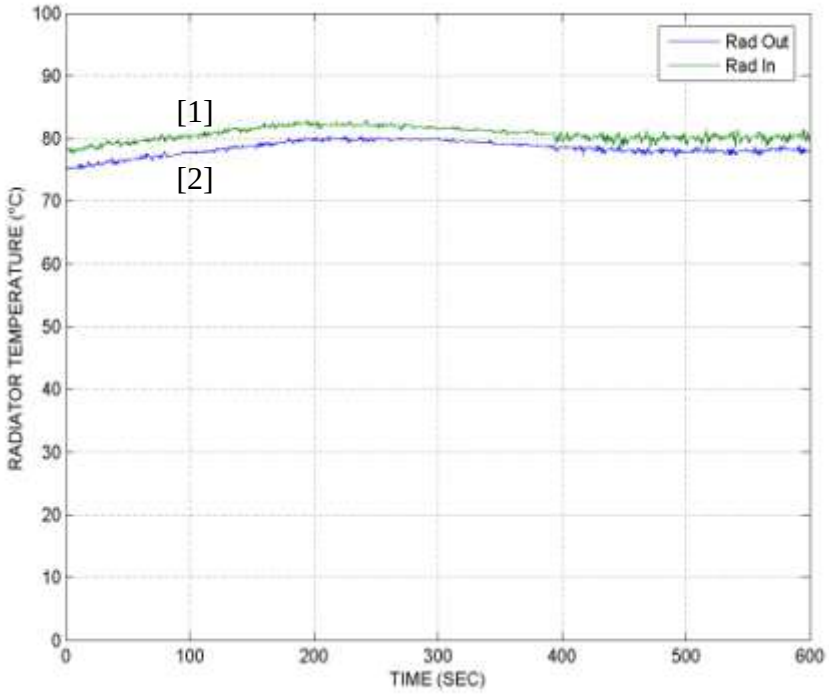
Rad Out
Rad In
[1]
[2]
RADIATOR TEMPERATURE (°C)
TIME (SEC)
0
10
20
30
40
50
60
70
80
90
100
0
100
200
300
400
500
600

(b)

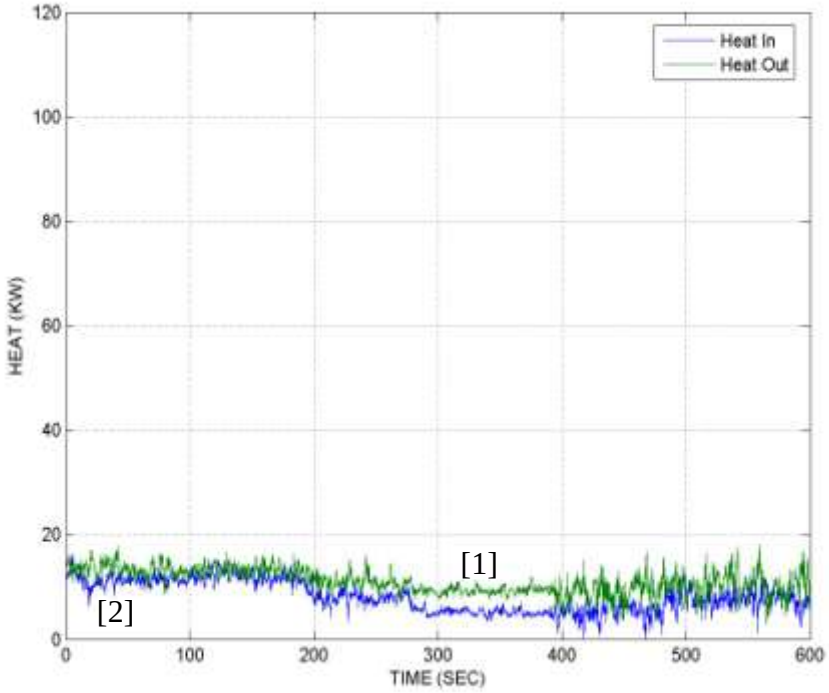

(c)

Figure A.1: Temperature and heat plots for Test #1 configuration at 1,000 RPM (a) heat exchanger inlet [1] and outlet [2] temperature, (b) radiator inlet [1] and outlet temperature [2] and, (c) heat input [1] and heat rejected [2].

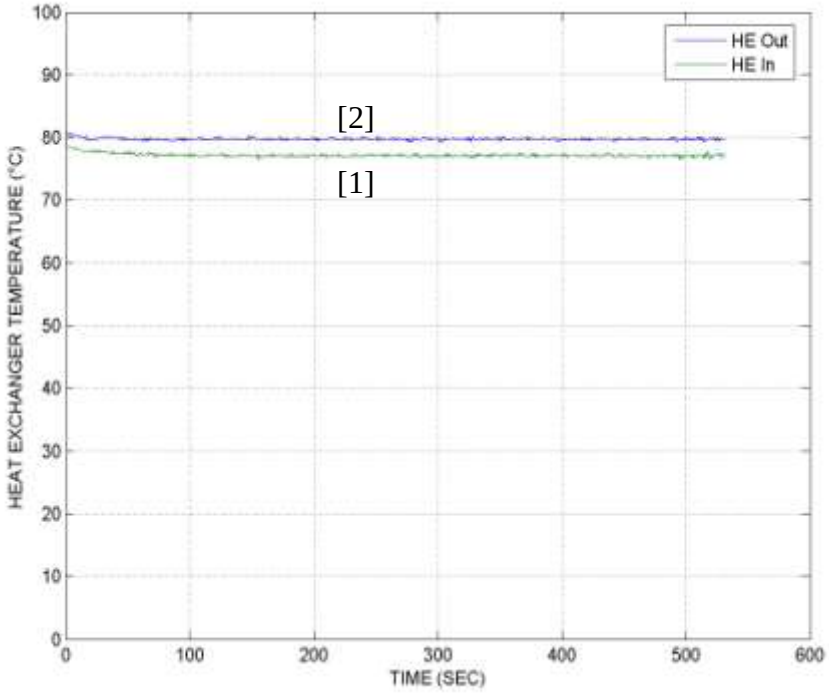
HE Out
HE In
[2]
[1]
HEAT EXCHANGER TEMPERATURE (°C)
TIME (SEC)
0
10
20
30
40
50
60
70
80
90
100
0
100
200
300
400
500
600

(a)

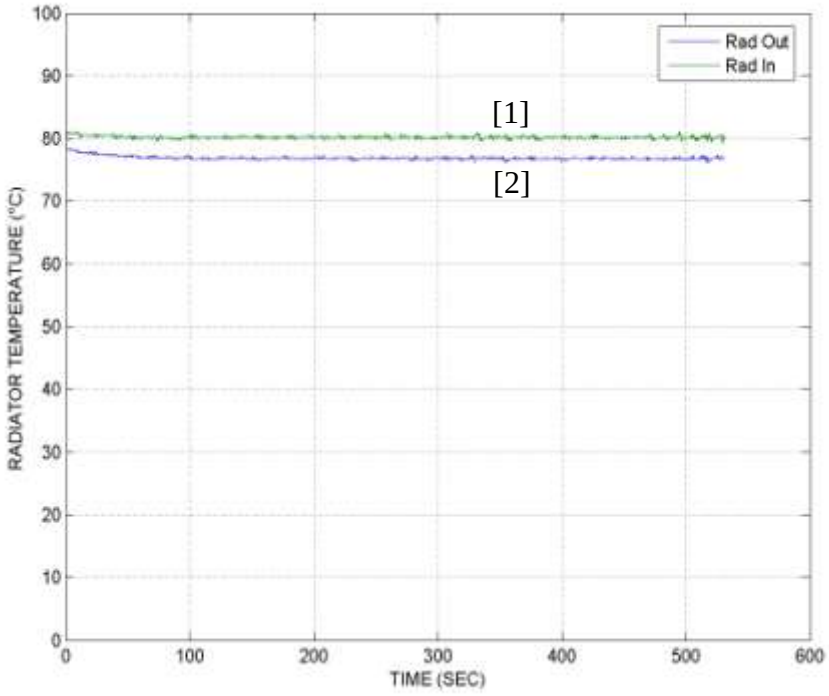
Rad Out
Rad In
[1]
[2]
RADIATOR TEMPERATURE (°C)
TIME (SEC)
0
10
20
30
40
50
60
70
80
90
100
0
100
200
300
400
500
600

(b)

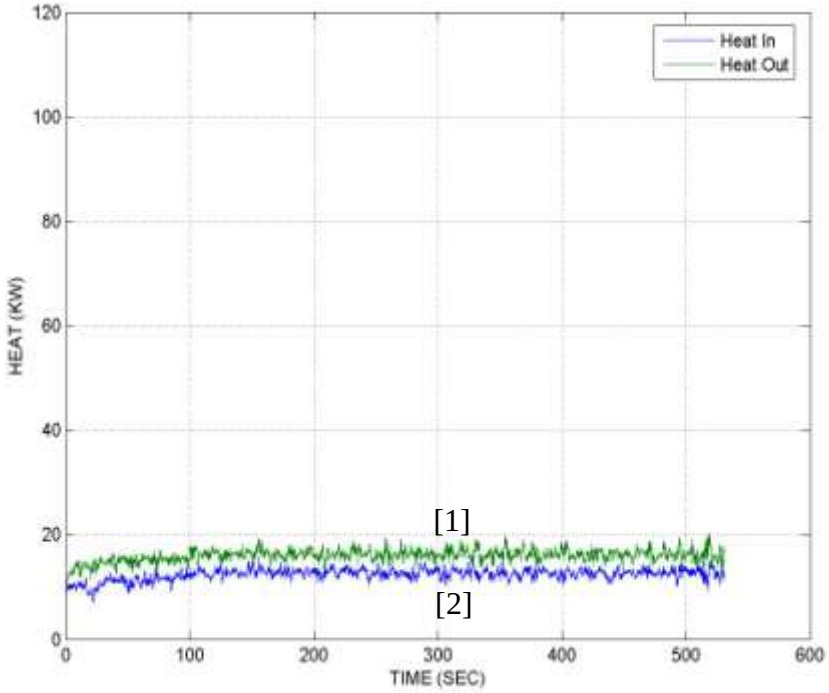

(c)

Figure A.2: Temperature and heat plots for Test #1 configuration at 2,000 RPM (a) heat exchanger inlet [1] and outlet [2] temperature, (b) radiator inlet [1] and outlet temperature [2] and, (c) heat input [1] and heat rejected [2].

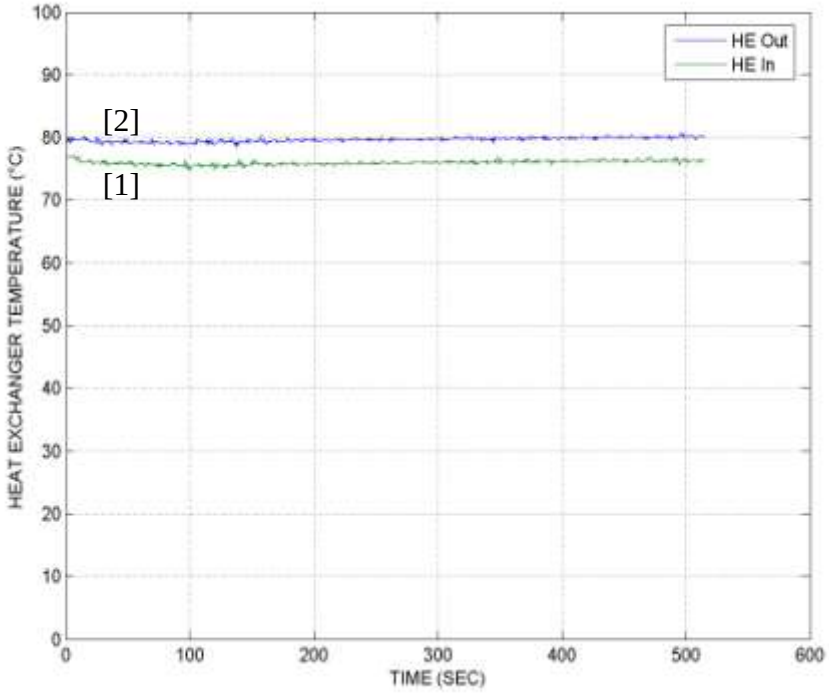
HE Out
HE In
[2]
[1]
HEAT EXCHANGER TEMPERATURE (°C)
TIME (SEC)
0
10
20
30
40
50
60
70
80
90
100
0
100
200
300
400
500
600

(a)

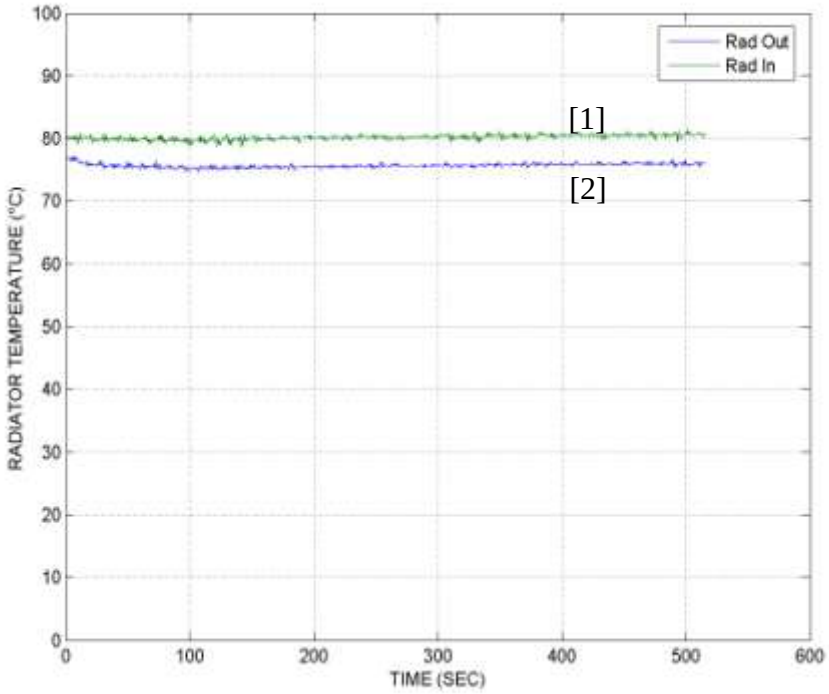
Rad Out
Rad In
[1]
[2]
RADIATOR TEMPERATURE (°C)
TIME (SEC)
0
10
20
30
40
50
60
70
80
90
100
0
100
200
300
400
500
600

(b)

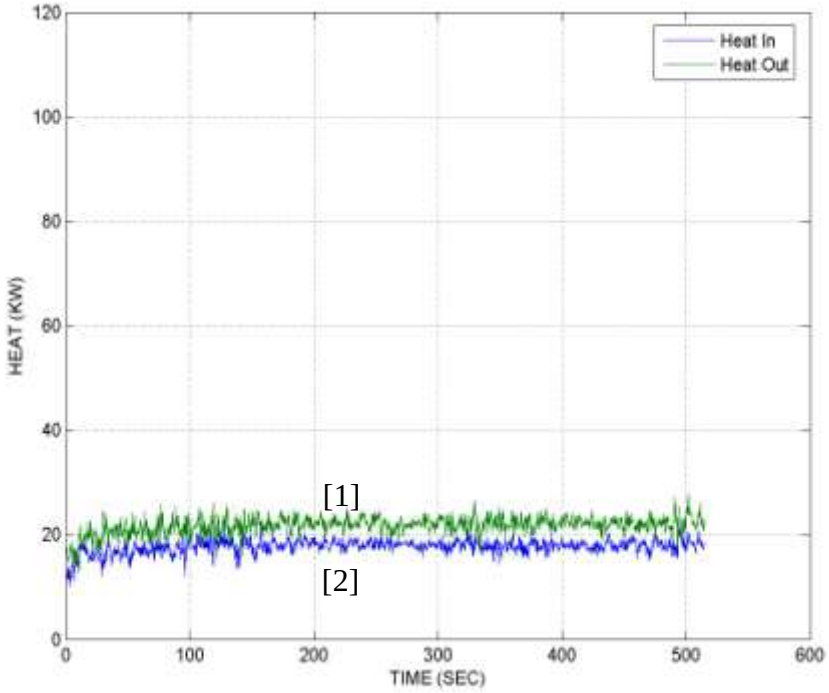

(c)

Figure A.3: Temperature and heat plots for Test #1 configuration at 3,000 RPM (a) heat exchanger inlet [1] and outlet [2] temperature, (b) radiator inlet [1] and outlet temperature [2] and, (c) heat input [1] and heat rejected [2].

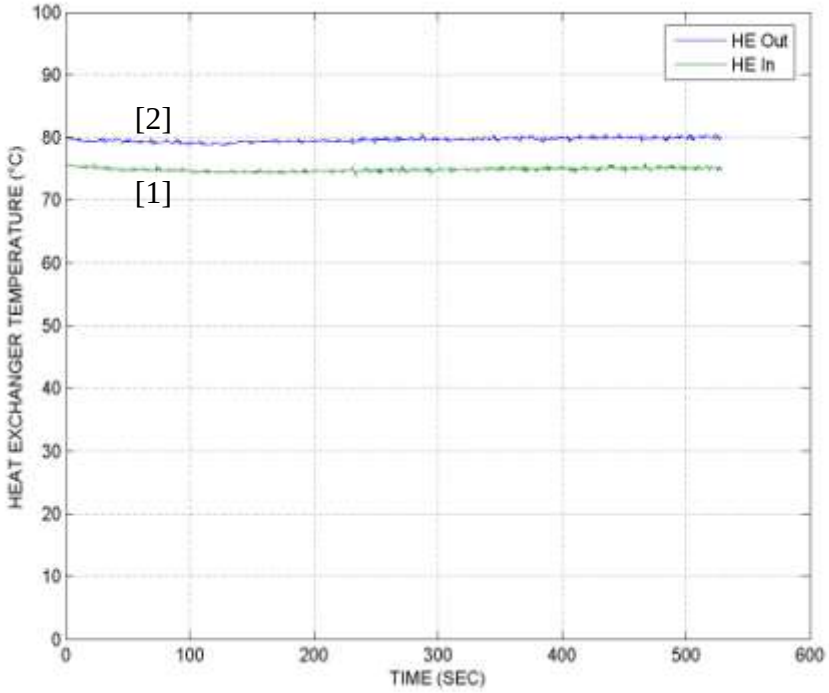
HE Out
HE In
[2]
[1]
HEAT EXCHANGER TEMPERATURE (°C)
TIME (SEC)
0
10
20
30
40
50
60
70
80
90
100
0
100
200
300
400
500
600

(a)

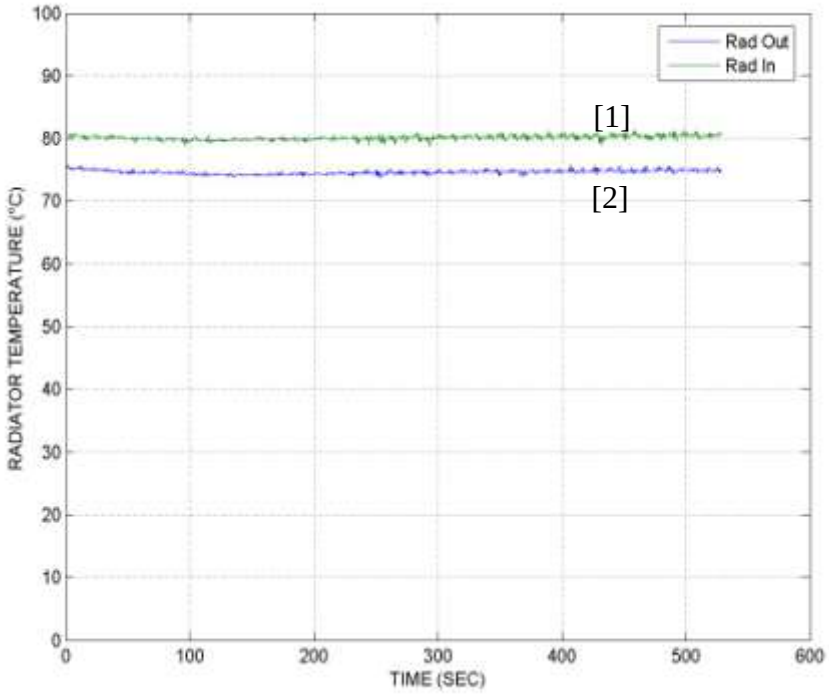
Rad Out
Rad In
[1]
[2]
RADIATOR TEMPERATURE (°C)
TIME (SEC)
0
10
20
30
40
50
60
70
80
90
100
0
100
200
300
400
500
600

(b)

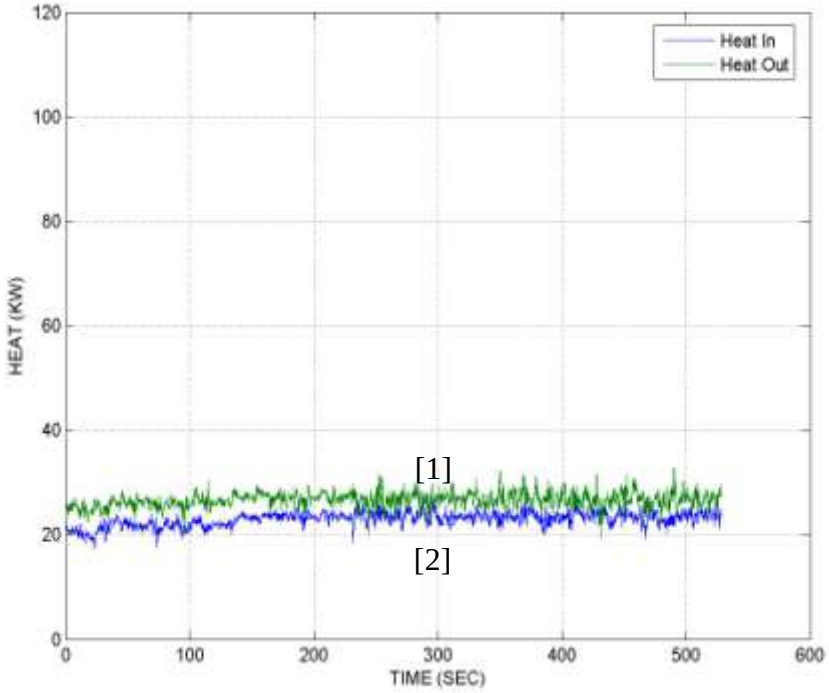

(c)

Figure A.4: Temperature and heat plots for Test #1 configuration at 4,000 RPM (a) heat exchanger inlet [1] and outlet [2] temperature, (b) radiator inlet [1] and outlet temperature [2] and, (c) heat input [1] and heat rejected [2].

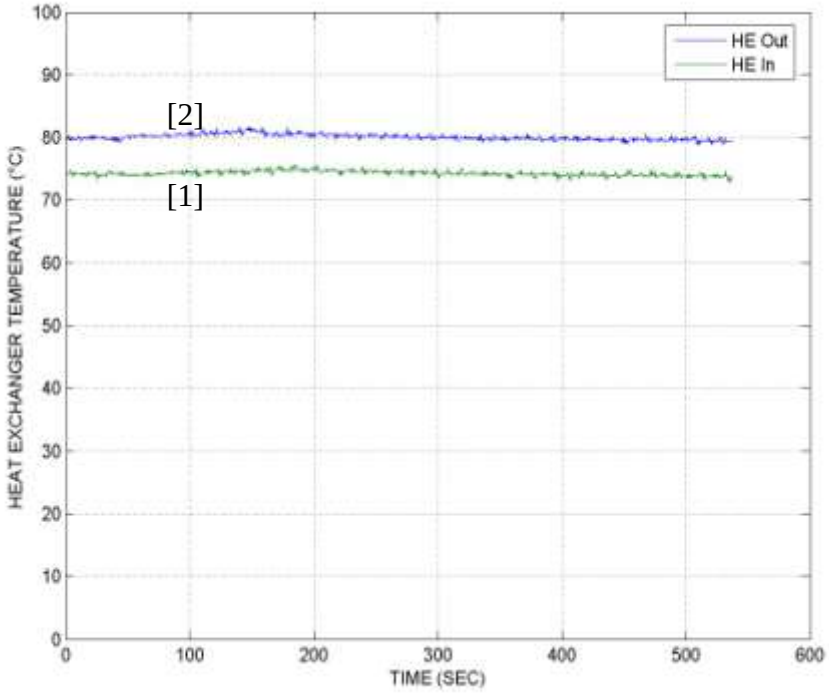
HE Out
HE In
[2]
[1]
HEAT EXCHANGER TEMPERATURE (°C)
TIME (SEC)
0
10
20
30
40
50
60
70
80
90
100
0
100
200
300
400
500
600

(a)

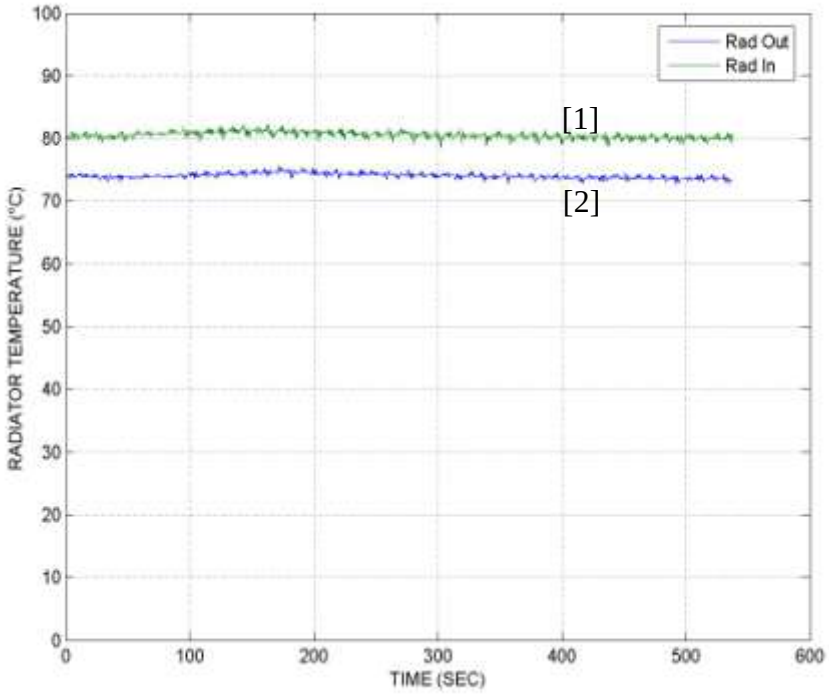
Rad Out
Rad In
[1]
[2]
RADIATOR TEMPERATURE (°C)
TIME (SEC)
0
10
20
30
40
50
60
70
80
90
100
0
100
200
300
400
500
600

(b)

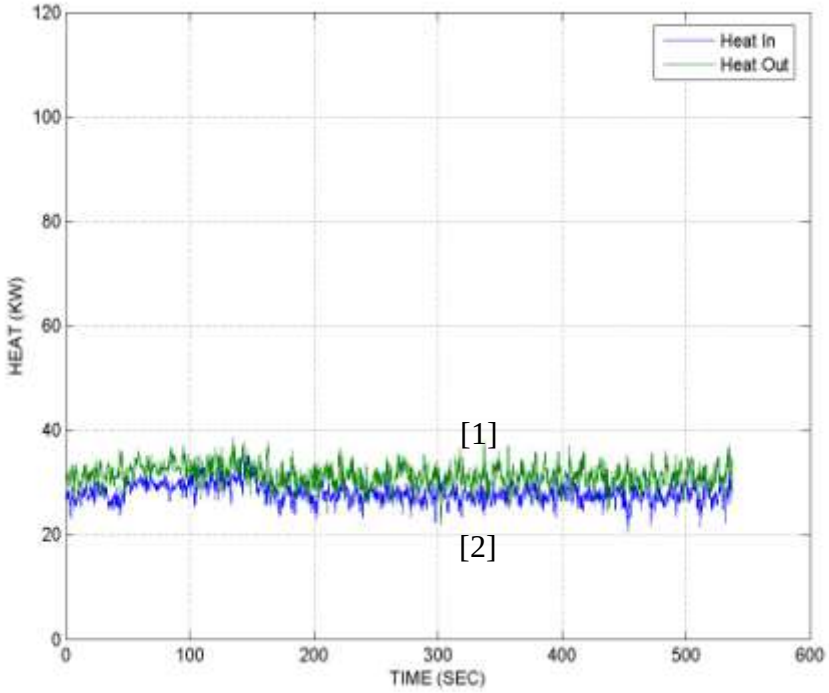

(c)

Figure A.5: Temperature and heat plots for Test #1 configuration at 5,000 RPM (a) heat exchanger inlet [1] and outlet [2] temperature, (b) radiator inlet [1] and outlet temperature [2] and, (c) heat input [1] and heat rejected [2].

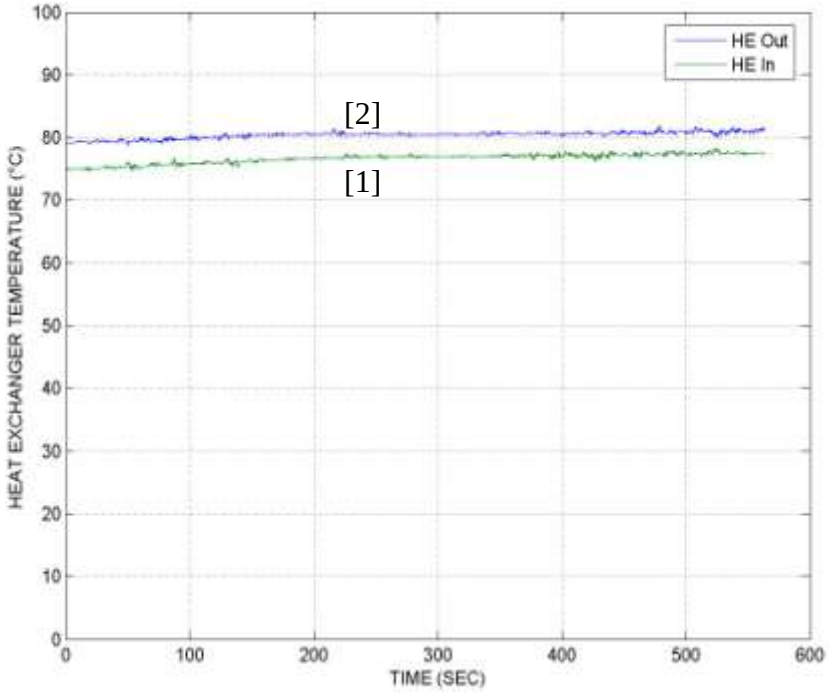
HE Out
HE In
[2]
[1]
HEAT EXCHANGER TEMPERATURE (°C)
TIME (SEC)
0
10
20
30
40
50
60
70
80
90
100
0
100
200
300
400
500
600

(a)

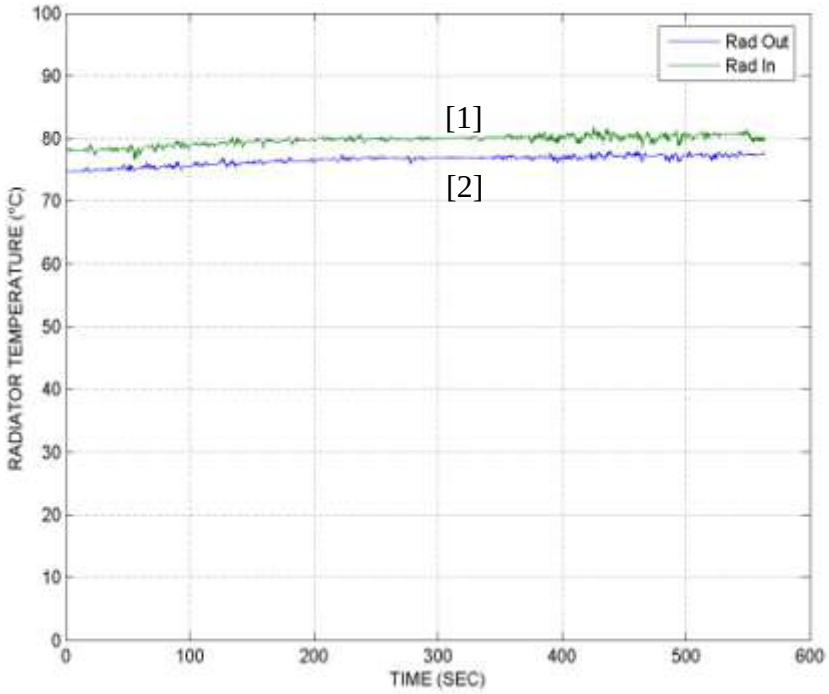
Rad Out
Rad In
[1]
[2]
RADIATOR TEMPERATURE (°C)
TIME (SEC)
0
10
20
30
40
50
60
70
80
90
100
0
100
200
300
400
500
600

(b)

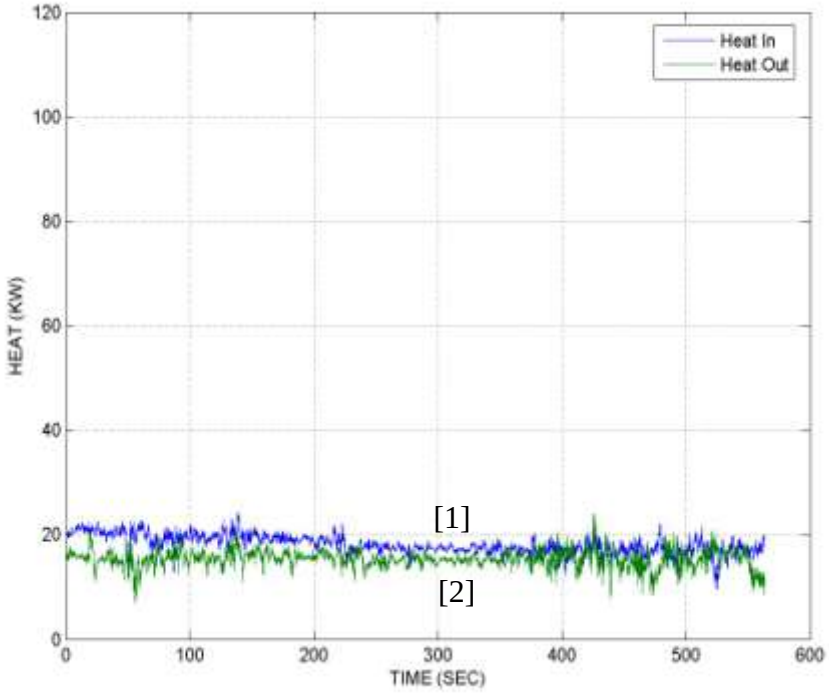

(c)

Figure A.6: Temperature and heat plots for Test #2 configuration at 1,000 RPM (a) heat exchanger inlet [1] and outlet [2] temperature, (b) radiator inlet [1] and outlet temperature [2] and, (c) heat input [1] and heat rejected [2].

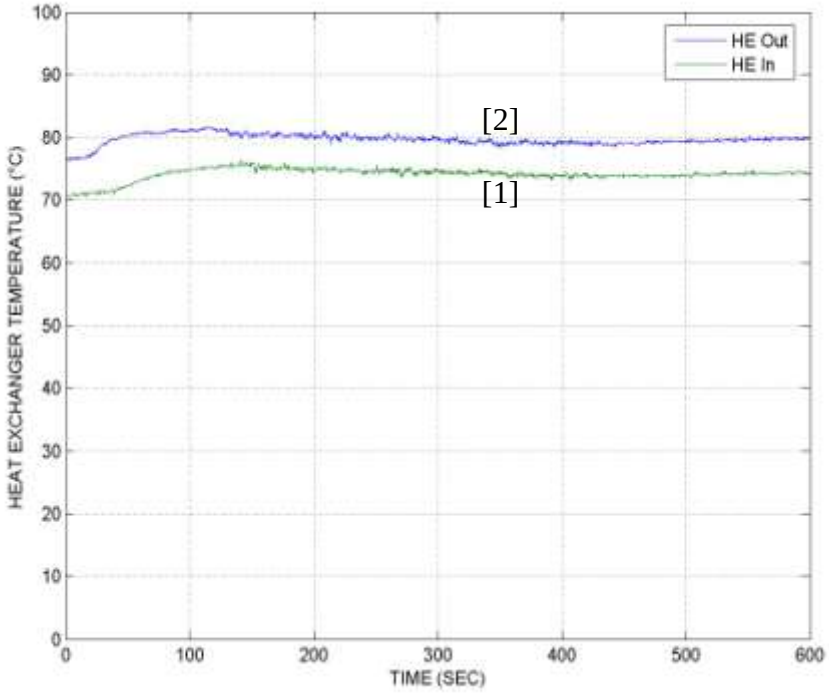
HE Out
HE In
[2]
[1]
HEAT EXCHANGER TEMPERATURE (°C)
TIME (SEC)
0
10
20
30
40
50
60
70
80
90
100
0
100
200
300
400
500
600

(a)

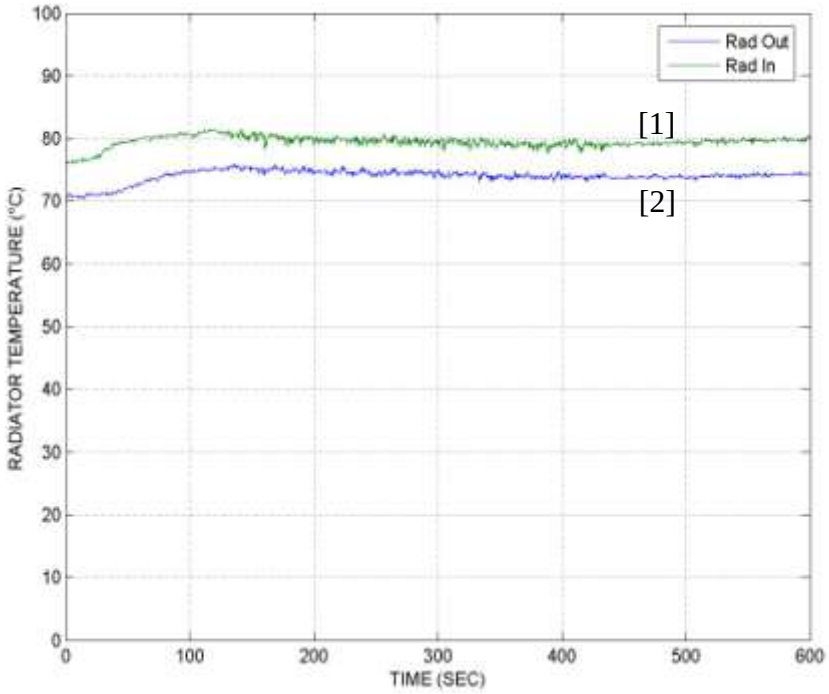
Rad Out
Rad In
[1]
[2]
RADIATOR TEMPERATURE (°C)
TIME (SEC)
0
10
20
30
40
50
60
70
80
90
100
0
100
200
300
400
500
600

(b)

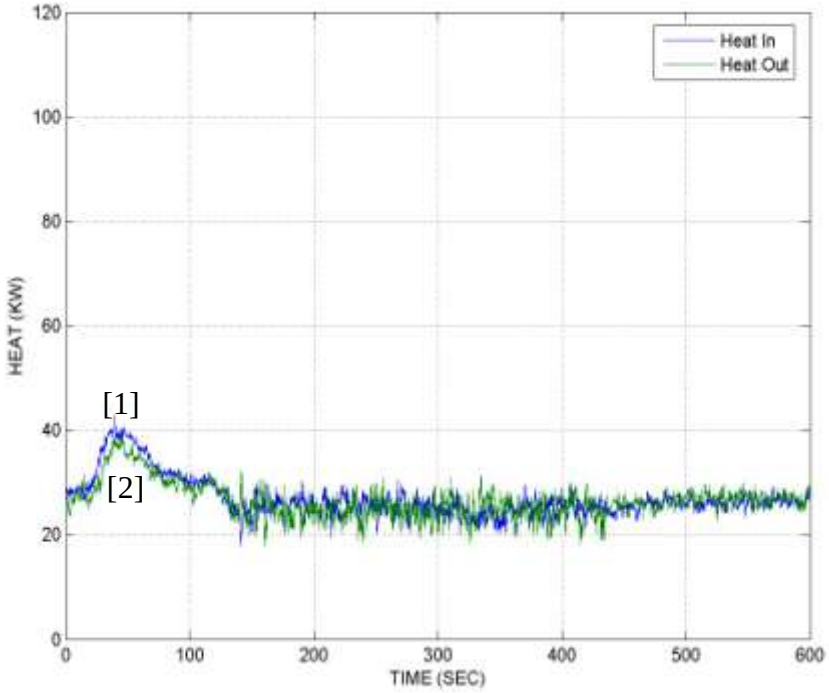

(c)

Figure A.7: Temperature and heat plots for Test #2 configuration at 2,000 RPM (a) heat exchanger inlet [1] and outlet [2] temperature, (b) radiator inlet [1] and outlet temperature [2] and, (c) heat input [1] and heat rejected [2].

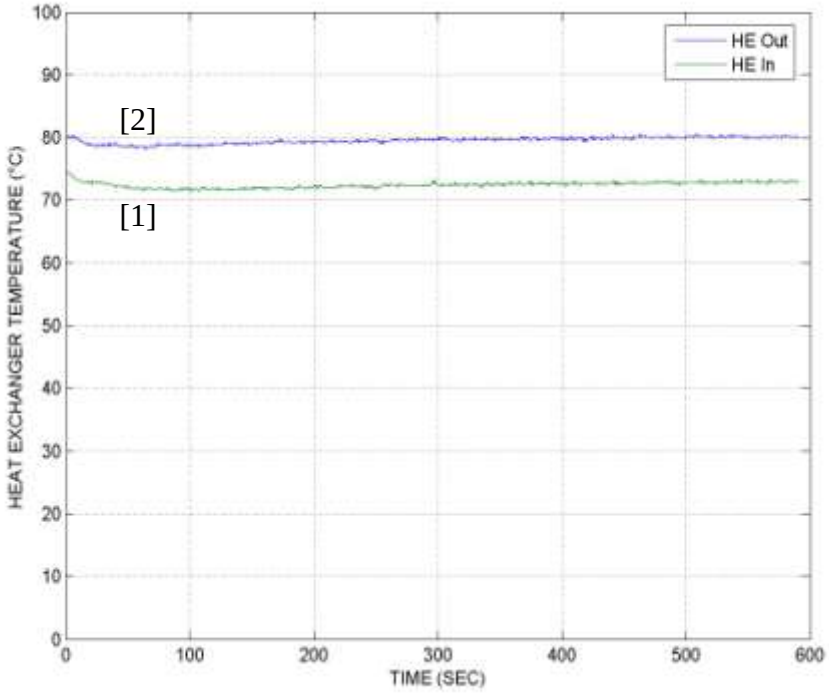
HE Out
HE In
[2]
[1]
HEAT EXCHANGER TEMPERATURE (°C)
TIME (SEC)
0
10
20
30
40
50
60
70
80
90
100
0
100
200
300
400
500
600

(a)

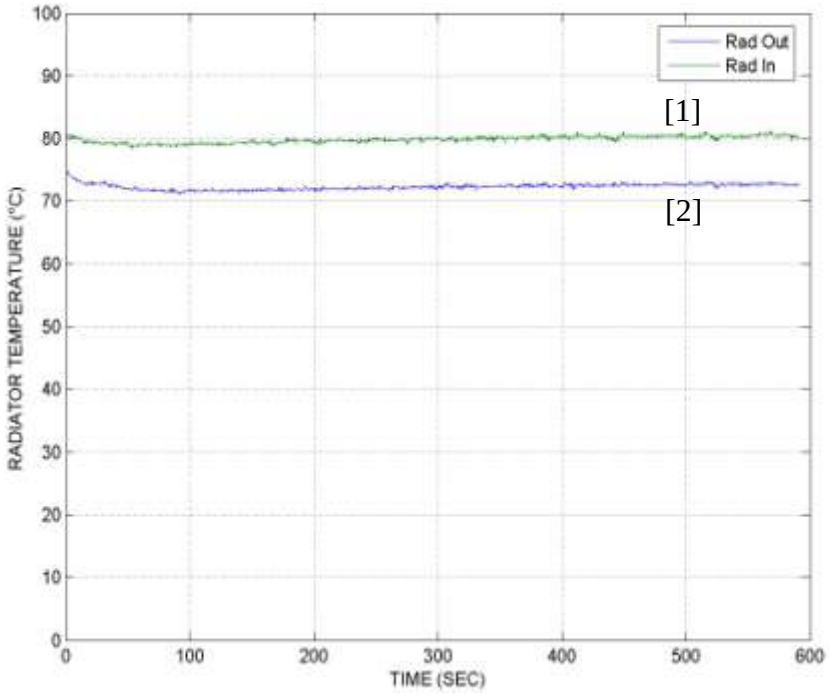
Rad Out
Rad In
[1]
[2]
RADIATOR TEMPERATURE (°C)
TIME (SEC)
0
10
20
30
40
50
60
70
80
90
100
0
100
200
300
400
500
600

(b)

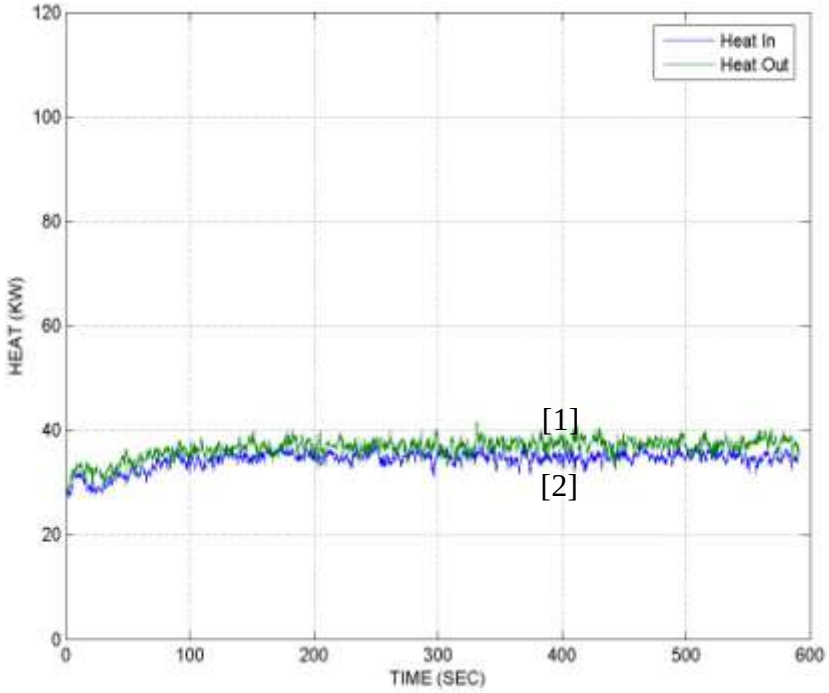

(c)

Figure A.8: Temperature and heat plots for Test #2 configuration at 3,000 RPM (a) heat exchanger inlet [1] and outlet [2] temperature, (b) radiator inlet [1] and outlet temperature [2] and, (c) heat input [1] and heat rejected [2].

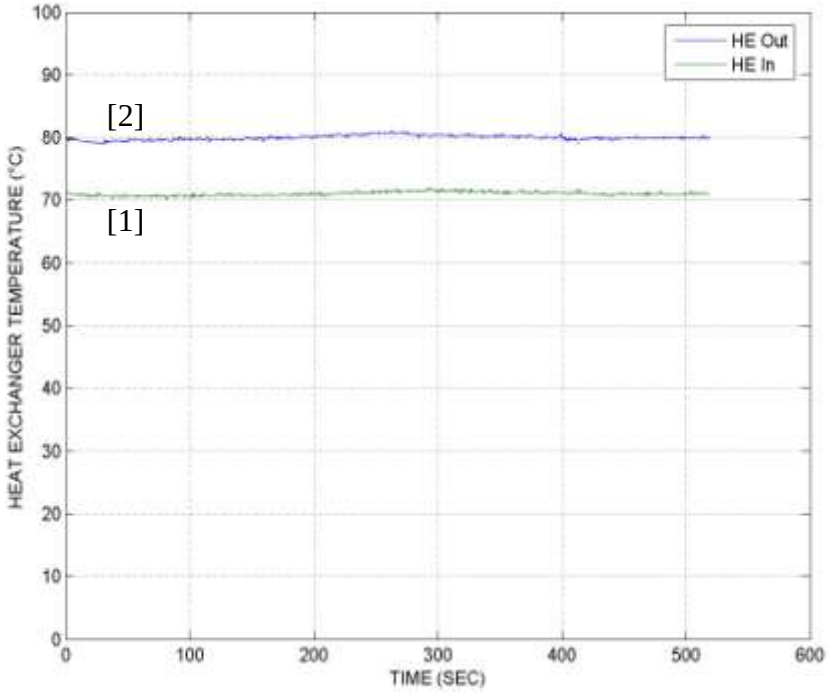
HE Out
HE In
[2]
[1]
HEAT EXCHANGER TEMPERATURE (°C)
TIME (SEC)
0
10
20
30
40
50
60
70
80
90
100
0
100
200
300
400
500
600

(a)

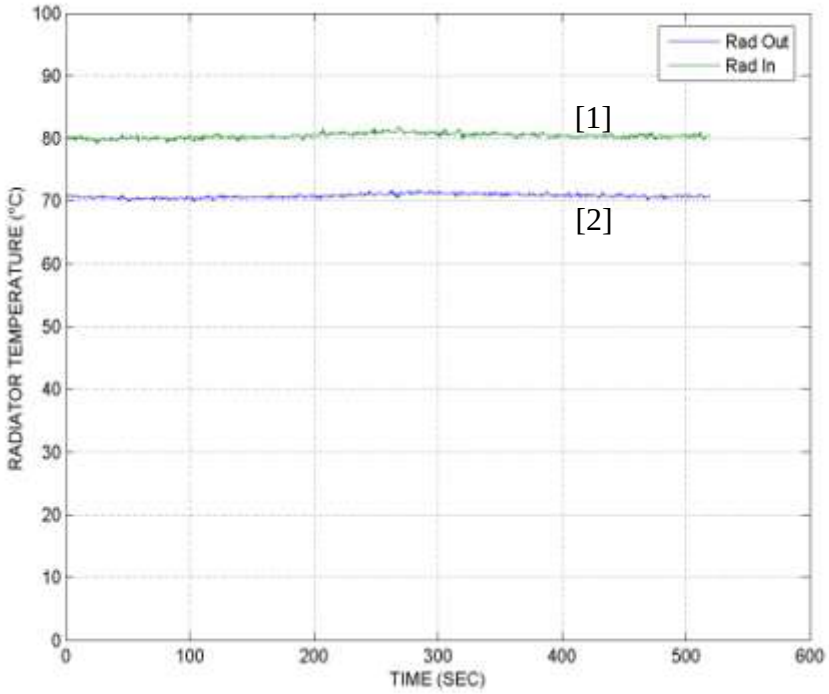
Rad Out
Rad In
[1]
[2]
RADIATOR TEMPERATURE (°C)
TIME (SEC)
0
10
20
30
40
50
60
70
80
90
100
0
100
200
300
400
500
600

(b)

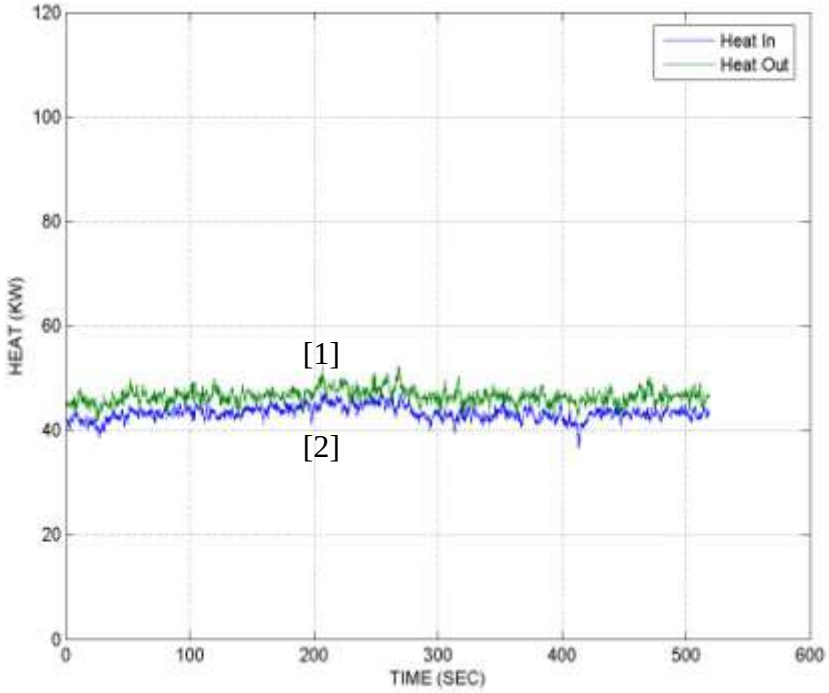

(c)

Figure A.9: Temperature and heat plots for Test #2 configuration at 4,000 RPM (a) heat exchanger inlet [1] and outlet [2] temperature, (b) radiator inlet [1] and outlet temperature [2] and, (c) heat input [1] and heat rejected [2].

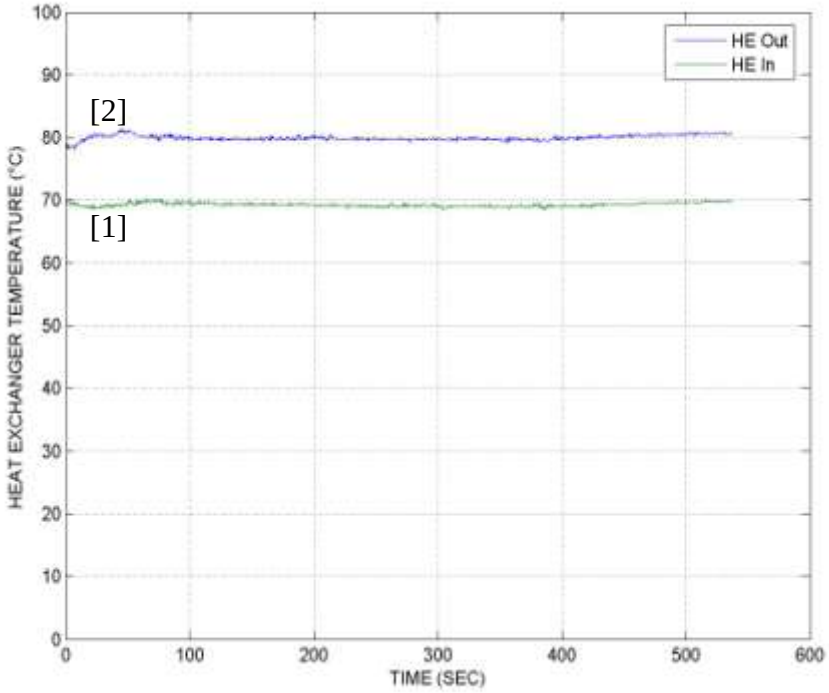
HE Out
HE In
[2]
[1]
HEAT EXCHANGER TEMPERATURE (°C)
TIME (SEC)
0
10
20
30
40
50
60
70
80
90
100
0
100
200
300
400
500
600

(a)

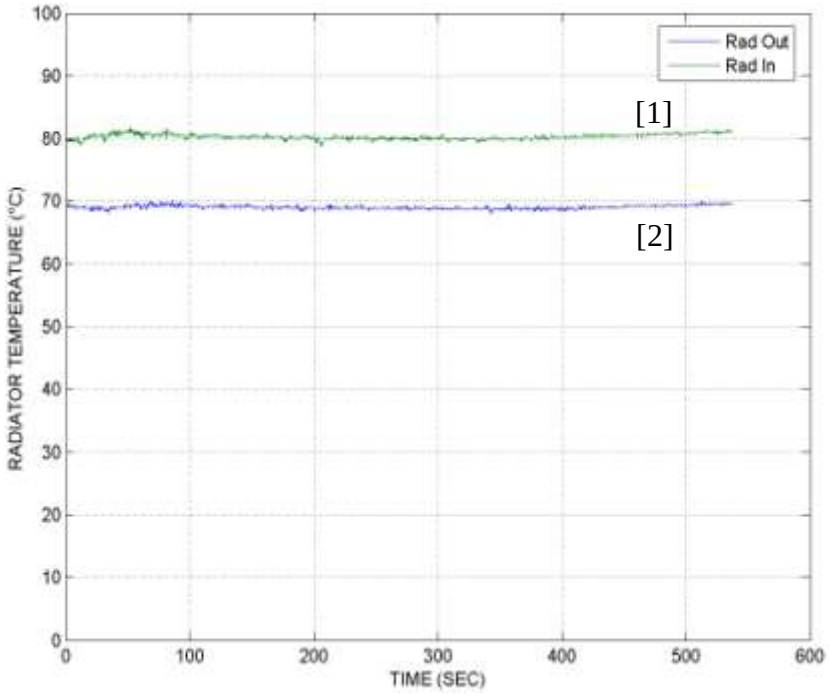
Rad Out
Rad In
[1]
[2]
RADIATOR TEMPERATURE (°C)
TIME (SEC)
0
10
20
30
40
50
60
70
80
90
100
0
100
200
300
400
500
600

(b)

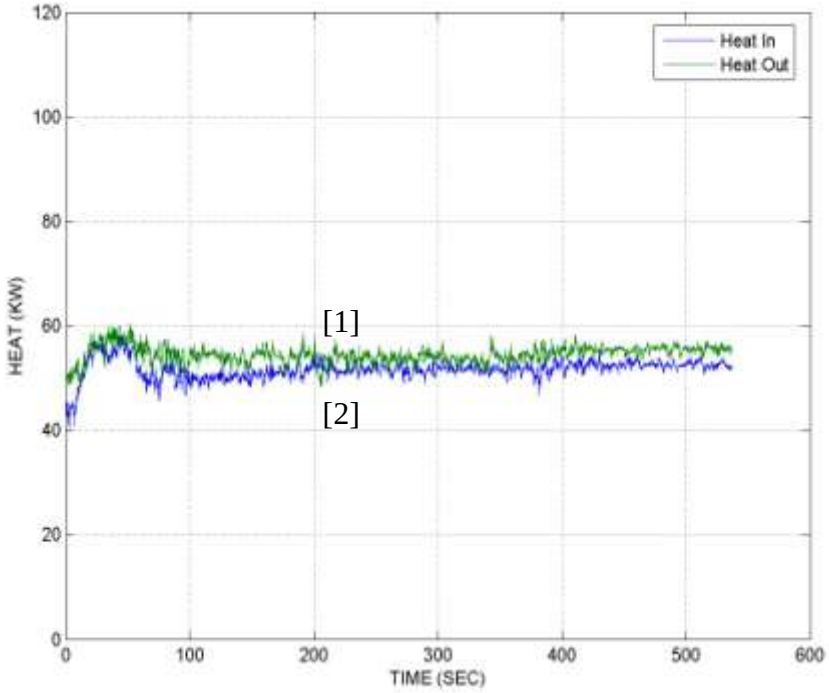

(c)

Figure A.10: Temperature and heat plots for Test #2 configuration at 5,000 RPM (a) heat exchanger inlet [1] and outlet [2] temperature, (b) radiator inlet [1] and outlet temperature [2] and, (c) heat input [1] and heat rejected [2].

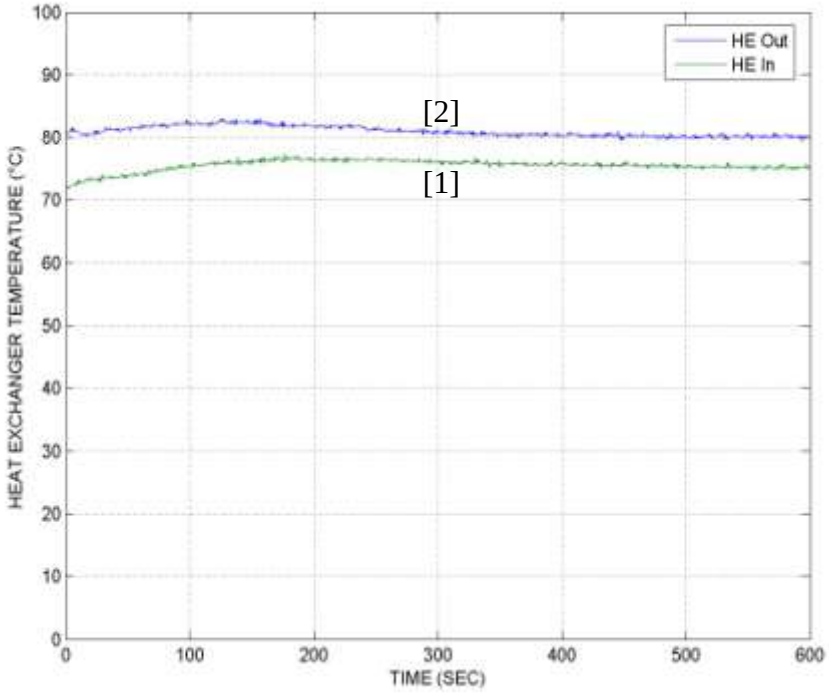
HE Out
HE In
[2]
[1]
HEAT EXCHANGER TEMPERATURE (°C)
TIME (SEC)
0
10
20
30
40
50
60
70
80
90
100
0
100
200
300
400
500
600

(a)

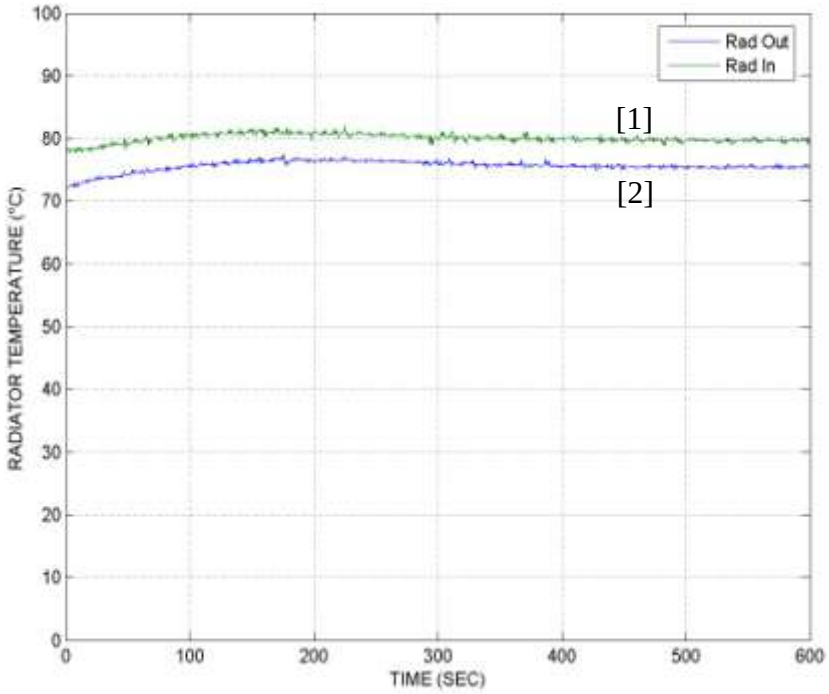
Rad Out
Rad In
[1]
[2]
RADIATOR TEMPERATURE (°C)
TIME (SEC)
0
10
20
30
40
50
60
70
80
90
100
0
100
200
300
400
500
600

(b)

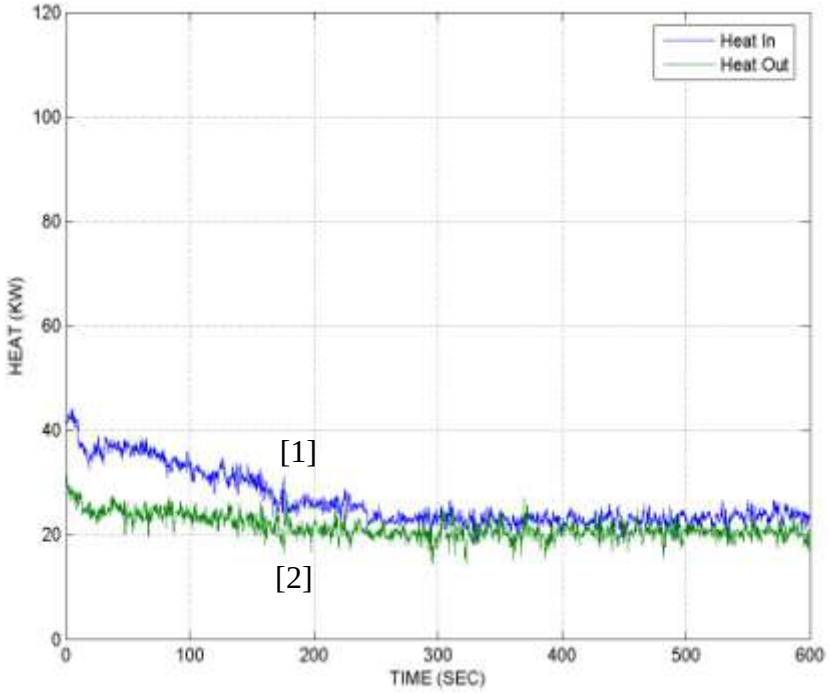

(c)

Figure A.11: Temperature and heat plots for Test #3 configuration at 1,000 RPM (a) heat exchanger inlet [1] and outlet [2] temperature, (b) radiator inlet [1] and outlet temperature [2] and, (c) heat input [1] and heat rejected [2].

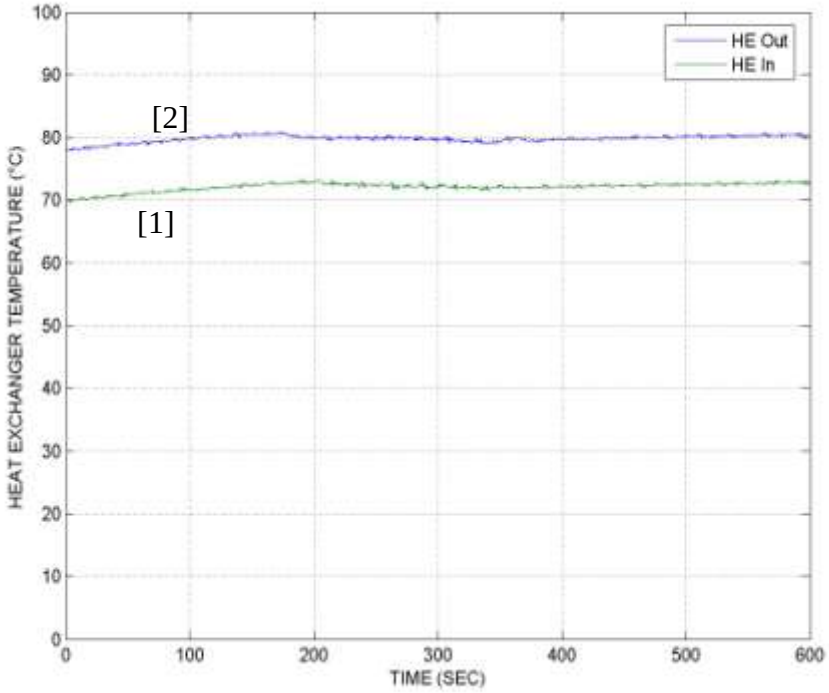
HE Out
HE In
[2]
[1]
HEAT EXCHANGER TEMPERATURE (°C)
TIME (SEC)
0
10
20
30
40
50
60
70
80
90
100
0
100
200
300
400
500
600

(a)

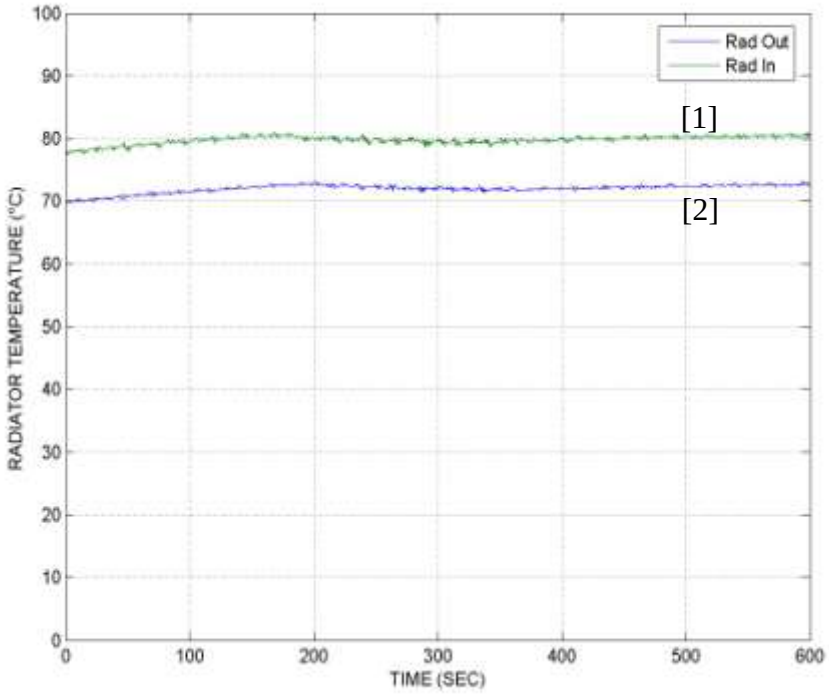
Rad Out
Rad In
[1]
[2]
RADIATOR TEMPERATURE (°C)
TIME (SEC)
0
10
20
30
40
50
60
70
80
90
100
0
100
200
300
400
500
600

(b)

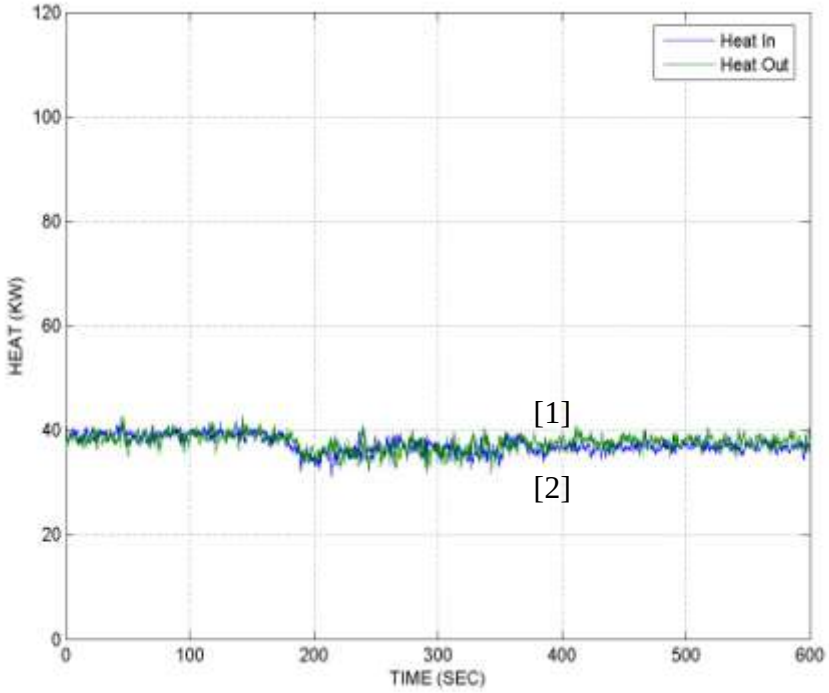

(c)

Figure A.12: Temperature and heat plots for Test #3 configuration at 2,000 RPM (a) heat exchanger inlet [1] and outlet [2] temperature, (b) radiator inlet [1] and outlet temperature [2] and, (c) heat input [1] and heat rejected [2].

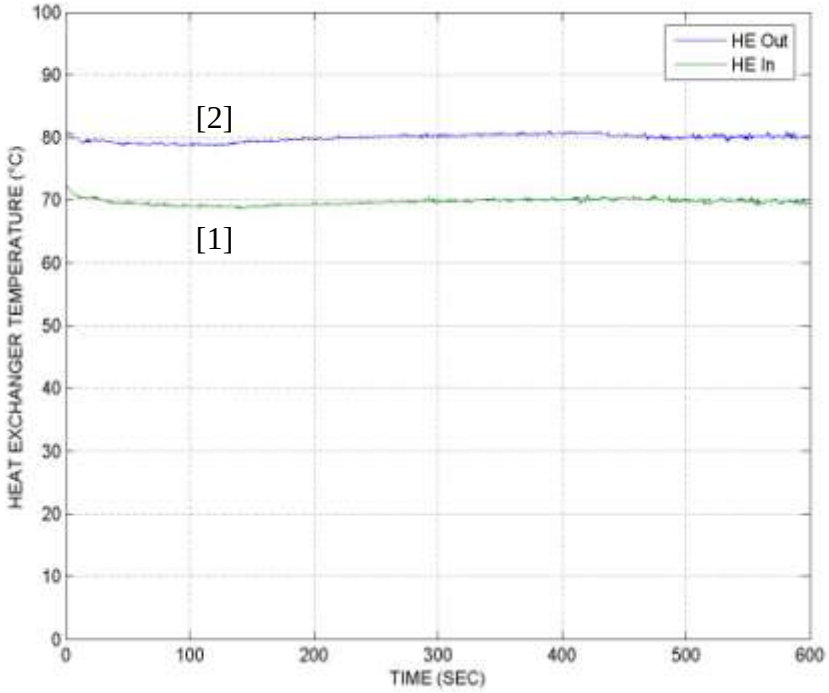
HE Out
HE In
[2]
[1]
HEAT EXCHANGER TEMPERATURE (°C)
TIME (SEC)
0
10
20
30
40
50
60
70
80
90
100
0
100
200
300
400
500
600

(a)

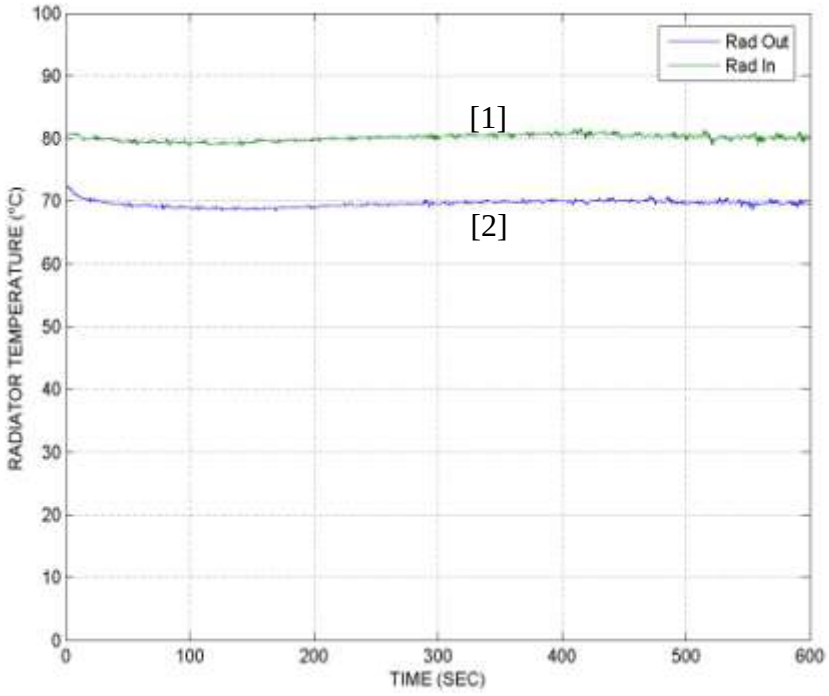
Rad Out
Rad In
[1]
[2]
RADIATOR TEMPERATURE (°C)
TIME (SEC)
0
10
20
30
40
50
60
70
80
90
100
0
100
200
300
400
500
600

(b)

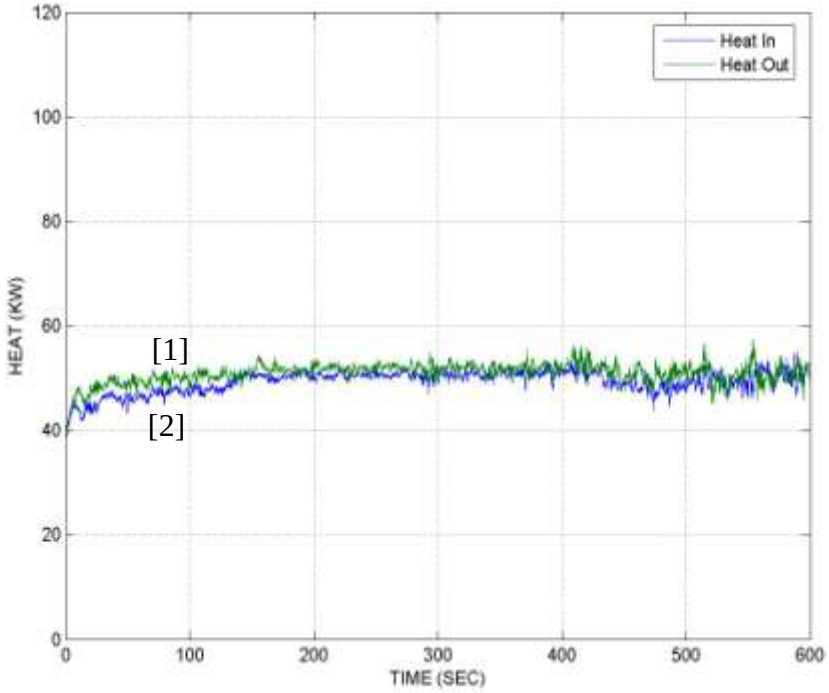

(c)

Figure A.13: Temperature and heat plots for Test #3 configuration at 3,000 RPM (a) heat exchanger inlet [1] and outlet [2] temperature, (b) radiator inlet [1] and outlet temperature [2] and, (c) heat input [1] and heat rejected [2].

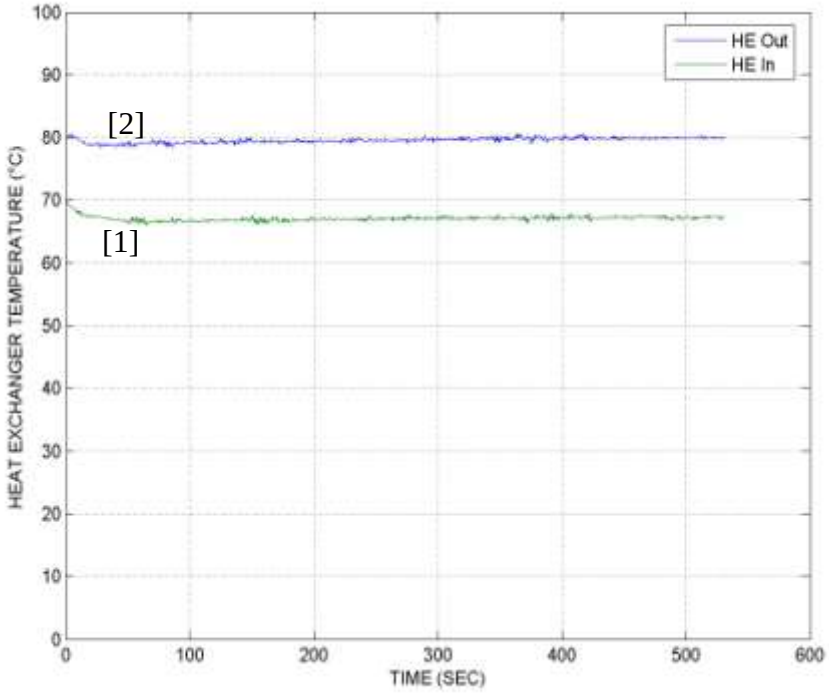
HE Out
HE In
[2]
[1]
HEAT EXCHANGER TEMPERATURE (°C)
TIME (SEC)
0
10
20
30
40
50
60
70
80
90
100
0
100
200
300
400
500
600

(a)

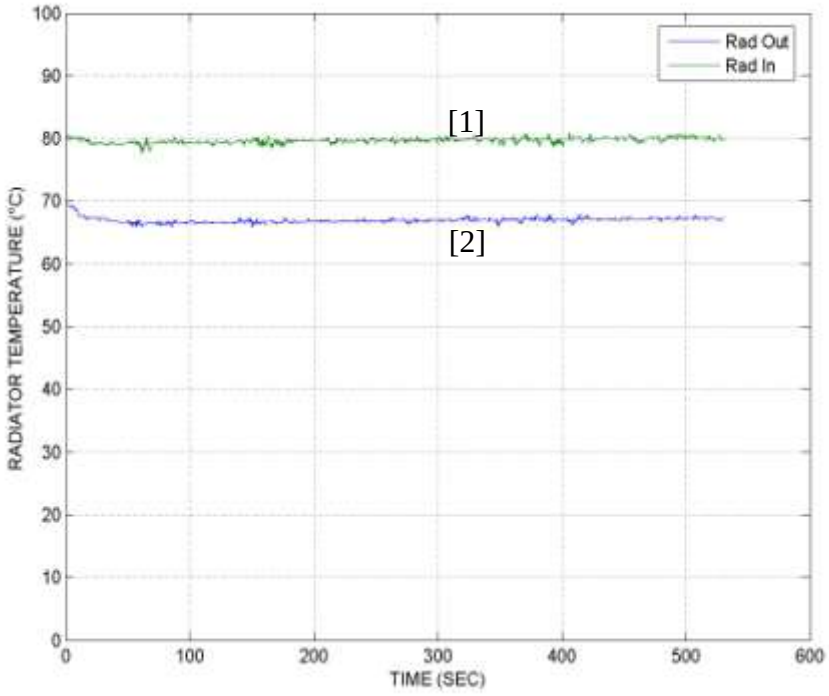
Rad Out
Rad In
[1]
[2]
RADIATOR TEMPERATURE (°C)
TIME (SEC)
0
10
20
30
40
50
60
70
80
90
100
0
100
200
300
400
500
600

(b)

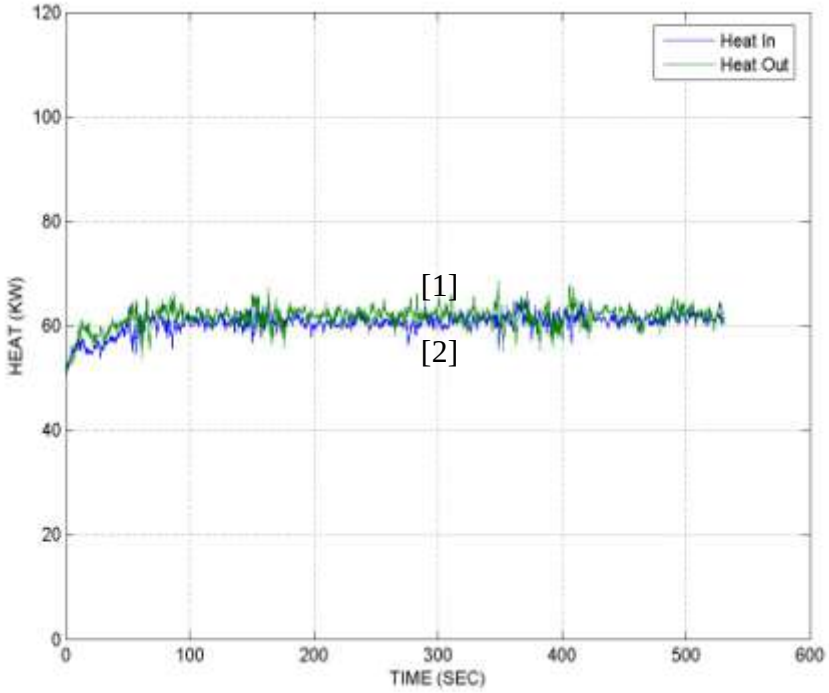

(c)

Figure A.14: Temperature and heat plots for Test #3 configuration at 4,000 RPM (a) heat exchanger inlet [1] and outlet [2] temperature, (b) radiator inlet [1] and outlet temperature [2] and, (c) heat input [1] and heat rejected [2].

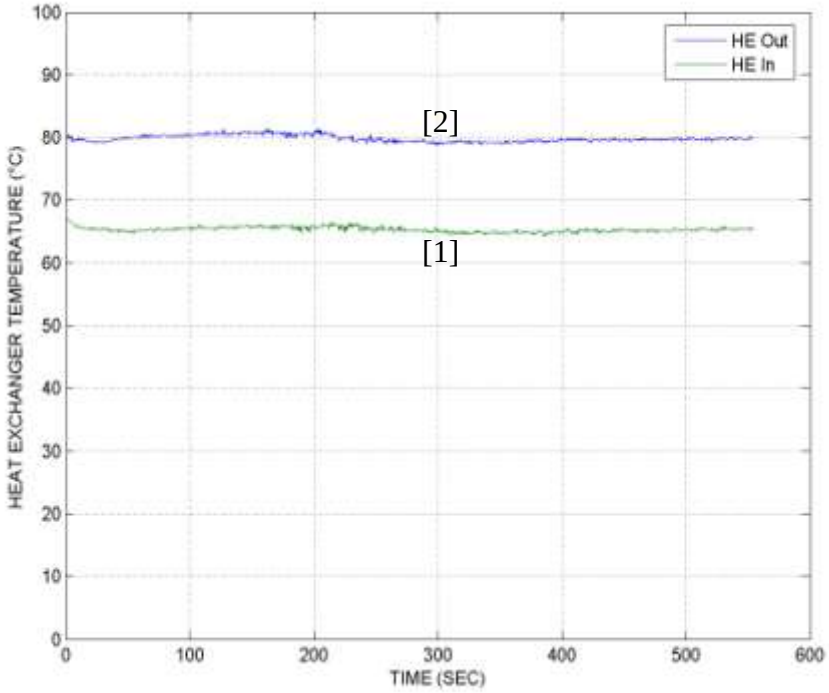
HE Out
HE In
[2]
[1]
HEAT EXCHANGER TEMPERATURE (°C)
TIME (SEC)
0
10
20
30
40
50
60
70
80
90
100
0
100
200
300
400
500
600

(a)

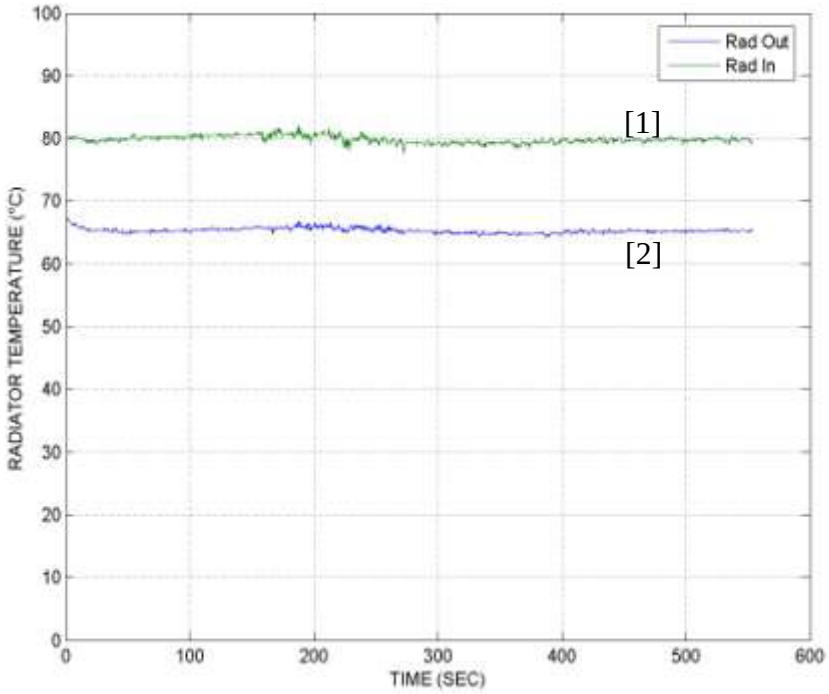
Rad Out
Rad In
[1]
[2]
RADIATOR TEMPERATURE (°C)
TIME (SEC)
0
10
20
30
40
50
60
70
80
90
100
0
100
200
300
400
500
600

(b)

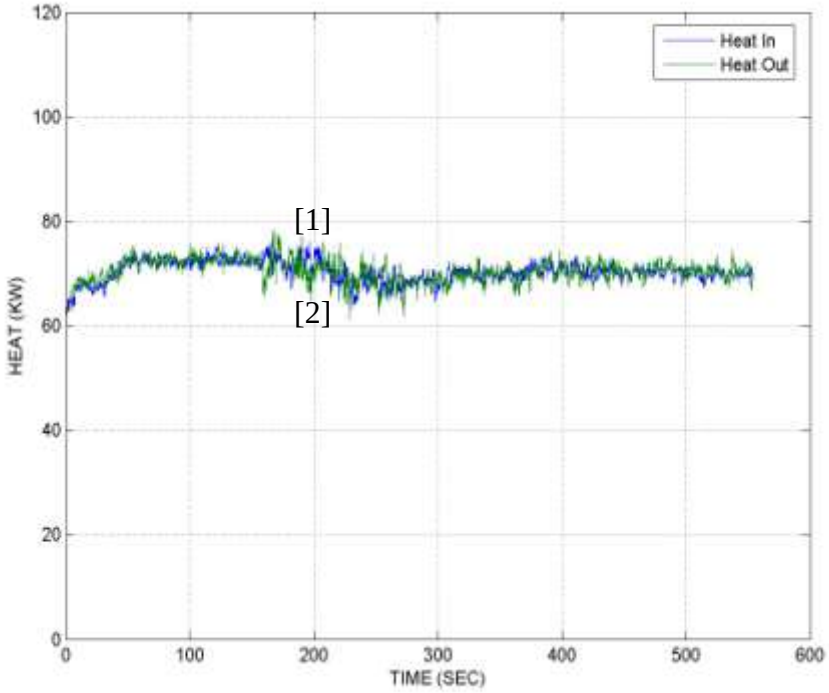

(c)

Figure A.15: Temperature and heat plots for Test #3 configuration at 5,000 RPM (a) heat exchanger inlet [1] and outlet [2] temperature, (b) radiator inlet [1] and outlet temperature [2] and, (c) heat input [1] and heat rejected [2].

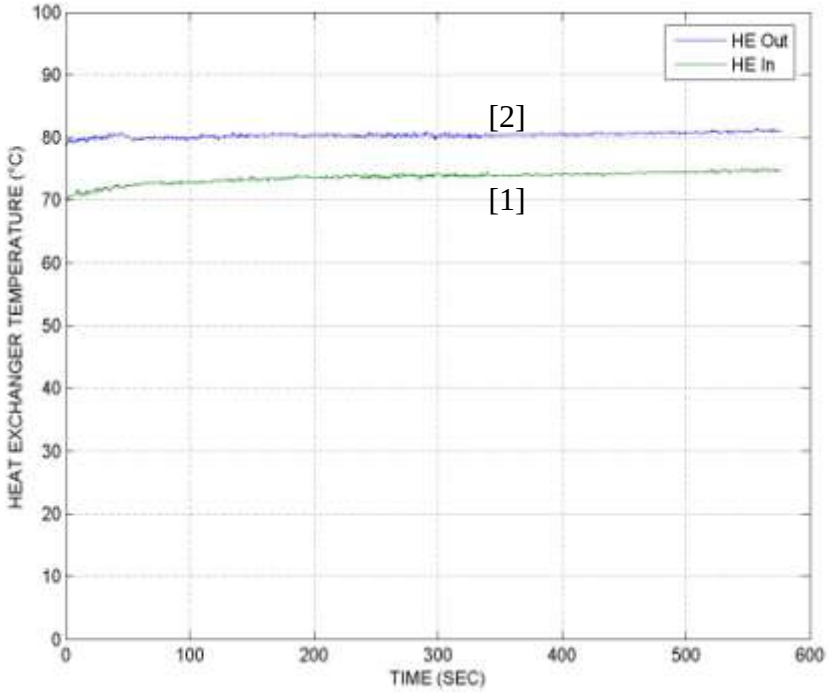
HE Out
HE In
[2]
[1]
HEAT EXCHANGER TEMPERATURE (°C)
TIME (SEC)
0
10
20
30
40
50
60
70
80
90
100
0
100
200
300
400
500
600

(a)

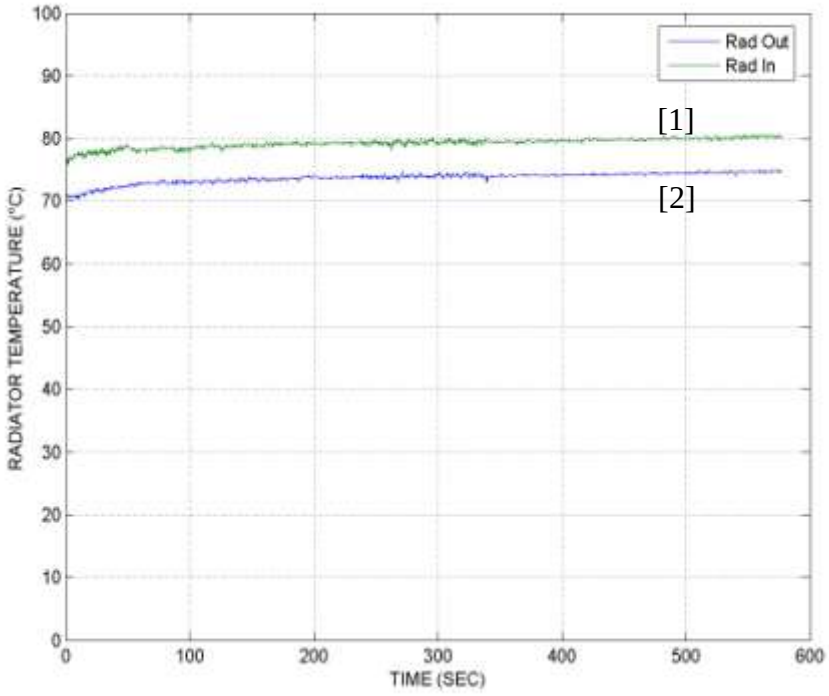
Rad Out
Rad In
[1]
[2]
RADIATOR TEMPERATURE (°C)
TIME (SEC)
0
10
20
30
40
50
60
70
80
90
100
0
100
200
300
400
500
600

(b)

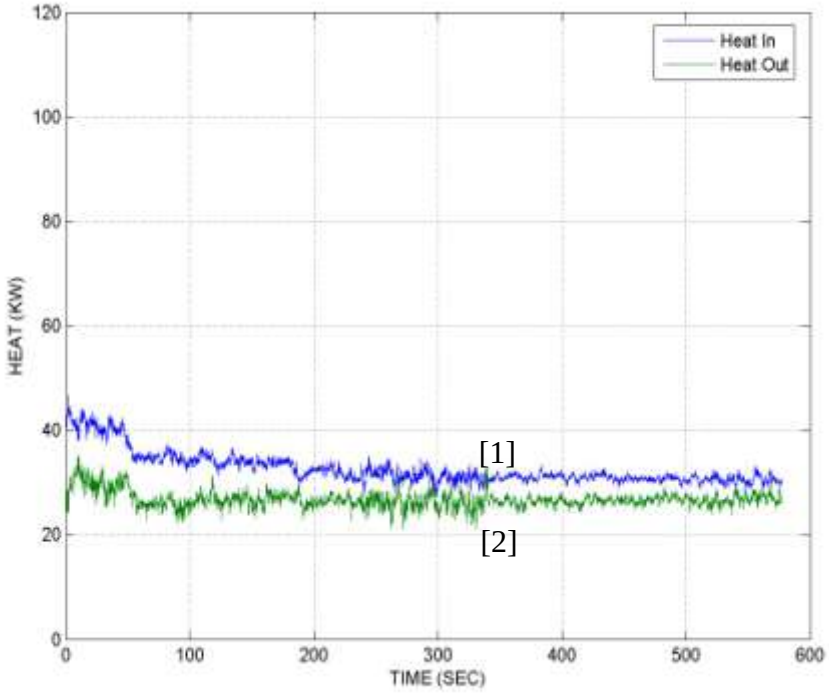

(c)

Figure A.16: Temperature and heat plots for Test #4 configuration at 1,000 RPM (a) heat exchanger inlet [1] and outlet [2] temperature, (b) radiator inlet [1] and outlet temperature [2] and, (c) heat input [1] and heat rejected [2].

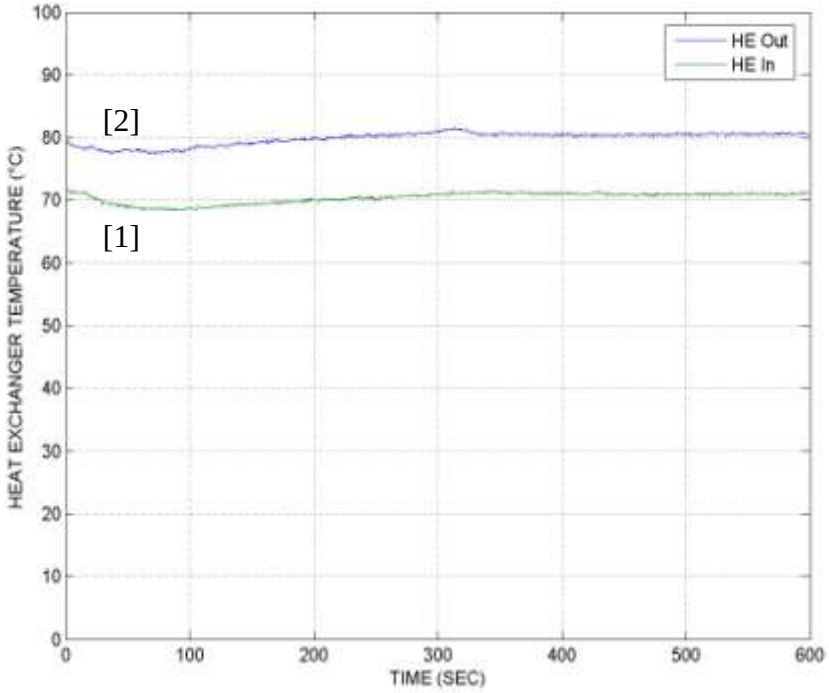
HE Out
HE In
[2]
[1]
HEAT EXCHANGER TEMPERATURE (°C)
TIME (SEC)
0
10
20
30
40
50
60
70
80
90
100
0
100
200
300
400
500
600

(a)

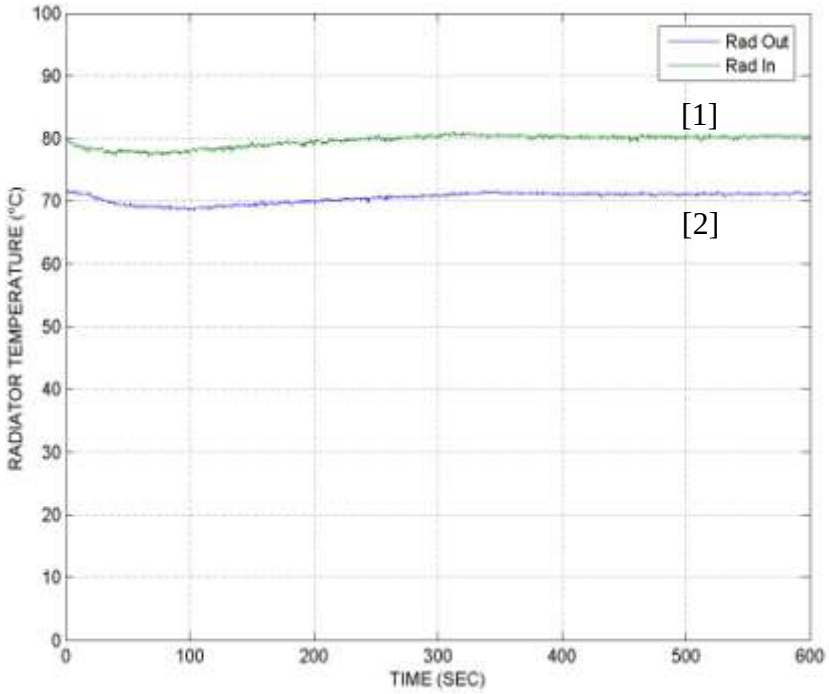
Rad Out
Rad In
[1]
[2]
RADIATOR TEMPERATURE (°C)
TIME (SEC)
0
10
20
30
40
50
60
70
80
90
100
0
100
200
300
400
500
600

(b)

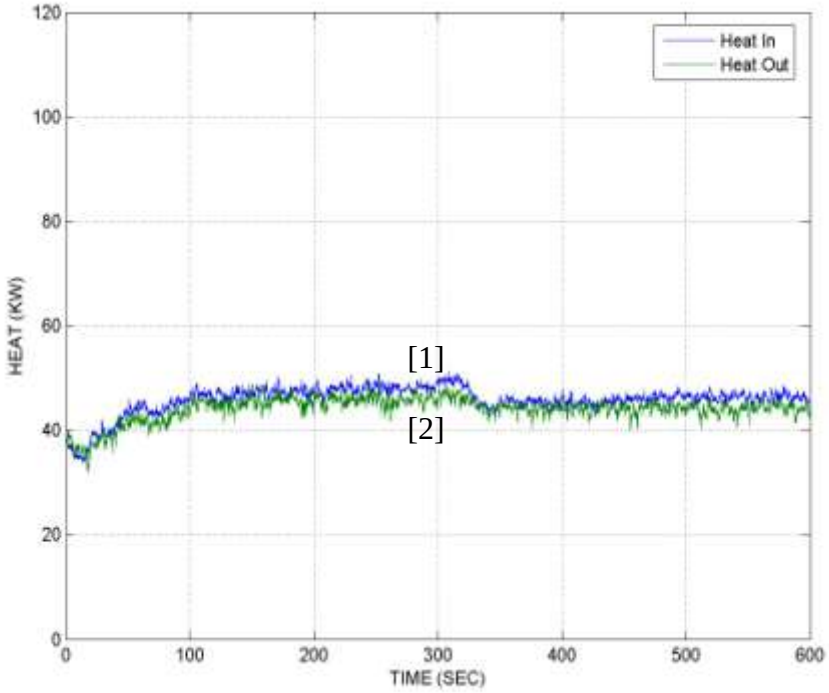

(c)

Figure A.17: Temperature and heat plots for Test #4 configuration at 2,000 RPM (a) heat exchanger inlet [1] and outlet [2] temperature, (b) radiator inlet [1] and outlet temperature [2] and, (c) heat input [1] and heat rejected [2].

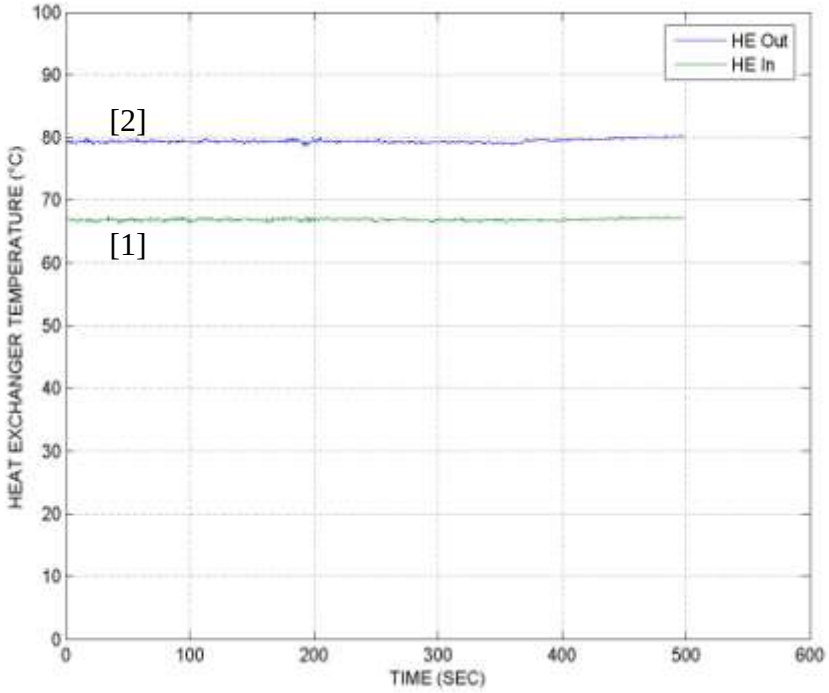
HE Out
HE In
[2]
[1]
HEAT EXCHANGER TEMPERATURE (°C)
TIME (SEC)
0
10
20
30
40
50
60
70
80
90
100
0
100
200
300
400
500
600

(a)

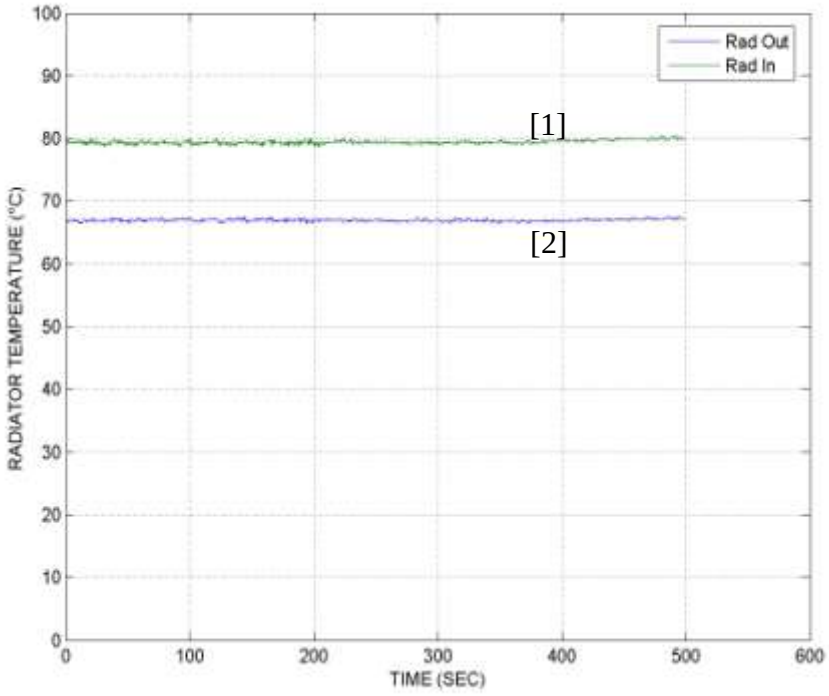
Rad Out
Rad In
[1]
[2]
RADIATOR TEMPERATURE (°C)
TIME (SEC)
0
10
20
30
40
50
60
70
80
90
100
0
100
200
300
400
500
600

(b)

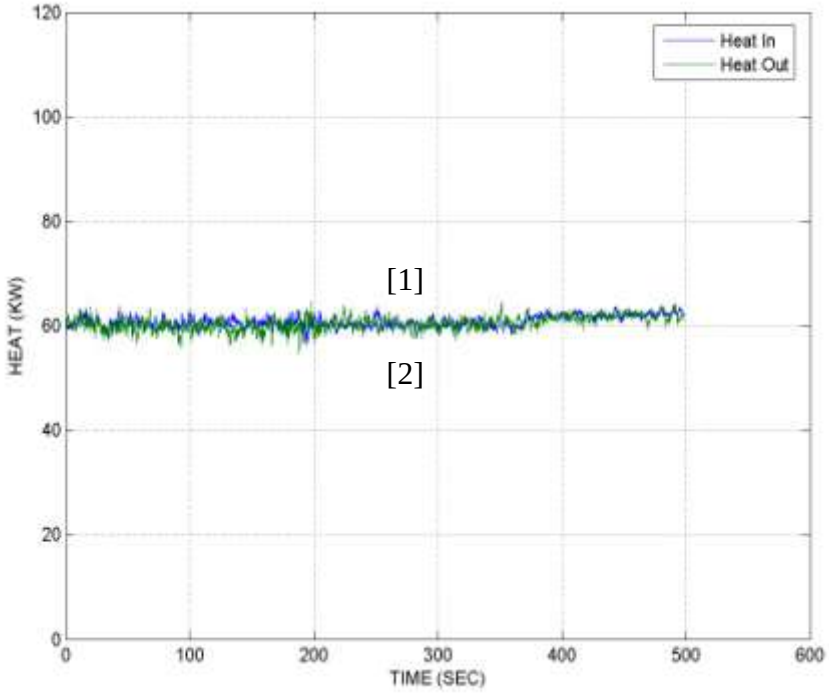

(c)

Figure A.18: Temperature and heat plots for Test #4 configuration at 3,000 RPM (a) heat exchanger inlet [1] and outlet [2] temperature, (b) radiator inlet [1] and outlet temperature [2] and, (c) heat input [1] and heat rejected [2].

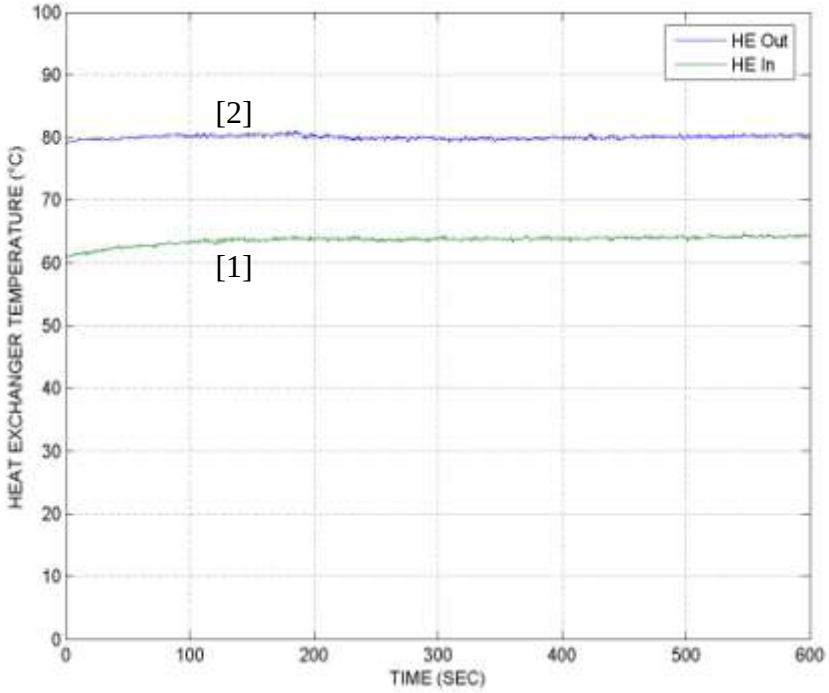
HE Out
HE In
[2]
[1]
HEAT EXCHANGER TEMPERATURE (°C)
TIME (SEC)
0
10
20
30
40
50
60
70
80
90
100
0
100
200
300
400
500
600

(a)

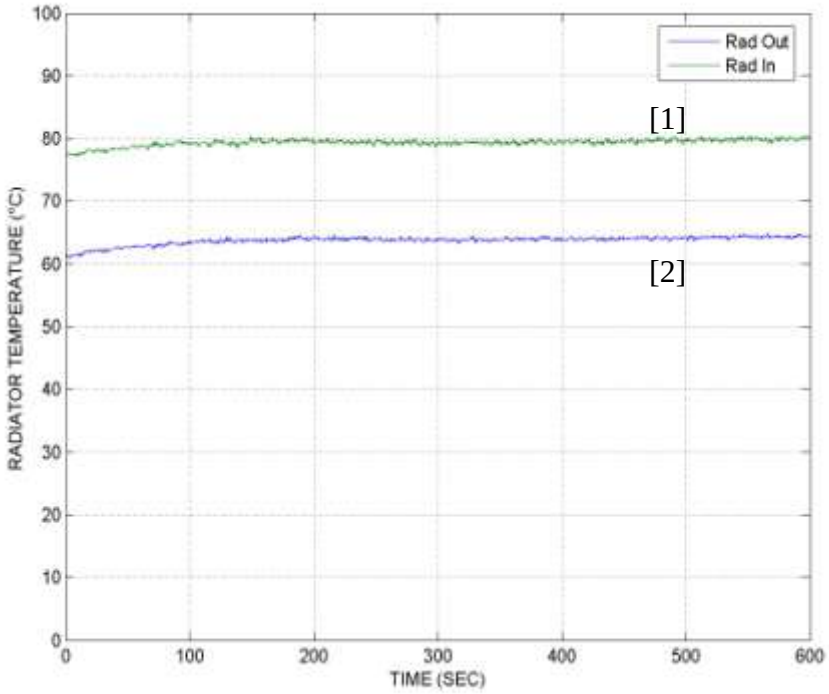
Rad Out
Rad In
[1]
[2]
RADIATOR TEMPERATURE (°C)
TIME (SEC)
0
10
20
30
40
50
60
70
80
90
100
0
100
200
300
400
500
600

(b)

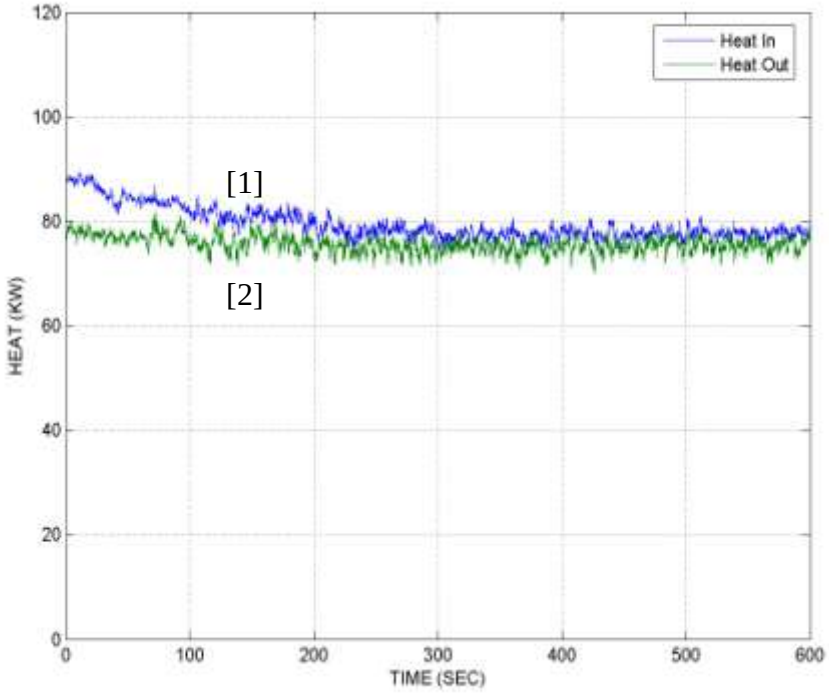

(c)

Figure A.19: Temperature and heat plots for Test #4 configuration at 4,000 RPM (a) heat exchanger inlet [1] and outlet [2] temperature, (b) radiator inlet [1] and outlet temperature [2] and, (c) heat input [1] and heat rejected [2].

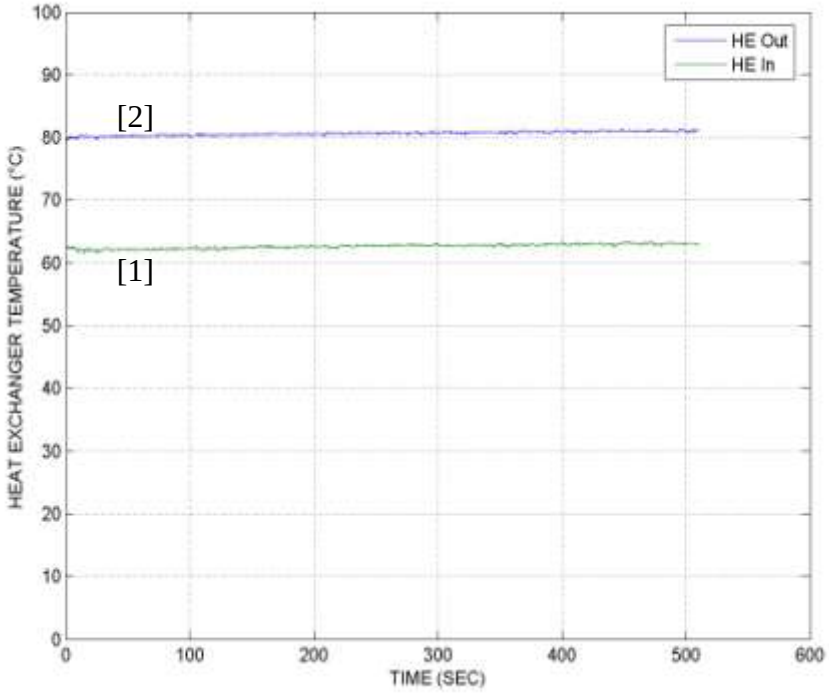
HE Out
HE In
[2]
[1]
HEAT EXCHANGER TEMPERATURE (°C)
TIME (SEC)
0
10
20
30
40
50
60
70
80
90
100
0
100
200
300
400
500
600

(a)

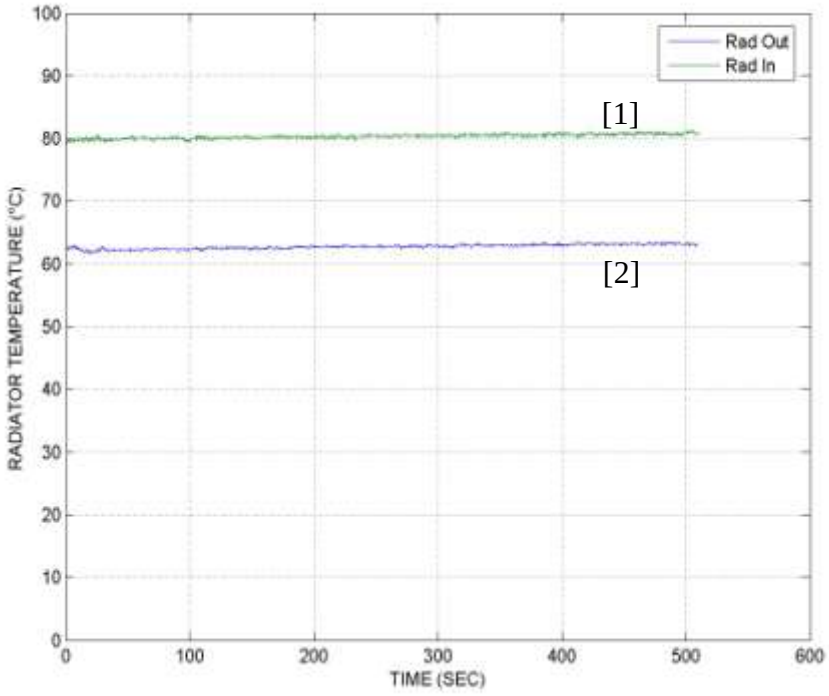
Rad Out
Rad In
[1]
[2]
RADIATOR TEMPERATURE (°C)
TIME (SEC)
0
10
20
30
40
50
60
70
80
90
100
0
100
200
300
400
500
600

(b)

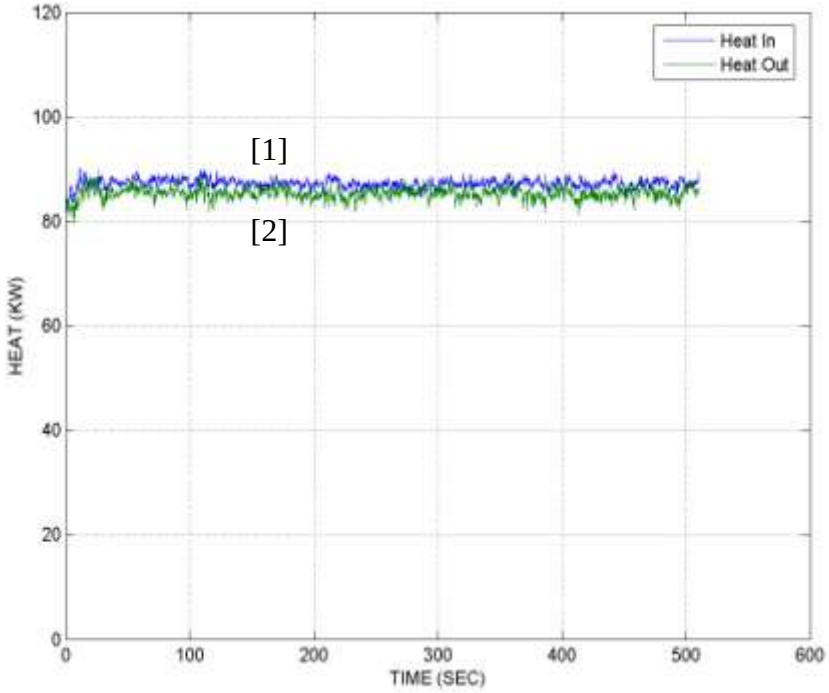

(c)

Figure A.20: Temperature and heat plots for Test #4 configuration at 5,000 RPM (a) heat exchanger inlet [1] and outlet [2] temperature, (b) radiator inlet [1] and outlet temperature [2] and, (c) heat input [1] and heat rejected [2].

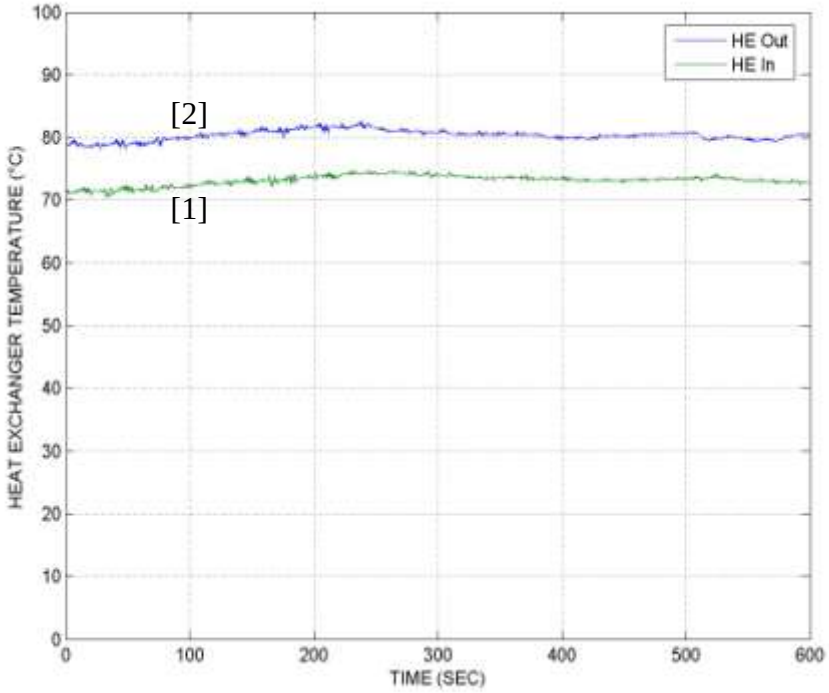
HE Out
HE In
[2]
[1]
HEAT EXCHANGER TEMPERATURE (°C)
TIME (SEC)
0
10
20
30
40
50
60
70
80
90
100
0
100
200
300
400
500
600

(a)

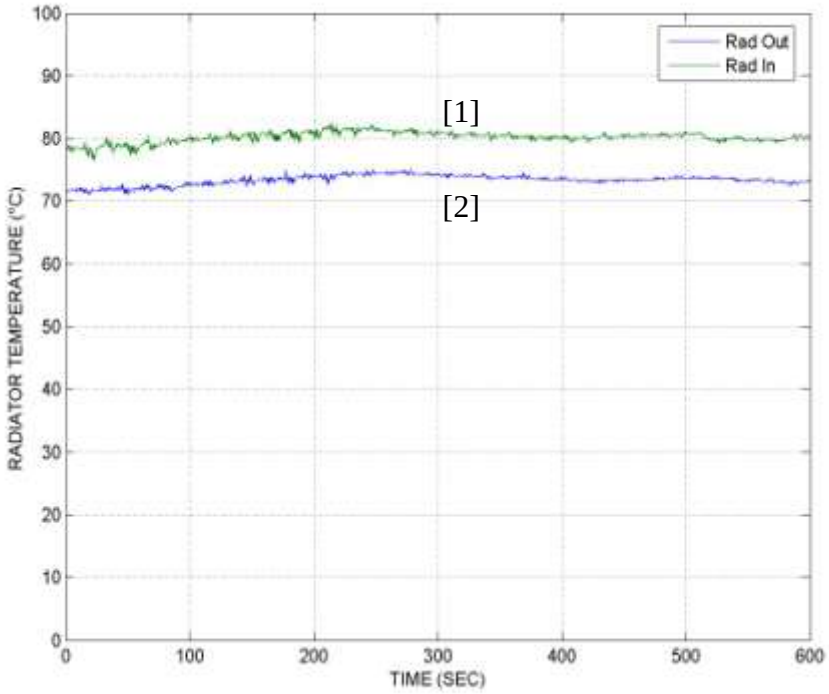
Rad Out
Rad In
[1]
[2]
RADIATOR TEMPERATURE (°C)
TIME (SEC)
0
10
20
30
40
50
60
70
80
90
100
0
100
200
300
400
500
600

(b)

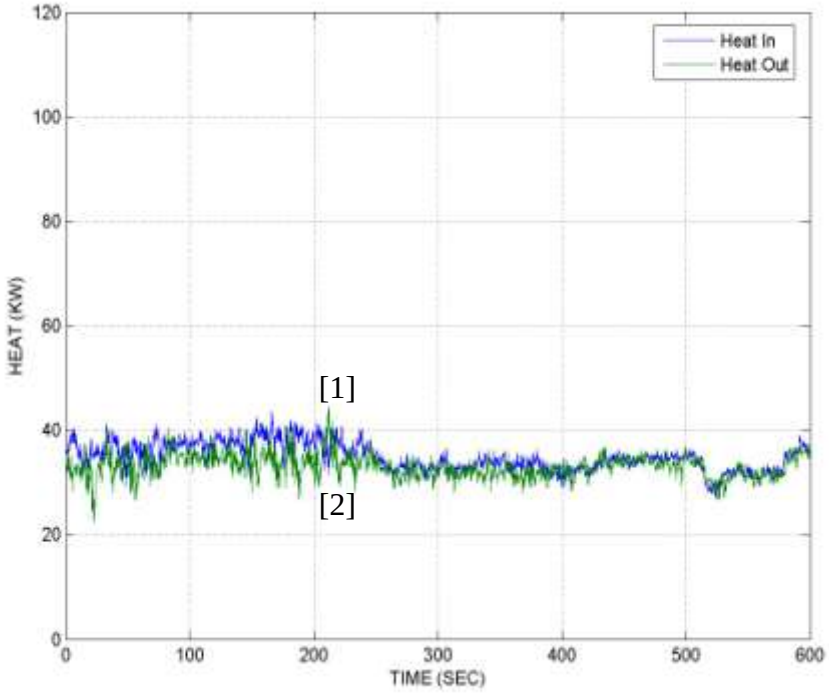

(c)

Figure A.21: Temperature and heat plots for Test #5 configuration at 1,000 RPM (a) heat exchanger inlet [1] and outlet [2] temperature, (b) radiator inlet [1] and outlet temperature [2] and, (c) heat input [1] and heat rejected [2] at 1,000 RPM.

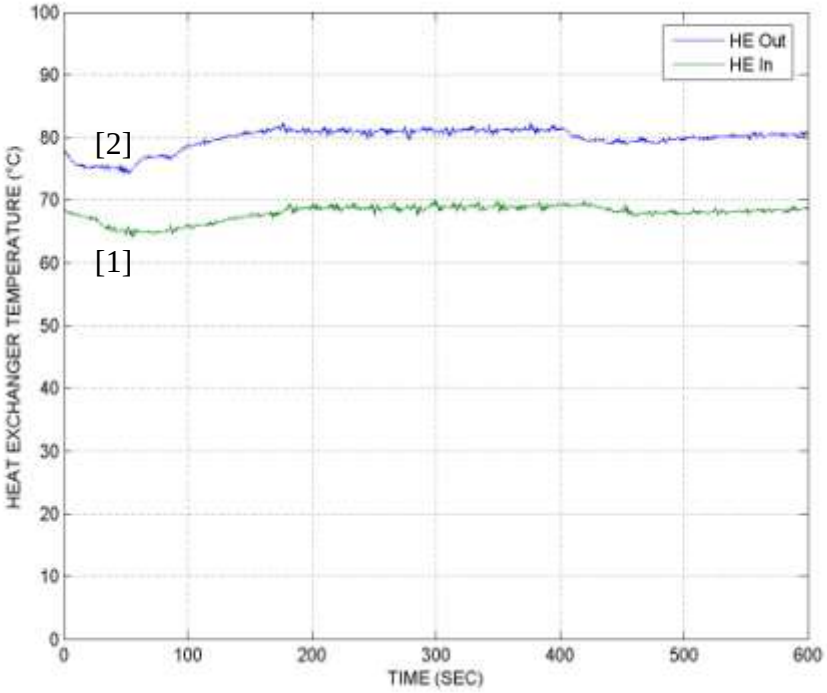
HE Out
HE In
[2]
[1]
HEAT EXCHANGER TEMPERATURE (°C)
TIME (SEC)
0
10
20
30
40
50
60
70
80
90
100
0
100
200
300
400
500
600

(a)

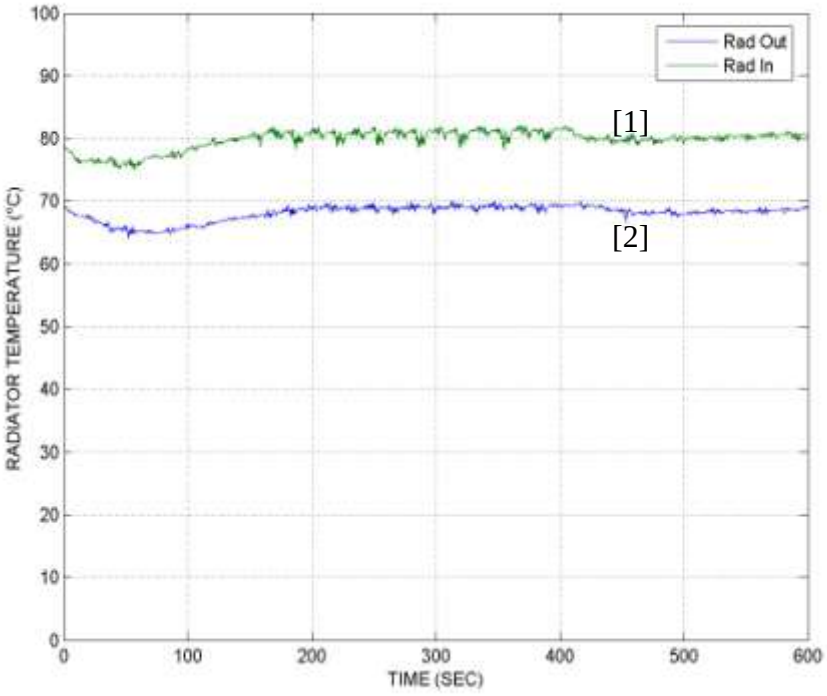
Rad Out
Rad In
[1]
[2]
RADIATOR TEMPERATURE (°C)
TIME (SEC)
0
10
20
30
40
50
60
70
80
90
100
0
100
200
300
400
500
600

(b)

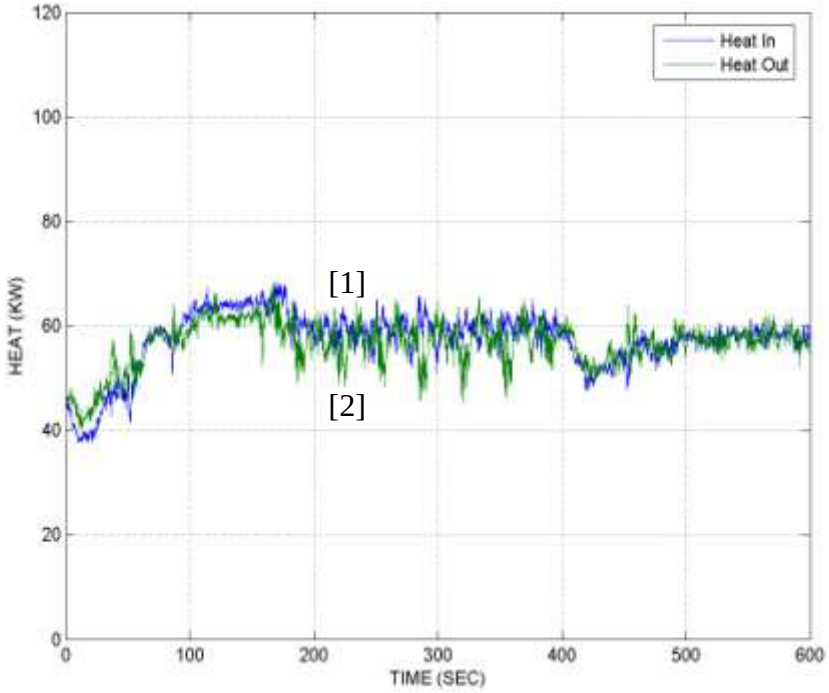

(c)

Figure A.22: Temperature and heat plots for Test #5 configuration at 2,000 RPM (a) heat exchanger inlet [1] and outlet [2] temperature, (b) radiator inlet [1] and outlet temperature [2] and, (c) heat input [1] and heat rejected [2].

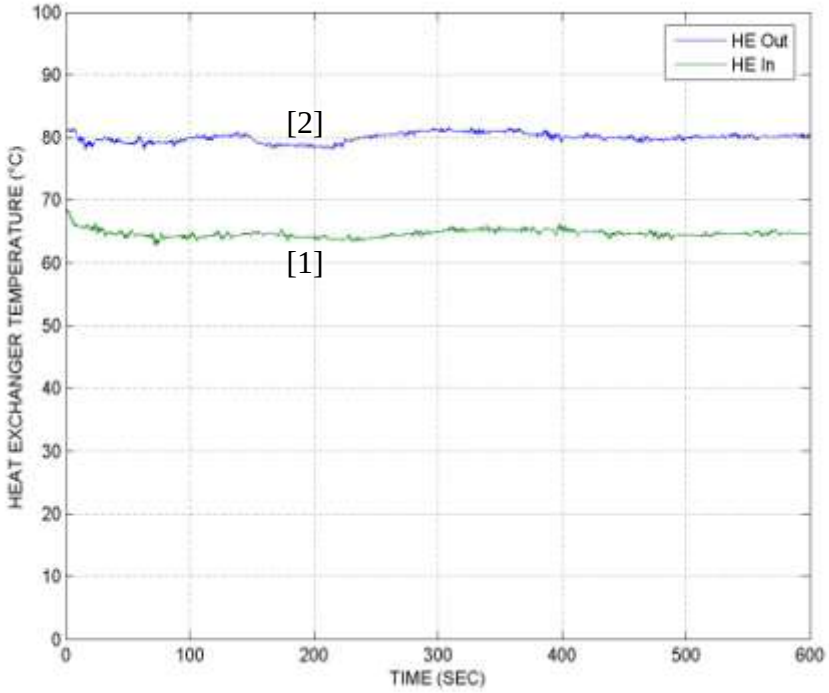
HE Out
HE In
[2]
[1]
HEAT EXCHANGER TEMPERATURE (°C)
TIME (SEC)
0
10
20
30
40
50
60
70
80
90
100
0
100
200
300
400
500
600

(a)

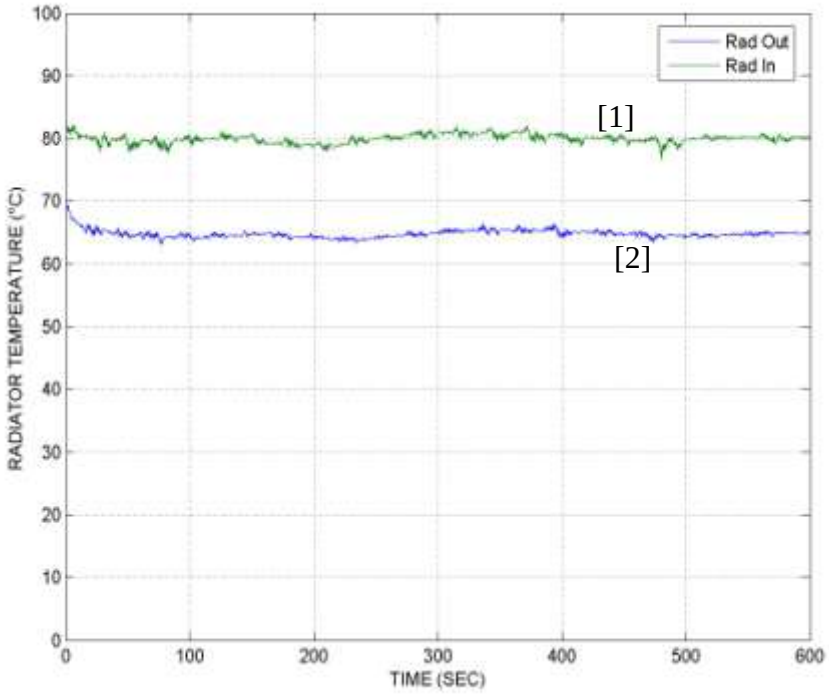
Rad Out
Rad In
[1]
[2]
RADIATOR TEMPERATURE (°C)
TIME (SEC)
0
10
20
30
40
50
60
70
80
90
100
0
100
200
300
400
500
600

(b)

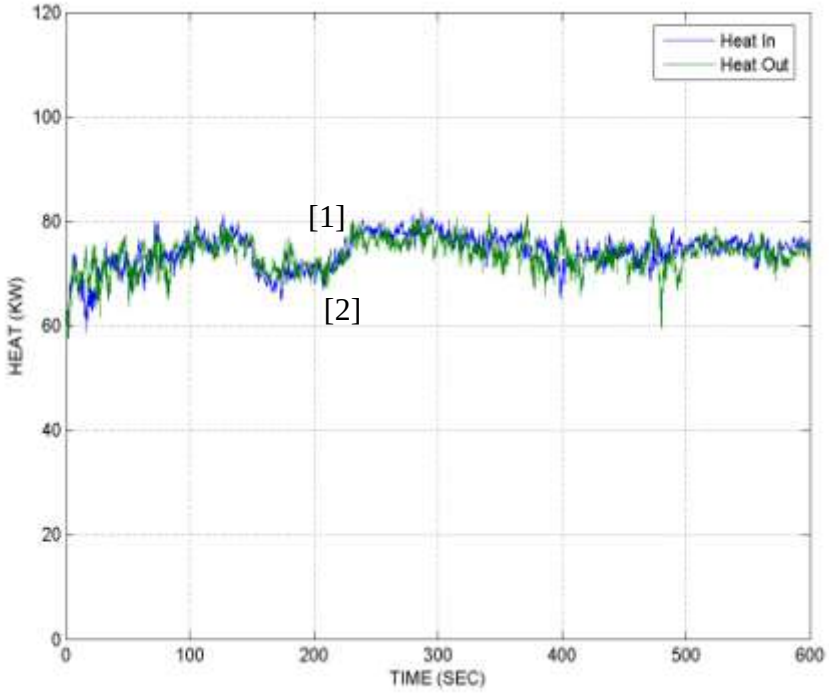

(c)

Figure A.23: Temperature and heat plots for Test #5 configuration at 3,000 RPM (a) heat exchanger inlet [1] and outlet [2] temperature, (b) radiator inlet [1] and outlet temperature [2] and, (c) heat input [1] and heat rejected [2].

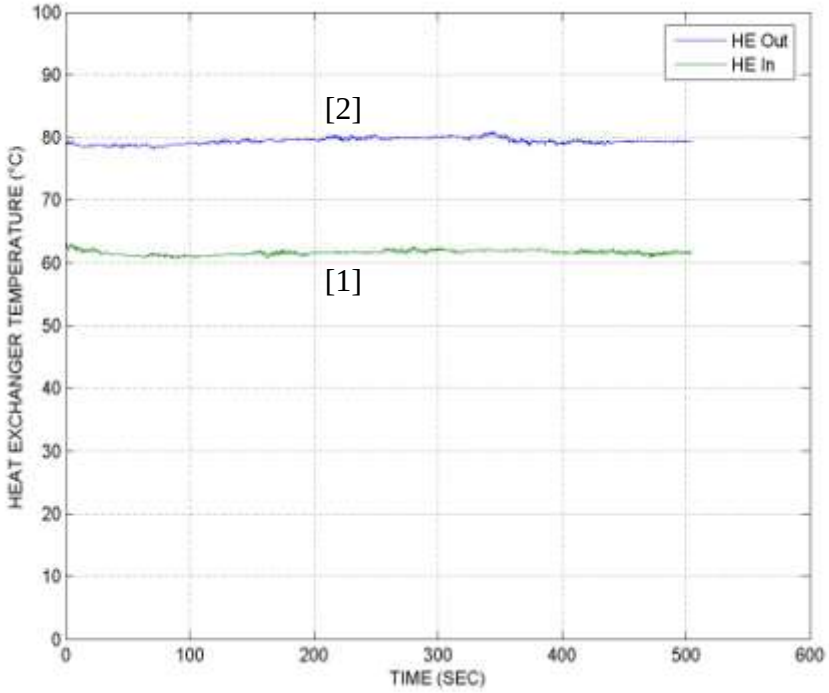
HE Out
HE In
[2]
[1]
HEAT EXCHANGER TEMPERATURE (°C)
TIME (SEC)
0
10
20
30
40
50
60
70
80
90
100
0
100
200
300
400
500
600

(a)

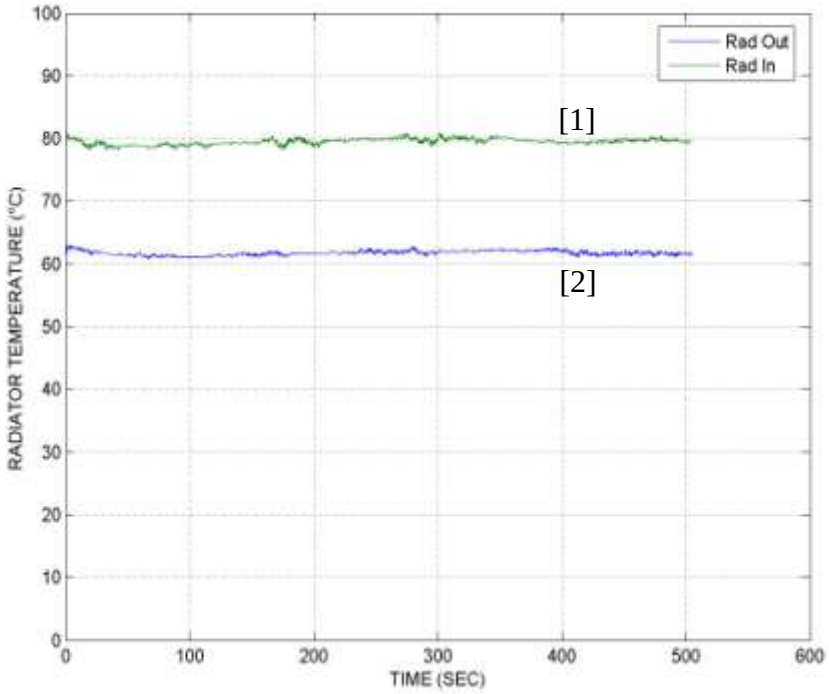
Rad Out
Rad In
[1]
[2]
RADIATOR TEMPERATURE (°C)
TIME (SEC)
0
10
20
30
40
50
60
70
80
90
100
0
100
200
300
400
500
600

(b)

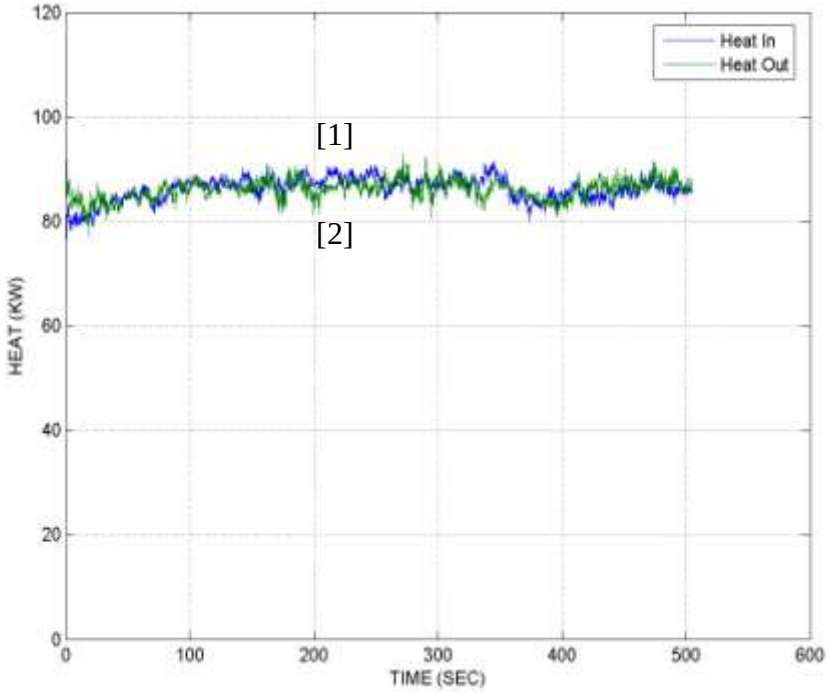

(c)

Figure A.24: Temperature and heat plots for Test #5 configuration at 4,000 RPM (a) heat exchanger inlet [1] and outlet [2] temperature, (b) radiator inlet [1] and outlet temperature [2] and, (c) heat input [1] and heat rejected [2] at 4,000 RPM.

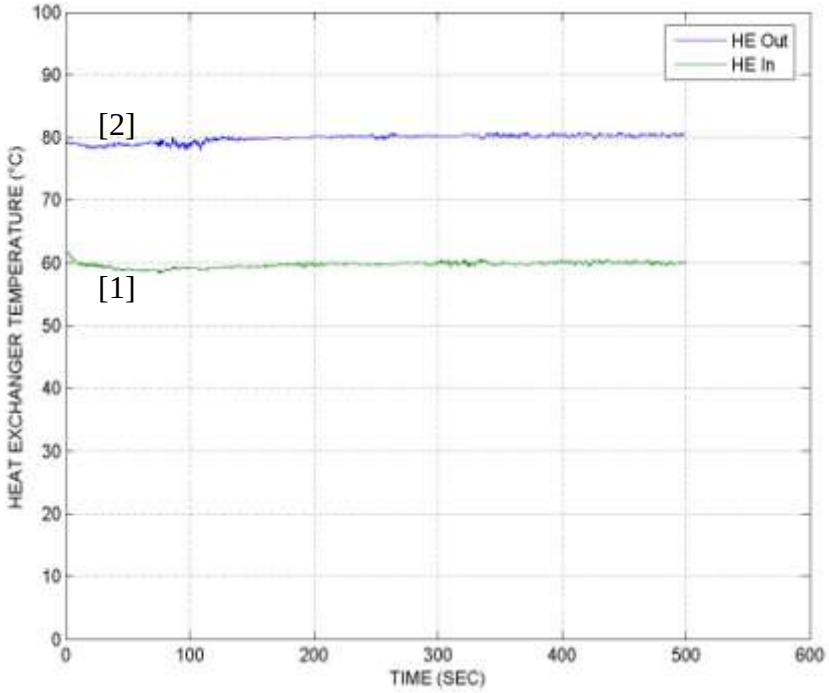
HE Out
HE In
[2]
[1]
HEAT EXCHANGER TEMPERATURE (°C)
TIME (SEC)
0
10
20
30
40
50
60
70
80
90
100
0
100
200
300
400
500
600

(a)

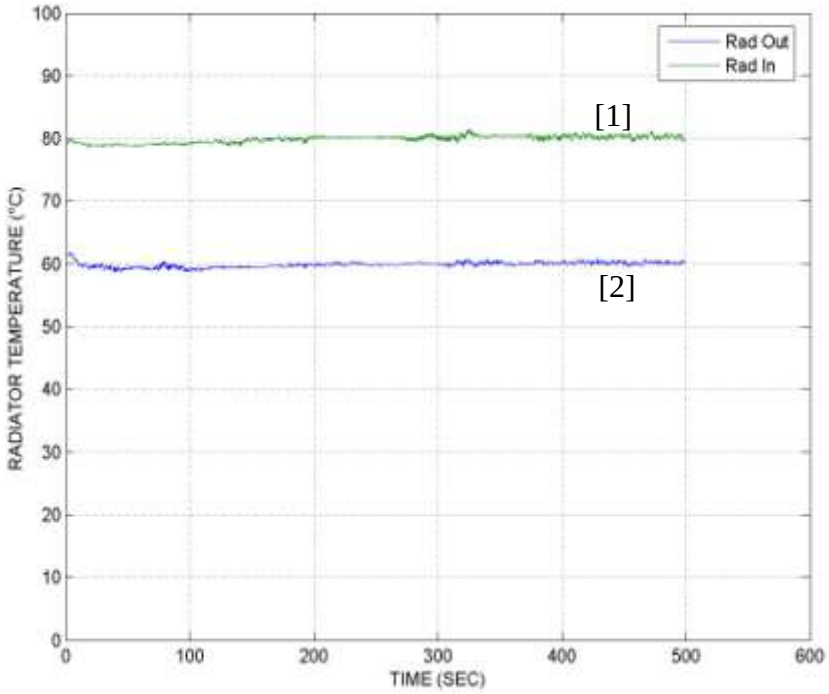
Rad Out
Rad In
[1]
[2]
RADIATOR TEMPERATURE (°C)
TIME (SEC)
0
10
20
30
40
50
60
70
80
90
100
0
100
200
300
400
500
600

(b)

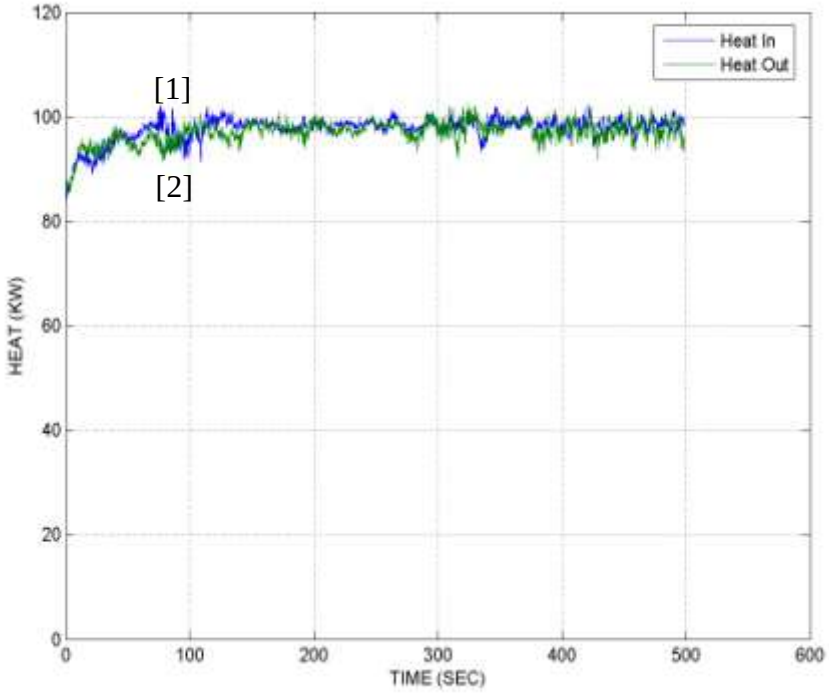

(c)

Figure A.25: Temperature and heat plots for Test #5 configuration at 5,000 RPM (a) heat exchanger inlet [1] and outlet [2] temperature, (b) radiator inlet [1] and outlet temperature [2] and, (c) heat input [1] and heat rejected [2].

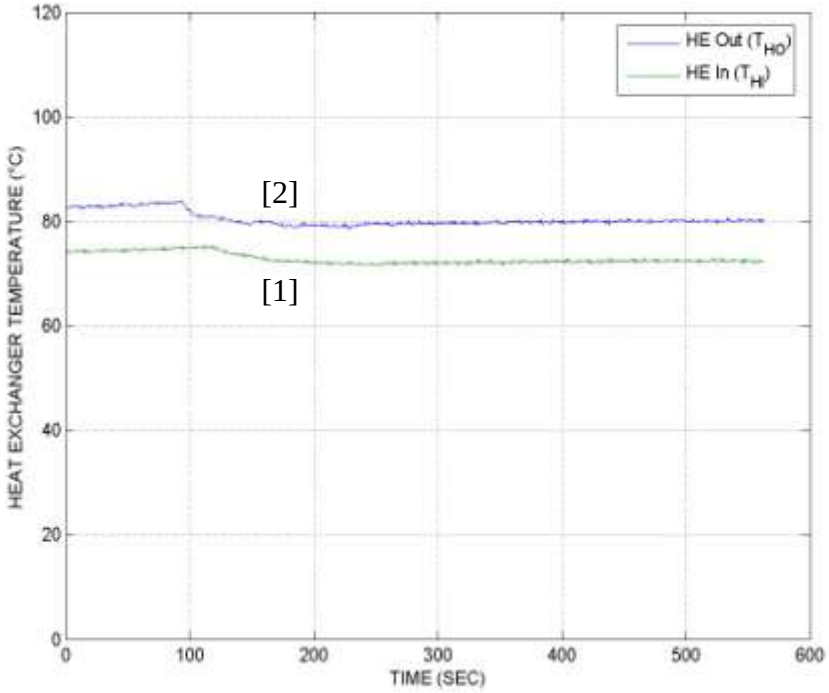
HE Out (T_{HO})
HE In (T_{HI})
[2]
[1]
HEAT EXCHANGER TEMPERATURE (°C)
TIME (SEC)
0
20
40
60
80
100
120
0
100
200
300
400
500
600

(a)

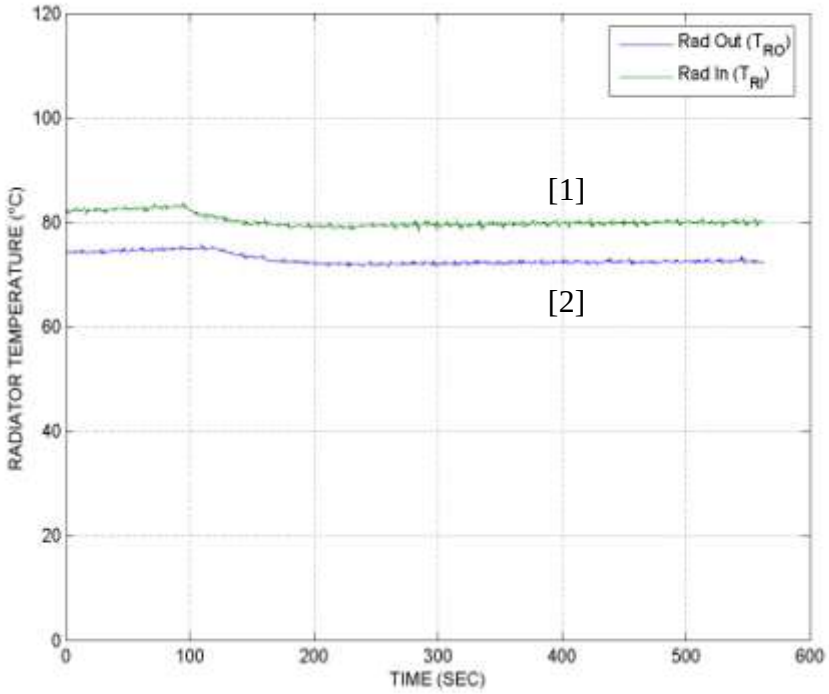
Rad Out (T_{RO})
Rad In (T_{RI})
[1]
[2]
RADIATOR TEMPERATURE (°C)
TIME (SEC)
0
20
40
60
80
100
120
0
100
200
300
400
500
600

(b)

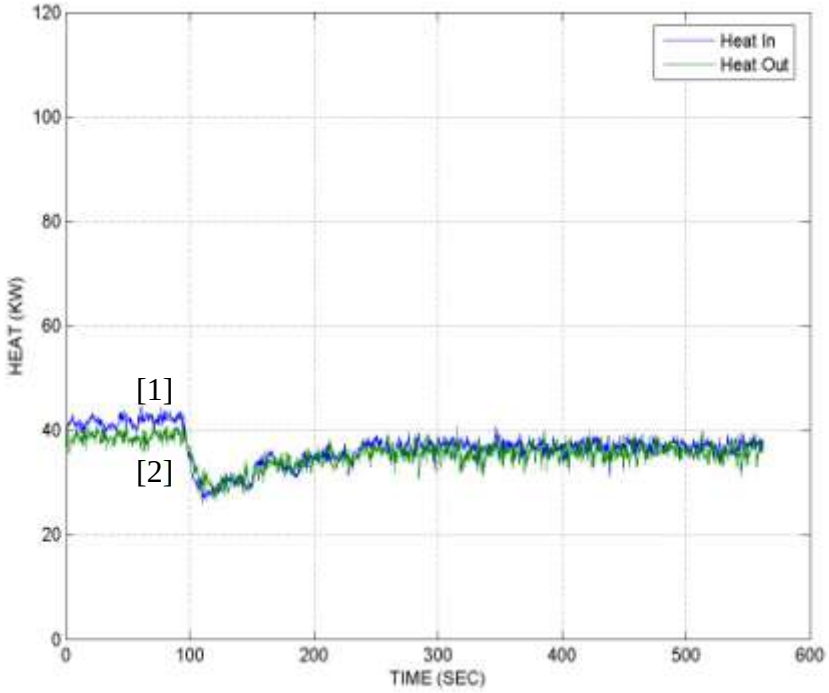

(c)

Figure A.26: Temperature and heat plots for Test #6 configuration at 1,000 RPM (a) heat exchanger inlet [1] and outlet [2] temperature, (b) radiator inlet [1] and outlet temperature [2] and, (c) heat input [1] and heat rejected [2].

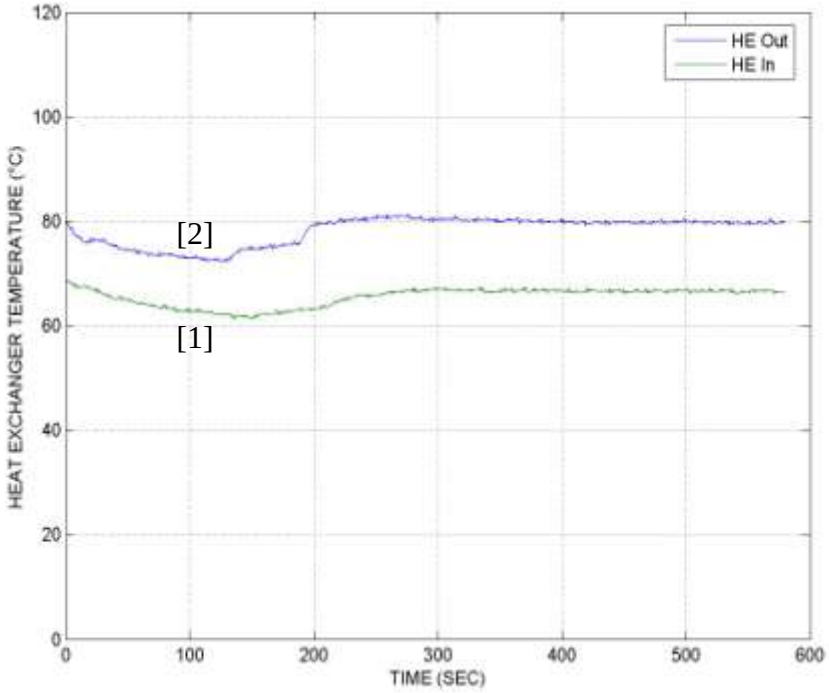
HE Out
HE In
[2]
[1]
HEAT EXCHANGER TEMPERATURE (°C)
TIME (SEC)
0
20
40
60
80
100
120
0
100
200
300
400
500
600

(a)

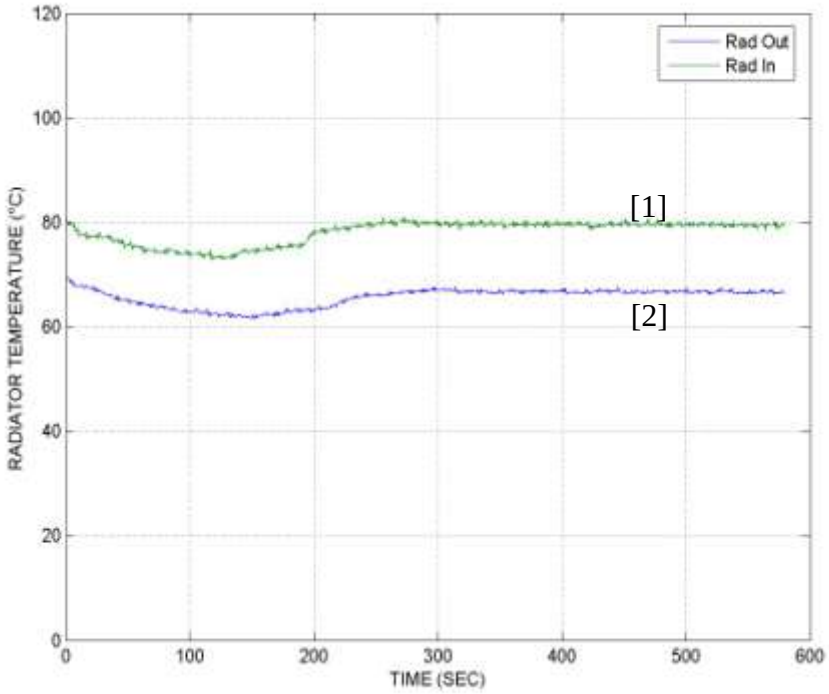
Rad Out
Rad In
[1]
[2]
RADIATOR TEMPERATURE (°C)
TIME (SEC)
0
20
40
60
80
100
120
0
100
200
300
400
500
600

(b)

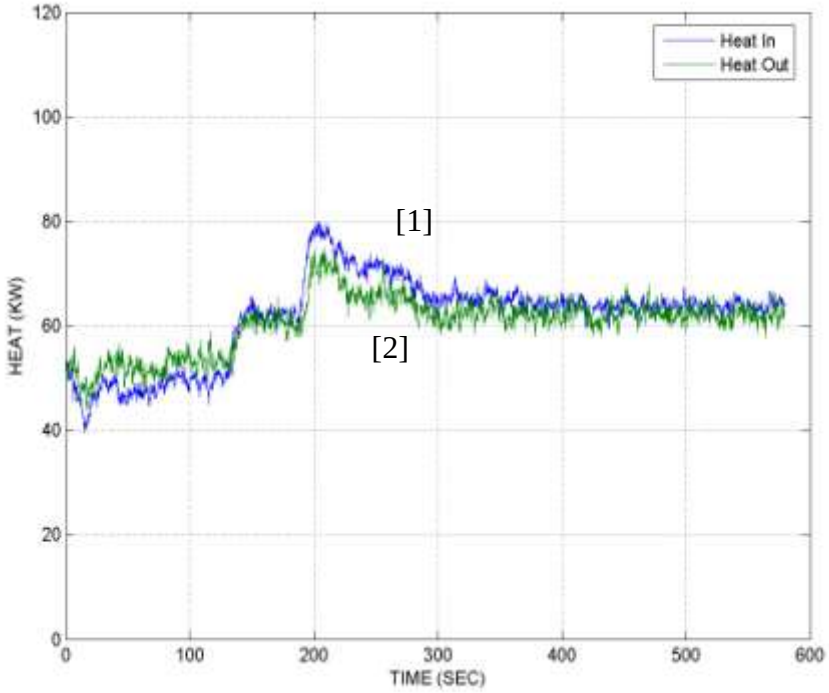

(c)

Figure A.27: Temperature and heat plots for Test #6 configuration at 2,000 RPM (a) heat exchanger inlet [1] and outlet [2] temperature, (b) radiator inlet [1] and outlet temperature [2] and, (c) heat input [1] and heat rejected [2].

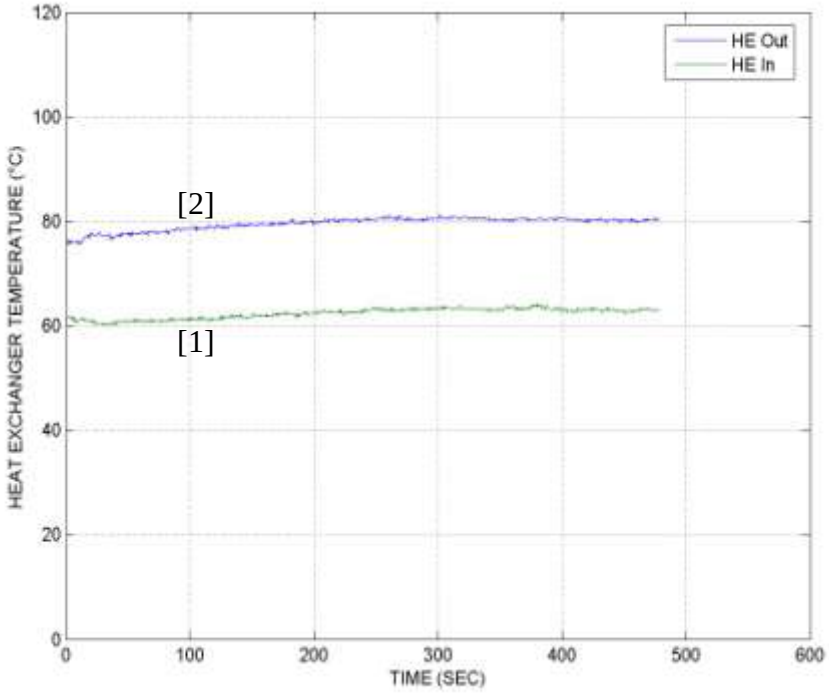
HE Out
HE In
[2]
[1]
HEAT EXCHANGER TEMPERATURE (°C)
TIME (SEC)
0
20
40
60
80
100
120
0
100
200
300
400
500
600

(a)

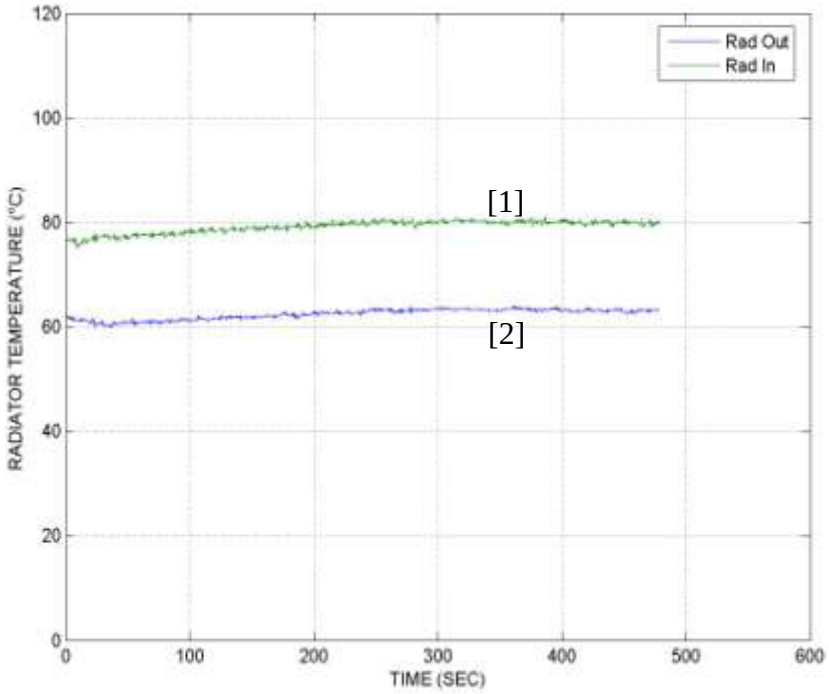
Rad Out
Rad In
[1]
[2]
RADIATOR TEMPERATURE (°C)
TIME (SEC)
0
20
40
60
80
100
120
0
100
200
300
400
500
600

(b)

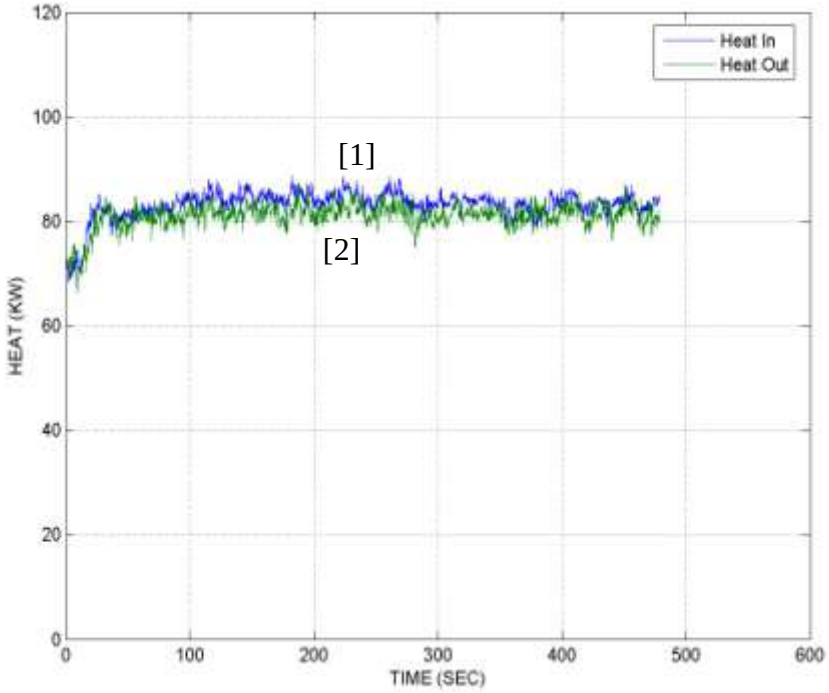

(c)

Figure A.28: Temperature and heat plots for Test #6 configuration at 3,000 RPM (a) heat exchanger inlet [1] and outlet [2] temperature, (b) radiator inlet [1] and outlet temperature [2] and, (c) heat input [1] and heat rejected [2].

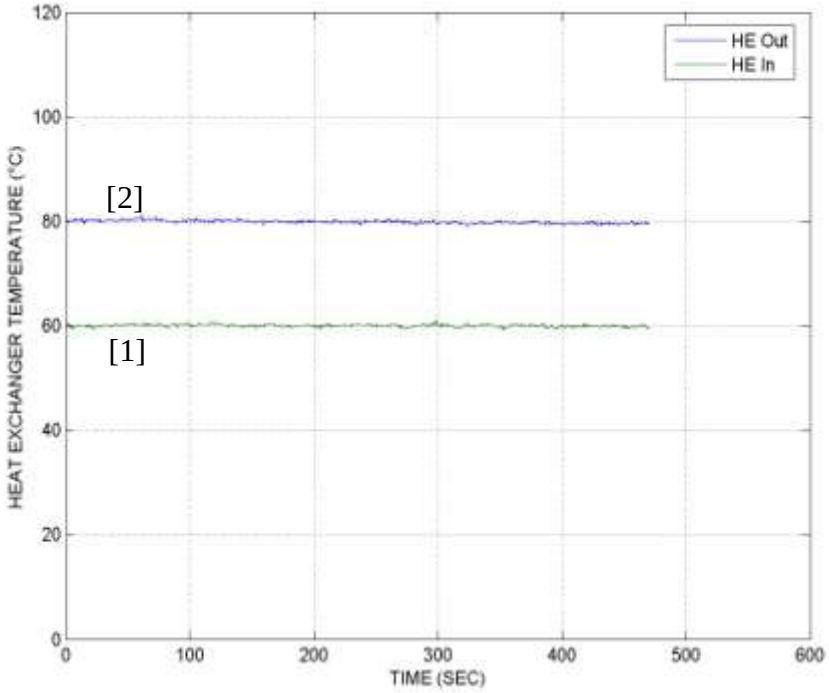
HE Out
HE In
[2]
[1]
HEAT EXCHANGER TEMPERATURE (°C)
TIME (SEC)
0
20
40
60
80
100
120
0
100
200
300
400
500
600

(a)

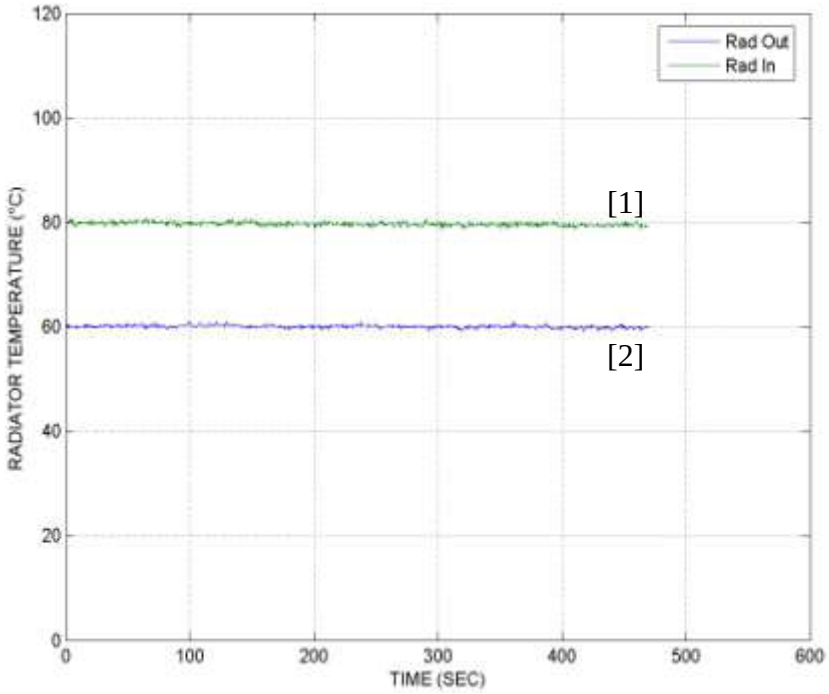
Rad Out
Rad In
[1]
[2]
RADIATOR TEMPERATURE (°C)
TIME (SEC)
0
20
40
60
80
100
120
0
100
200
300
400
500
600

(b)

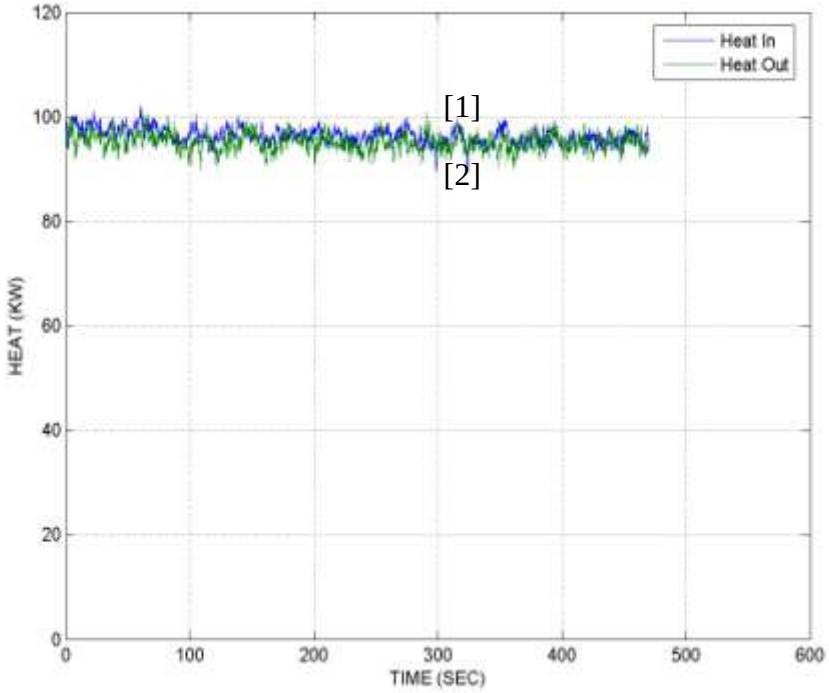

(c)

Figure A.29: Temperature and heat plots for Test #6 configuration at 4,000 RPM (a) heat exchanger inlet [1] and outlet [2] temperature, (b) radiator inlet [1] and outlet temperature [2] and, (c) heat input [1] and heat rejected [2].

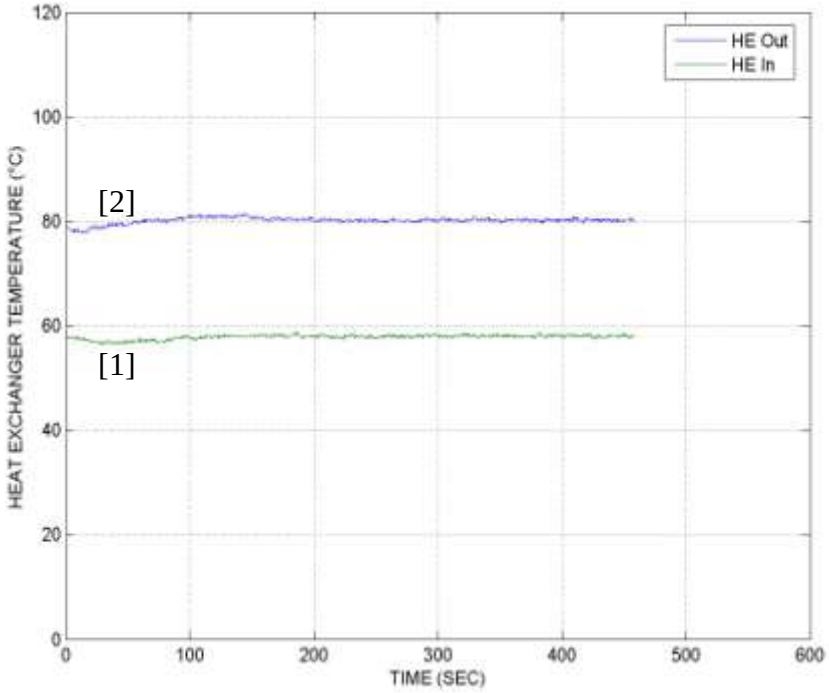
HE Out
HE In
[2]
[1]
HEAT EXCHANGER TEMPERATURE (°C)
TIME (SEC)
0
20
40
60
80
100
120
0
100
200
300
400
500
600

(a)

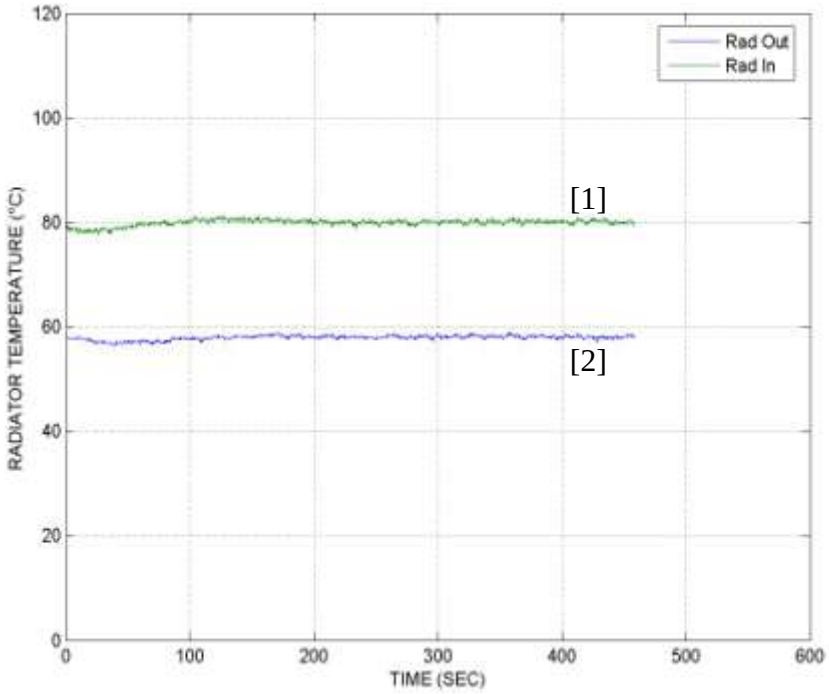
Rad Out
Rad In
[1]
[2]
RADIATOR TEMPERATURE (°C)
TIME (SEC)
0
20
40
60
80
100
120
0
100
200
300
400
500
600

(b)

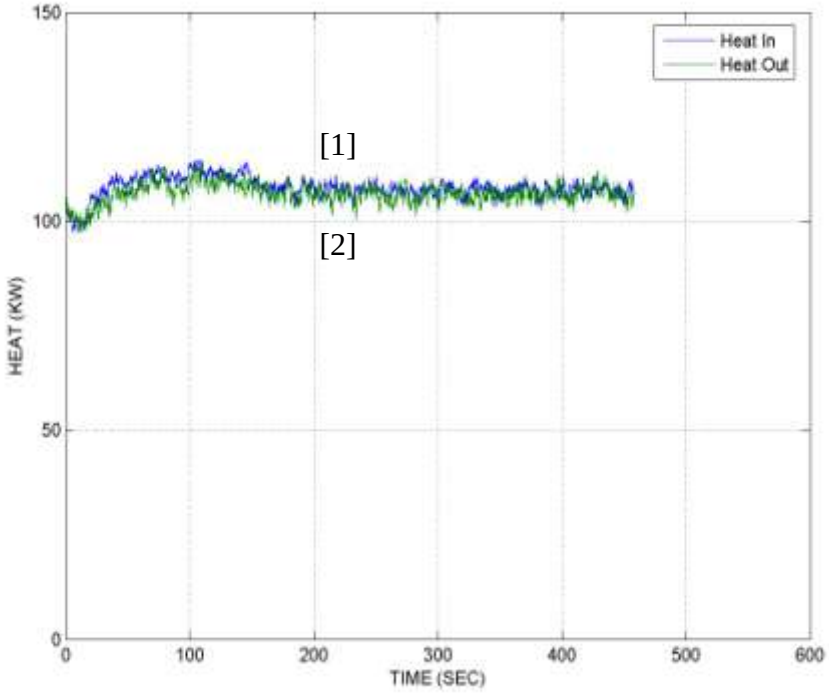

(c)

Figure A.30: Temperature and heat plots for Test #6 configuration at 5,000 RPM (a) heat exchanger inlet [1] and outlet [2] temperature, (b) radiator inlet [1] and outlet temperature [2] and, (c) heat input [1] and heat rejected [2].

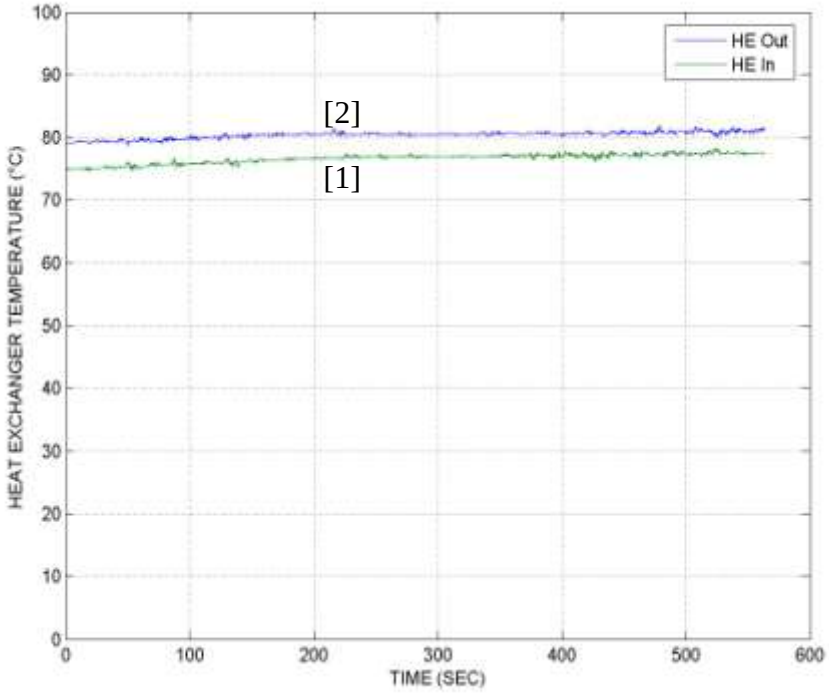
HE Out
HE In
[2]
[1]
HEAT EXCHANGER TEMPERATURE (°C)
TIME (SEC)
0
10
20
30
40
50
60
70
80
90
100
0
100
200
300
400
500
600

(a)

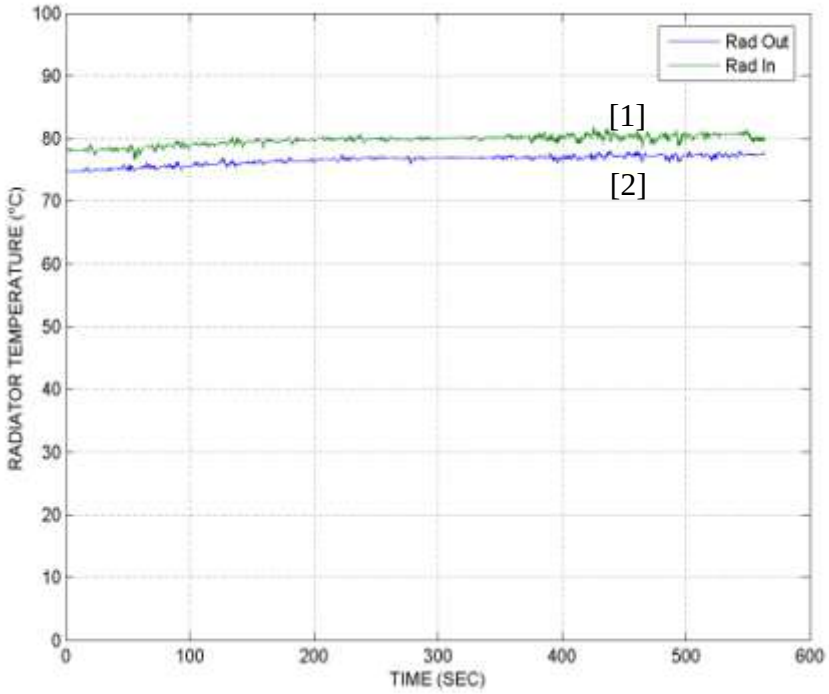
Rad Out
Rad In
[1]
[2]
RADIATOR TEMPERATURE (°C)
TIME (SEC)
0
10
20
30
40
50
60
70
80
90
100
0
100
200
300
400
500
600

(b)

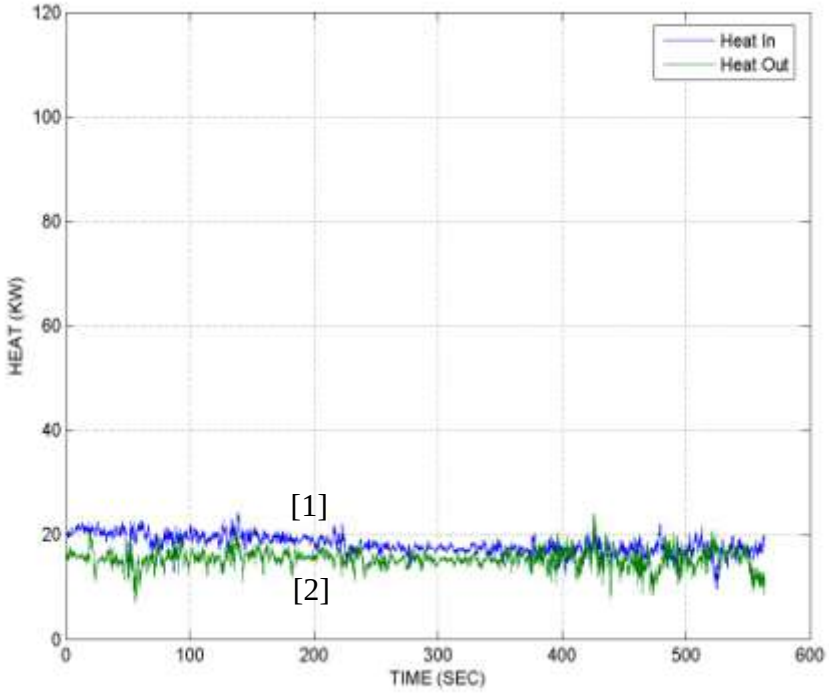

(c)

Figure A.31: Temperature and heat plots for Test #7 configuration at 1,000 RPM (a) heat exchanger inlet [1] and outlet [2] temperature, (b) radiator inlet [1] and outlet temperature [2] and, (c) heat input [1] and heat rejected [2].

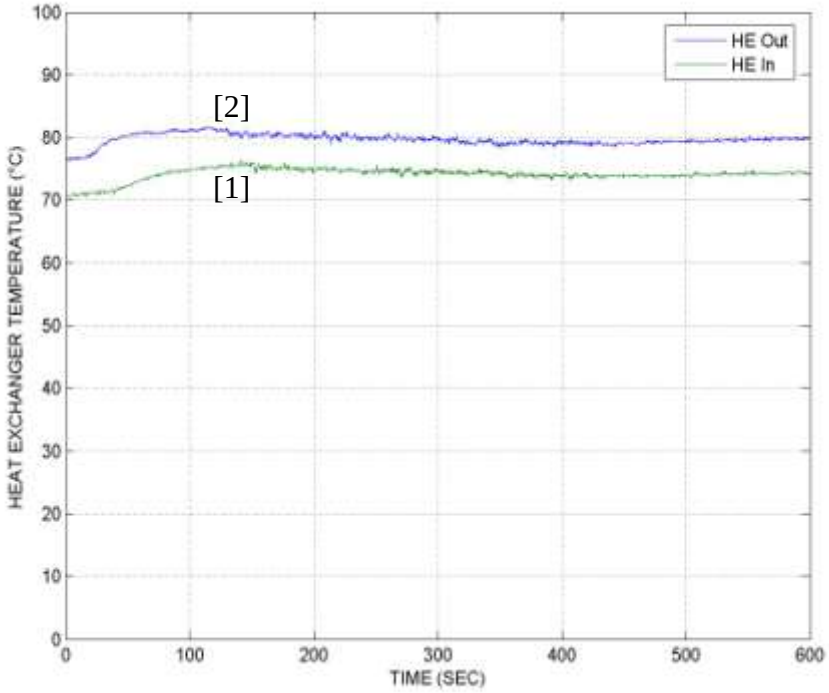
HE Out
HE In
[2]
[1]
HEAT EXCHANGER TEMPERATURE (°C)
TIME (SEC)
0
10
20
30
40
50
60
70
80
90
100
0
100
200
300
400
500
600

(a)

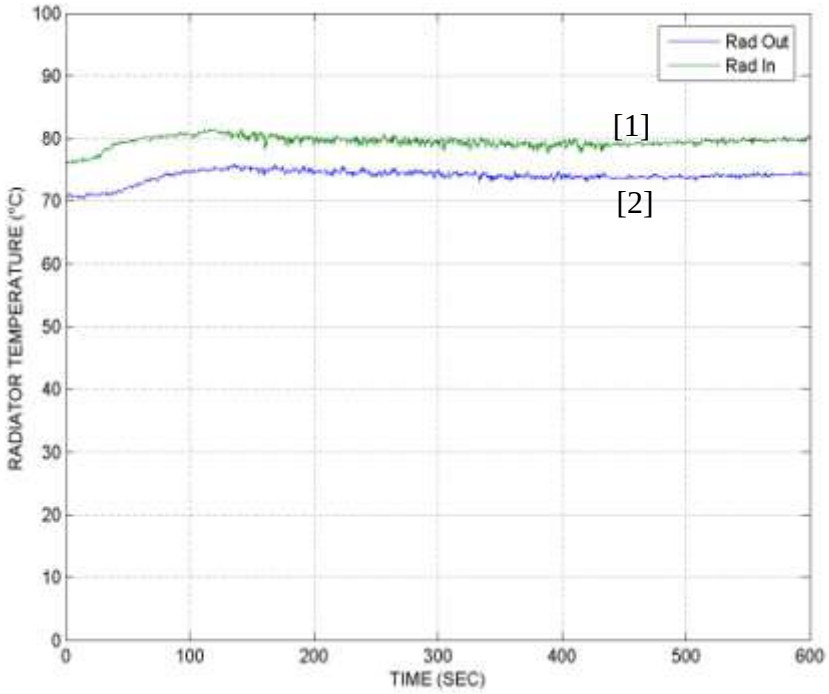
Rad Out
Rad In
[1]
[2]
RADIATOR TEMPERATURE (°C)
TIME (SEC)
0
10
20
30
40
50
60
70
80
90
100
0
100
200
300
400
500
600

(b)

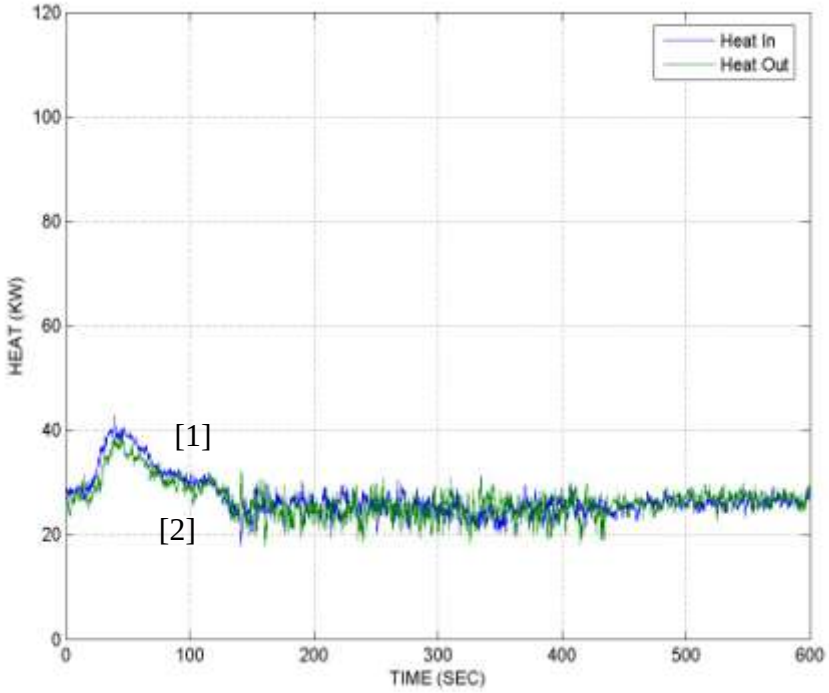

(c)

Figure A.32: Temperature and heat plots for Test #7 configuration at 2,000 RPM (a) heat exchanger inlet [1] and outlet [2] temperature, (b) radiator inlet [1] and outlet temperature [2] and, (c) heat input [1] and heat rejected [2].

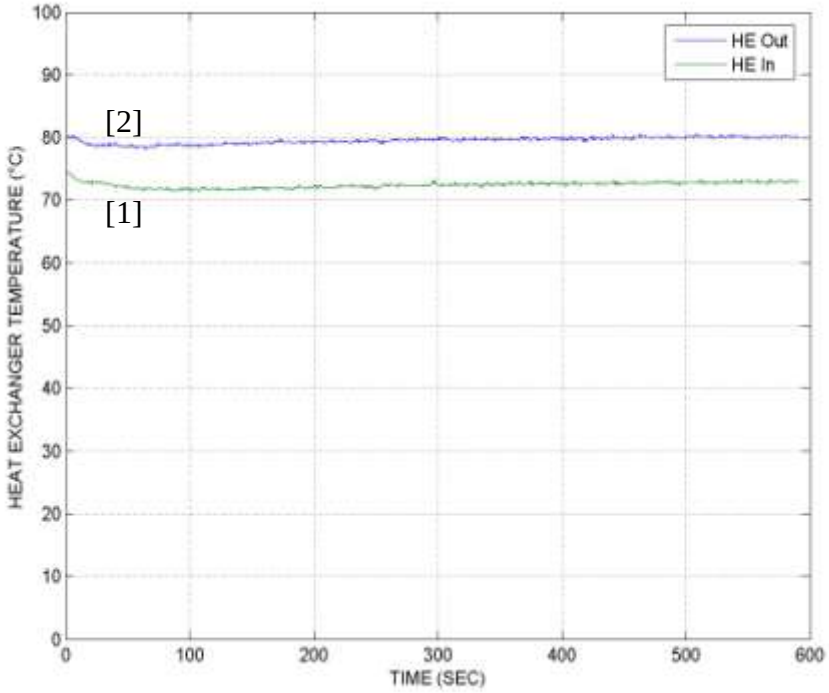
HE Out
HE In
[2]
[1]
HEAT EXCHANGER TEMPERATURE (°C)
TIME (SEC)
0
10
20
30
40
50
60
70
80
90
100
0
100
200
300
400
500
600

(a)

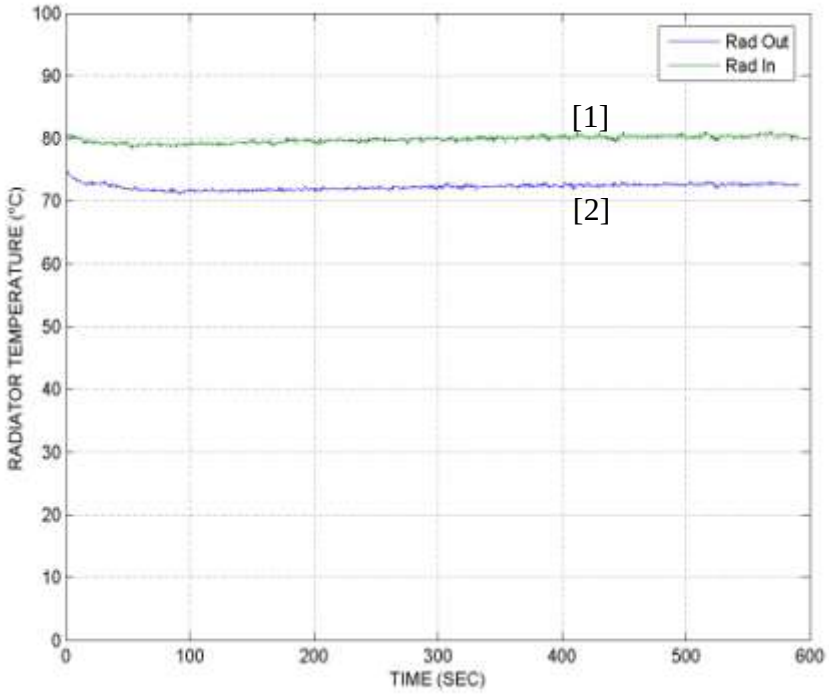
Rad Out
Rad In
[1]
[2]
RADIATOR TEMPERATURE (°C)
TIME (SEC)
0
10
20
30
40
50
60
70
80
90
100
0
100
200
300
400
500
600

(b)

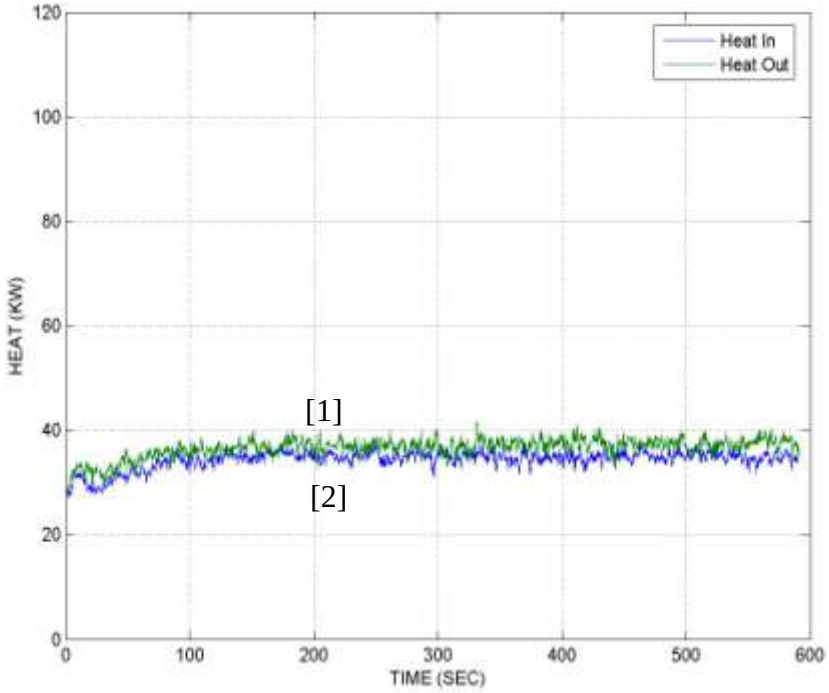

(c)

Figure A.33: Temperature and heat plots for Test #7 configuration at 3,000 RPM (a) heat exchanger inlet [1] and outlet [2] temperature, (b) radiator inlet [1] and outlet temperature [2] and, (c) heat input [1] and heat rejected [2].

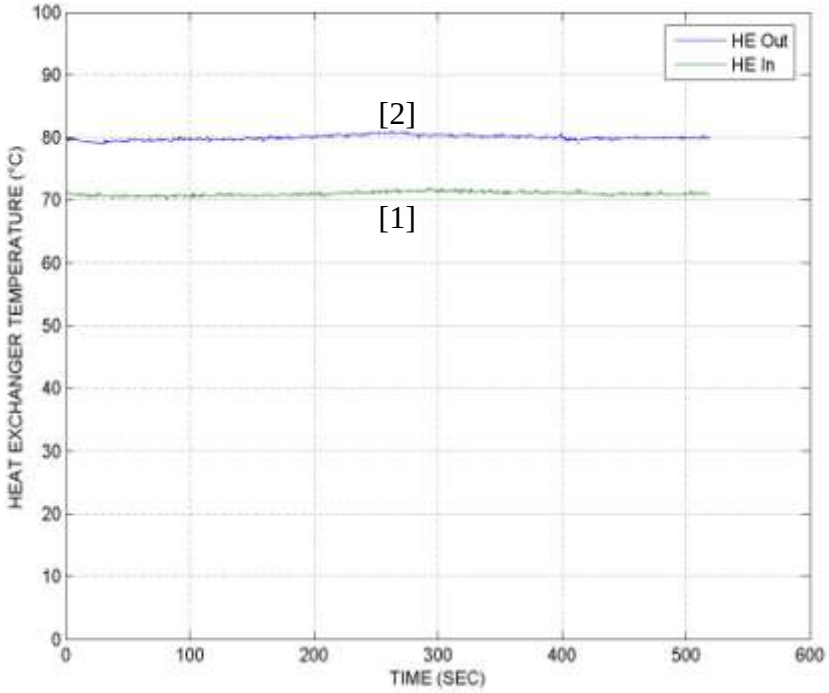
HE Out
HE In
[2]
[1]
HEAT EXCHANGER TEMPERATURE (°C)
TIME (SEC)
0
10
20
30
40
50
60
70
80
90
100
0
100
200
300
400
500
600

(a)

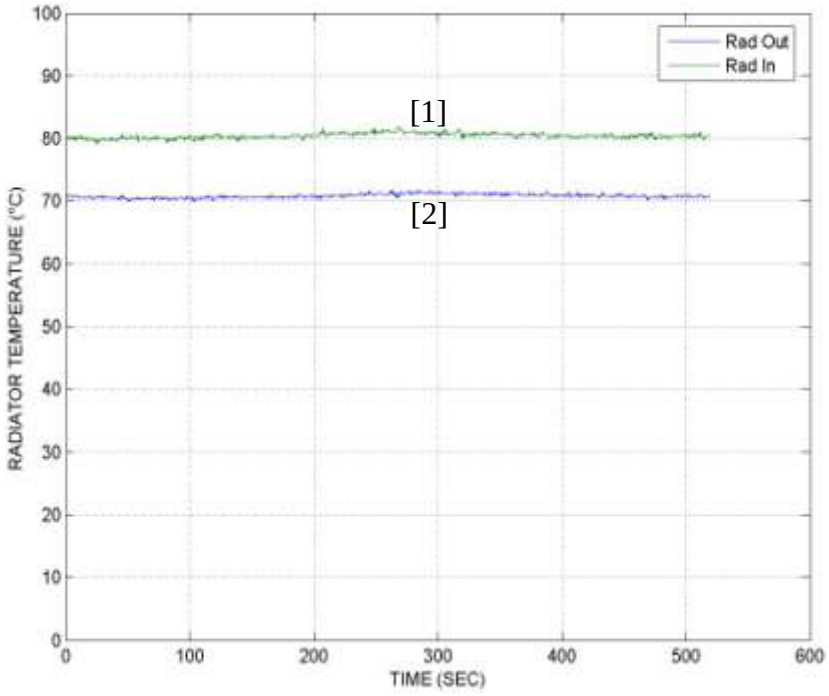
Rad Out
Rad In
[1]
[2]
RADIATOR TEMPERATURE (°C)
TIME (SEC)
0
10
20
30
40
50
60
70
80
90
100
0
100
200
300
400
500
600

(b)

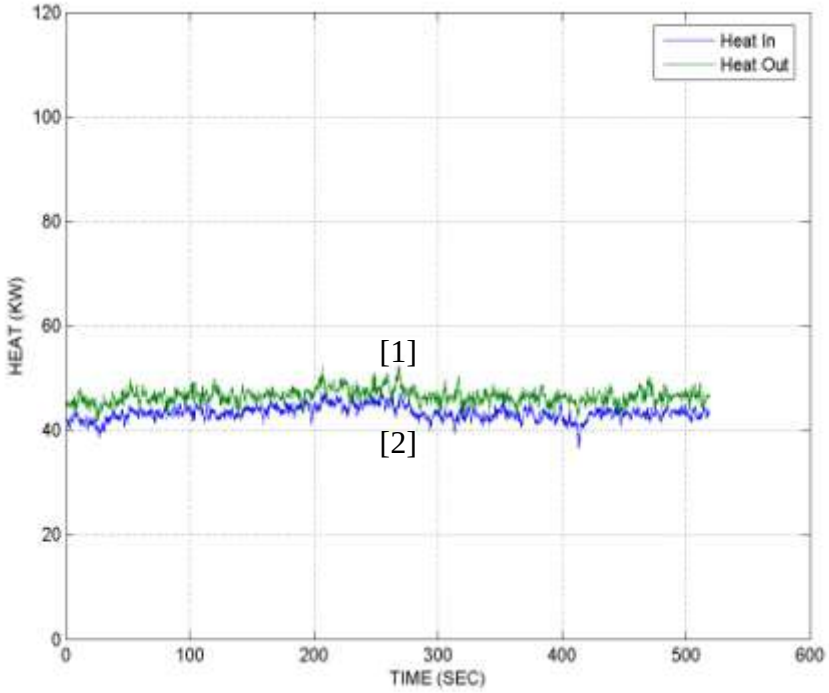

(c)

Figure A.34: Temperature and heat plots for Test #7 configuration at 4,000 RPM (a) heat exchanger inlet [1] and outlet [2] temperature, (b) radiator inlet [1] and outlet temperature [2] and, (c) heat input [1] and heat rejected [2].

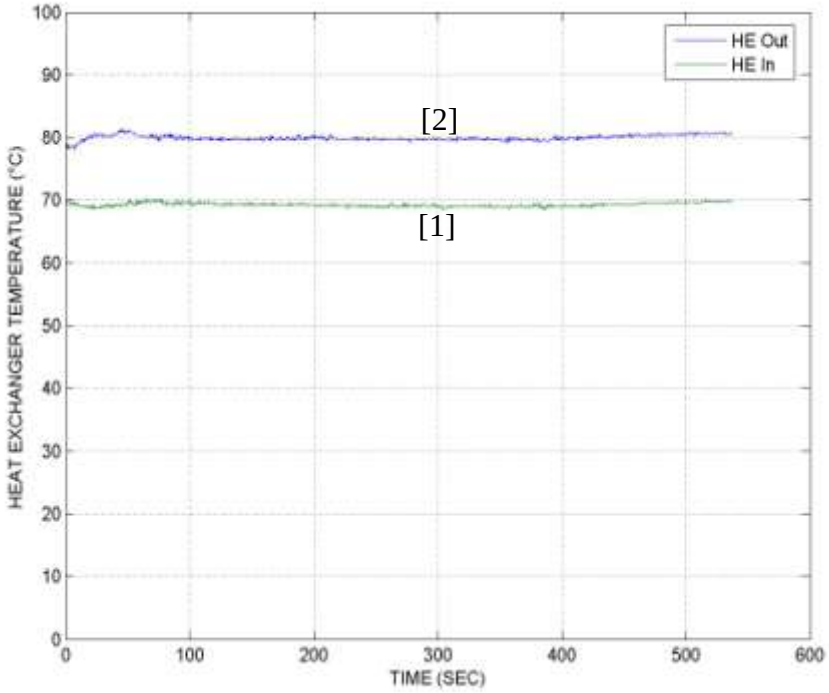
HE Out
HE In
[2]
[1]
HEAT EXCHANGER TEMPERATURE (°C)
TIME (SEC)
0
10
20
30
40
50
60
70
80
90
100
0
100
200
300
400
500
600

(a)

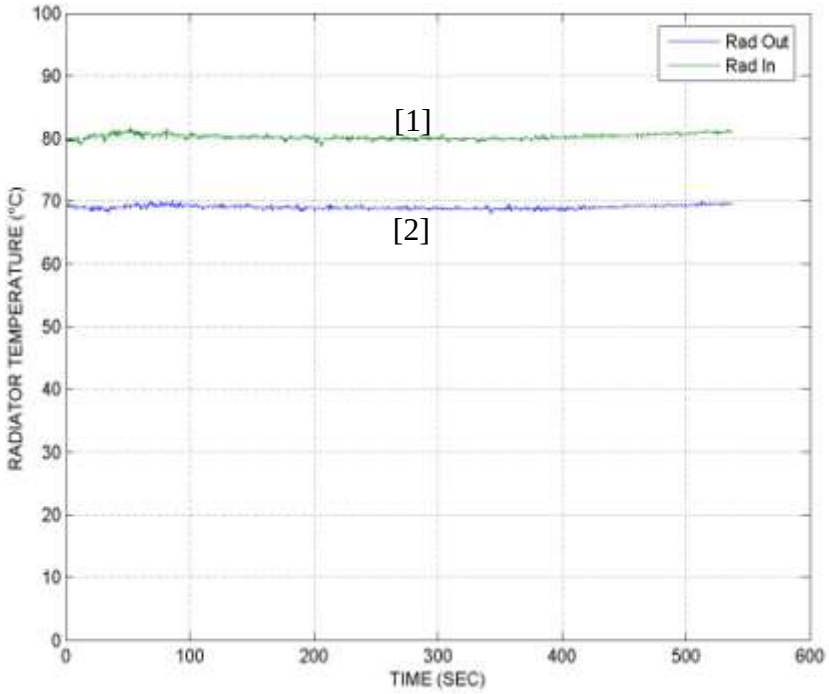
Rad Out
Rad In
[1]
[2]
RADIATOR TEMPERATURE (°C)
TIME (SEC)
0
10
20
30
40
50
60
70
80
90
100
0
100
200
300
400
500
600

(b)

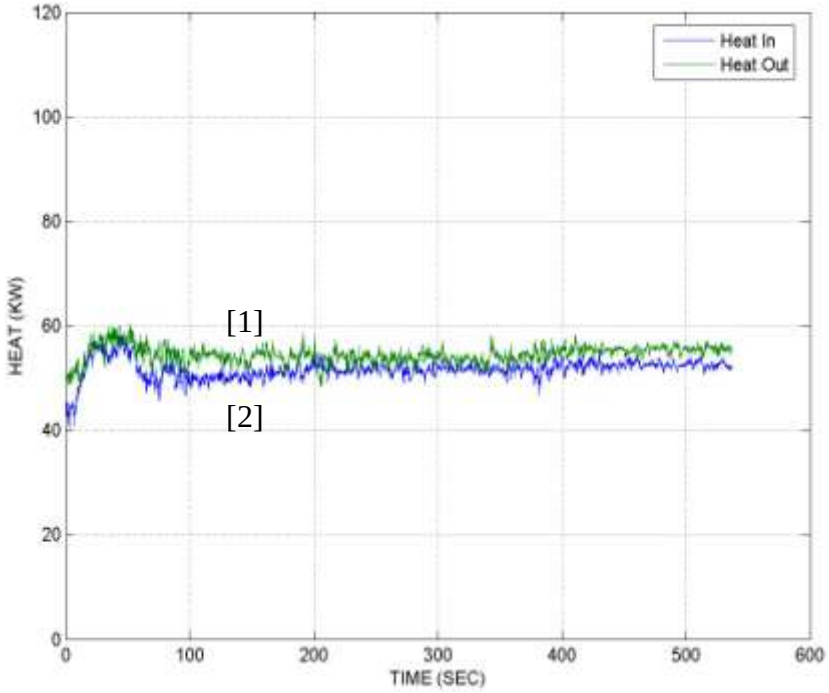

(c)

Figure A.35: Temperature and Heat plots for Test #7 configuration at 5,000 RPM (a) heat exchanger inlet [1] and outlet [2] temperature, (b) radiator inlet [1] and outlet temperature [2] and, (c) heat input [1] and heat rejected [2].

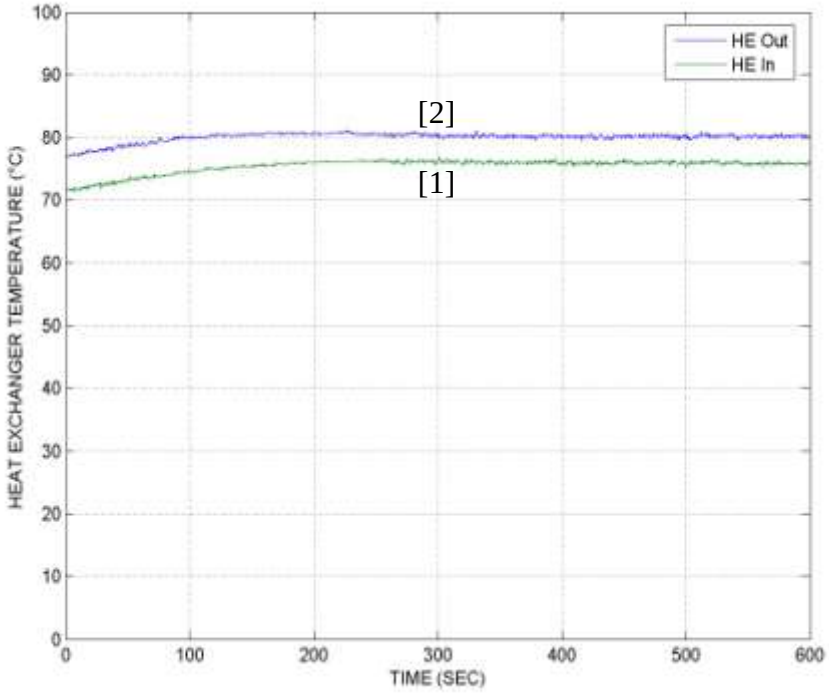
HE Out
HE In
[2]
[1]
HEAT EXCHANGER TEMPERATURE (°C)
TIME (SEC)
0
10
20
30
40
50
60
70
80
90
100
0
100
200
300
400
500
600

(a)

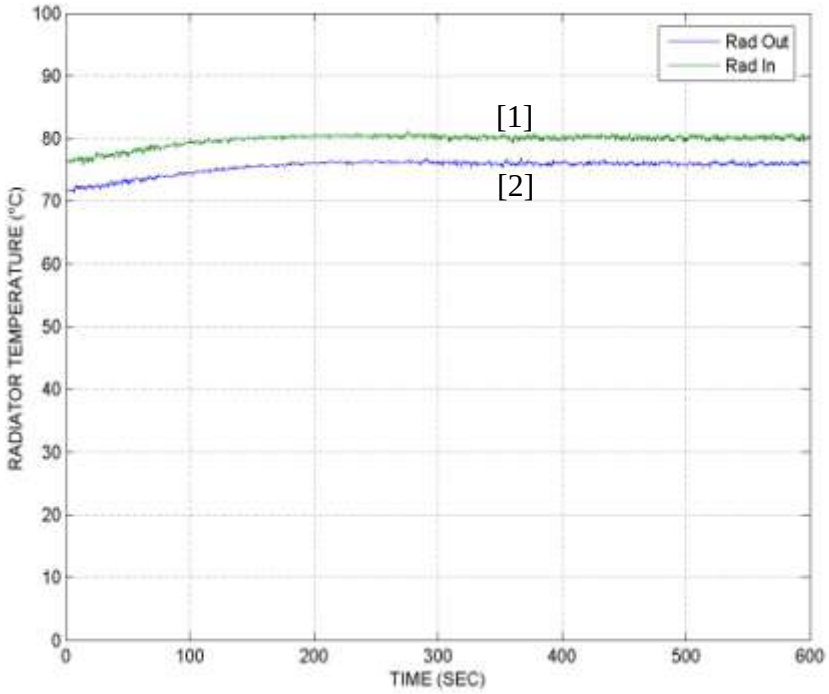
Rad Out
Rad In
[1]
[2]
RADIATOR TEMPERATURE (°C)
TIME (SEC)
0
10
20
30
40
50
60
70
80
90
100
0
100
200
300
400
500
600

(b)

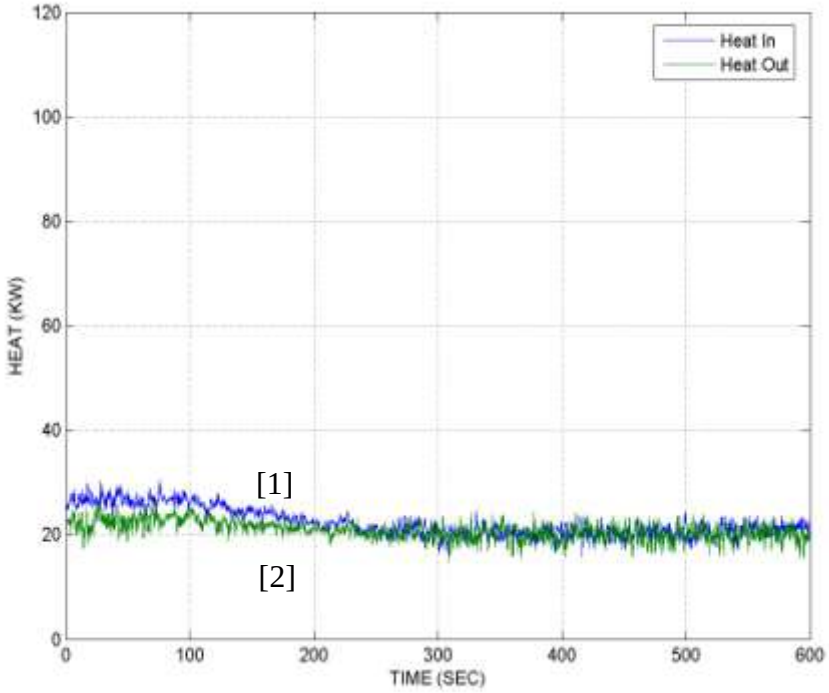

(c)

Figure A.36: Temperature and heat plots for Test #8 configuration at 1,000 RPM (a) heat exchanger inlet [1] and outlet [2] temperature, (b) radiator inlet [1] and outlet temperature [2] and, (c) heat input [1] and heat rejected [2].

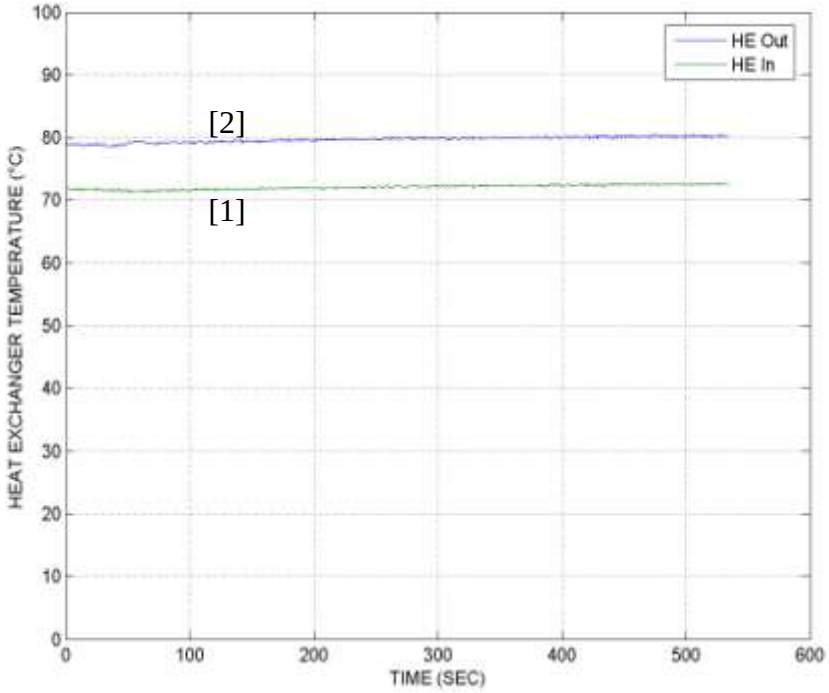
HE Out
HE In
[2]
[1]
HEAT EXCHANGER TEMPERATURE (°C)
TIME (SEC)
0
10
20
30
40
50
60
70
80
90
100
0
100
200
300
400
500
600

(a)

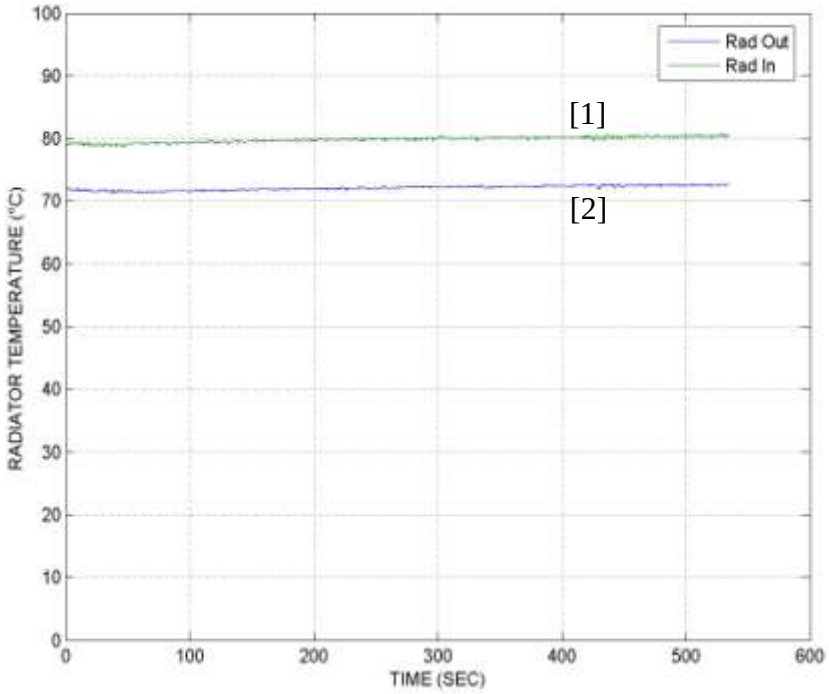
Rad Out
Rad In
[1]
[2]
RADIATOR TEMPERATURE (°C)
TIME (SEC)
0
10
20
30
40
50
60
70
80
90
100
0
100
200
300
400
500
600

(b)

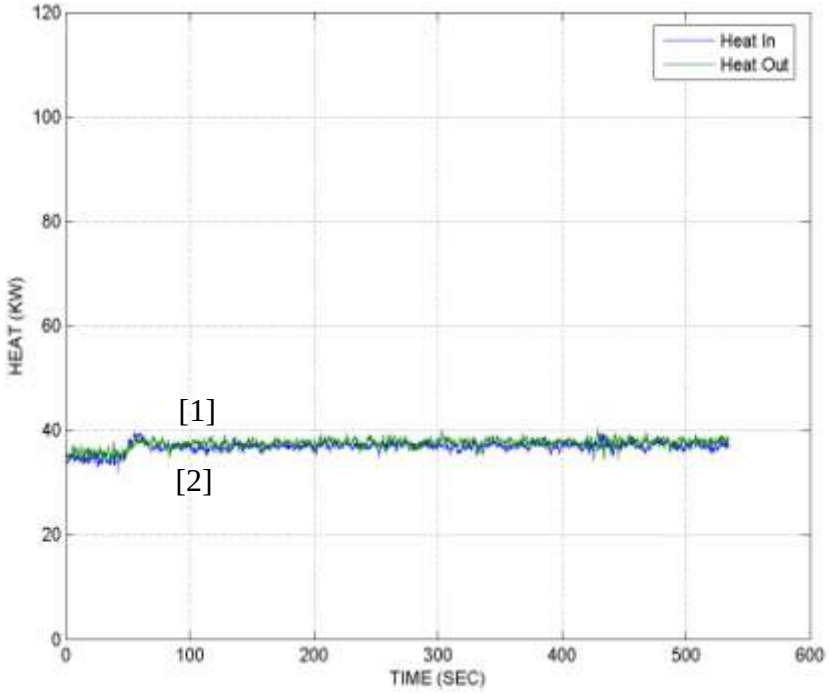

(c)

Figure A.37: Temperature and heat plots for Test #8 configuration at 2,000 RPM (a) heat exchanger inlet [1] and outlet [2] temperature, (b) radiator inlet [1] and outlet temperature [2] and, (c) heat input [1] and heat rejected [2].

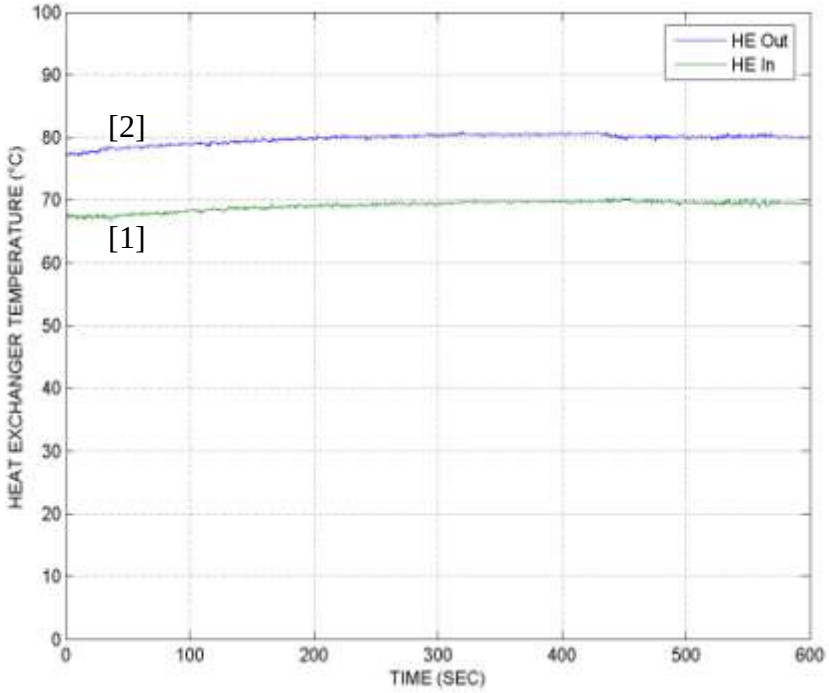
HE Out
HE In
[2]
[1]
HEAT EXCHANGER TEMPERATURE (°C)
TIME (SEC)
0
10
20
30
40
50
60
70
80
90
100
0
100
200
300
400
500
600

(a)

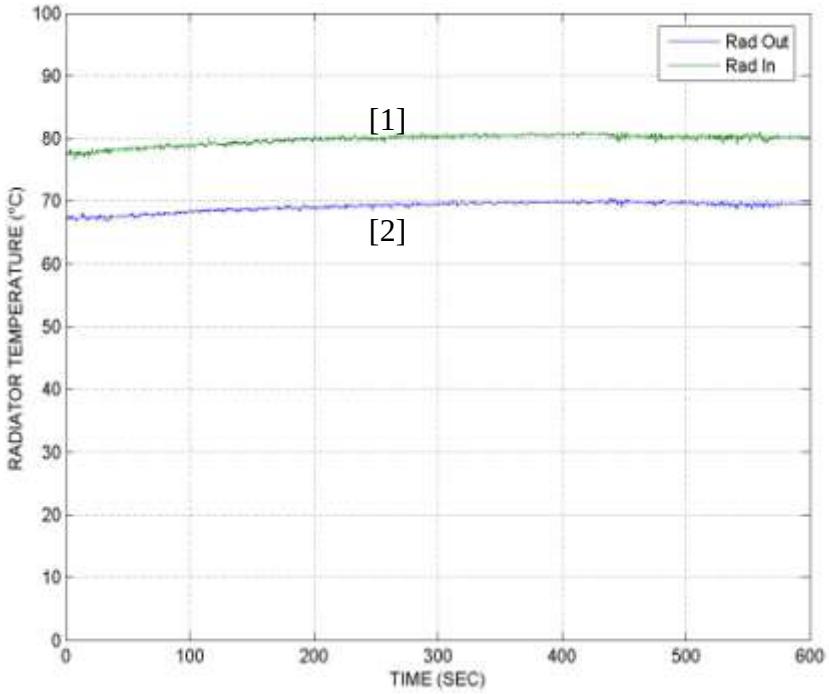
Rad Out
Rad In
[1]
[2]
RADIATOR TEMPERATURE (°C)
TIME (SEC)
0
10
20
30
40
50
60
70
80
90
100
0
100
200
300
400
500
600

(b)

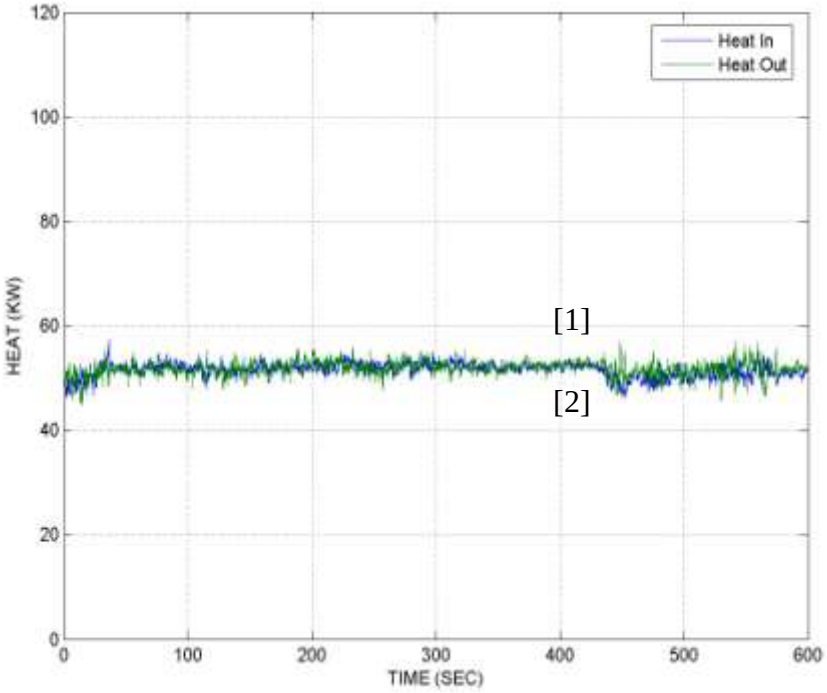

(c)

Figure A.38: Temperature and heat plots for Test #8 configuration at 3,000 RPM (a) heat exchanger inlet [1] and outlet [2] temperature, (b) radiator inlet [1] and outlet temperature [2] and, (c) heat input [1] and heat rejected [2].

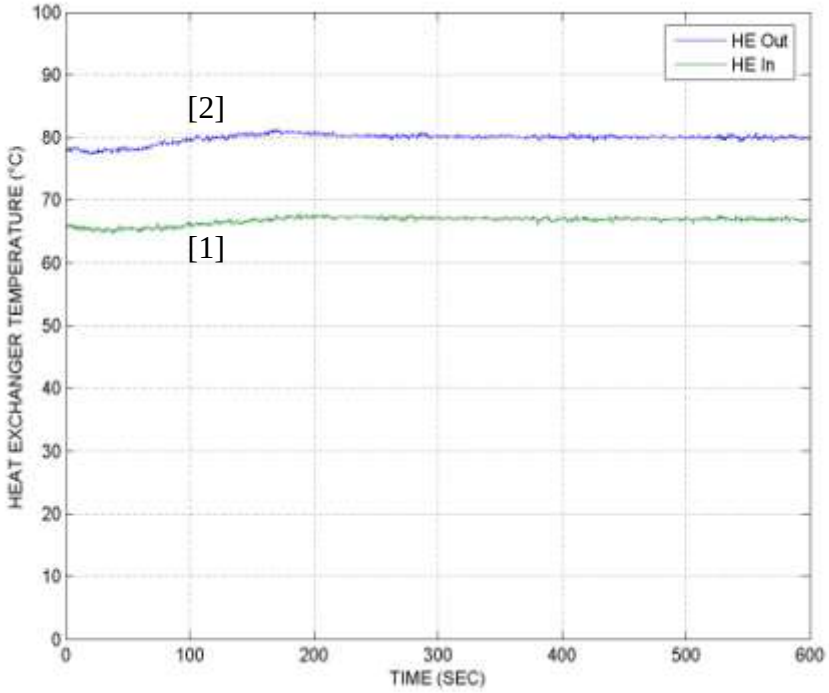
HE Out
HE In
[2]
[1]
HEAT EXCHANGER TEMPERATURE (°C)
TIME (SEC)
0
10
20
30
40
50
60
70
80
90
100
0
100
200
300
400
500
600

(a)

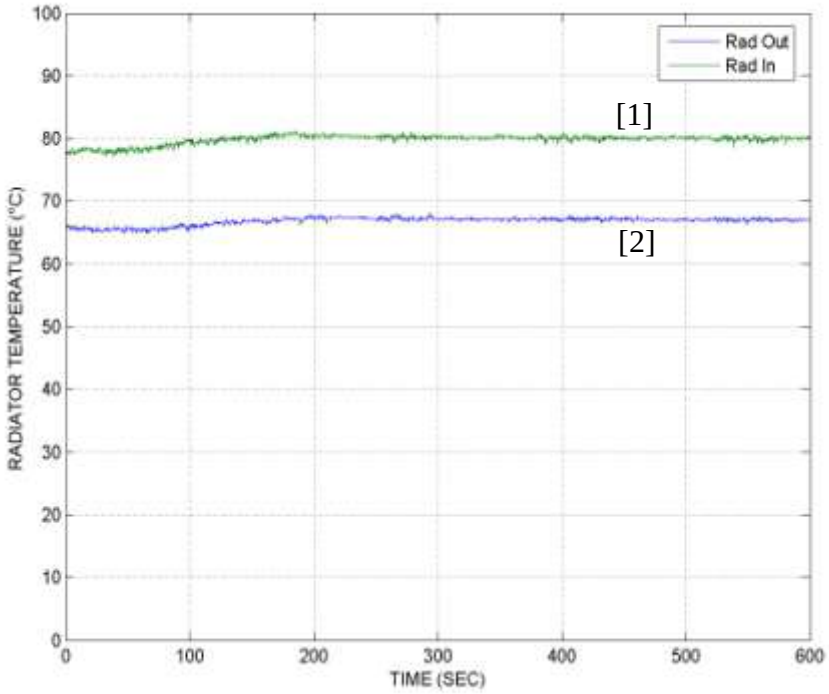
Rad Out
Rad In
[1]
[2]
RADIATOR TEMPERATURE (°C)
TIME (SEC)
0
10
20
30
40
50
60
70
80
90
100
0
100
200
300
400
500
600

(b)

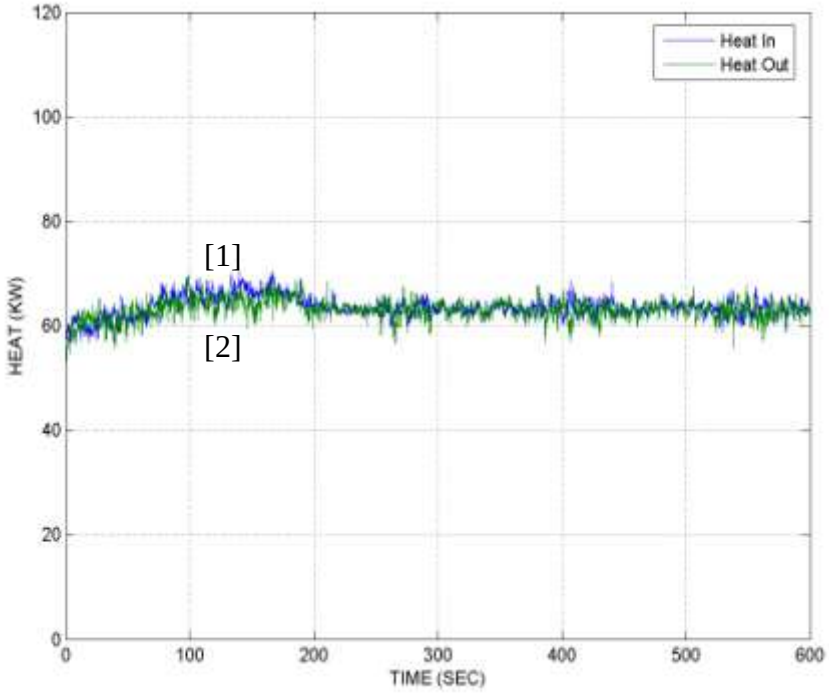

(c)

Figure A.39: Temperature and heat plots for Test #8 configuration at 4,000 RPM (a) heat exchanger inlet [1] and outlet [2] temperature, (b) radiator inlet [1] and outlet temperature [2] and, (c) heat input [1] and heat rejected [2].

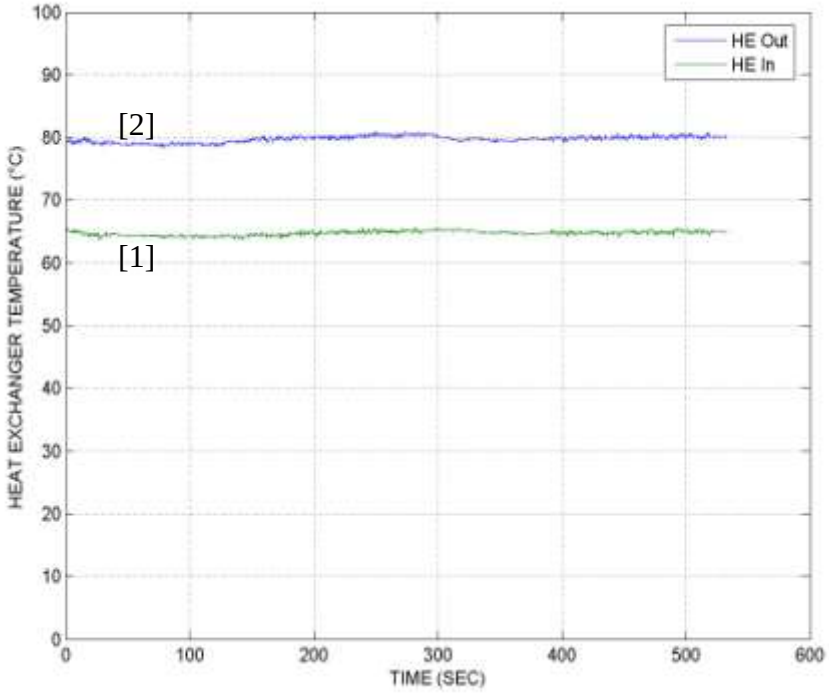
HE Out
HE In
[2]
[1]
HEAT EXCHANGER TEMPERATURE (°C)
TIME (SEC)
0
10
20
30
40
50
60
70
80
90
100
0
100
200
300
400
500
600

(a)

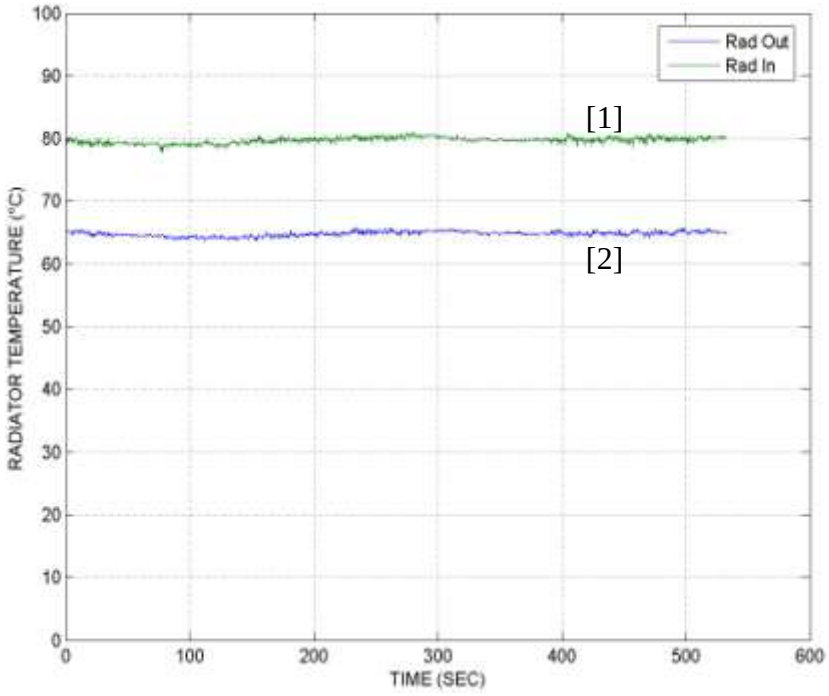
Rad Out
Rad In
[1]
[2]
RADIATOR TEMPERATURE (°C)
TIME (SEC)
0
10
20
30
40
50
60
70
80
90
100
0
100
200
300
400
500
600

(b)

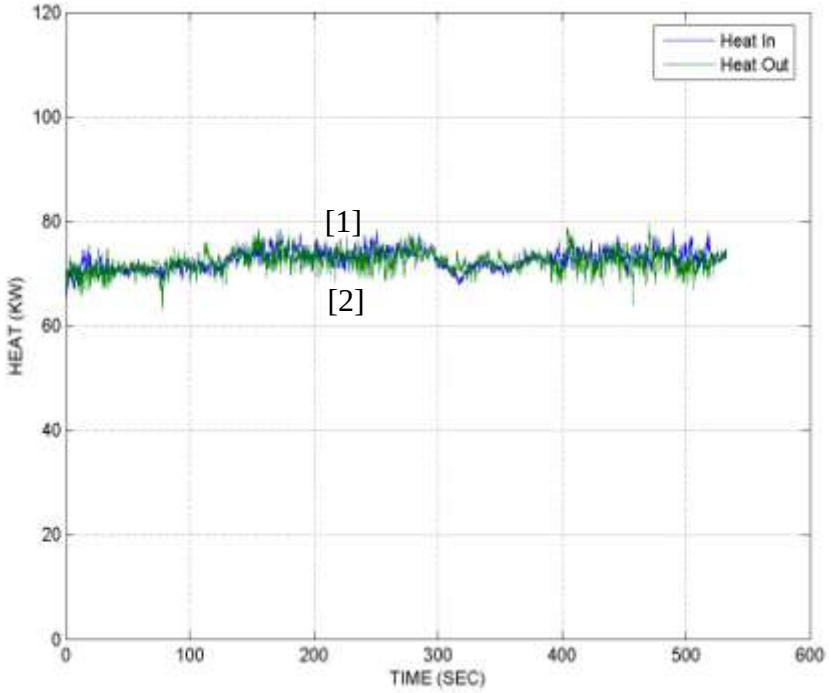

(c)

Figure A.40: Temperature and heat plots for Test #8 configuration at 5,000 RPM (a) heat exchanger inlet [1] and outlet [2] temperature, (b) radiator inlet [1] and outlet temperature [2] and, (c) heat input [1] and heat rejected [2] at 5,000 RPM.

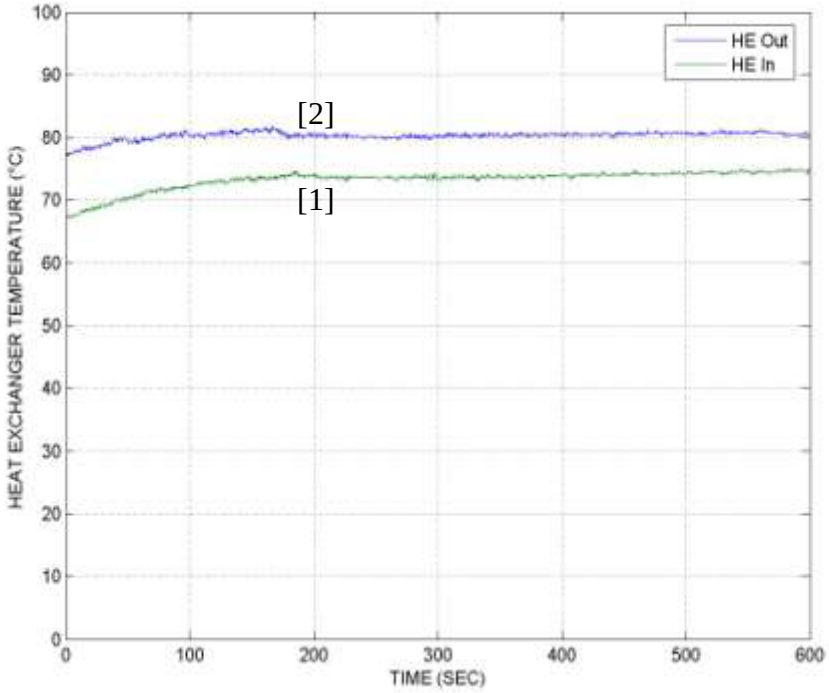
HE Out
HE In
[2]
[1]
HEAT EXCHANGER TEMPERATURE (°C)
TIME (SEC)
0
10
20
30
40
50
60
70
80
90
100
0
100
200
300
400
500
600

(a)

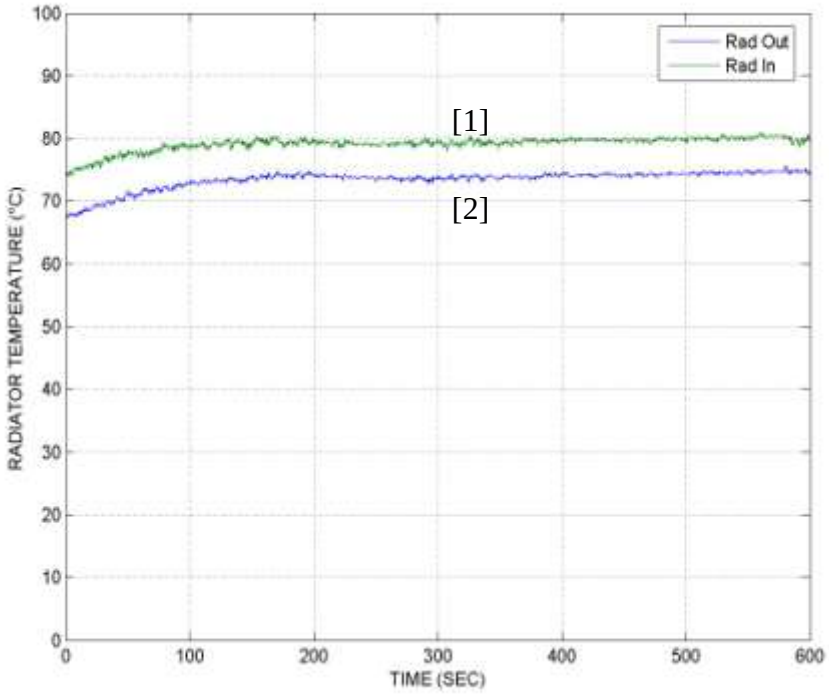
Rad Out
Rad In
[1]
[2]
RADIATOR TEMPERATURE (°C)
TIME (SEC)
0
10
20
30
40
50
60
70
80
90
100
0
100
200
300
400
500
600

(b)

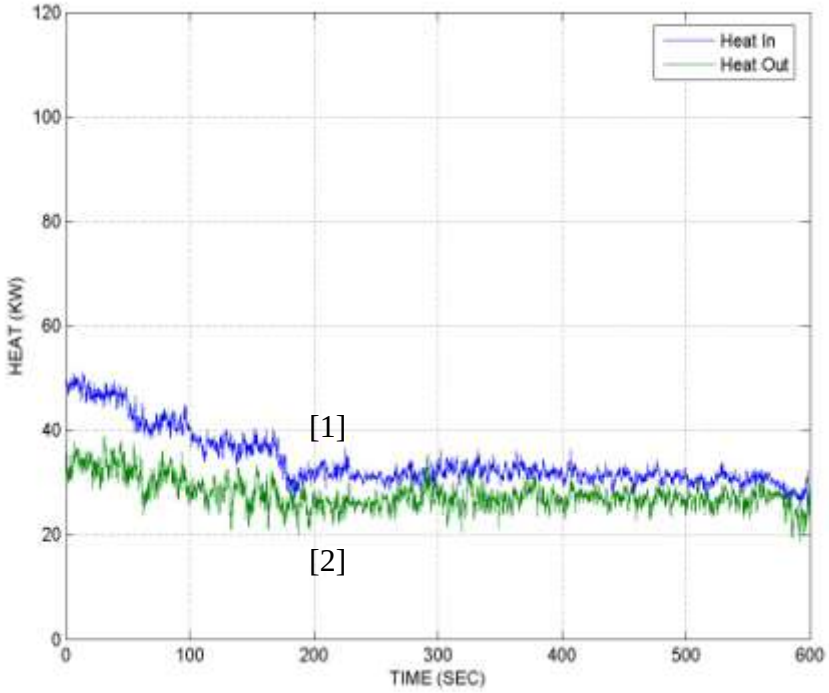

(c)

Figure A.41: Temperature and heat plots for Test #9 configuration at 1,000 RPM (a) heat exchanger inlet [1] and outlet [2] temperature, (b) radiator inlet [1] and outlet temperature [2] and, (c) heat input [1] and heat rejected [2].

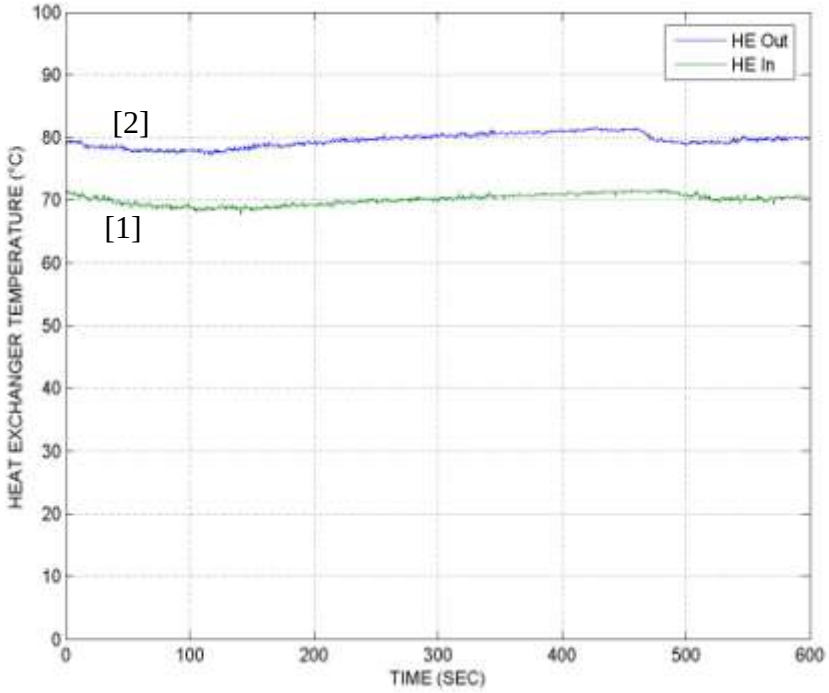
HE Out
HE In
[2]
[1]
HEAT EXCHANGER TEMPERATURE (°C)
TIME (SEC)
0
10
20
30
40
50
60
70
80
90
100
0
100
200
300
400
500
600

(a)

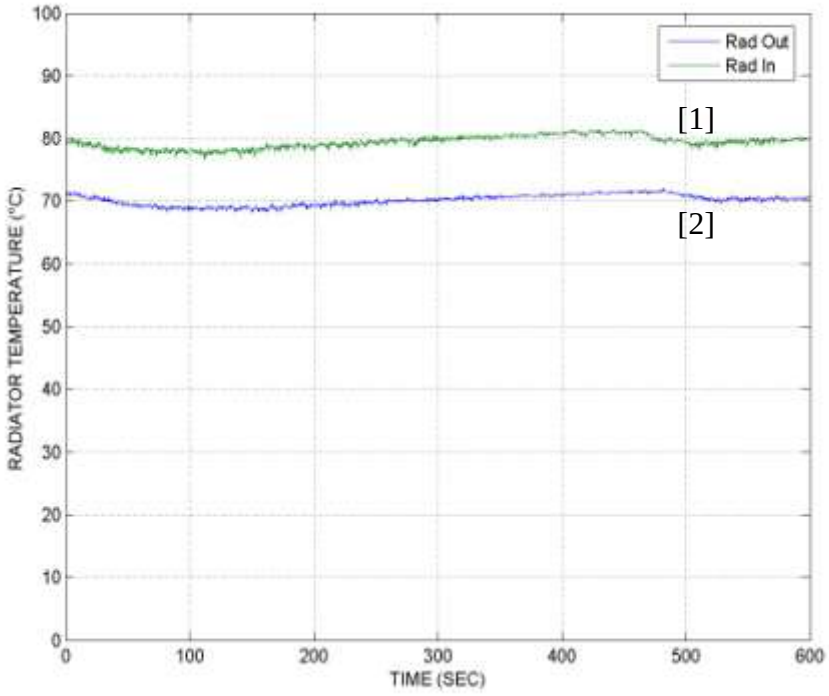
Rad Out
Rad In
[1]
[2]
RADIATOR TEMPERATURE (°C)
TIME (SEC)
0
10
20
30
40
50
60
70
80
90
100
0
100
200
300
400
500
600

(b)

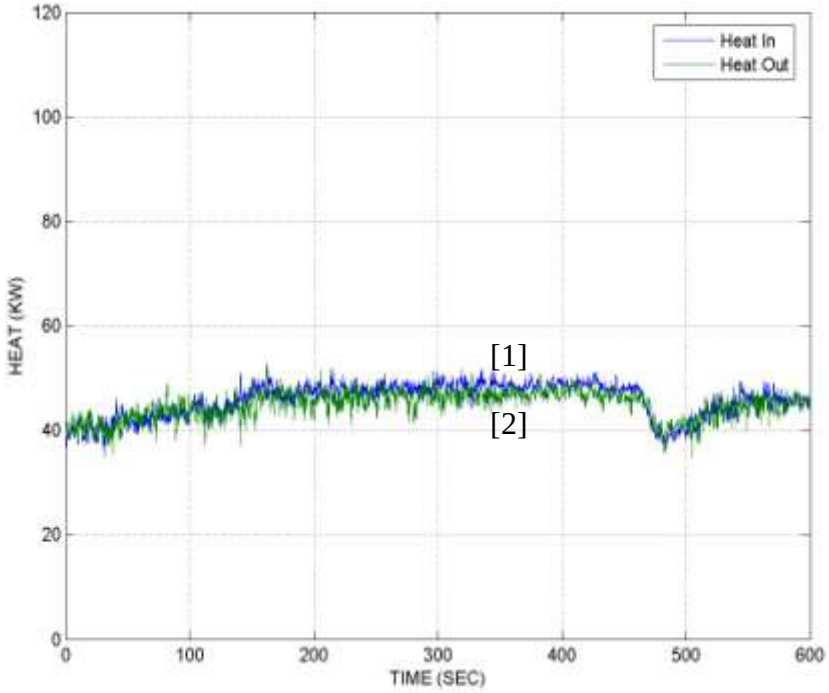

(c)

Figure A.42: Temperature and heat plots for Test #9 configuration at 2,000 RPM (a) heat exchanger inlet [1] and outlet [2] temperature, (b) radiator inlet [1] and outlet temperature [2] and, (c) heat input [1] and heat rejected [2].

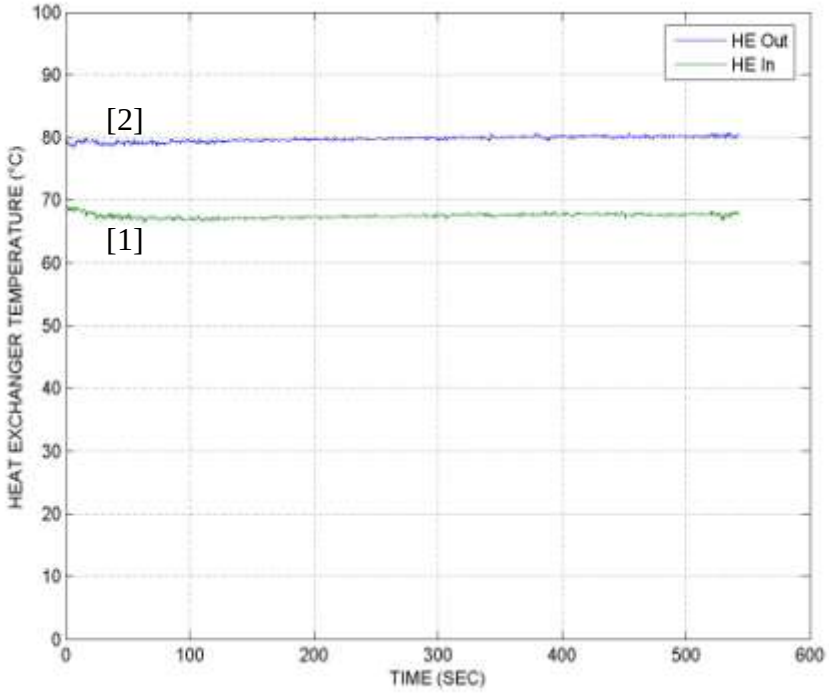
HE Out
HE In
[2]
[1]
HEAT EXCHANGER TEMPERATURE (°C)
TIME (SEC)
0
10
20
30
40
50
60
70
80
90
100
0
100
200
300
400
500
600

(a)

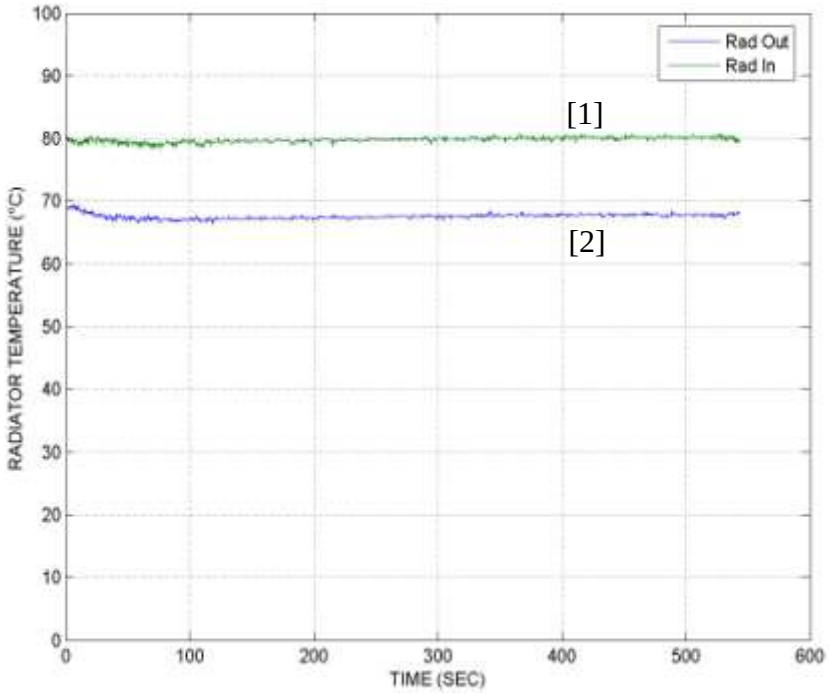
Rad Out
Rad In
[1]
[2]
RADIATOR TEMPERATURE (°C)
TIME (SEC)
0
10
20
30
40
50
60
70
80
90
100
0
100
200
300
400
500
600

(b)

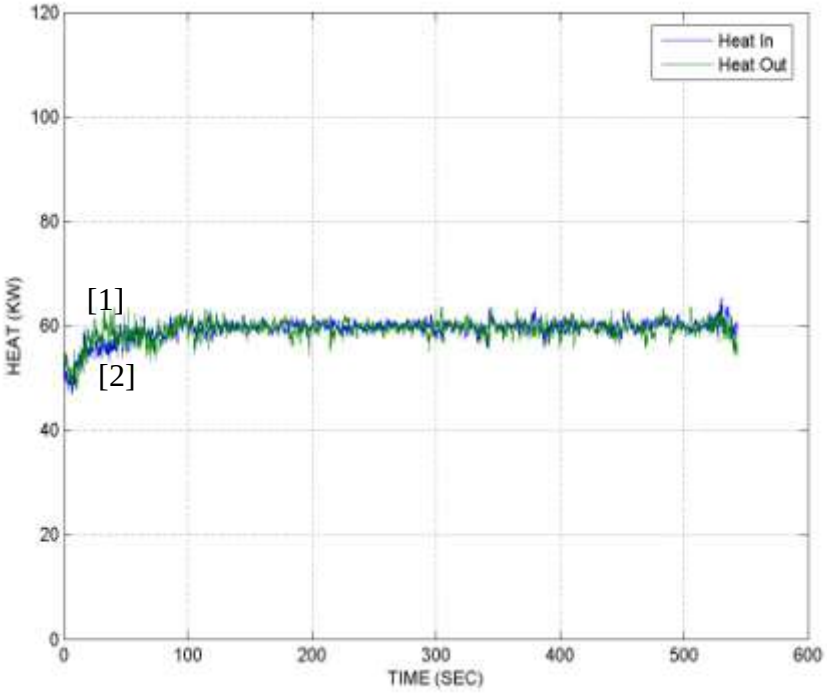

(c)

Figure A.43: Temperature and heat plots for Test #9 configuration at 3,000 RPM (a) heat exchanger inlet [1] and outlet [2] temperature, (b) radiator inlet [1] and outlet temperature [2] and, (c) heat input [1] and heat rejected [2] at 3,000 RPM.

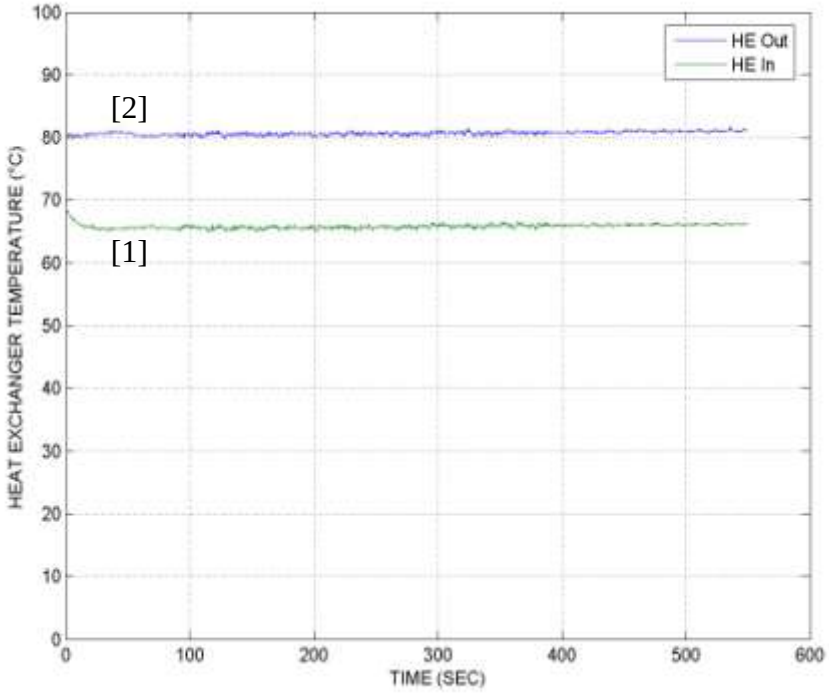
HE Out
HE In
[2]
[1]
HEAT EXCHANGER TEMPERATURE (°C)
TIME (SEC)
0
10
20
30
40
50
60
70
80
90
100
0
100
200
300
400
500
600

(a)

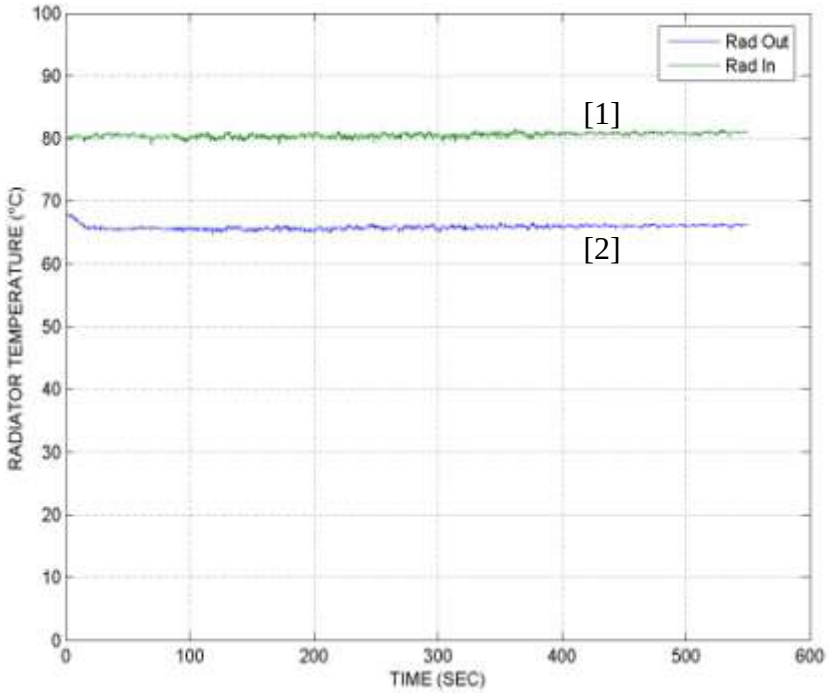
Rad Out
Rad In
[1]
[2]
RADIATOR TEMPERATURE (°C)
TIME (SEC)
0
10
20
30
40
50
60
70
80
90
100
0
100
200
300
400
500
600

(b)

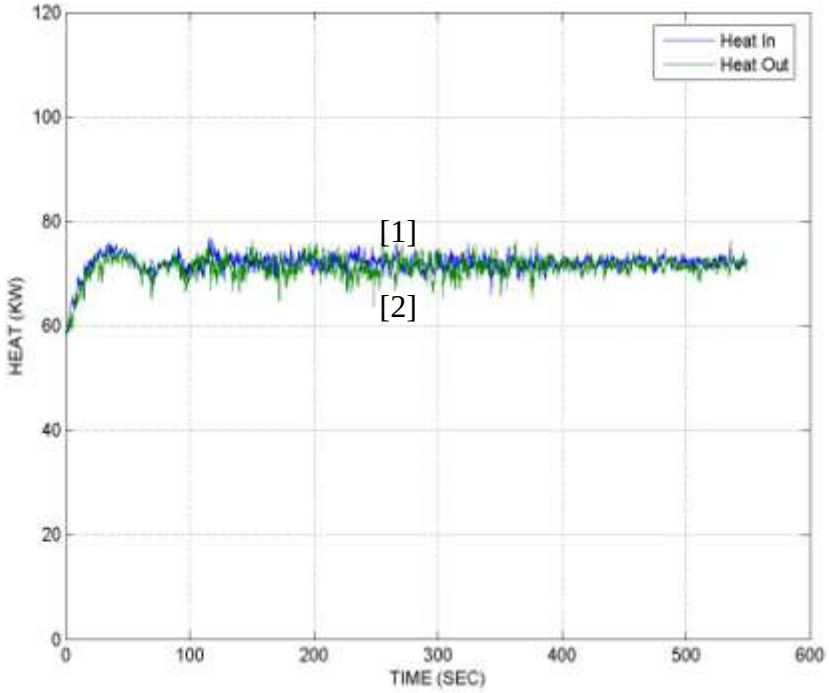

(c)

Figure A.44: Temperature and heat plots for Test #9 configuration at 4,000 RPM (a) heat exchanger inlet [1] and outlet [2] temperature, (b) radiator inlet [1] and outlet temperature [2] and, (c) heat input [1] and heat rejected [2].

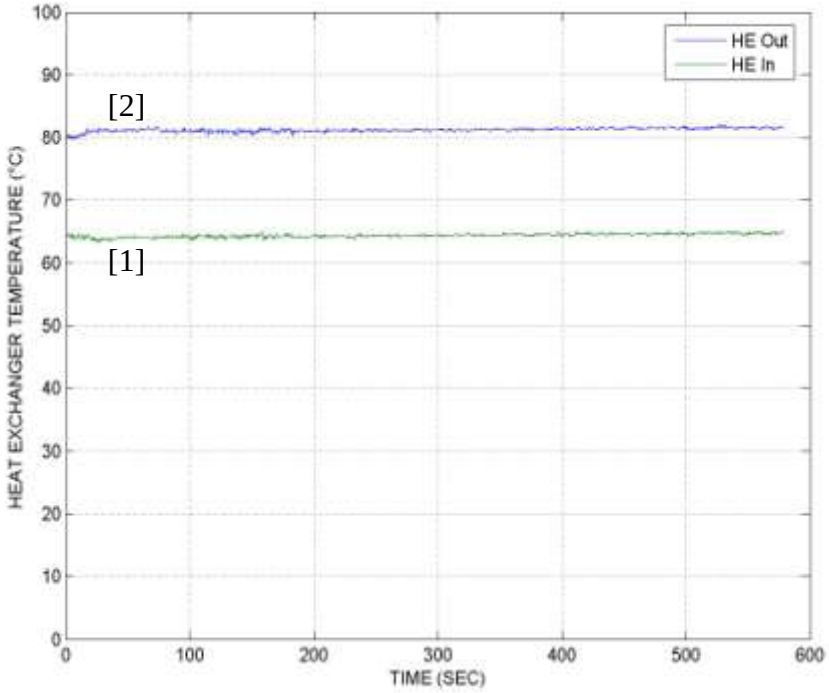
HE Out
HE In
[2]
[1]
HEAT EXCHANGER TEMPERATURE (°C)
TIME (SEC)
0
10
20
30
40
50
60
70
80
90
100
0
100
200
300
400
500
600

(a)

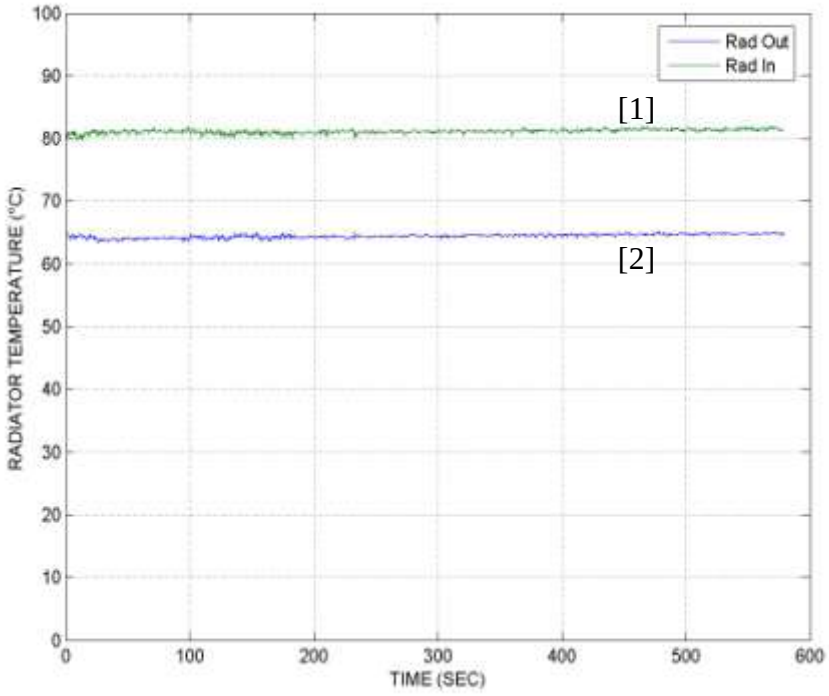
Rad Out
Rad In
[1]
[2]
RADIATOR TEMPERATURE (°C)
TIME (SEC)
0
10
20
30
40
50
60
70
80
90
100
0
100
200
300
400
500
600

(b)

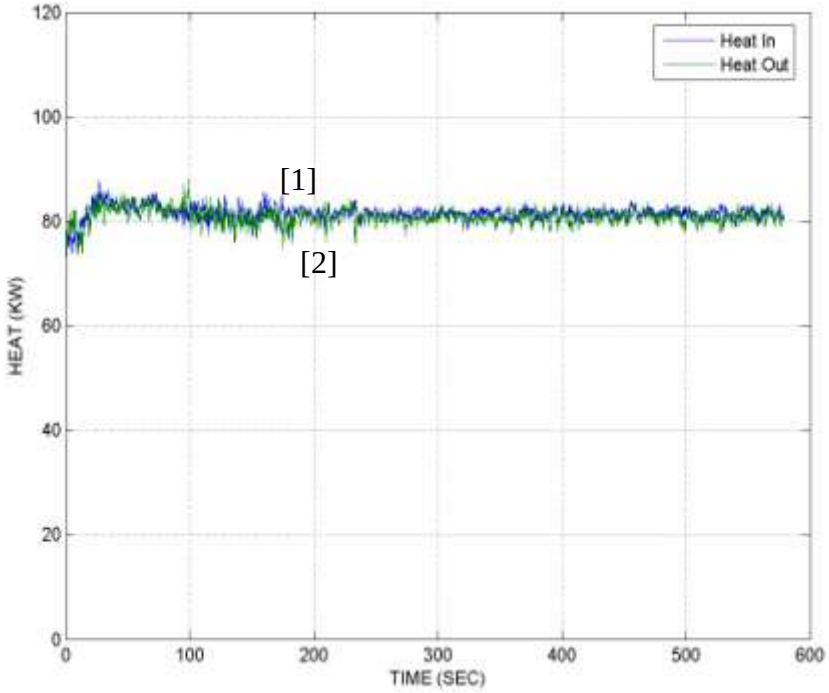

(c)

Figure A.45: Temperature and heat plots for Test #9 configuration at 5,000 RPM (a) heat exchanger inlet [1] and outlet [2] temperature, (b) radiator inlet [1] and outlet temperature [2] and, (c) heat input [1] and heat rejected [2].

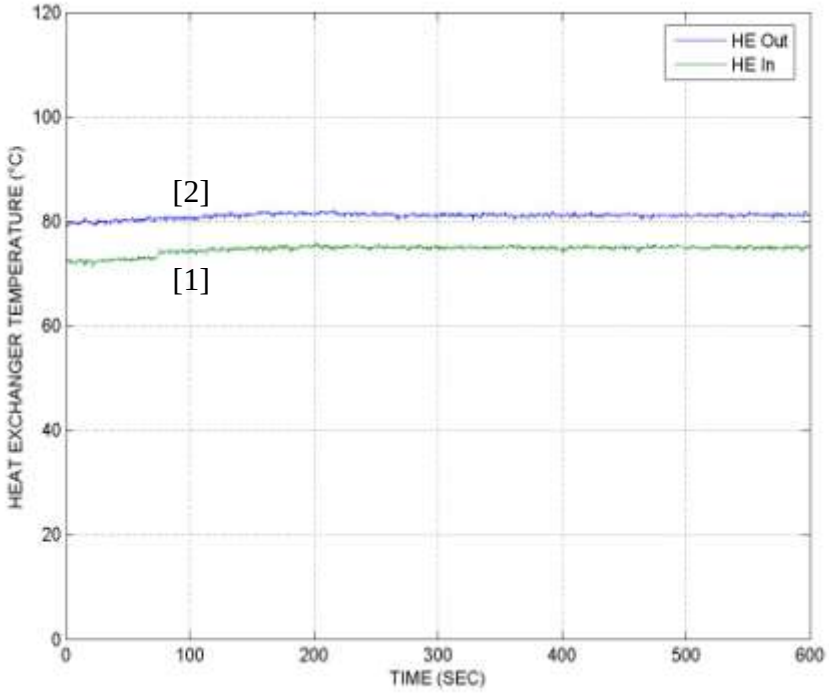
HE Out
HE In
[2]
[1]
HEAT EXCHANGER TEMPERATURE (°C)
TIME (SEC)
0
20
40
60
80
100
120
0
100
200
300
400
500
600

(a)

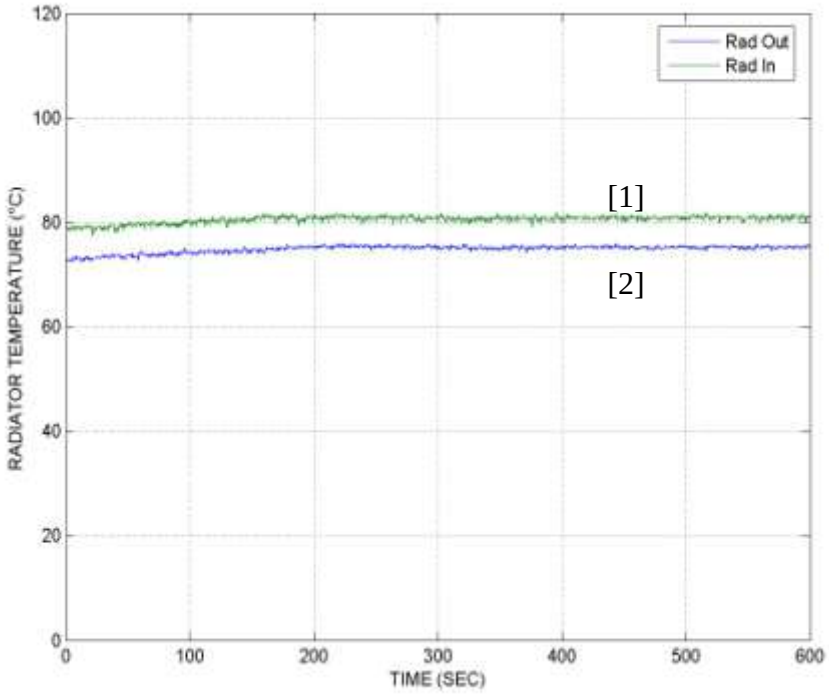
Rad Out
Rad In
[1]
[2]
RADIATOR TEMPERATURE (°C)
TIME (SEC)
0
20
40
60
80
100
120
0
100
200
300
400
500
600

(b)

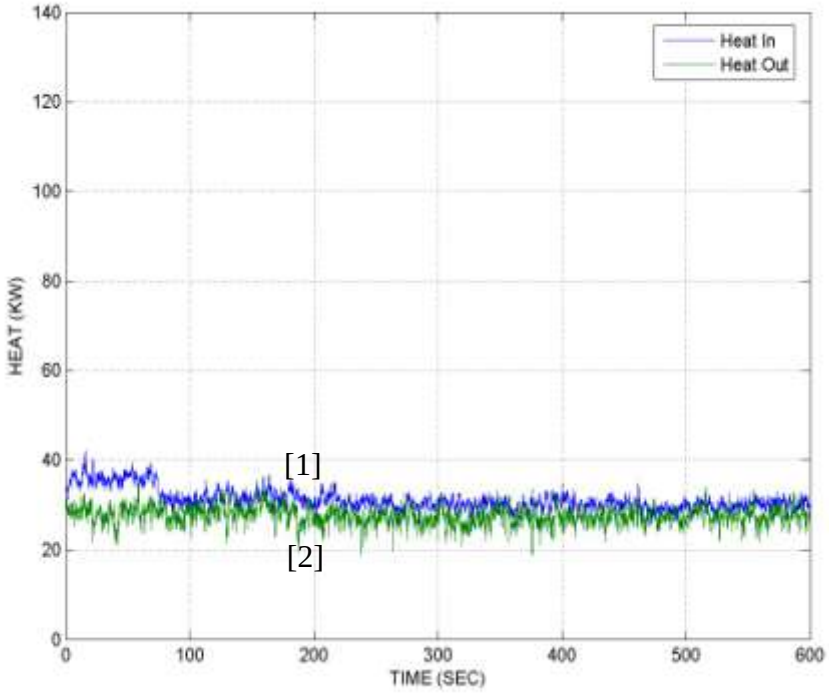

(c)

Figure A.46: Temperature and heat plots for Test #10 configuration at 1,000 RPM (a) heat exchanger inlet [1] and outlet [2] temperature, (b) radiator inlet [1] and outlet temperature [2] and, (c) heat input [1] and heat rejected [2].

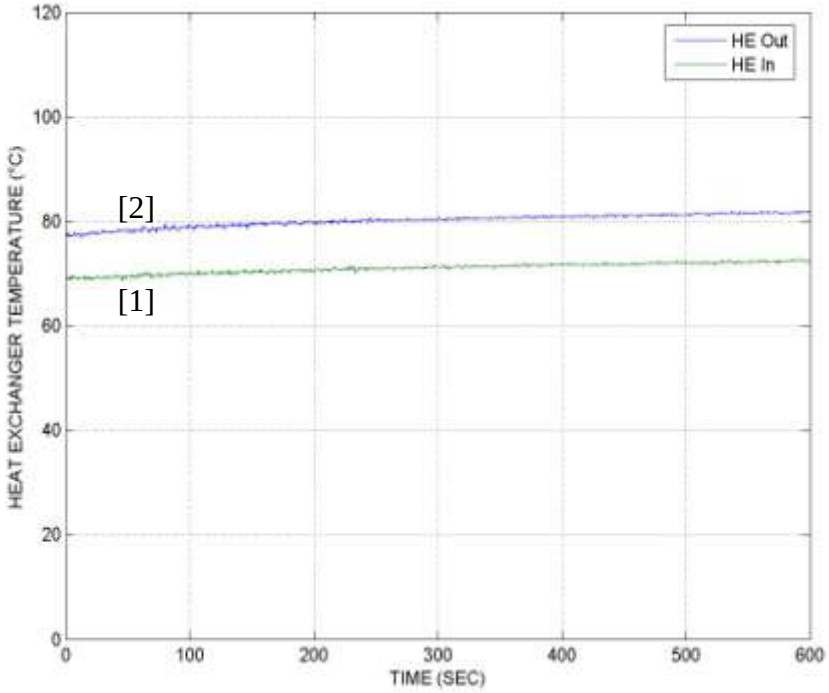
HE Out
HE In
[2]
[1]
HEAT EXCHANGER TEMPERATURE (°C)
TIME (SEC)
0
20
40
60
80
100
120
0
100
200
300
400
500
600

(a)

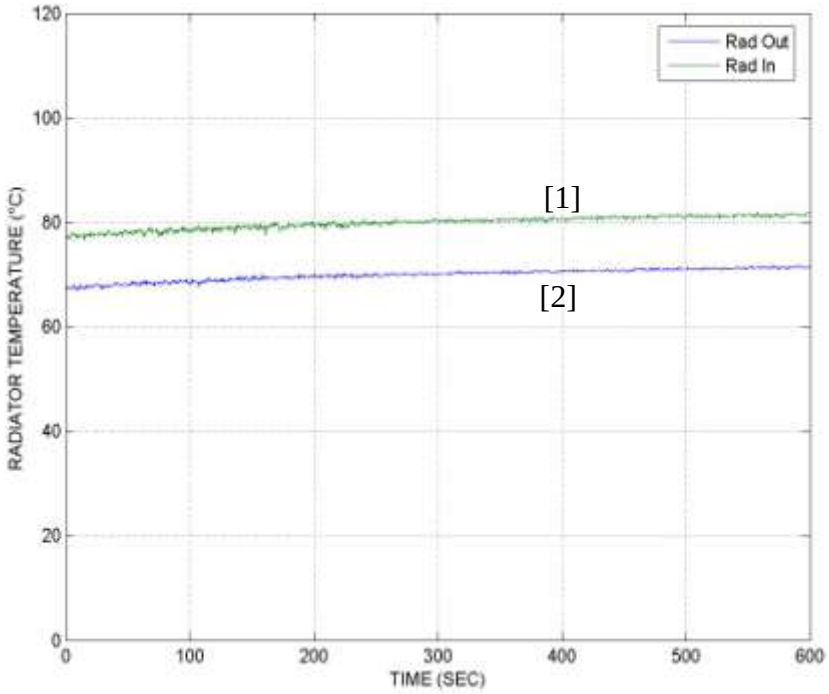
Rad Out
Rad In
[1]
[2]
RADIATOR TEMPERATURE (°C)
TIME (SEC)
0
20
40
60
80
100
120
0
100
200
300
400
500
600

(b)

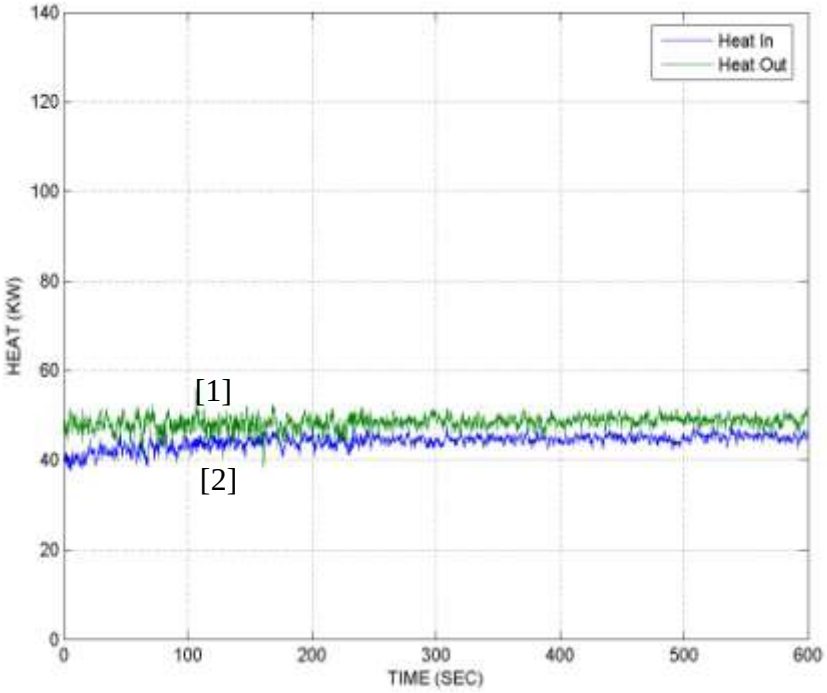

(c)

Figure A.47: Temperature and heat plots for Test #10 configuration at 2,000 RPM (a) heat exchanger inlet [1] and outlet [2] temperature, (b) radiator inlet [1] and outlet temperature [2] and, (c) heat input [1] and heat rejected [2].

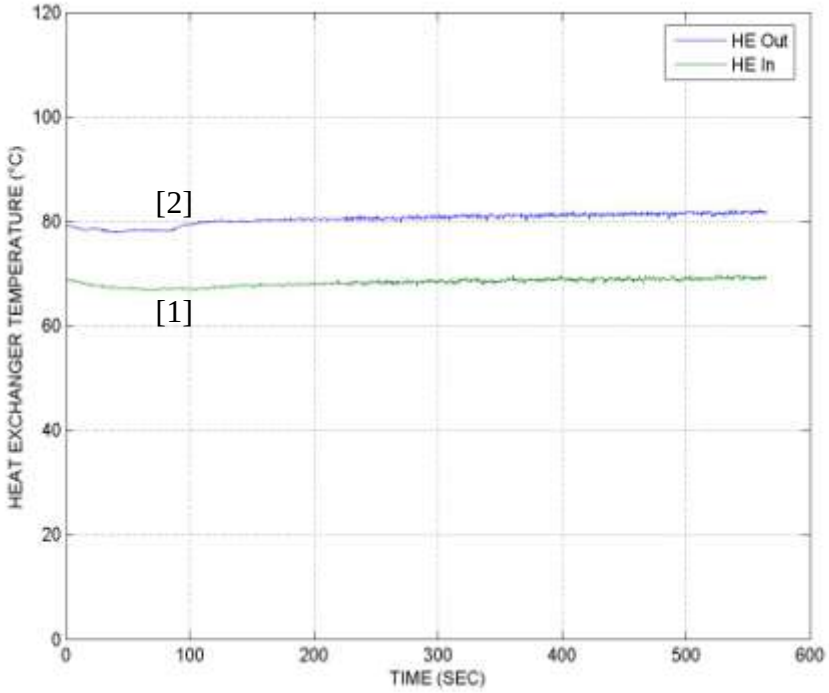
HE Out
HE In
[2]
[1]
HEAT EXCHANGER TEMPERATURE (°C)
TIME (SEC)
0
20
40
60
80
100
120
0
100
200
300
400
500
600

(a)

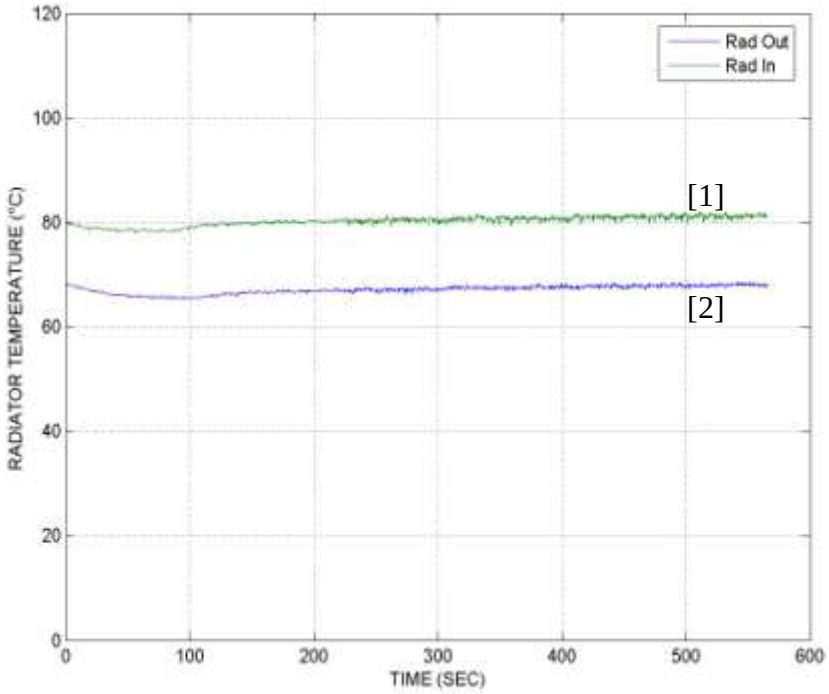
Rad Out
Rad In
[1]
[2]
RADIATOR TEMPERATURE (°C)
TIME (SEC)
0
20
40
60
80
100
120
0
100
200
300
400
500
600

(b)

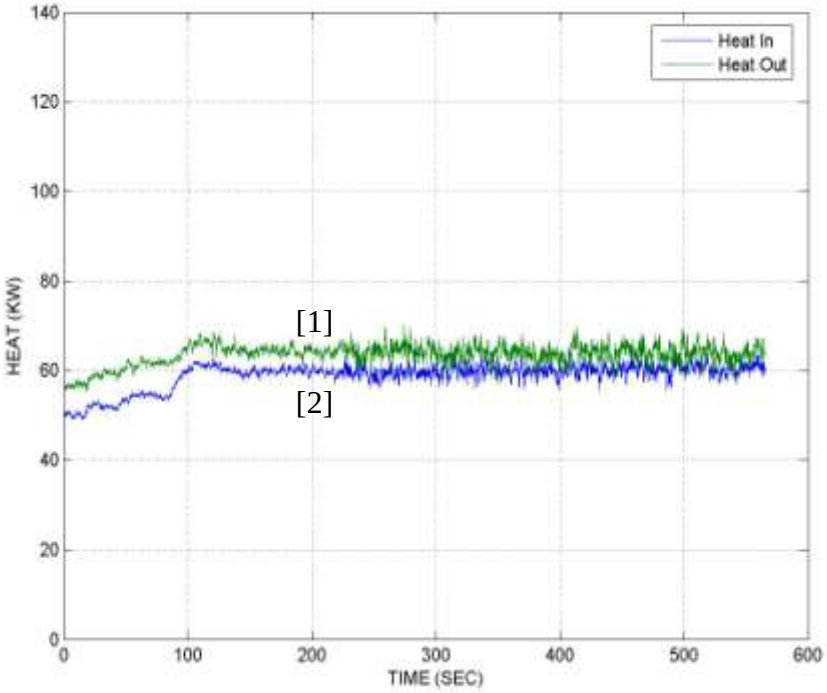

(c)

Figure A.48: Temperature and heat plots for Test #10 configuration at 3,000 RPM (a) heat exchanger inlet [1] and outlet [2] temperature, (b) radiator inlet [1] and outlet temperature [2] and, (c) heat input [1] and heat rejected [2].

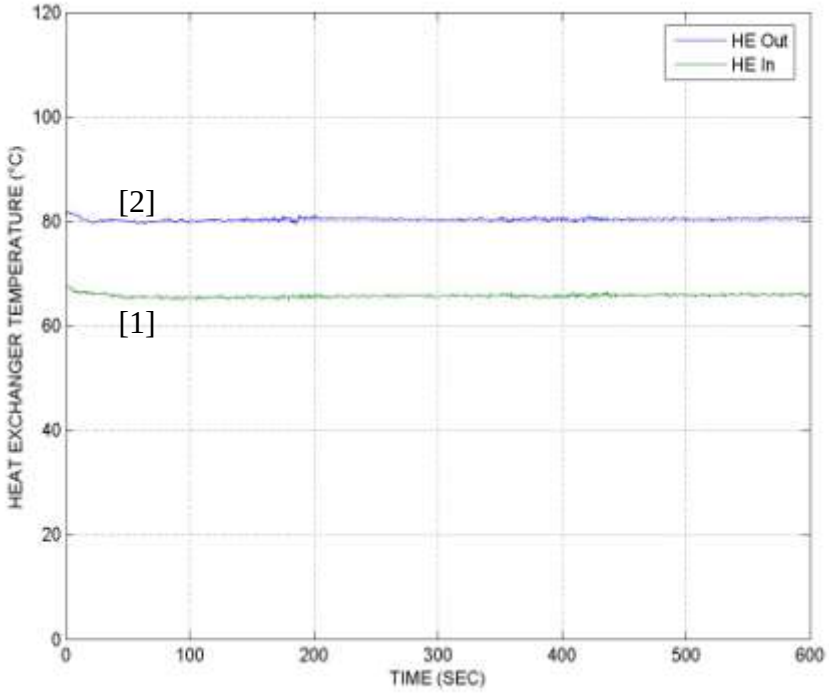
HE Out
HE In
[2]
[1]
HEAT EXCHANGER TEMPERATURE (°C)
TIME (SEC)
0
20
40
60
80
100
120
0
100
200
300
400
500
600

(a)

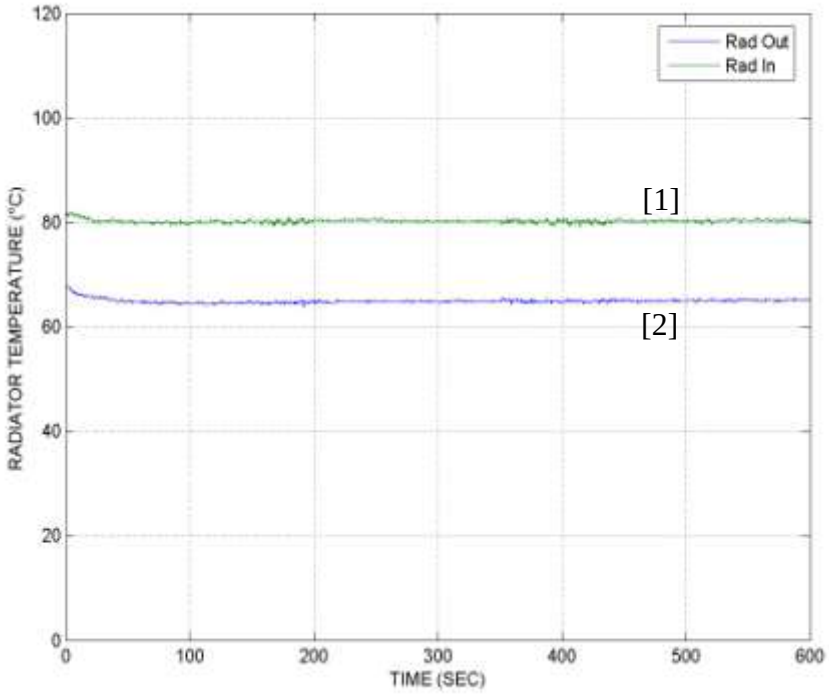
Rad Out
Rad In
[1]
[2]
RADIATOR TEMPERATURE (°C)
TIME (SEC)
0
20
40
60
80
100
120
0
100
200
300
400
500
600

(b)

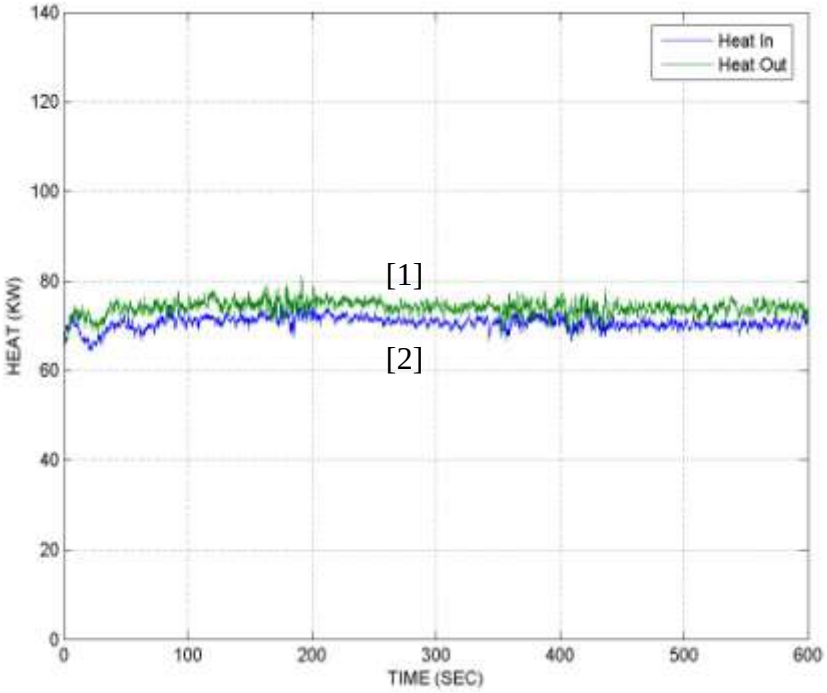

(c)

Figure A.49: Temperature and heat plots for Test #10 configuration at 4,000 RPM (a) heat exchanger inlet [1] and outlet [2] temperature, (b) radiator inlet [1] and outlet temperature [2] and, (c) heat input [1] and heat rejected [2].

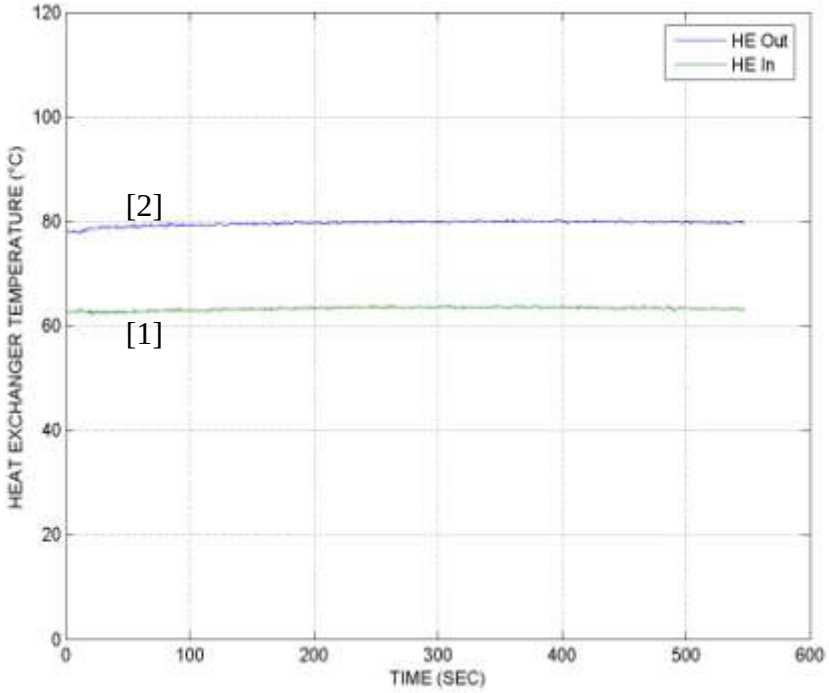
HE Out
HE In
[2]
[1]
HEAT EXCHANGER TEMPERATURE (°C)
TIME (SEC)
0
20
40
60
80
100
120
0
100
200
300
400
500
600

(a)

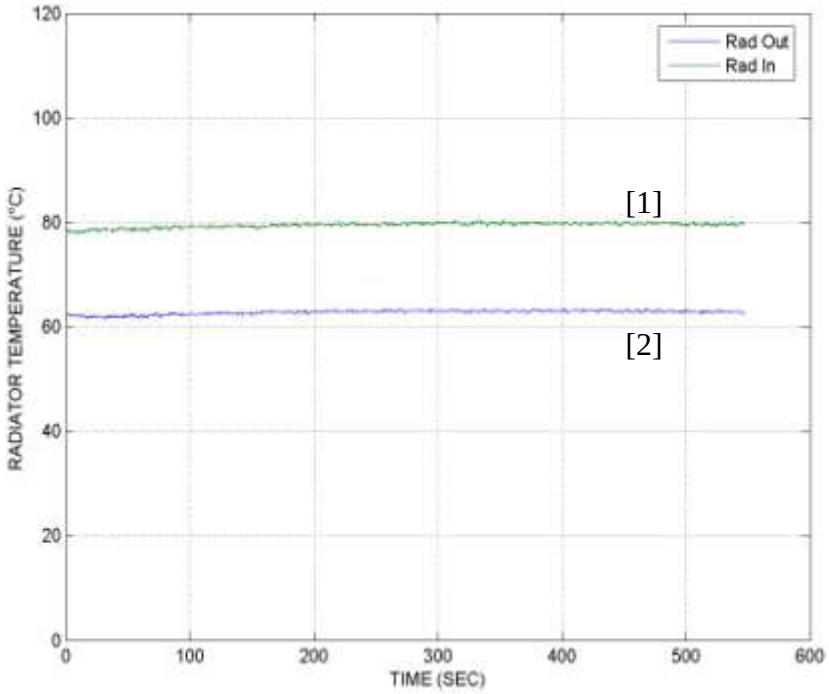
Rad Out
Rad In
[1]
[2]
RADIATOR TEMPERATURE (°C)
TIME (SEC)
0
20
40
60
80
100
120
0
100
200
300
400
500
600

(b)

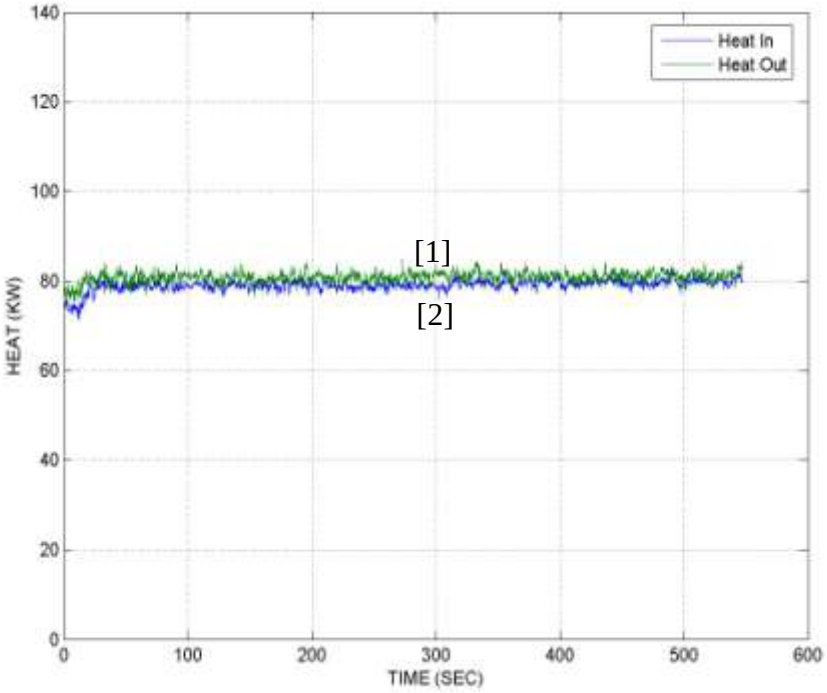

(c)

Figure A.50: Temperature and heat plots for Test #10 configuration at 5,000 RPM (a) heat exchanger inlet [1] and outlet [2] temperature, (b) radiator inlet [1] and outlet temperature [2] and, (c) heat input [1] and heat rejected [2].

Appendix B

Air Speed Measurement

The experimental air speed readings collected at different fan combinations (refer to Table 4.7) and air speed surface plots will be presented in this Section. Note the radiator view is from rear side with fan motors located behind the radiator.

Fan Speed 1000 RPM											
Air Speed (m/sec)											
Point	**1**	**2**	**3**	**4**	**5**	**6**	**7**	**8**	**9**	**10**	**11**
1	0	0	0	0	0	0	0	0	0	0	0
2	0	1.425	1.248	1.258	1.096	1.165	1.132	1.052	1.137	1.274	0
3	0	0.335	0.835	1.237	1.14	1.253	0.634	0.252	1.126	1.357	0
4	0	1.252	1.081	0.961	0.949	1.014	1.124	1.153	1.153	1.381	0
5	0	1.351	1.135	1.109	0.936	0.765	1.162	1.163	1.149	1.253	0
6	0	1.192	1.351	1.203	1.065	1.032	1.124	1.352	1.154	1.353	0
7	0	1.745	1.354	0.498	0.22	1.352	1.457	1.361	0.668	1.081	0
8	0	1.355	1.204	1.152	0.952	1.29	1.153	1.134	1.146	1.151	0
9	0	1.221	1.155	1.163	1.031	0.913	1.154	1.042	1.156	1.155	0
10	0	1.351	1.184	1.202	1.056	1.046	0.898	1.136	1.122	1.152	0
11	0	1.254	1.074	1.154	1.154	1.156	1.159	0.912	0.513	1.154	0
12	0	1.151	0.132	0.872	1.162	1.134	1.084	1.076	0.326	1.225	0
13	0	0	0	0	0	0	0	0	0	0	0

Table B.1: Air speed readings for all fans operating at 1,000 RPM.

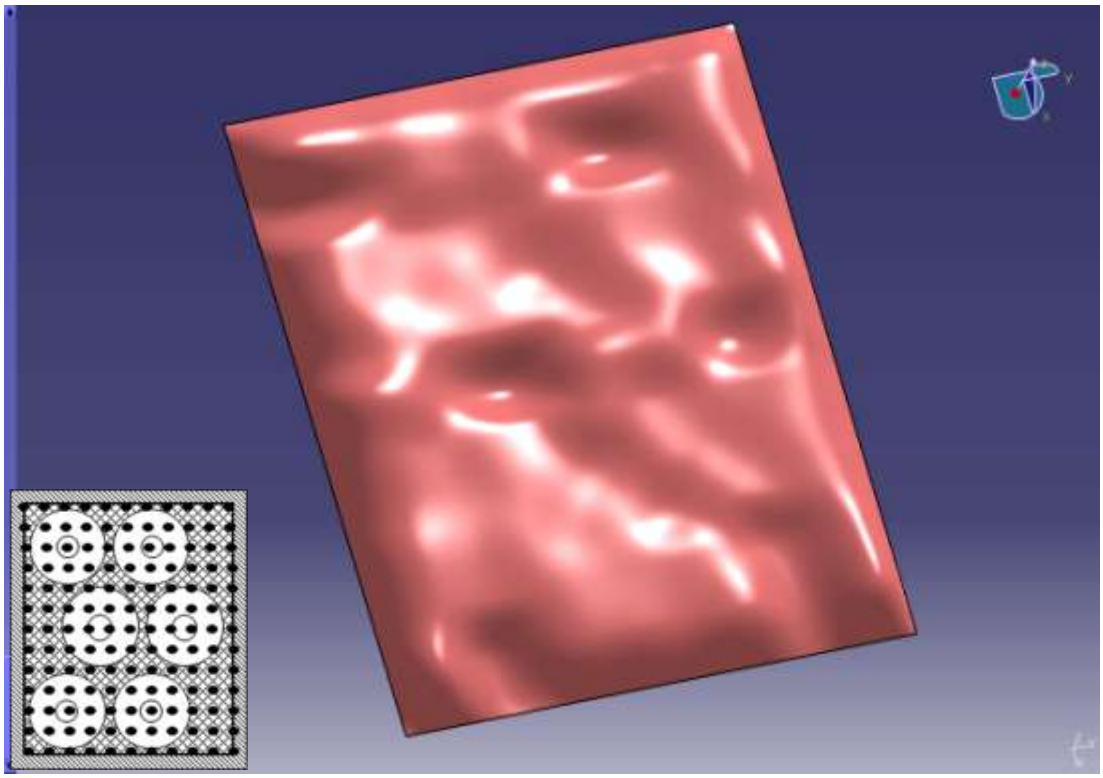

Figure B.1: Air speed profile for all fans operating at 1,000 RPM.

Fan speed 2000 RPM											
Air Speed (m/sec)											
Point	**1**	**2**	**3**	**4**	**5**	**6**	**7**	**8**	**9**	**10**	**11**
1	0	0	0	0	0	0	0	0	0	0	0
2	0	2.967	2.818	2.921	2.224	2.395	2.275	2.114	2.25	2.452	0
3	0	1.498	1.506	2.901	2.631	2.868	1.966	0.434	2.153	2.71	0
4	0	2.348	2.358	2.152	2.127	2.143	2.313	2.354	2.414	2.921	0
5	0	2.751	2.441	2.533	2.127	2.018	2.445	2.351	2.497	2.883	0
6	0	2.367	2.755	2.36	2.53	2.471	2.249	2.826	2.357	2.782	0
7	0	3.313	2.983	1.12	1.154	2.965	3.13	3.158	1.821	2.227	0
8	0	2.652	2.606	2.337	2.428	2.874	2.635	2.57	2.25	2.776	0
9	0	2.545	2.362	2.78	2.273	2.142	2.617	2.389	2.623	2.612	0
10	0	2.84	2.47	2.659	2.162	2.318	2.011	2.383	2.552	2.554	0
11	0	2.657	2.036	2.613	2.288	2.433	2.452	1.828	1.882	2.571	0
12	0	2.654	0.847	2.269	2.818	2.472	2.528	2.357	1.76	2.836	0
13	0	0	0	0	0	0	0	0	0	0	0

Table B.2: Air speed readings for all fans operating at 2,000 RPM.

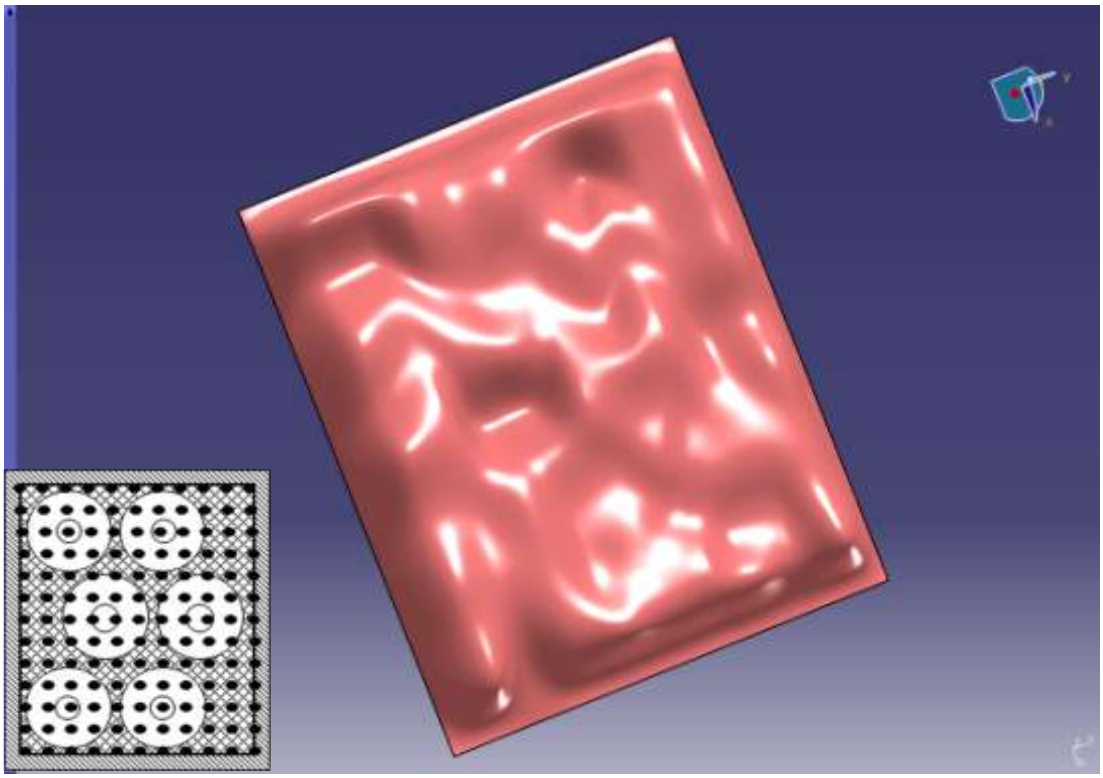

Figure B.2: Air speed profile for all fans operating at 2,000 RPM.

Fan speed 3000 RPM											
Air Speed (m/sec)											
Point	**1**	**2**	**3**	**4**	**5**	**6**	**7**	**8**	**9**	**10**	**11**
1	0	0	0	0	0	0	0	0	0	0	0
2	0	4.76	4.573	4.921	3.52	3.555	3.471	3.256	3.422	3.694	0
3	0	3.246	2.259	4.654	4.445	4.584	3.1	0.606	3.126	3.956	0
4	0	3.75	3.634	3.505	3.076	3.484	3.829	3.66	3.875	4.359	0
5	0	4.244	3.951	3.914	3.553	3.179	3.724	3.846	4.113	4.645	0
6	0	3.949	4.407	3.713	4.033	3.952	3.598	4.523	3.691	4.638	0
7	0	5.046	4.651	1.661	2.173	4.718	4.888	4.759	3.417	3.442	0
8	0	4.253	4.232	3.634	4.082	4.535	4.178	4.32	3.327	4.246	0
9	0	4.032	3.934	4.272	3.644	3.674	3.474	3.823	4.286	4.428	0
10	0	4.374	4.138	4.235	3.217	3.533	3.234	3.506	3.962	4.068	0
11	0	4.182	2.977	4.248	3.432	3.962	4.143	2.547	2.713	4.091	0
12	0	4.251	1.749	3.954	4.522	4.015	4.244	3.913	3.384	4.598	0
13	0	0	0	0	0	0	0	0	0	0	0

Table B.3: Air speed readings for all fans operating at 3,000 RPM.

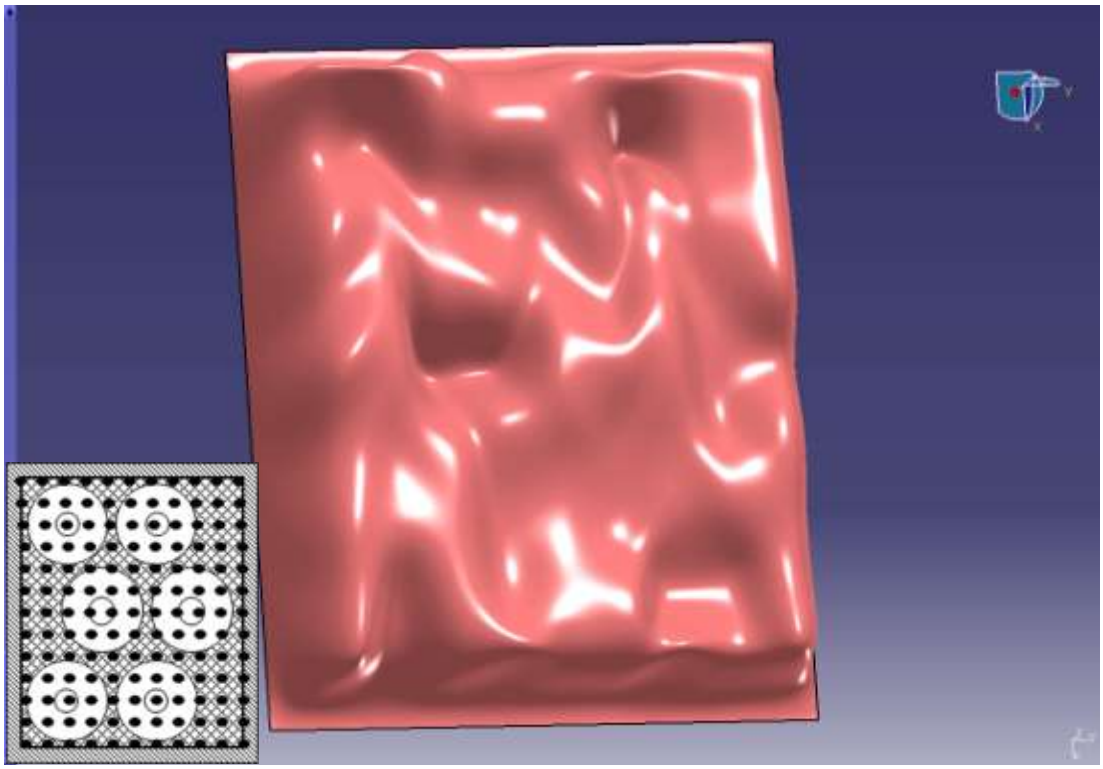

Figure B.3: Air speed profile for all fans operating at 3,000 RPM.

Fan speed 4000 RPM											
Air Speed (m/sec)											
Point	**1**	**2**	**3**	**4**	**5**	**6**	**7**	**8**	**9**	**10**	**11**
1	0	0	0	0	0	0	0	0	0	0	0
2	0	6.82	6.72	7.456	5.036	4.908	4.833	4.645	4.705	5.145	0
3	0	4.268	2.097	6.957	6.556	6.625	4.424	0.752	4.218	5.396	0
4	0	5.438	5.068	4.958	4.366	4.956	5.738	5.135	5.409	6.171	0
5	0	6.195	5.591	5.408	4.978	4.427	5.352	5.146	5.953	6.619	0
6	0	5.558	6.685	5.183	5.442	5.876	5.387	6.714	5.447	6.636	0
7	0	7.437	6.753	2.417	2.605	6.997	6.913	6.739	4.648	4.808	0
8	0	6.241	6.128	5.359	5.501	6.647	5.327	6.138	4.691	6.018	0
9	0	5.722	5.863	6.246	5.317	5.523	4.745	5.226	5.949	6.202	0
10	0	6.342	5.987	6.053	4.416	5.352	4.645	5.36	6.036	5.636	0
11	0	5.919	4.152	5.972	4.726	5.496	5.723	3.456	4.034	6.056	0
12	0	6.189	2.274	5.493	6.643	5.799	5.982	5.432	4.751	6.601	0
13	0	0	0	0	0	0	0	0	0	0	0

Table B.4: Air speed readings for all fans operating at 4,000 RPM.

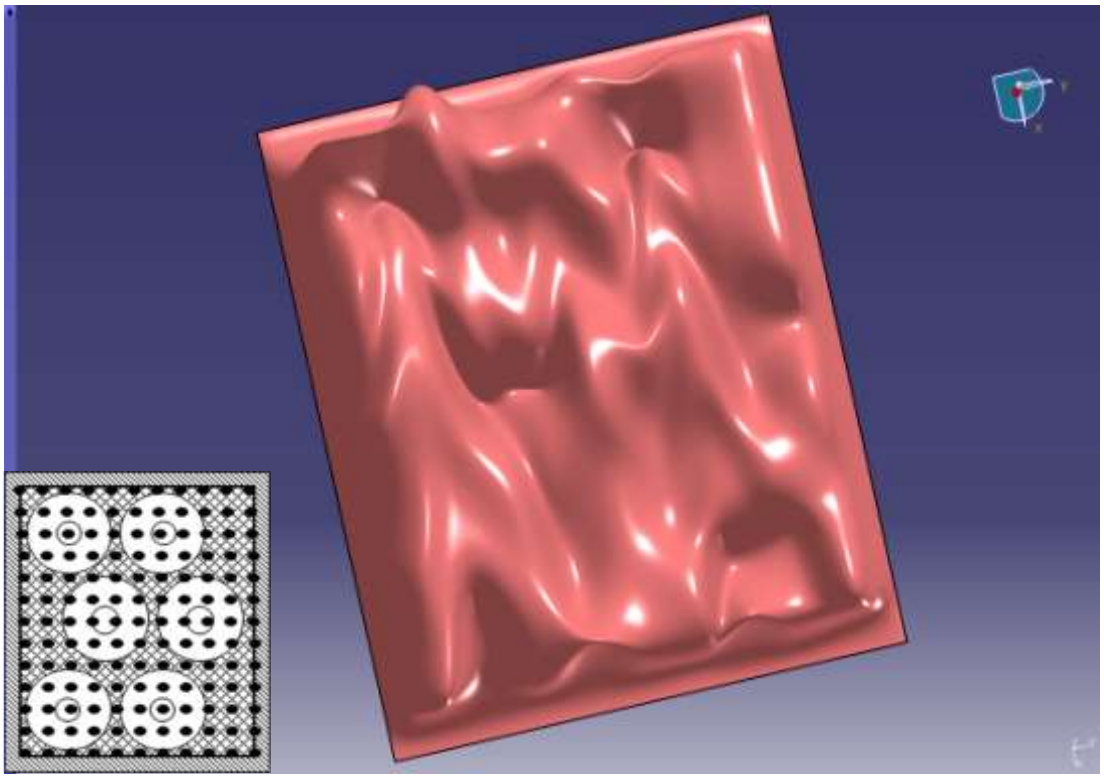

Figure B.4: Air speed profile for all fans operating at 4,000 RPM.

Fan speed 5000 RPM											
Air Speed (m/sec)											
Point	**1**	**2**	**3**	**4**	**5**	**6**	**7**	**8**	**9**	**10**	**11**
1	0	0	0	0	0	0	0	0	0	0	0
2	0	9.18	8.884	9.485	6.732	6.624	6.627	6.499	6.134	6.887	0
3	0	6.896	2.856	8.889	8.352	8.537	5.868	0.713	5.445	7.325	0
4	0	7.465	7.013	7.056	5.981	6.665	7.671	6.801	7.348	8.035	0
5	0	8.029	7.605	7.413	6.967	5.709	7.053	7.23	7.743	8.376	0
6	0	7.501	8.545	7.041	7.118	7.771	7.328	8.652	7.368	8.787	0
7	0	9.083	8.824	3.227	3.156	8.823	8.694	8.633	6.103	6.293	0
8	0	8.041	8.182	6.961	7.494	8.448	6.924	8.082	6.418	8.205	0
9	0	7.447	7.924	8.29	7.051	7.485	6.148	7.678	8.007	8.196	0
10	0	8.076	7.738	8.052	5.864	7.44	6.338	6.773	8.092	7.503	0
11	0	7.875	5.238	7.976	6.256	7.488	7.542	4.433	5.782	8.058	0
12	0	8.262	3.406	7.153	8.616	7.575	8.173	7.536	6.04	8.608	0
13	0	0	0	0	0	0	0	0	0	0	0

Table B.5: Air speed readings for all fans operating at 5,000 RPM.

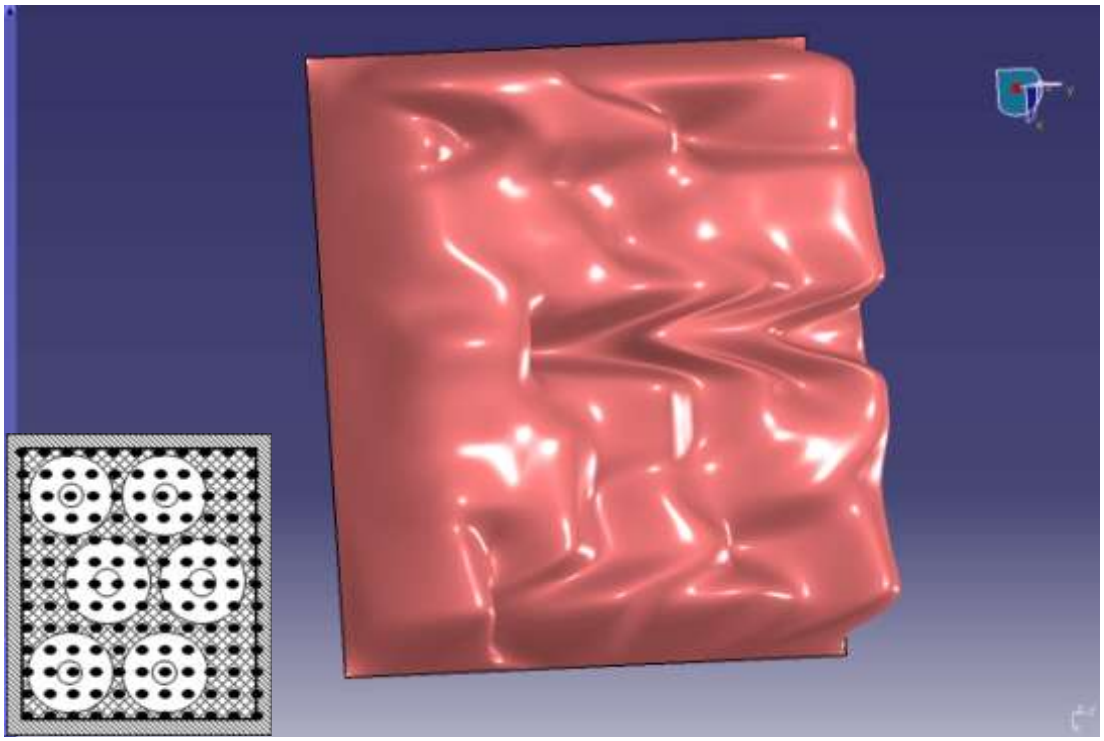

Figure B.5: Air speed profile for all fans operating at 5,000 RPM.

Fan speed 1000 RPM											
Air Speed (m/sec)											
Point	**1**	**2**	**3**	**4**	**5**	**6**	**7**	**8**	**9**	**10**	**11**
1	0	0	0	0	0	0	0	0	0	0	0
2	0	0.856	1.119	0.955	0.453	0.838	0.965	0.386	0.397	0.658	0
3	0	0.385	0.685	0.902	0.515	0.957	0.825	0.275	0.05	0.639	0
4	0	0.115	0.095	0.999	0.553	0.894	0.751	0.347	0.375	0.752	0
5	0	0.308	0.825	0.47	0.287	0.461	0.738	0.875	0.736	0.455	0
6	0	0.257	0.182	0.062	0.276	0.308	0.281	0.351	0.348	0.303	0
7	0	0.155	0.122	0.146	0.248	0.255	0.175	0.206	0.177	0.236	0
8	0	0.141	0.115	0.106	0.121	0.118	0.283	0.248	0.145	0.286	0
9	0	0.15	0.143	0.149	0.125	0.157	0.249	0.218	0.257	0.319	0
10	0	0.267	0.168	0.151	0.154	0.202	0.252	0.217	0.263	0.266	0
11	0	0.209	0.208	0.189	0.253	0.248	0.263	0.168	0.235	0.258	0
12	0	0.28	0.255	0.262	0.24	0.263	0.274	0.248	0.157	0.188	0
13	0	0	0	0	0	0	0	0	0	0	0

Table B.6: Air speed readings for fans 1-2 operating at 1,000 RPM.

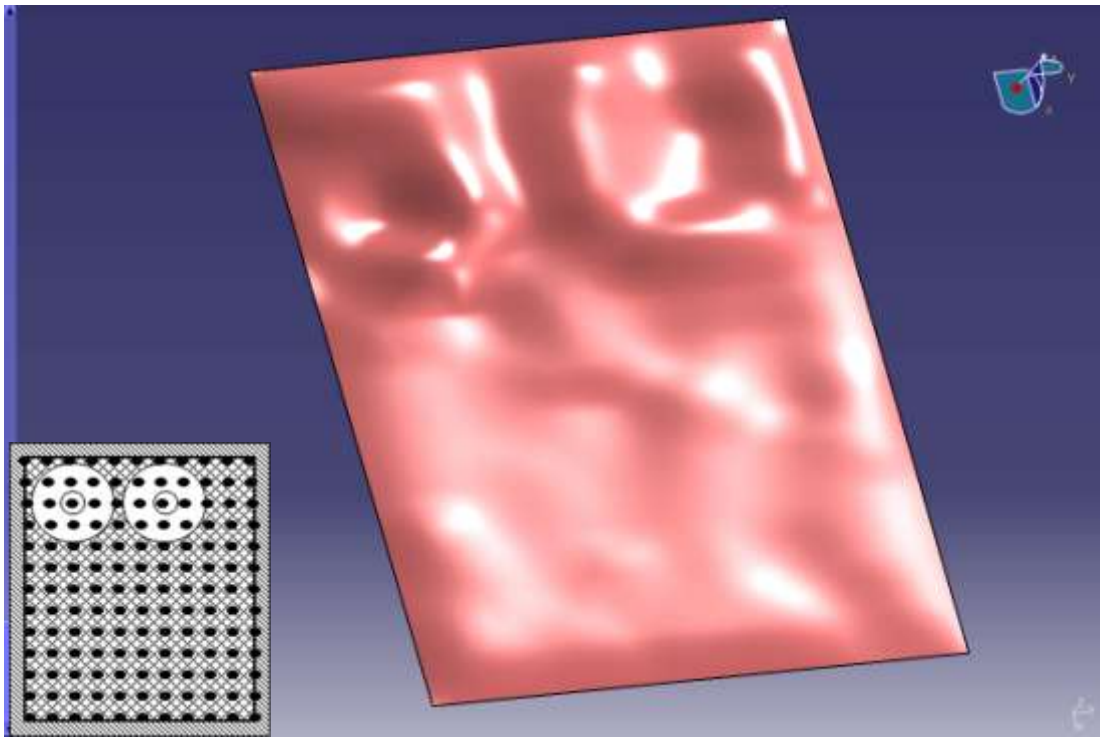

Figure B.6: Air speed profile for fans 1-2 operating at 1,000 RPM.

Fan speed 5000 RPM											
Air Speed (m/sec)											
Point	**1**	**2**	**3**	**4**	**5**	**6**	**7**	**8**	**9**	**10**	**11**
1	0	0	0	0	0	0	0	0	0	0	0
2	0	4.371	4.135	5.564	2.945	4.473	6.347	3.238	3.718	5.46	0
3	0	2.097	1.654	4.352	4.278	4.852	4.22	1.587	0.766	4.273	0
4	0	0.684	0.923	5.1	3.374	4.564	3.764	3.516	1.191	4.435	0
5	0	3.736	3.898	4.048	1.307	2.58	4.118	4.086	4.596	3.311	0
6	0	2.124	2.348	1.274	0.654	1.258	0.902	2.043	1.341	0.655	0
7	0	1.256	0.757	0.923	0.984	1.056	0.949	0.789	0.682	1.183	0
8	0	0.31	0.238	0.633	0.943	0.358	0.642	1.046	0.928	1.042	0
9	0	0.574	0.548	0.862	0.784	0.421	0.868	1.204	1.146	1.182	0
10	0	1.082	0.844	1.042	1.021	0.848	1.056	1.118	1.062	1.177	0
11	0	1.198	1.008	1.126	1.144	1.156	1.13	1.129	0.825	1.297	0
12	0	1.322	1.138	1.417	1.316	1.374	1.256	0.956	0.613	1.281	0
13	0	0	0	0	0	0	0	0	0	0	0

Table B.7: Air speed readings for fans 1-2 operating at 5,000 RPM.

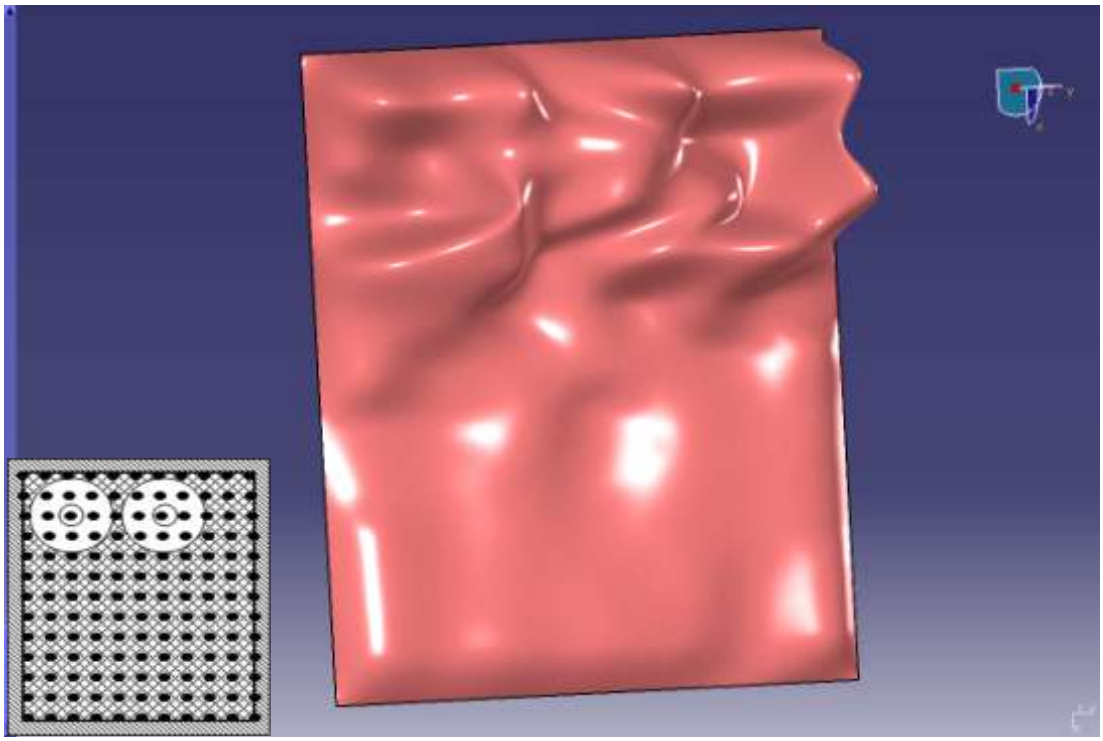

Figure B.7: Air speed profile for fans 1-2 operating at 5,000 RPM.

Fan speed 1000 RPM											
Air Speed (m/sec)											
Point	**1**	**2**	**3**	**4**	**5**	**6**	**7**	**8**	**9**	**10**	**11**
1	0	0	0	0	0	0	0	0	0	0	0
2	0	0.152	0.046	0.044	0.052	0.119	0.141	0.098	0.05	0.043	0
3	0	0.163	0.044	0.05	0.073	0.127	0.138	0.111	0.102	0.147	0
4	0	0.133	0.163	0.052	0.047	0.129	0.157	0.087	0.167	0.244	0
5	0	0.276	0.468	0.476	0.206	0.239	0.244	0.422	0.537	0.586	0
6	0	0.645	0.319	0.368	0.546	0.375	0.456	0.648	0.245	0.356	0
7	0	0.912	0.218	0.071	0.352	1.068	0.854	0.94	0.374	0.294	0
8	0	0.668	0.248	0.271	0.493	0.665	0.342	0.747	0.238	0.352	0
9	0	0.358	0.455	0.699	0.516	0.266	0.349	0.423	0.762	0.791	0
10	0	0.148	0.135	0.089	0.05	0.067	0.287	0.11	0.247	0.226	0
11	0	0.058	0.058	0.05	0.048	0.049	0.108	0.048	0.042	0.086	0
12	0	0.103	0.112	0.04	0.045	0.054	0.056	0.055	0.051	0.054	0
13	0	0	0	0	0	0	0	0	0	0	0

Table B.8: Air speed readings for fans 3-4 operating at 1,000 RPM.

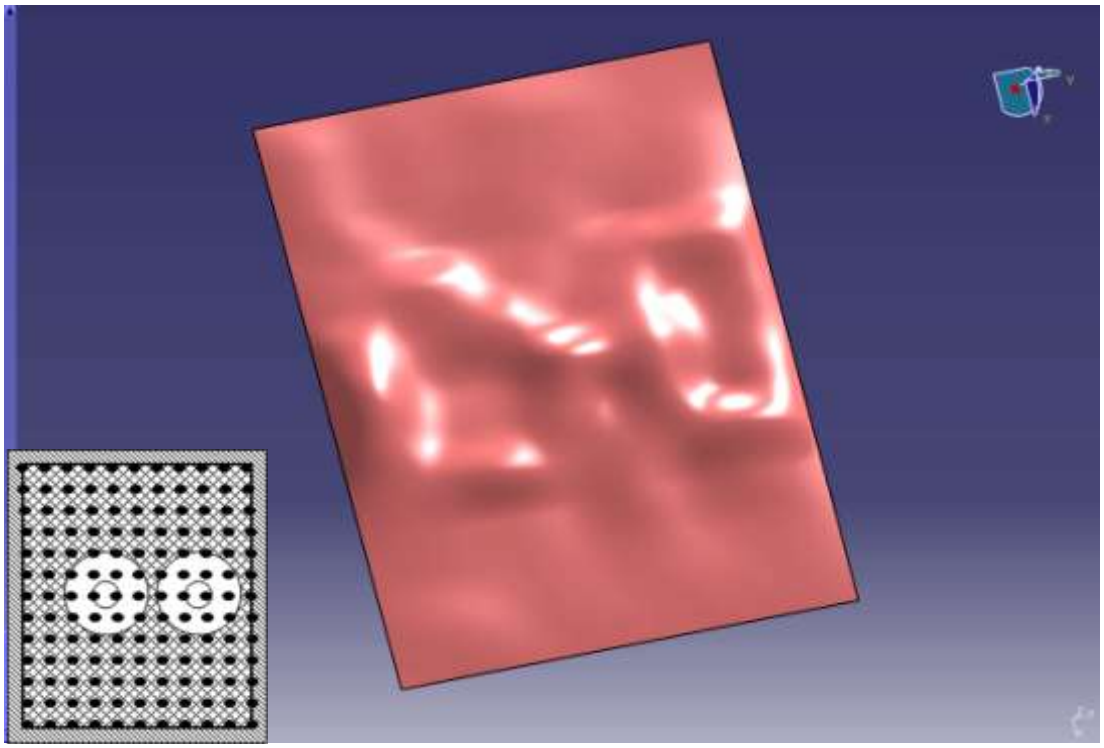

Figure B.8: Air speed profile for fans 3-4 operating at 1,000 RPM.

Fan speed 5000 RPM											
Air Speed (m/sec)											
Point	**1**	**2**	**3**	**4**	**5**	**6**	**7**	**8**	**9**	**10**	**11**
1	0	0	0	0	0	0	0	0	0	0	0
2	0	1.238	0.857	0.563	0.359	0.764	1.217	0.963	0.506	0.565	0
3	0	1.147	0.253	0.146	0.187	0.724	1.103	0.834	0.735	0.868	0
4	0	0.773	0.486	0.151	0.191	0.943	0.944	0.658	0.785	1.062	0
5	0	2.269	4.635	4.576	2.068	1.568	1.555	3.994	4.648	5.057	0
6	0	4.772	2.786	2.758	3.12	2.968	4.554	4.726	1.839	3.642	0
7	0	5.542	2.433	0.39	2.156	7.252	5.123	5.962	0.846	2.278	0
8	0	4.573	2.298	2.168	3.446	5.154	3.497	4.862	2.847	2.742	0
9	0	2.578	4.633	4.976	4.486	3.207	2.273	3.184	4.837	4.69	0
10	0	1.046	0.876	1.164	0.991	0.972	1.089	1.153	1.212	1.79	0
11	0	1.053	0.788	0.668	0.506	0.814	0.857	0.536	0.459	1.024	0
12	0	1.068	1.057	0.727	0.564	0.583	0.942	0.334	0.436	0.6	0
13	0	0	0	0	0	0	0	0	0	0	0

Table B.9: Air speed readings for fans 3-4 operating at 5,000 RPM.

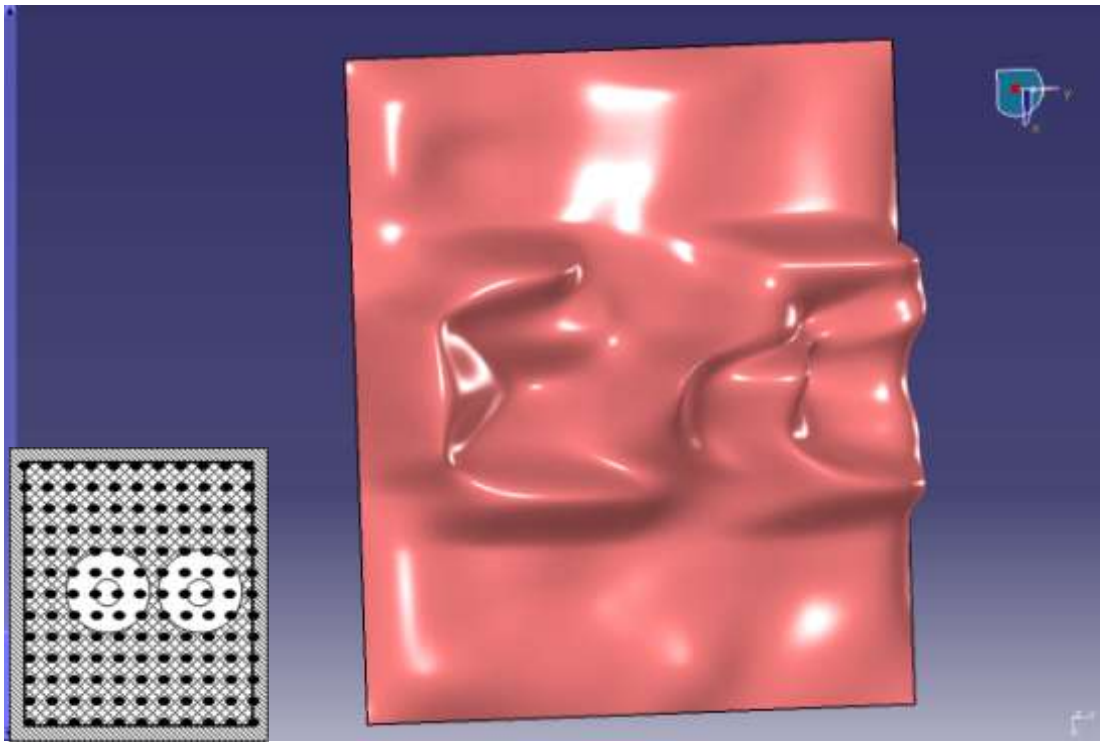

Figure B.9: Air speed profile for fans 3-4 operating at 5,000 RPM.

Fan speed 1000 RPM											
Air Speed (m/sec)											
Point	**1**	**2**	**3**	**4**	**5**	**6**	**7**	**8**	**9**	**10**	**11**
1	0	0	0	0	0	0	0	0	0	0	0
2	0	0.173	0.093	0.254	0.253	0.217	0.146	0.143	0.143	0.184	0
3	0	0.186	0.151	0.187	0.245	0.257	0.256	0.168	0.138	0.222	0
4	0	0.164	0.174	0.203	0.193	0.238	0.171	0.211	0.133	0.213	0
5	0	0.169	0.21	0.053	0.112	0.093	0.159	0.149	0.155	0.172	0
6	0	0.155	0.137	0.162	0.132	0.157	0.219	0.197	0.156	0.143	0
7	0	0.295	0.238	0.254	0.246	0.156	0.248	0.238	0.273	0.268	0
8	0	0.158	0.169	0.128	0.12	0.051	0.048	0.136	0.162	0.146	0
9	0	0.75	0.454	0.441	0.364	0.255	0.318	0.823	0.656	0.253	0
10	0	0.296	0.274	0.575	0.536	0.518	0.628	0.338	0.043	0.103	0
11	0	0.174	0.162	0.774	0.582	0.619	0.909	0.347	0.323	0.522	0
12	0	0.554	0.545	0.924	0.376	0.322	0.857	0.865	0.563	0.574	0
13	0	0	0	0	0	0	0	0	0	0	0

Table B.10: Air speed readings for fans 5-6 operating at 1,000 RPM.

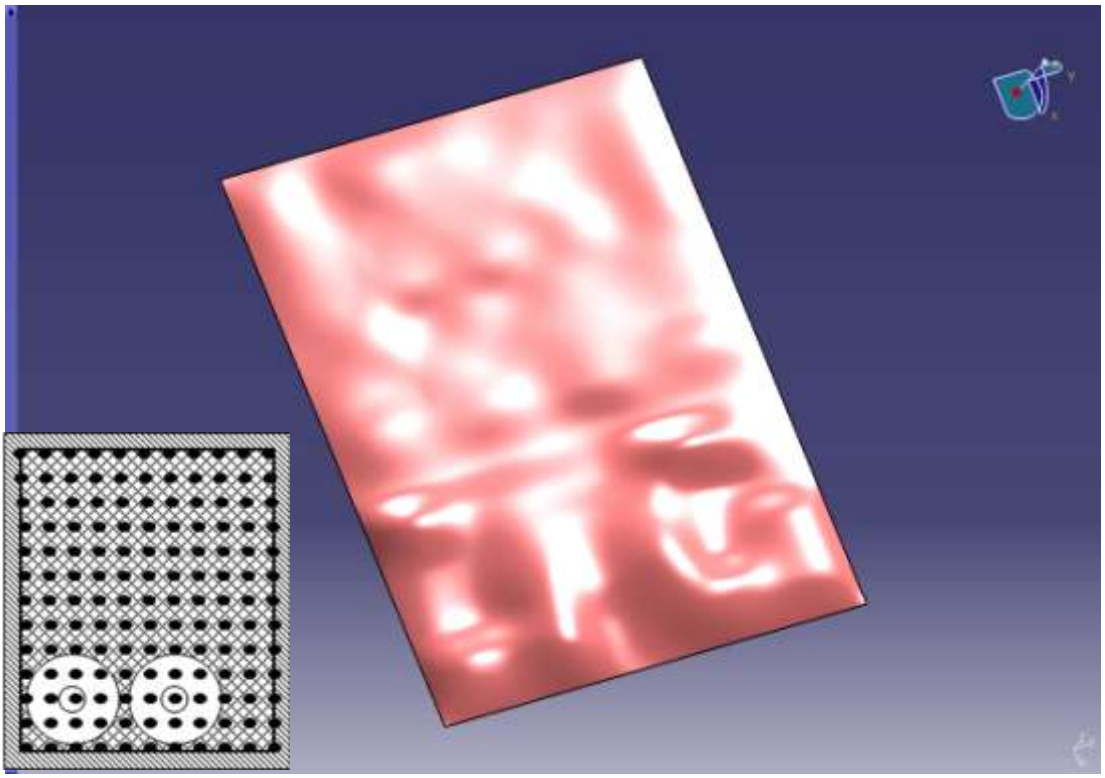

Figure B.10: Air speed profile for fans 5-6 operating at 1,000 RPM.

Fan speed 5000 RPM											
Air Speed (m/sec)											
Point	**1**	**2**	**3**	**4**	**5**	**6**	**7**	**8**	**9**	**10**	**11**
1	0	0	0	0	0	0	0	0	0	0	0
2	0	1.322	1.081	1.236	1.227	1.408	1.284	1.275	1.272	1.632	0
3	0	1.214	1.117	1.098	1.236	1.351	1.262	1.036	1.457	1.376	0
4	0	1.157	1.295	1.194	1.286	1.253	1.177	1.04	1.153	1.425	0
5	0	1.127	1.198	0.924	0.899	1.296	1.156	1.16	1.139	1.027	0
6	0	0.924	1.034	0.856	0.684	1.235	1.057	1.13	1.01	0.815	0
7	0	1.744	1.297	1.113	1.132	1.366	1.258	1.128	1.103	0.888	0
8	0	1.492	1.243	0.851	1.016	0.356	0.331	0.918	0.901	0.432	0
9	0	4.649	4.668	2.797	1.902	1.424	3.766	4.2	3.517	2.41	0
10	0	2.043	1.979	4.851	3.727	4.268	4.603	1.776	0.498	1.085	0
11	0	1.284	1.516	5.328	3.479	3.842	4.058	2.275	0.962	1.912	0
12	0	4.567	4.624	5.689	3.091	3.379	5.816	6.175	5.332	4.874	0
13	0	0	0	0	0	0	0	0	0	0	0

Table B.11: Air speed readings for fans 5-6 operating at 5,000 RPM.

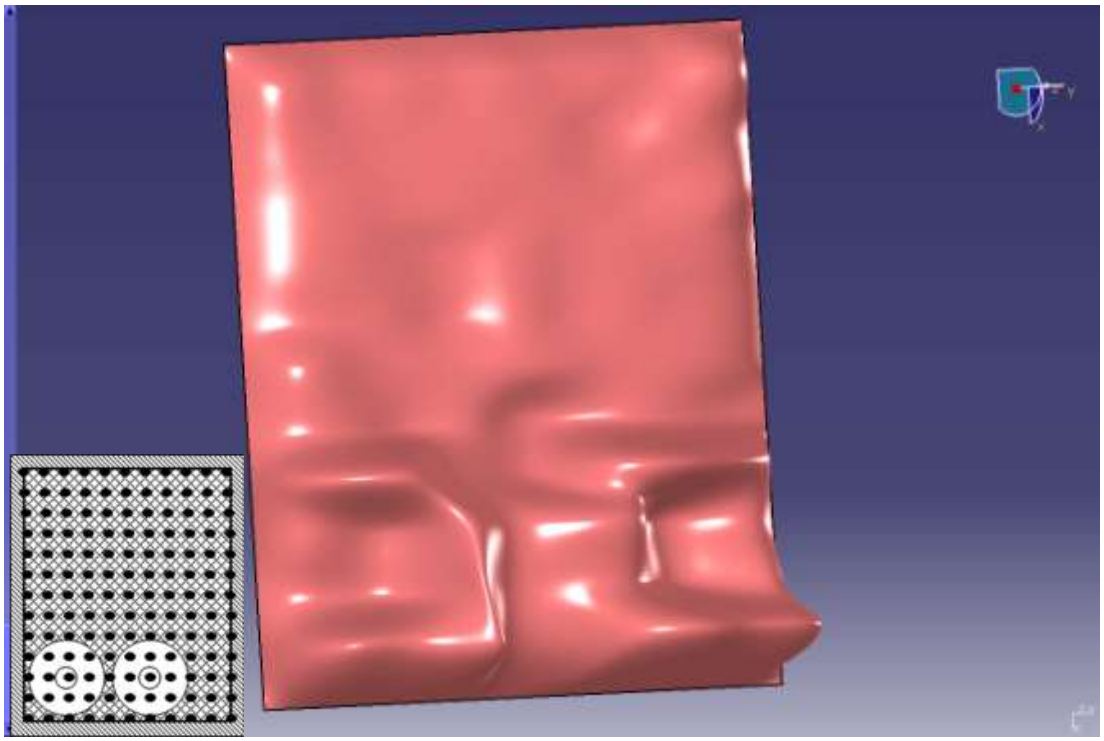

Figure B.11: Air speed profile for fans 5-6 operating at 5,000 RPM.

Fan speed 1000 RPM											
Air Speed (m/sec)											
Point	**1**	**2**	**3**	**4**	**5**	**6**	**7**	**8**	**9**	**10**	**11**
1	0	0	0	0	0	0	0	0	0	0	0
2	0	0.765	0.386	0.648	0.572	0.331	0.292	0.306	0.368	0.462	0
3	0	0.903	0.718	0.963	0.84	0.461	0.314	0.252	0.319	0.523	0
4	0	1.175	1.149	1.005	0.562	0.356	0.26	0.276	0.372	0.664	0
5	0	1.115	1.069	1.032	0.841	0.457	0.213	0.303	0.464	0.574	0
6	0	0.772	1.114	0.704	0.476	0.699	0.275	0.215	0.371	0.348	0
7	0	1.361	1.39	0.825	0.285	0.846	0.836	0.413	0.435	0.353	0
8	0	0.878	1.157	0.938	0.915	0.86	0.883	0.288	0.223	0.328	0
9	0	0.782	0.883	1.017	0.669	0.601	0.357	0.263	0.264	0.344	0
10	0	1.028	0.554	0.976	0.813	0.411	0.351	0.322	0.358	0.438	0
11	0	0.78	0.317	0.063	0.278	0.463	0.338	0.357	0.372	0.409	0
12	0	1.112	0.757	0.328	0.164	0.166	0.325	0.356	0.353	0.455	0
13	0	0	0	0	0	0	0	0	0	0	0

Table B.12: Air speed readings for fans 1-3-5 operating at 1,000 RPM.

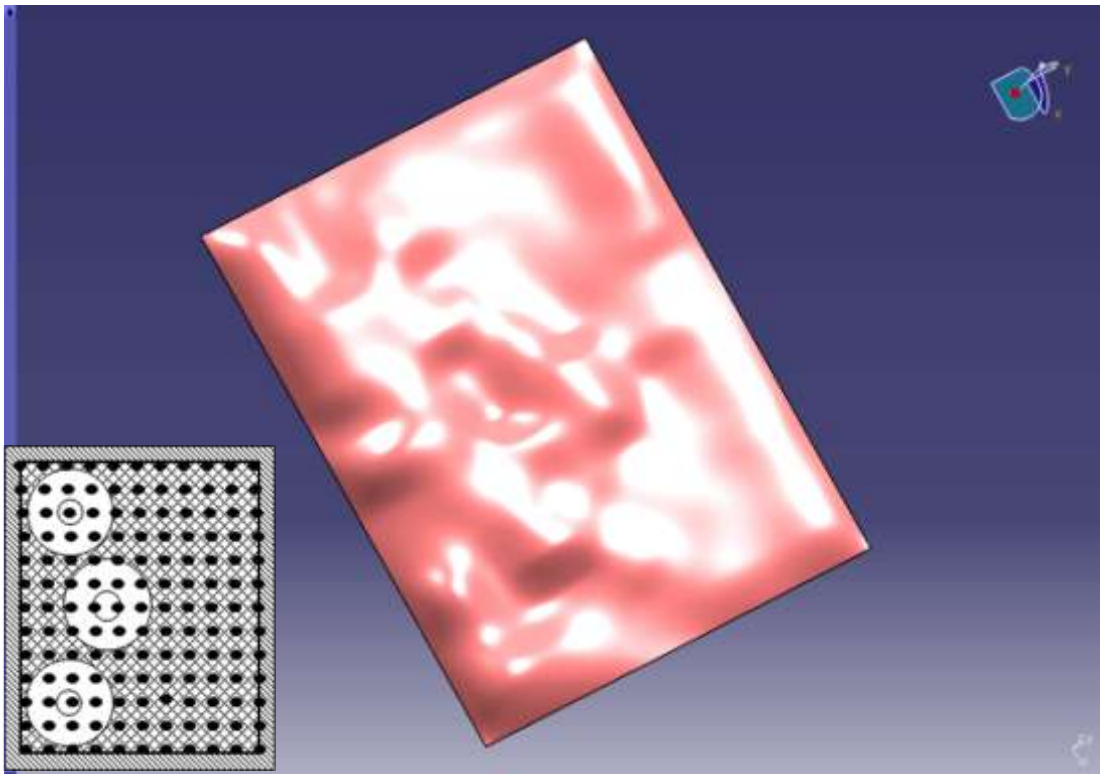

Figure B.12: Air speed profile for fans 1-3-5 operating at 1,000 RPM.

Fan speed 5000 RPM											
Air Speed (m/sec)											
Point	**1**	**2**	**3**	**4**	**5**	**6**	**7**	**8**	**9**	**10**	**11**
1	0	0	0	0	0	0	0	0	0	0	0
2	0	5.132	1.871	3.876	3.956	1.486	0.972	1.258	1.028	2.486	0
3	0	5.178	3.23	4.712	4.182	2.536	1.236	1.331	1.658	2.528	0
4	0	7.172	6.597	5.692	3.164	1.928	1.342	1.692	2.198	2.643	0
5	0	5.927	5.968	6.543	4.702	2.728	1.465	1.956	2.476	3.356	0
6	0	4.718	6.678	4.412	3.336	3.942	1.852	1.579	2.26	2.834	0
7	0	8.018	8.216	4.063	1.632	4.075	5.173	1.257	1.1	1.74	0
8	0	5.624	6.632	5.633	5.274	4.982	2.598	1.392	1.026	1.142	0
9	0	4.229	5.826	5.146	4.414	3.035	1.767	1.218	1.02	1.788	0
10	0	5.488	4.332	4.468	4.268	2.368	1.568	1.496	1.582	1.95	0
11	0	3.842	1.849	0.798	2.912	2.336	1.554	1.849	1.812	2.268	0
12	0	6.806	4.021	2.568	1.832	1.984	1.803	1.841	1.946	2.459	0
13	0	0	0	0	0	0	0	0	0	0	0

Table B.13: Air speed readings for fans 1-3-5 operating at 5,000 RPM.

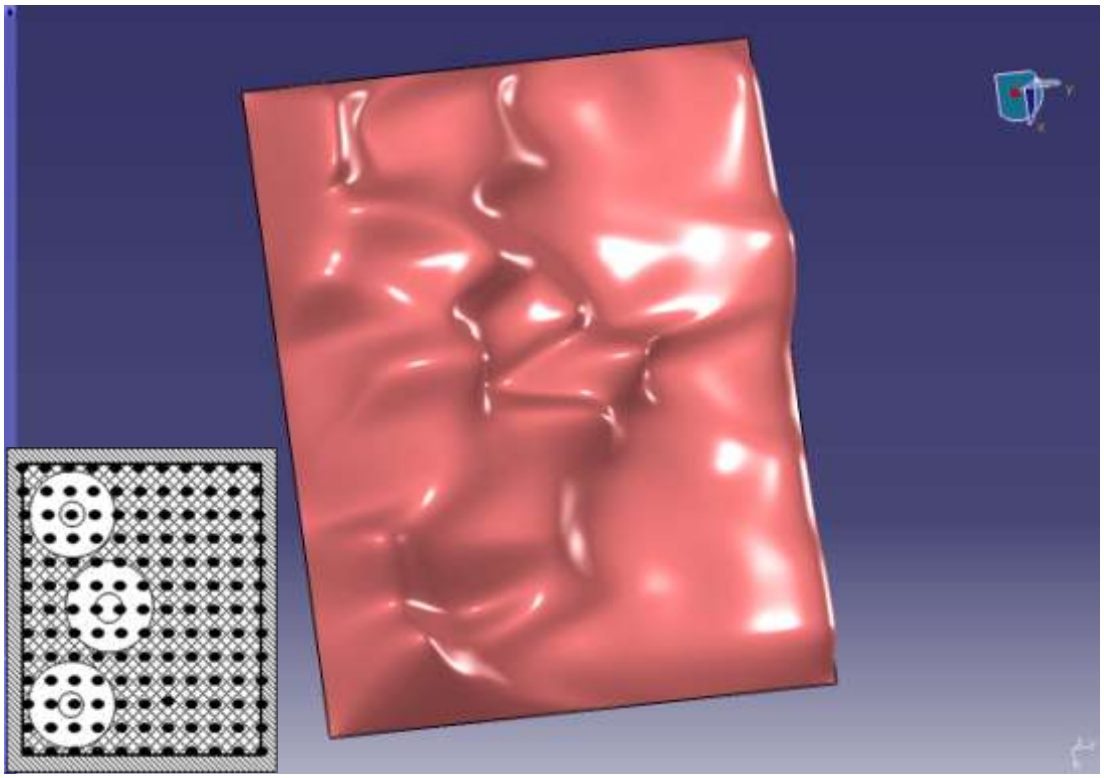

Figure B.13: Air speed profile for fans 1-3-5 operating at 5,000 RPM.

Fan speed 1000 RPM											
Air Speed (m/sec)											
Point	**1**	**2**	**3**	**4**	**5**	**6**	**7**	**8**	**9**	**10**	**11**
1	0	0	0	0	0	0	0	0	0	0	0
2	0	0.347	0.368	0.333	0.216	0.371	0.365	0.633	0.848	0.493	0
3	0	0.318	0.346	0.34	0.356	0.062	0.063	0.322	0.818	0.785	0
4	0	0.282	0.336	0.344	0.428	0.668	0.343	0.573	0.916	0.498	0
5	0	0.152	0.208	0.292	0.372	0.328	0.854	1.751	0.75	0.834	0
6	0	0.533	0.389	0.347	0.312	0.446	0.737	0.926	0.793	1.008	0
7	0	0.639	0.415	0.424	0.404	0.454	0.844	0.493	0.399	0.864	0
8	0	0.394	0.245	0.328	0.358	0.342	0.507	0.541	0.671	0.981	0
9	0	0.216	0.268	0.318	0.364	0.495	0.713	0.813	0.824	0.748	0
10	0	0.238	0.261	0.325	0.362	0.886	0.928	1.056	1.065	0.836	0
11	0	0.368	0.356	0.359	0.458	0.952	0.547	0.179	0.436	1.045	0
12	0	0.487	0.403	0.366	0.452	0.859	0.602	0.538	1.078	0.869	0
13	0	0	0	0	0	0	0	0	0	0	0

Table B.14: Air speed readings for fans 2-4-6 operating at 1,000 RPM.

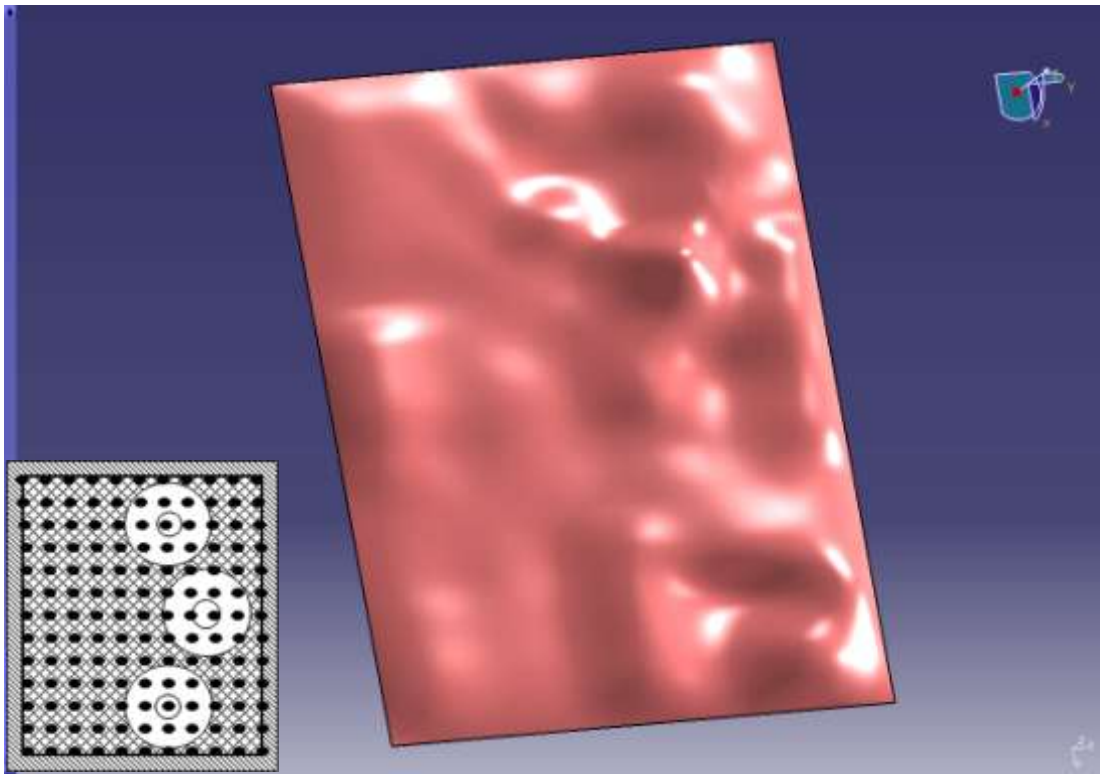

Figure B.14: Air speed profile for fans 2-4-6 operating at 1,000 RPM.

Fan speed 5000 RPM											
Air Speed (m/sec)											
Point	**1**	**2**	**3**	**4**	**5**	**6**	**7**	**8**	**9**	**10**	**11**
1	0	0	0	0	0	0	0	0	0	0	0
2	0	2.281	0.916	1.193	0.718	1.301	3.563	3.323	1.915	4.922	0
3	0	2.49	1.467	1.352	1.131	2.254	4.097	4.864	3.198	5.012	0
4	0	2.612	2.049	1.569	1.289	1.733	3.252	5.563	6.15	6.547	0
5	0	3.372	2.336	1.834	1.563	2.896	4.698	6.345	5.47	5.776	0
6	0	2.93	2.158	1.69	1.866	3.462	3.194	4.342	6.113	4.454	0
7	0	1.68	0.962	1.171	5.094	3.935	1.546	4.095	8.141	7.781	0
8	0	1.035	1.263	1.243	2.295	4.315	5.283	5.348	6.329	5.432	0
9	0	1.842	0.985	1.165	1.675	2.357	3.951	4.987	5.585	4.058	0
10	0	2.031	1.466	1.372	1.633	2.118	4.176	4.48	1.071	3.439	0
11	0	2.173	1.745	1.794	1.384	1.462	2.711	1.016	3.423	6.703	0
12	0	2.756	1.878	1.812	1.529	0.859	1.544	2.243	1.078	0.869	0
13	0	0	0	0	0	0	0	0	0	0	0

Table B.15: Air speed readings for fans 2-4-6 operating at 5,000 RPM.

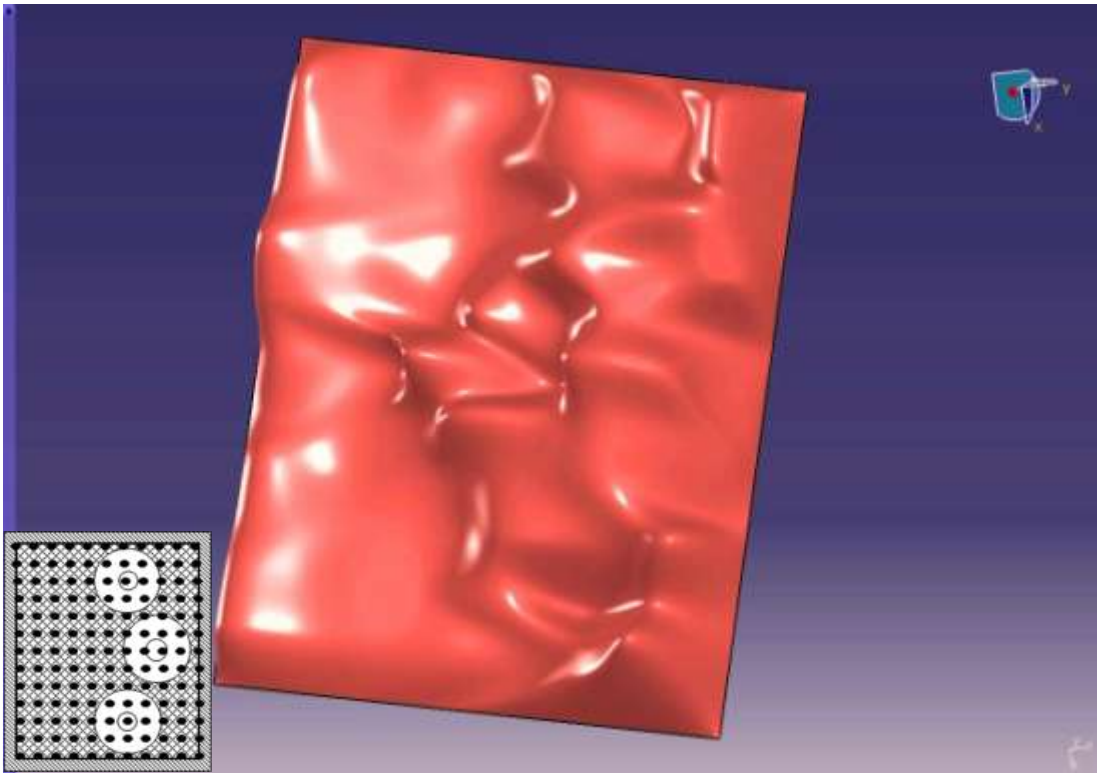

Figure B.15: Air speed profile for fans 2-4-6 operating at 5,000 RPM.

Appendix C

MATLAB/Simulink models

Following figures illustrate the Simulink models used for data processing and feedback. The models for data acquisition, data processing and display.

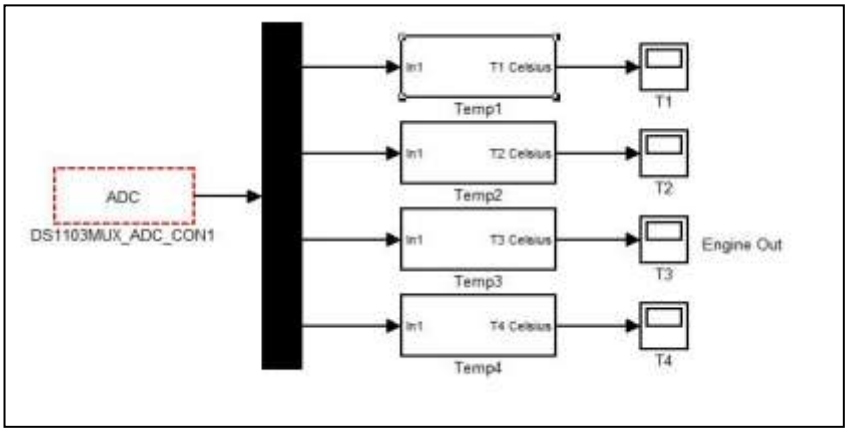

Figure C.1: Analog-to-digital converter (ADC) 4 ports plus mux with signal processing blocks in MATLAB/ Simulink

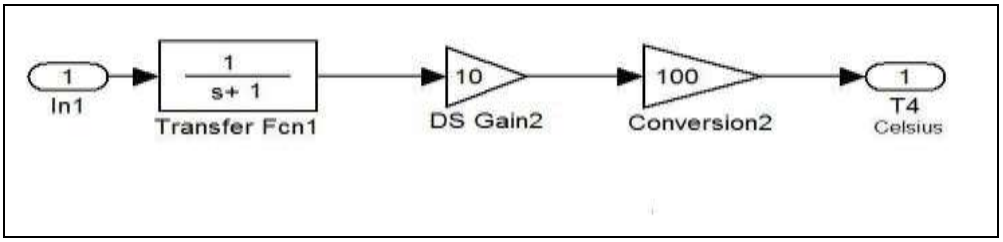

Figure C.2: Transfer function and gains to convert dSPACE signal to actual temperature (K type)

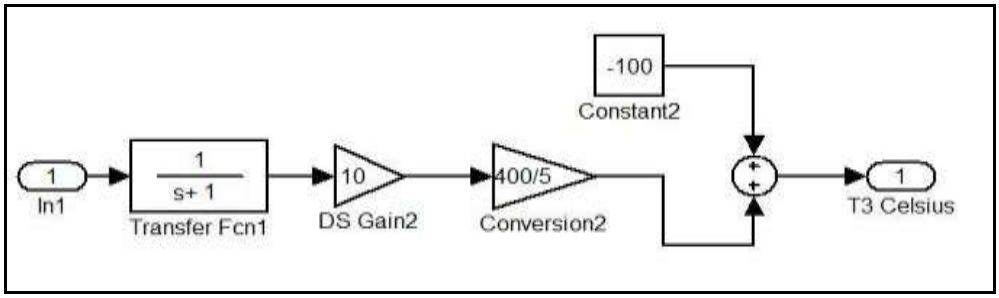

Figure C.3: Transfer function and gains to convert dSPACE signal to actual temperature (J type)

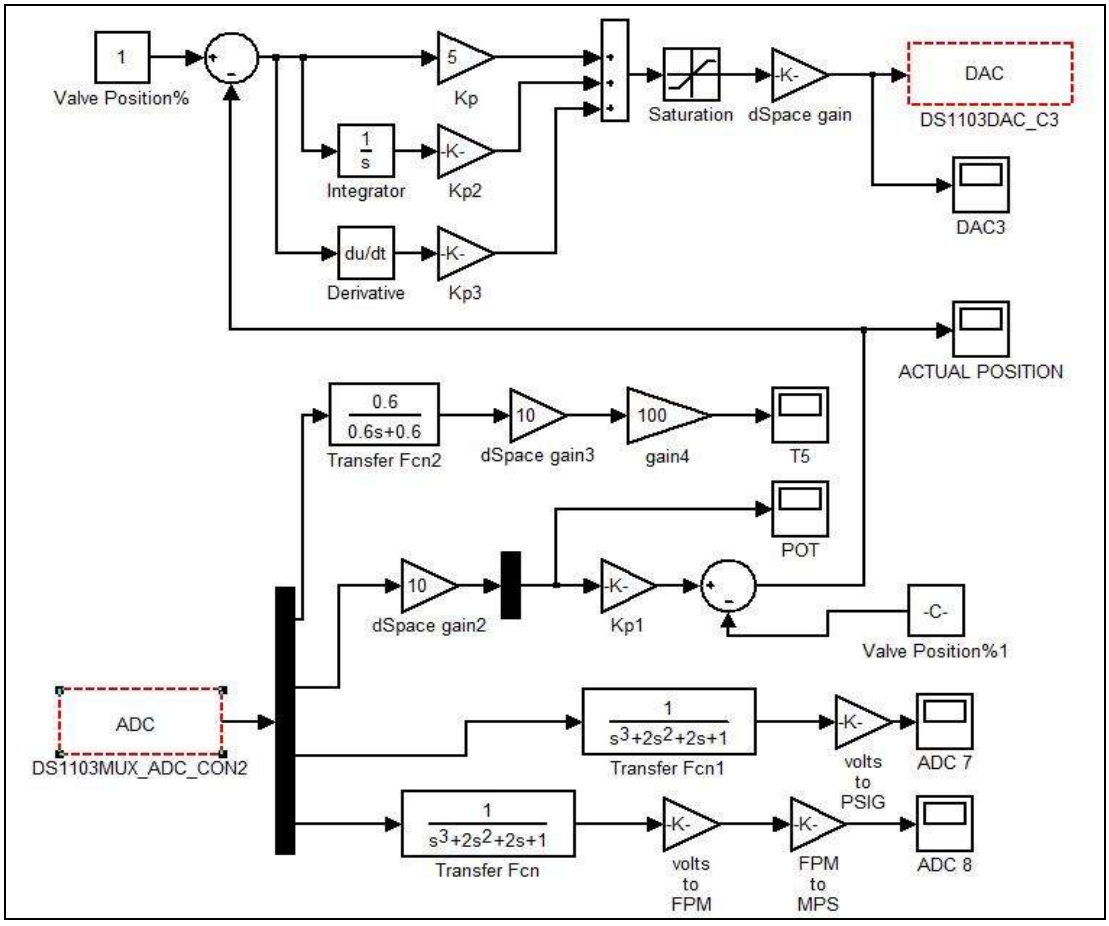

Figure C.4: MATLAB/Simulink algorithm for meqasirement of parametes : air speed, valve position and pressure readings. Also shown are the low pass filters and the required gains.

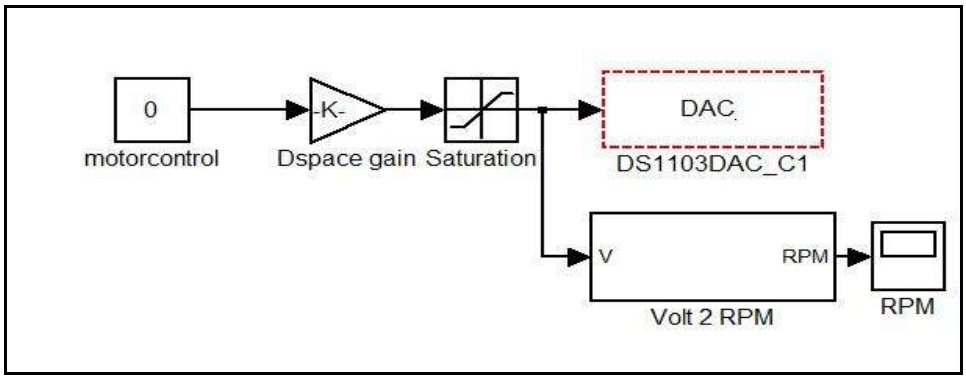

Figure C.5: Motor control and control desk interface.

Appendix D

Plus+1 BLDC Motor Model

Following figures illustrate the Plus+1 models used for CAN signals for BLDC motor control.

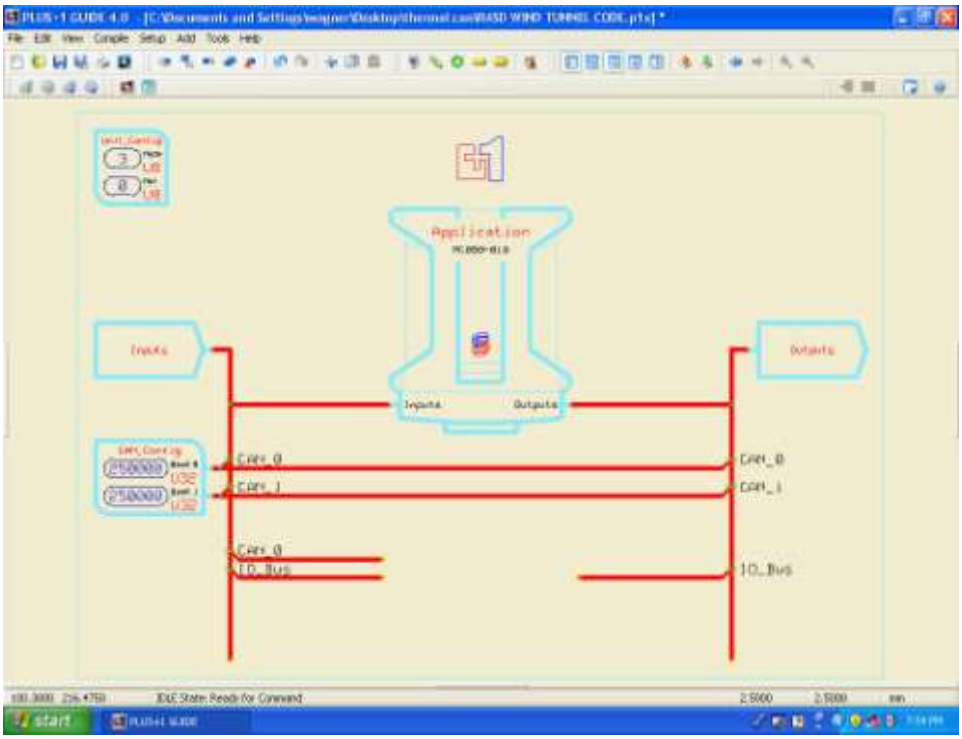

Figure D.1: Fan motor controller overall layout with microprocessor input/output ports.

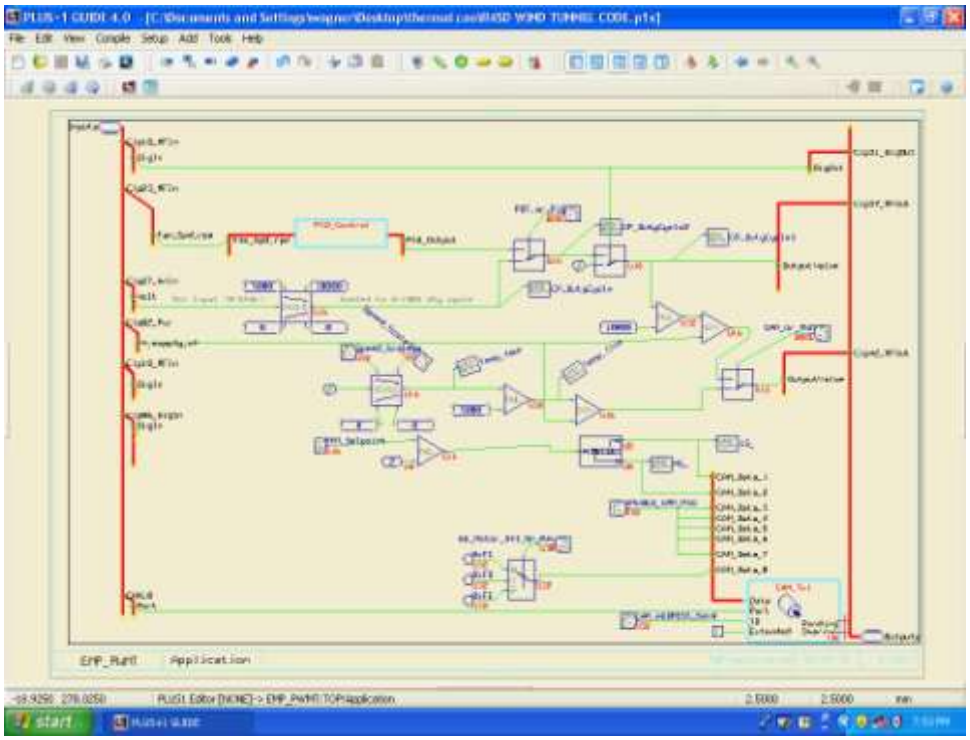

Figure D.2: Motor control signal flow block diagram with external variable interface.

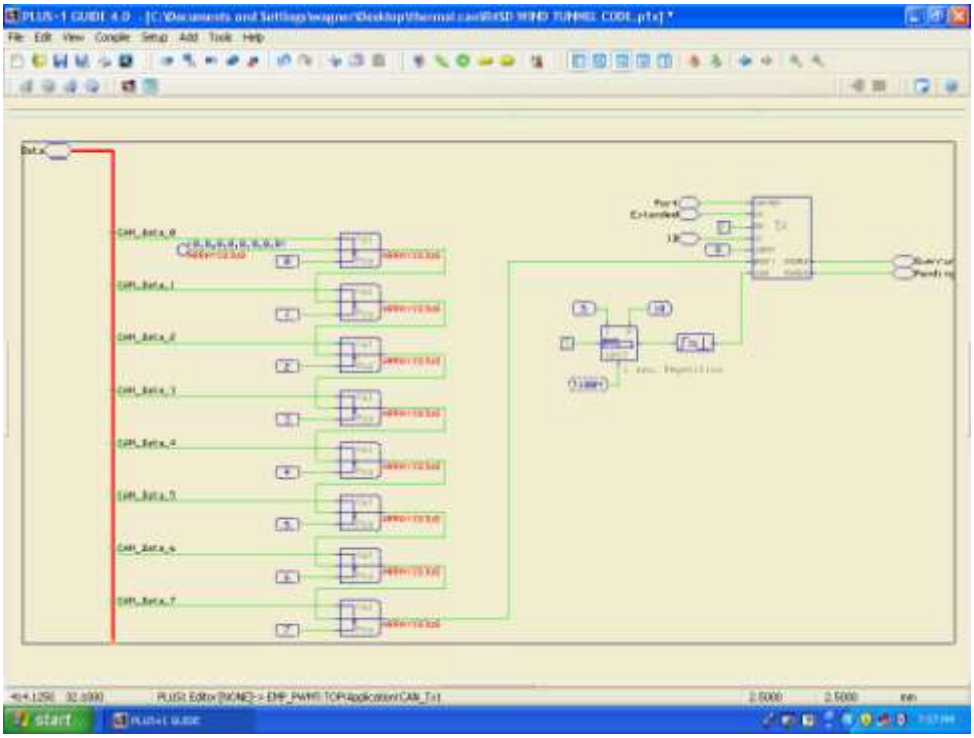

Figure D.3: Motor control signal flow schematic (8 bit format).

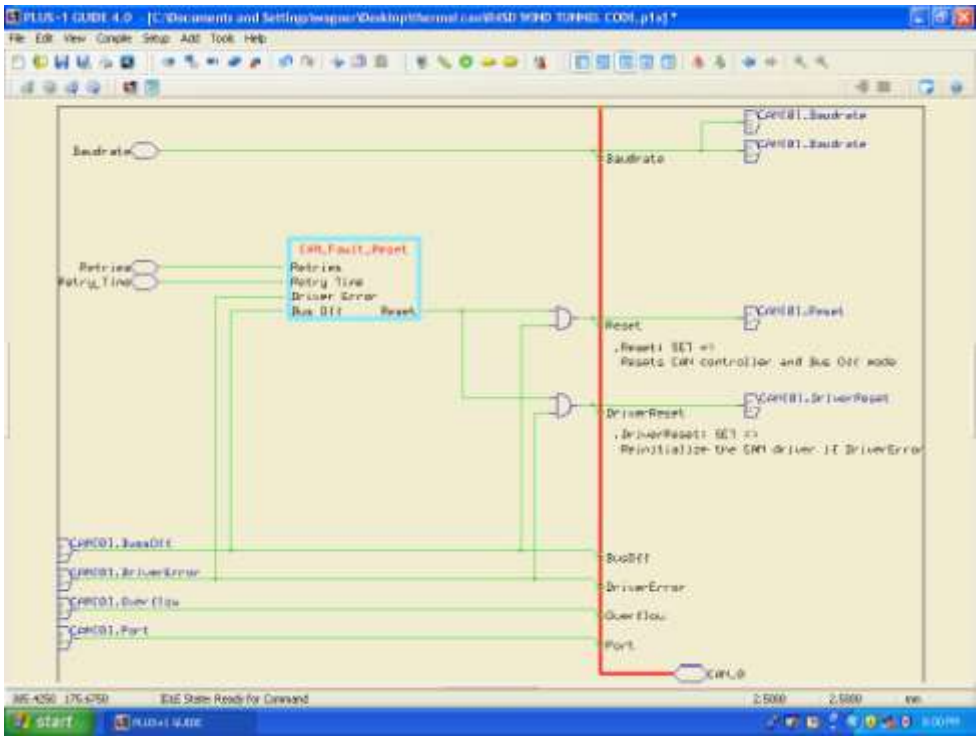

Figure D.4: Signal flow in CAN format.

REFERENCES

Alfano, D., and Judkins J., "Intelligent Thermal Management Using Brushless DC Fans", proceedings of Wescon/98 Conference, ISBN: 0-7803-5078-2 Anaheim, CA, September 1998.

Allen, D., and Lasecki, M., "Thermal Management Evolution and Controlled Coolant Flow", proceedings of the Vehicle Thermal Management Systems Conference & Exposition, SAE Paper Number: 2001-01-1732, Nashville, TN, May 2001.

Badekar, R., Mahajan, J., Kakaye, S., Khire, P., and Gopalkrishna, K., "Development of Control System for Electrical Radiator Fan Using Dual Sensor & Microprocessor Based Electronic Unit", proceedings of the SAE World Congress & Exhibition, SAE Paper Number: 2006-01-1035, Detroit, MI, April 2006.

Chalgren, R., and Allen, D., "Light Duty Diesel Advanced Thermal Management", proceedings of the Vehicle Thermal Management Systems Conference & Exposition, SAE Paper Number: 2005-01-2020, Toronto, Canada, May 2005.

Chalgren, R., "Thermal Comfort and Engine Warm-up Optimization of a Low-Flow Advanced Thermal Management System", proceedings of the SAE World Congress & Exhibition, SAE Paper Number: 2004-01-0047, Detroit, MI, March 2004.

Chalgren, R., Parker, G., Arici, O., and Johnson, J., "A Controlled EGR Cooling System for Heavy Duty Diesel Applications Using the Vehicle Engines Cooling System Simulation", proceedings of the SAE World Congress & Exhibition, SAE Paper Number: 2002-01-0076, Detroit, MI, March 2002.

Chanfreau, M., and Joseph, A., "Advanced Engine Cooling Thermal Management System on a Dual Voltage 42V-14V Minivan", proceedings of the Vehicle Thermal Management Systems Conference & Exposition, SAE Paper Number: 2001-01-1742, Nashville, TN, May 2001.

Chanfreau, M., Gessier, B., Farkh, A., and Geels, P., "The Need for an Electrical Water Valve in a THErmal Management Intelligent System (THEMIS)", proceedings of the SAE World Congress & Exhibition, SAE Paper Number: 2003-01-0274, Detroit, MI, March 2003.

Cho, H., Jung, D., Filipi, Z., and Assanis, D., "Application of Controllable Electric Coolant Pump for Fuel Economy and Cooling Performance Improvement", proceedings of the *ASME Journal of Engineering for Gas Turbine and Power*, vol. 129, Issue no. 1, pp- 239-244, January 2007.

Choi, K., Kim, H., Cho, W., and Lee, K., "Investigation of Emission Reduction Effect by Controlling Cooling System in a Diesel Engine", proceedings of the Powertrain & Fluid Systems Conference and Exhibition, SAE Paper Number: 2007-01-4064, Chicago, IL, October 2007.

Choi, K., Kim, K., and Lee, K., "Effect of New Cooling System in a Diesel Engine on Engine Performance and Emission Characteristics", proceedings of the SAE World Congress & Exhibition, SAE Paper Number: 2009-01-0177, Detroit, MI, April 2009.

Choukroun, A., and Chanfreau, M., "Automatic Control of Electronic Actuators for an Optimized Engine Cooling Thermal Management", proceedings of the Vehicle Thermal Management Systems Conference & Exposition, SAE Paper Number: 2001-01-1758, Nashville, TN, May 2001.

Figliola, R., and Beasley, D., "Theory and Design for Mechanical Measurements", Edition 2, Published By, John Wiley & Sons Inc, ISBN: 0-471-00089-2, 1995.

Fulton, J., and Repple, W., "Efficient Controllable Variable Flow (CVF) Cooling System for Modern Engines", SAE Paper Number: 2008-01-2766, Warrendale, PA, December 2008.

Heinz, H., "Advanced Engine Technology", Edition. 1, Published By. SAE International, ISBN: 978-1-56091-734-2, October 1995.

Heywood, J., "Internal Combustion Engine Fundamentals", Edition. 88, Published By McGraw-Hill, ISBN13**:** 9780070286375, April 1988.

Hyun, K., and Heon, J .,"Development of A Continuous Variable Speed Viscous Fan Clutch for Engine Cooling System", proceedings of the SAE World Congress & Exposition, SAE Paper Number: 980838, Detroit, MI, February 1998.

Jiangjiang, W., Chunfa, Z., Youyin, J., and Dawei, A., "Design of Radiator Thermal Characteristics Measurement and Control System Based on Virtual Instruments", proceedings of The Eighth International Conference on Electronic Measurement and Instruments, ISBN: 978-1-4244-1136-8, Xi'an, China, August 2007.

Jorgensen, R., "Fan Engineering",Edition 8,Published By Buffalo Forge Company, September, 1982.

Koch, F., and Haubner, F., "Cooling System Development and Optimization for DI Engines", proceedings of the SAE World Congress, SAE Paper Number: 2000-01-0283, Detroit, MI, March 2000.

Kopac, M, and Kokturk, L, "Determination of Optimum Speed of an Internal Combustion Engine by Exergy Analysis", *International Journal of Exergy 2005* - vol. *2*, No.1 pp. 40 - 54, 2005.

Mahmoud, K., Loibner, E., and Weisler, B., "Simulation-Based Vehicle Thermal Management System- Concept and Methodology", proceedings of the SAE World Congress & Exhibition, SAE Paper Number: 2003-01-0276, Detroit, MI, March 2003.

Mitchell, T., Salah, M., Wagner, J., and Dawson, D., "Automotive Thermal Valve Configurations: Enhanced Warm-Up Perfromance", *ASME Journal of Dynamic Systems, Measurement and Control.* vol. 131, Issue no. 4, pp- 239-244, July 2009

Page, R ., Hnatczuk, W., and Kozierowski, J., "Thermal Management for the 21st Century- Improved Thermal Control and fuel Economy in an Army Medium Tactical Vehicle", proceedings of the Vehicle Thermal Management Systems Conference & Exposition, SAE Paper Number: 2005-01-2068, Toronto, Canada, May 2005.

Rahman, S., and Sun, R., "Robust Engineering of Engine Cooling System", proceedings of the SAE World Congress & Exhibition, SAE Paper Number: 2003-01-0149, Detroit, MI, March 2003.

Redfield, J., Surampudi, B., Ray, G., and Montemayor, A., "Accessory Electrification in Class 8 Tractors", proceedings of the SAE World Congress & Exhibition, SAE Paper Number: 2006-01-0215, Detroit, MI, April 2006.

Rocklage, G., Riehl, G., and Vogt, R., "Requirements on New Components for Future Cooling Systems", proceedings of the Vehicle Thermal Management Systems Conference & Exposition, SAE Paper Number: 2001-01-1767, Nashville, TN, May 2001.

Setlur, P., Wagner, J., Dawson, D., and Egidio Marotta, "An Advanced Engine Thermal Management System: Nonlinear Control and Test", IEEE/ASME Transactions on Mechatronics, vol. no 10, Issue no. 2, DOI: 1083-4435, September 2005.

Staunton, N., Pickert, V., and Maughan, R., "Assessment of Advanced Thermal Management Systems for Micro-Hybrid Trucks and Heavy Duty Diesel Vehicles", proceedings of the IEEE Vehicle Power and Propulsion Conference, ISBN: 978-1-4244-1849-7/08, Harbin, China, September 2008.

Stephens, T., and Cross, T., "Fan and Heat Exchanger Flow Interactions", proceedings of the Vehicle Thermal Management Systems Conference & Exposition, SAE Paper Number: 2005-01-2004, Toronto, Canada, May 2005.

Takashi, S., Yasufumi, O., and Masake, Y., "Heat Transfer in Internal Combustion Engines", proceedings of the SAE World Congress, SAE Paper Number: 2000-01-0300, Detroit, MI, March 2000.

Taylor, C., and Toong, T., "Heat Transfer in Internal-Combustion Engine", proceedings of the ASME-AiChE Heat Transfer Conference, ASME Paper Number: 295, University Park, PA, August 1957.

Wagner, J., Ghone, M., and Dawson, D., "Cooling Flow Control Strategy for Automotive Thermal Management Systems", proceedings of the SAE World Congress & Exhibition, SAE Paper Number: 2002-01-0713, Detroit, MI, March 2002.

Wambsganss, M, "Thermal Management Concepts for Higher-Efficiency Heavy Vehicles", proceedings of the Government Industry Meeting, SAE Paper Number: 1999-01-2240 Washington, DC, April 1999.